

TERNARY NANOCOMPOSITES OF LOW DENSITY,
HIGH DENSITY AND LINEAR LOW DENSITY POLYETHYLENES
WITH THE COMPATIBILIZERS E-MA-GMA AND E-BA-MAH

A THESIS SUBMITTED TO
THE GRADUATE SCHOOL OF NATURAL AND APPLIED SCIENCES
OF
MIDDLE EAST TECHNICAL UNIVERSITY

BY

FATMA IŞIK COŞKUNSES

IN PARTIAL FULFILLMENT OF THE REQUIREMENTS
FOR
THE DEGREE OF DOCTOR OF PHILOSOPHY
IN
CHEMICAL ENGINEERING

JUNE 2011

Approval of the thesis:

**TERNARY NANOCOMPOSITES OF LOW DENSITY,
HIGH DENSITY AND LINEAR LOW DENSITY POLYETHYLENES
WITH THE COMPATIBILIZERS E-MA-GMA AND E-BA-MAH**

submitted by **FATMA IŞIK COŞKUNSES** in partial fulfillment of the requirements for the degree of **Doctor of Philosophy in Chemical Engineering Department, Middle East Technical University** by,

Prof. Dr. Canan Özgen
Dean, Graduate School of **Natural and Applied Sciences**

Prof. Dr. Deniz Üner
Head of Department, **Chemical Engineering**

Prof. Dr. Ülkü Yilmazer
Supervisor, **Chemical Engineering Dept., METU**

Examining Committee Members:

Prof. Dr. Güngör Gündüz
Chemical Engineering Dept., METU

Prof. Dr. Ülkü Yilmazer
Chemical Engineering Dept., METU

Prof. Dr. Teoman Tinçer
Chemistry Dept., METU

Prof. Dr. Göknur Bayram
Chemical Engineering Dept., METU

Assist. Prof. Dr. Güralp Özkoç
Chemical Engineering Dept., Kocaeli University

Date: 14 .06. 2011

I hereby declare that all information in this document has been obtained and presented in accordance with academic rules and ethical conduct. I also declare that, as required by these rules and conduct, I have fully cited and referenced all material and results that are not original to this work.

Name, Last name: **Fatma IŐIK COŐKUNSES**

Signature:

ABSTRACT

TERNARY NANOCOMPOSITES OF LOW DENSITY, HIGH DENSITY AND LINEAR LOW DENSITY POLYETHYLENES WITH THE COMPATIBILIZERS E-MA-GMA AND E-BA-MAH

Işık Coşkunes, Fatma

Ph.D., Department of Chemical Engineering

Supervisor: Prof. Dr. Ülkü YILMAZER

June 2011, 198 pages

The effects of polyethylene, (PE), type, compatibilizer type and organoclay type on the morphology, rheological, thermal, and mechanical properties of ternary low density polyethylene (LDPE), high density polyethylene (HDPE), and linear low density polyethylene (LLDPE), matrix nanocomposites were investigated in this study. Ethylene – Methyl acrylate – Glycidyl methacrylate terpolymer (E-MA-GMA) and Ethylene – Butyl acrylate- Maleic anhydride terpolymer (E-BA-MAH) were used as the compatibilizers. The organoclays selected for the study were Cloisite® 30B and Nanofil® 8. Nanocomposites were prepared by means of melt blending via co-rotating twin screw extrusion process. Extruded samples were injection molded to be used for material characterization tests.

Optimum amounts of ingredients of ternary nanocomposites were determined based on to the mechanical test results of binary blends of PE/Compatibilizer and binary nanocomposites of PE/Organoclay. Based on the tensile test results, the optimum contents of compatibilizer and organoclay were determined as 5 wt % and 2 wt %, respectively.

XRD and TEM analysis results indicated that intercalated and partially exfoliated structures were obtained in the ternary nanocomposites. In these

nanocomposites E-MA-GMA compatibilizer produced higher d-spacing in comparison to E-BA-MAH, owing to its higher reactivity. HDPE exhibited the highest basal spacing among all the nanocomposite types with E-MA-GMA/30B system. Considering the polymer type, better dispersion was achieved in the order of LDPE<LLDPE<HDPE, owing to the linearity of HDPE, and short branches of LLDPE.

MFI values were decreased by the addition of compatibilizer and organoclay to the matrix polymers. Compatibilizers imparted the effect of sticking the polymer blends on the walls of test apparatus, and addition of organoclay showed the filler effect and increased the viscosity.

DSC analysis showed that addition of compatibilizer or organoclay did not significantly affect the melting behavior of the nanocomposites. Degree of crystallinity of polyethylene matrices decreased with organoclay addition. Nanoscale organoclays prevented the alignment of polyethylene chains and reduced the degree of crystallinity.

Ternary nanocomposites had improved tensile properties. Effect of compatibilizer on property enhancement was observed in mechanical results. Tensile strength and Young's modulus of nanocomposites increased significantly in the presence of compatibilizers.

Keywords: low density polyethylene, high density polyethylene, linear low density polyethylene, compatibilizer, organoclay, nanocomposite, extrusion

ÖZ

E-MA-GMA VE E-BA-MAH UYUM SAĞLAYICILARI İÇEREN ALÇAK YOĞUNLUK, YÜKSEK YOĞUNLUK VE LİNEER ALÇAK YOĞUNLUK POLİETİLENLERİN ÜÇLÜ SİSTEM NANOKOMPOZİTLERİ

Işık Coşkunes, Fatma
Doktora, Kimya Mühendisliği
Tez Yöneticisi: Prof. Dr. Ülkü Yılmaz

Haziran 2011, 198 sayfa

Bu çalışmada polietilen (PE), uyum sağlayıcı ve organik kil çeşidinin, üçlü alçak yoğunluk polietilen AYPE, yüksek yoğunluk polietilen YYPE ve lineer alçak yoğunluk polietilen LAYPE, matrisli nanokompozitlerin morfolojileri, reolojik, ısı ve mekanik özellikleri üzerindeki etkileri incelenmiştir. Etilen/metil akrilat/glisidil metakrilat (E-MA-GMA), ve etilen/bütül akrilat/maleik anhidrit (E-BA-MAH) terpolimerleri uyum sağlayıcı olarak kullanılmıştır. Çalışma için seçilen organik killer Cloisite® 30B ve Nanofil® 8 dir. Nanokompozitler eriyik karıştırma yöntemi ile aynı yönde dönen çift vidalı ekstruder kullanılarak hazırlanmıştır. Karakterizasyon testlerinde kullanılmak üzere, ekstrüzyonla karıştırılmış numuneler enjeksiyonlu kalıplama yöntemi ile hazırlanmıştır.

PE/Uyum sağlayıcı ikili alaşımları ve PE/Organikkil ikili nanokompozitlerin mekanik test sonuçlarına göre üçlü nanokompozitlerin optimum içerik miktarları belirlenmiştir. Gerilme testi sonuçlarına göre içerik miktarları uyum sağlayıcı için ağırlıkça % 5, organik kil için ağırlıkça % 2 olarak belirlenmiştir.

X-Işını kırınımı ve TEM analizleri sonuçları üçlü nanokompozitlerde aralanmış ve kısmi saçılmış yapıların elde edildiğini belirtmektedir. Bu üçlü nanokompozitlerde E-MA-GMA, daha yüksek reaktivitesinden dolayı E-BA-MAH uyumlaştırıcısından daha yüksek d-aralığına neden olmuştur.

Tüm nanokompozit çeşitleri arasında en yüksek kil tabakası aralığına YYPE ve E-MA-GMA/30B sistemlerinde rastlanmıştır. Polietilen tipi dikkate alındığında daha iyi organik kil dağılımı sırası ile YYPE, LAYPE ve AYPE de elde edilmiştir; bunun nedeni YYPE' nin lineer zincirlere, LAYPE' nin de kısa yan zincirlere sahip olmasıdır.

Polimerlere uyum sağlayıcı ve organik kil eklendiğinde eriyik akış indeks değerleri düşmüştür. Uyum sağlayıcılar, polimer karışımlarının test cihazının metal yüzeylerine yapışmasını sağlayarak, organik kil eklenmesi ise katkı maddesi etkisi sağlayarak vizkoziteyi arttırmıştır.

DSC analiz sonuçlarına göre, uyum sağlayıcı ve/veya organik kil eklenmesi, nanokompozitlerin erime davranışlarını belirgin olarak etkilememiştir. Polietilen matrislerinin kristallenme derecesi organik kil eklenmesi ile azalmıştır. Nano boyuttaki organik killer polietilen zincirlerinin kristal yapı oluşturmasını engellemiş ve kristallenme derecesini azaltmıştır.

Üçlü nanokompozit sistemlerinin gerilme özellikleri geliştirilmiştir. Mekanik sonuçlarda, uyum sağlayıcının özelliklerin artırılmasına etkisi gözlenmiştir. Nanokompozitlerin gerilme mukavemetleri ve Young modülleri uyum sağlayıcının katılımı ile önemli miktarda artış göstermiştir.

Anahtar Sözcükler: Alçak yoğunluk polietilen, yüksek yoğunluk polietilen, lineer alçak yoğunluk polietilen, uyum sağlayıcı, organik kil, nanokompozit, ekstrüzyon

To My Daughter Defne & My Mother Hatice

ACKNOWLEDGMENTS

I would like to express my deepest gratitude to my thesis supervisor Prof. Dr. Ülkü Yılmaz for his guidance, understanding, kind support, encouraging advice, criticism, and valuable discussions throughout my thesis.

I am greatly indebted to Prof. Dr. Gökür Bayram from Department of Chemical Engineering for her contributions to completion of the thesis and providing me every opportunity to use the instruments in her laboratory, and Prof. Dr. Teoman Tinçer for his helpful advice necessary for the completion of this study.

I would like to thank to Mihrican Açıkgöz from METU – CHE Department for DSC analysis, Necmi Avcı from METU - METE Department for XRD analysis, Cengiz Tan from METU - METE Department for SEM analysis, Mustafa Güler from UNAM Bilkent University for TEM sample preparation, Tuğba Endoğan and Seçkin Öztürk from METU Central Laboratory for TEM analysis, Prof. Dr. Necati Özkan from METU Central Laboratory for rheological analysis.

I express my special thanks to my friends, İlknur Çakar, Dr. Sertan Yeşil, Dr. Işıl Işık, Dr. Güralp Özkoç, Aslı Tolga Baysal, Dr. Mert Kılınc, Canan Yeniova, Fadile Ezeroğlu, Dr. Özcan Köysüren, Ali Sinan Dike, Dr. Tijen Seyidoğlu, Dr. Wisam Abdallah, Eda Açıık, and Nisa Ilgaz for friendship and cooperation, and helping me in all the possible ways.

It is with immense pleasure that I dedicate this dissertation to each and every member of my family who always offered their love, care and support. I also express my sincerest love and thanks to my daughter Defne and my husband Fatih for their endless love and happiness they gave me in every moment of my life. It would not have been possible without their love and support to complete this study.

Special thanks to the Scientific and Technological Research Council of Turkey (TUBITAK) for supporting me throughout my graduate study by the National Scholarship Program for Ph.D. students. In addition, this thesis work has been supported by the BAP-2008-03-04-09, and BAP-2006-07-02-00-01.

TABLE OF CONTENTS

ABSTRACT	iv
ÖZ	vi
ACKNOWLEDGMENTS	ix
TABLE OF CONTENTS	xi
LIST OF TABLES	xv
LIST OF FIGURES	xviii
NOMENCLATURE	xxix
CHAPTERS	
1 INTRODUCTION	1
2 BACKGROUND INFORMATION	5
2.1 Nanocomposites	5
2.2 Polymer Layered Silicate Nanocomposites (PLSN)	5
2.3 Layered Silicates	7
2.4 Cation Exchange Process of Layered Silicates	9
2.5 Polymer Layered Silicate Nanocomposite Structures	11
2.6 Synthesis Methods of PLSN	13
2.7 Polymer Organoclay Interaction	15
2.8 Polyethylene	16
2.8.1 Low Density Polyethylene	18
2.8.2 High Density Polyethylene	18
2.8.3 Linear Low Density Polyethylene	19
2.9 Polymer Processing Methods to Produce Nanocomposites	20
2.9.1 Extrusion Process	20

2.9.2 Injection Molding Process	22
2.10 Previous Studies	22
3 EXPERIMENTAL SECTION	26
3.1 Materials	26
3.1.1 Polymer Matrix	26
3.1.2 Compatibilizers	28
3.1.3 Organoclays	31
3.2 Experimental Work	33
3.2.1 Drying Conditions	34
3.2.2 Melt Blending Process	35
3.2.2.1 Sample Compositions	37
3.2.3 Injection Molding	40
3.3 Characterization Experiments	41
3.3.1 Morphological Characterization	42
3.3.1.1 X-Ray Diffraction (XRD) Analysis	42
3.3.1.2 Scanning Electron Microscopy (SEM) Analysis	42
3.3.1.3 Transmission Electron Microscopy (TEM) Analysis	43
3.3.2 Rheological Characterization	44
3.3.2.1 Melt Flow Index Test	44
3.3.2.2 Capillary Rheometer Analysis	45
3.3.4 Thermal Characterization	45
3.3.4.1 Differential Scanning Calorimetry (DSC) Analysis	45
3.3.5 Mechanical Characterization	46
3.3.5.1 Tensile tests	46
4 RESULTS AND DISCUSSION	49
4.1 Determination of Process Parameters	49

4.1.1 Determination of Nanocomposite Production Temperature-----	49
4.1.2 Determination of Number of Extrusion Passes-----	51
4.2 Morphological Analysis -----	53
4.2.1 XRD Analysis-----	53
4.2.1.1 XRD Analysis Results of Organoclays -----	54
4.2.1.2 XRD Analysis Results of LDPE Matrix Nanocomposites-----	55
4.2.1.2.1 LDPE Matrix Nanocomposites Containing Organoclay Cloisite® 30B-----	55
4.2.1.2.2 LDPE Matrix Nanocomposites Containing Organoclay Nanofil® 8-----	59
4.2.1.3 XRD Analysis Results of HDPE Matrix Nanocomposites -----	61
4.2.1.3.1 HDPE Matrix Nanocomposites Containing Organoclay Cloisite® 30B-----	62
4.2.1.3.2 HDPE Matrix Nanocomposites Containing Organoclay Nanofil® 8-----	65
4.2.1.4 XRD Analysis Results of LLDPE Matrix Nanocomposites -----	68
4.2.1.4.1 LLDPE Matrix Nanocomposites Containing Organoclay Cloisite® 30B-----	68
4.2.1.4.2 LLDPE Matrix Nanocomposites Containing Organoclay Nanofil® 8-----	71
4.2.2 TEM Analysis-----	76
4.2.2.1 TEM Analysis Results of Nanocomposites with LDPE Matrix-----	76
4.2.2.2 TEM Analysis Results of Nanocomposites with HDPE Matrix ----	79
4.2.2.3 TEM Analysis Results of Nanocomposites with LLDPE Matrix ---	82
4.2.3 SEM Analysis -----	85
4.2.3.1 SEM Analysis Results of Samples with LDPE Matrix -----	85

4.2.3.2 SEM Analysis Results of Samples with HDPE Matrix -----	90
4.2.3.3 SEM Analysis Results of Samples with LLDPE Matrix -----	95
4.3 Flow Properties-----	101
4.3.1 MFI Test Results -----	101
4.3.1.1 MFI Test Results of Samples with LDPE Matrix -----	102
4.3.1.2 MFI Test Results of Samples with HDPE Matrix -----	104
4.3.1.3 MFI Test Results of Samples with LLDPE Matrix -----	106
4.4 Thermal Characterization -----	108
4.4.1 DSC Analysis Test Results -----	108
4.5 Mechanical Characterization -----	111
4.5.1 Tensile Test Results -----	111
4.5.1.1 Tensile Test Results of PE/Compatibilizer Blends-----	111
4.5.1.3 Tensile Test Results of PE/Compatibilizer/Organoclay Ternary Nanocomposites-----	129
5 CONCLUSIONS-----	140
REFERENCES -----	143
APPENDICES	
A. XRD ANALYSIS -----	163
B. DSC ANALYSIS -----	166
C. TENSILE TEST RESULTS -----	180
D. STRESS-STRAIN CURVES-----	189
CURRICULUM VITAE -----	197

LIST OF TABLES

TABLES

Table 3.1	Properties of LDPE.....	47
Table 3.2	Properties of HDPE.....	47
Table 3.3	Properties of LLDPE.....	48
Table 3.4	Properties of E-MA-GMA.....	49
Table 3.5	Properties of E-BA-MAH.....	50
Table 3.6	Typical physical properties of Cloisite® 30B.....	52
Table 3.7	Typical physical properties of Nanofil® 8.....	53
Table 3.8	Drying conditions.....	55
Table 3.9	LDPE matrix sample compositions.....	58
Table 3.10	HDPE matrix sample compositions.....	59
Table 3.11	LLDPE matrix sample compositions.....	60
Table 3.12	Dimensions of the tensile test samples.....	67
Table 4.1	XRD results of LD/E-MA-GMA/30B samples.....	52
Table 4.2	Tensile test results of LD/E-MA-GMA/30B samples	53
Table 4.3	Basal spacing data of nanocomposites containing organoclay Cloisite® 30B with LDPE matrix.....	55
Table 4.4	Basal spacing data of nanocomposites containing organoclay Nanofil® 8 with LDPE matrix.....	59

Table 4.5	Basal spacing data of nanocomposites containing organoclay Cloisite® 30B with HDPE matrix.....	62
Table 4.6	Basal spacing data of nanocomposites containing organoclay Nanofil® 8 with HDPE matrix.....	65
Table 4.7	Basal spacing data of nanocomposites containing organoclay Cloisite® 30B with LLDPE matrix.....	68
Table 4.8	Basal spacing data of nanocomposites containing organoclay Nanofil® 8 with LLDPE matrix.....	71
Table 4.9	Basal spacing data (Δd_1 %) of ternary nanocomposites of LDPE, HDPE and LLDPE containing 2 wt % organoclay and 5 wt % compatibilizer.....	73
Table 4.10-a	MFI test results of neat polyethylenes at 190 °C.....	101
Table 4.10-b	MFI test results of neat compatibilizers at 160 °C, 180 °C and 235 °C.....	102
Table 4.11	MFI test results of LDPE/Compatibilizer blends at 160 °C.....	102
Table 4.12	MFI test results of LDPE/Organoclay nanocomposites at 160 °C.....	103
Table 4.13	MFI test results of LDPE/Compatibilizer/Organoclay nanocomposites at 160 °C.....	104
Table 4.14	MFI test results of HDPE/Compatibilizer blends at 235 °C.....	105
Table 4.15	MFI test results of HDPE/Organoclay nanocomposites at 235 °C.....	105
Table 4.16	MFI test results of HDPE/Compatibilizer/Organoclay nanocomposites at 235 °C.....	105
Table 4.17	MFI test results of LLDPE/Compatibilizer blends at 180 °C.....	106

Table 4.18	MFI test results of LLDPE/Organoclay nanocomposites at 180 °C.....	107
Table 4.19	MFI test results of LLDPE/Compatibilizer/Organoclay nanocomposites at 180 °C.....	107
Table 4.20	DSC analysis results of samples with LDPE matrix.....	109
Table 4.21	DSC analysis results of samples with HDPE matrix.....	110
Table 4.22	DSC analysis results of samples with LLDPE matrix.....	110
Table 4.23	Change of tensile properties of binary blends of LDPE, HDPE and LLDPE containing 5 wt % and 10 wt % compatibilizer.....	120
Table 4.24	Change of tensile properties of binary nanocomposites of LDPE, HDPE and LLDPE with 2 wt % organoclay content.....	129
Table 4.25	Comparison of tensile properties of ternary nanocomposites of LDPE, HDPE and LLDPE containing 2 wt % organoclay and 5 wt % compatibilizer.....	139
Table C.1	Tensile strength data of samples with LDPE matrix.....	180
Table C.2	Tensile strength data of samples with HDPE matrix.....	181
Table C.3	Tensile strength data of samples with LLDPE matrix.....	182
Table C.4	Young's Modulus data of samples with LDPE matrix.....	183
Table C.5	Young's Modulus data of samples with HDPE matrix.....	184
Table C.6	Young's Modulus data of samples with LLDPE matrix.....	185
Table C.7	Percent elongation at break data of samples with LDPE matrix.....	186
Table C.8	Percent elongation at break data of samples with HDPE matrix.....	187
Table C.9	Percent elongation at break data of samples with LLDPE matrix.....	188

LIST OF FIGURES

FIGURES

Figure 2.1	Nanocomposite structures	7
Figure 2.2	2:1 layered phyllosilicates structure	9
Figure 2.3	Cation Exchange Process	10
Figure 2.4	Possible types of arrangements of alkylammonium ions in the galleries of layered silicates.....	11
Figure 2.5	Morphological structures of nanocomposite.....	12
Figure 2.6	Melt Intercalation Method.....	15
Figure 2.7	Schematic of dispersion of clay platelets during melt blending....	16
Figure 2.8	PE repeating unit and space filling model.....	21
Figure 2.9	Chemical architecture of LDPE, HDPE, and LLDPE.....	23
Figure 2.10	Single Screw Extruder.....	27
Figure 2.11	Twin Screw Extruder.....	28
Figure 3.1	Chemical structure of E-MA-GMA; Lotader® AX 8900.....	29
Figure 3.2	Chemical structure of E-BA-MAH; Lotader® 2210.....	30
Figure 3.3	Chemical structure of organic modifier (MT2EtOH) and anion (Cl ⁻) of Cloisite® 30B.....	31
Figure 3.4	Chemical structure of organic modifier (2M2HT) and anion (Cl ⁻) of Nanofil® 8.....	32
Figure 3.5	Flowchart of the experimental work.....	34
Figure 3.6	Thermo Prism TSE 16 TC twin screw extruder.....	35
Figure 3.7	Screw configuration of Thermo Prism TSE 16 TC twin screw extruder.....	36

Figure 3.8	DSM Micro 10cc Injection Molding Machine.....	41
Figure 3.9	A photograph of injected molded HDPE.....	41
Figure 3.10	A photograph of specimen in liquid nitrogen.....	43
Figure 3.11	Omega Melt Flow Indexer.....	45
Figure 3.12	Shimadzu AG-IS 100 kN test machine.....	46
Figure 3.13	Dog bone shape of the tensile test specimen.....	47
Figure 4.1	MFI values of pristine LDPE, HDPE, and LLDPE.....	50
Figure 4.2	Apparent viscosity of pristine polyethylenes at different temperatures.....	51
Figure 4.3	XRD analyses of LDPE/E-MA-GMA/30B samples.....	52
Figure 4.4	XRD patterns for binary nanocomposites of LD/30B.....	56
Figure 4.5	XRD patterns for ternary nanocomposites of LD/Compatibilizer/30B.....	58
Figure 4.6	XRD patterns for binary nanocomposites of LD/NF8.....	60
Figure 4.7	XRD patterns for ternary nanocomposites of LD/Compatibilizer/NF8.....	61
Figure 4.8	XRD patterns for binary nanocomposites of HD/30B.....	63
Figure 4.9	XRD patterns for ternary nanocomposites of HD/Compatibilizer/30B.....	64
Figure 4.10	XRD patterns for binary nanocomposites of HD/NF8.....	66
Figure 4.11	XRD patterns for ternary nanocomposites of HD/Compatibilizer/NF8.....	67
Figure 4.12	XRD patterns for binary nanocomposites of LIN/30B.....	69
Figure 4.13	XRD patterns for ternary nanocomposites of LIN/Compatibilizer/30B.....	70
Figure 4.14	XRD patterns for binary nanocomposites of LIN/NF8.....	72

Figure 4.15	XRD patterns for ternary nanocomposites of LIN/Compatibilizer/NF8.....	73
Figure 4.16	TEM micrographs of LD/E-MA-GMA/30B nanocomposite.....	77
Figure 4.17	TEM micrographs of LD/ E-BA-MAH /30B nanocomposite.....	77
Figure 4.18	TEM micrographs of LD/ E-MA-GMA /NF8 nanocomposite.....	78
Figure 4.19	TEM micrographs of LD/ E-BA-MAH /NF8 nanocomposite.....	78
Figure 4.20	TEM micrographs of HD/E-MA-GMA/30B nanocomposite.....	79
Figure 4.21	TEM micrographs of HD/ E-BA-MAH /30B nanocomposite.....	80
Figure 4.22	TEM micrographs of HD/ E-MA-GMA /NF8 nanocomposite.....	81
Figure 4.23	TEM micrographs of HD/ E-BA-MAH /NF8 nanocomposite.....	81
Figure 4.24	TEM micrographs of LIN/E-MA-GMA/30B nanocomposite.....	84
Figure 4.25	TEM micrographs of LIN/ E-BA-MAH /30B nanocomposite.....	83
Figure 4.26	TEM micrographs of LIN/ E-MA-GMA /NF8 nanocomposite.....	83
Figure 4.27	TEM micrographs of LIN/ E-BA-MAH /NF8 nanocomposite.....	84
Figure 4.28	SEM micrographs of pure LDPE (a) x250 magnification, (b) x3000 magnification.....	86
Figure 4.29	SEM micrographs of LD/E-MA-GMA blend (a) x250 magnification (b) x3000 magnification.....	86
Figure 4.30	SEM micrographs of LD/E-BA-MAH blend (a) x250 magnification (b) x3000 magnification.....	86
Figure 4.31	SEM micrographs of LD/30B binary nanocomposite (a) x250 magnification (b) x3000 magnification	87
Figure 4.32	SEM micrographs of LD/NF8 binary nanocomposite (a) x250 magnification (b) x3000 magnification.....	88
Figure 4.33	SEM micrographs of LD/ E-MA-GMA/30B ternary nanocomposite (a) x250 magnification (b) x3000 magnification.....	88

Figure 4.34	SEM micrographs of LD/ E-BA-MAH/30B ternary nanocomposite (a) x250 magnification (b) x3000 magnification.....	89
Figure 4.35	SEM micrographs of LD/ E-MA-GMA/ NF8 ternary nanocomposite (a) x250 magnification (b) x3000 magnification.....	89
Figure 4.36	SEM micrographs of LD/ E-BA-MAH/ NF8 ternary nanocomposite (a) x250 magnification (b) x3000 magnification.....	90
Figure 4.37	SEM micrographs of pure HD (a) x250 magnification, (b) x3000 magnification.....	90
Figure 4.38	SEM micrographs of HD/E-MA-GMA blend (a) x250 magnification (b) x3000 magnification.....	91
Figure 4.39	SEM micrographs of HD/E-BA-MAH blend (a) x250 magnification (b) x3000 magnification.....	91
Figure 4.40	SEM micrographs of HD/30B binary nanocomposite (a) x250 magnification (b) x3000 magnification.....	92
Figure 4.41	SEM micrographs of HD/NF8 binary nanocomposite (a) x250 magnification (b) x3000 magnification.....	92
Figure 4.42	SEM micrographs of HD/ E-MA-GMA/30B ternary nanocomposite (a) x250 magnification (b) x3000 magnification.....	93
Figure 4.43	SEM micrographs of HD/ E-BA-MAH/30B ternary nanocomposite (a) x250 magnification (b) x3000 magnification.....	94
Figure 4.44	SEM micrographs of HD/ E-MA-GMA/ NF8 ternary nanocomposite (a) x250 magnification (b) x3000 magnification.....	94
Figure 4.45	SEM micrographs of HD/ E-BA-MAH/ NF8 ternary nanocomposite (a) x250 magnification (b) x3000 magnification.....	95
Figure 4.46	SEM micrographs of pureLLDPE (a) x250 magnification , (b) x3000 magnification.....	96

Figure 4.47	SEM micrographs of LIN/E-MA-GMA blend (a) x250 magnification (b) x3000 magnification.....	96
Figure 4.48	SEM micrographs of LIN/E-BA-MAH blend (a) x250 magnification (b) x3000 magnification.....	97
Figure 4.49	SEM micrographs of LIN /30B binary nanocomposite (a) x250 magnification (b) x3000 magnification.....	97
Figure 4.50	SEM micrographs of LIN/NF8 binary nanocomposite (a) x250 magnification (b) x3000 magnification.....	98
Figure 4.51	SEM micrographs of LIN/ E-MA-GMA/30B ternary nanocomposite (a) x250 magnification (b) x3000 magnification.....	99
Figure 4.52	SEM micrographs of LIN/ E-BA-MAH/30B ternary nanocomposite (a) x250 magnification (b) x3000 magnification.....	99
Figure 4.53	SEM micrographs of LIN/ E-MA-GMA/ NF8 ternary nanocomposite (a) x250 magnification (b) x3000 magnification.....	100
Figure 4.54	SEM micrographs of LIN/ E-BA-MAH/ NF8 ternary nanocomposite (a) x250 magnification (b) x3000 magnification.....	100
Figure 4.55	Schematic of amorphous-crystalline polymer structure.....	108
Figure 4.56	Tensile stress-strain curve of neat LDPE.....	112
Figure 4.57	Tensile stress-strain curve of neat HDPE.....	113
Figure 4.58	Tensile stress-strain curve of neat LLDPE.....	113
Figure 4.59.	Effect of compatibilizer content on tensile strength of LD/Compatibilizer blends.....	115
Figure 4.60	Effect of compatibilizer content on Young's Modulus of LD/Compatibilizer blends.....	115
Figure 4.61	Effect of compatibilizer content on % elongation at break of LD/Compatibilizer blends.....	116

Figure 4.62	Effect of compatibilizer content on tensile strength of HD/Compatibilizer blends.....	116
Figure 4.63	Effect of compatibilizer content on Young's Modulus of HD/Compatibilizer blends.....	117
Figure 4.64	Effect of compatibilizer content on % elongation at break of HD/Compatibilizer blends.....	117
Figure 4.65	Effect of compatibilizer content on tensile strength of LIN/Compatibilizer blends.....	118
Figure 4.66	Effect of compatibilizer content on Young's Modulus of LIN/Compatibilizer blends.....	118
Figure 4.67	Effect of compatibilizer content on % elongation at break of LIN/Compatibilizer blends.....	119
Figure 4.68.	Effect of organoclay content on tensile strength of LD/Organoclay binary nanocomposites.....	122
Figure 4.69	Effect of organoclay content on Young's Modulus of LD/Organoclay binary nanocomposites.....	122
Figure 4.70	Effect of organoclay content on % elongation at break of LD/Organoclay binary nanocomposites.....	123
Figure 4.71	Effect of organoclay content on tensile strength of HD/Organoclay binary nanocomposites.....	125
Figure 4.72	Effect of organoclay content on Young's Modulus of HD/Organoclay binary nanocomposites.....	125
Figure 4.73	Effect of organoclay content on % elongation at break of HD/Organoclay binary nanocomposites.....	126
Figure 4.74	Effect of organoclay content on tensile strength of LIN/Organoclay binarynanocomposites.....	127

Figure 4.75	Effect of organoclay content on Young's Modulus of LIN/Organoclay binarynanocomposites.....	127
Figure 4.76	Effect of organoclay content on % elongation at break of LIN/Organoclay binarynanocomposites.....	128
Figure 4.77	Tensile strength values of LD/Compatibilizer/Organoclay ternary nanocomposites with 5 wt % compatibilizer and 2 wt % organoclay loading....	130
Figure 4.78	Young's Modulus values of LD/Compatibilizer/Organoclay ternary nanocomposites with 5 wt % compatibilizer and 2 wt % organoclay loading....	132
Figure 4.79	% Elongation at break values of LD/Compatibilizer/Organoclay ternary nanocomposites with 5 wt % compatibilizer and 2wt % organoclay loading.....	133
Figure 4.80	Tensile strength values of HD/Compatibilizer/Organoclay ternary nanocomposites with 5 wt % compatibilizer and 2 wt % organoclay loading....	134
Figure 4.81	Young's Modulus values of HD/Compatibilizer/Organoclay ternary nanocomposites with 5 wt % compatibilizer and 2 wt % organoclay loading....	134
Figure 4.82	% Elongation at break values of HD/Compatibilizer/Organoclay ternary nanocomposites with 5 wt % compatibilizer and 2 wt% organoclay loading.....	135
Figure 4.83	Tensile strength values of LIN/Compatibilizer/Organoclay ternary nanocomposites with 5 wt % compatibilizer and 2 wt % organoclay loading....	136
Figure 4.84	Young's Modulus values of LIN/Compatibilizer/Organoclay ternary nanocomposites with 5 wt % compatibilizer and 2 wt % organoclay loading....	137
Figure 4.85	% Elongation at break values of LIN/Compatibilizer/Organoclay ternary nanocomposites with 5 wt % compatibilizer and 2 wt% organoclay loading.....	138
Figure A.1	X-Ray diffraction pattern of organoclay Cloisite® 30B.....	163

Figure A.2	X-Ray diffraction pattern of organoclay Nanofil® 8.....	164
Figure A.3	X-Ray diffraction pattern of pure LDPE.....	164
Figure A.4	X-Ray diffraction pattern of pure HDPE.....	165
Figure A.5	X-Ray diffraction pattern of pure LLDPE.....	165
Figure B.1	DSC thermogram of neat LDPE.....	166
Figure B.2	DSC thermogram of LD/E-MA-GMA binary blend containing 5 wt % compatibilizer.....	167
Figure B.3	DSC thermogram of LD/E-BA-MAH binary blend containing 5 wt % compatibilizer.....	167
Figure B.4	DSC thermogram of LD/30B binary nanocomposites containing 2 wt % organoclay.....	168
Figure B.5	DSC thermogram of LD/NF8 binary nanocomposites containing 2 wt % organoclay.....	168
Figure B.6	DSC thermogram of LD/E-MA-GMA/30B ternary nanocomposites containing 5 wt % compatibilizer and 2 wt % organoclay.....	169
Figure B.7	DSC thermogram of LD/E-BA-MAH/30B ternary nanocomposites containing 5 wt % compatibilizer and 2 wt % organoclay.....	169
Figure B.8	DSC thermogram of LD/E-MA-GMA/NF8 ternary nanocomposites containing 5 wt % compatibilizer and 2 wt % organoclay.....	170
Figure B.9	DSC thermogram of LD/E-BA-MAH/NF8 ternary nanocomposites containing 5 wt % compatibilizer and 2 wt % organoclay.....	170
Figure B.10	DSC thermogram of neat HDPE.....	171
Figure B.11	DSC thermogram of HD/E-MA-GMA binary blend containing 5 wt % compatibilizer.....	171
Figure B.12	DSC thermogram of HD/E-BA-MAH binary blend containing 5 wt % compatibilizer.....	172

Figure B.13	DSC thermogram of HD/30B binary nanocomposites containing 2 wt % organoclay.....	172
Figure B.14	DSC thermogram of HD/NF8 binary nanocomposites containing 2 wt % organoclay.....	173
Figure B.15	DSC thermogram of HD/E-MA-GMA/30B ternary nanocomposites containing 5 wt % compatibilizer and 2 wt % organoclay.....	173
Figure B.16	DSC thermogram of HD/E-BA-MAH/30B ternary nanocomposites containing 5 wt % compatibilizer and 2 wt % organoclay.....	174
Figure B.17	DSC thermogram of HD/E-MA-GMA/NF8 ternary nanocomposites containing 5 wt % compatibilizer and 2 wt % organoclay.....	174
Figure B.18	DSC thermogram of HD/E-BA-MAH/NF8 ternary nanocomposites containing 5 wt % compatibilizer and 2 wt % organoclay.....	175
Figure B.19	DSC thermogram of neat LLDPE.....	175
Figure B.20	DSC thermogram of LIN/E-MA-GMA binary blend containing 5 wt % compatibilizer.....	176
Figure B.21	DSC thermogram of LIN/E-BA-MAH binary blend containing 5 wt % compatibilizer.....	176
Figure B.22	DSC thermogram of LIN/30B binary nanocomposites containing 2 wt % organoclay.....	177
Figure B.23	DSC thermogram of LIN/NF8 binary nanocomposites containing 2 wt % organoclay.....	177
Figure B.24	DSC thermogram of LIN/E-MA-GMA/30B ternary nanocomposites containing 5 wt % compatibilizer and 2 wt % organoclay.....	178
Figure B.25	DSC thermogram of LIN/E-BA-MAH/30B ternary nanocomposites containing 5 wt % compatibilizer and 2 wt % organoclay.....	178
Figure B.26	DSC thermogram of LIN/E-MA-GMA/NF8 ternary nanocomposites containing 5 wt % compatibilizer and 2 wt % organoclay.....	179

Figure B.27	DSC thermogram of LIN/E-BA-MAH/NF8 ternary nanocomposites containing 5 wt % compatibilizer and 2 wt % organoclay.....	179
Figure D.1	Tensile stress-strain curve of LD/Compatibilizer blends.....	189
Figure D.2	Tensile stress-strain curve of HD/Compatibilizer blends.....	190
Figure D.3	Tensile stress-strain curve of LIN/Compatibilizer blends.....	190
Figure D.4	Tensile stress-strain curves of LD/30B binary nanocomposites.....	191
Figure D.5	Tensile stress-strain curves of LD/NF8 binary nanocomposites.....	191
Figure D.6	Tensile stress-strain curves of HD/30B binary nanocomposites.....	192
Figure D.7	Tensile stress-strain curves of HD/NF8 binary nanocomposites.....	192
Figure D.8	Tensile stress-strain curves of LIN/30B binary nanocomposites.....	193
Figure D.9	Tensile stress-strain curves of LIN/NF8 binary nanocomposites.....	193
Figure D.10	Tensile stress-strain curves of LD/E-MA-GMA/Organoclay ternary nanocomposites with 5 wt % compatibilizer and 2 wt % organoclay loading....	194
Figure D.11	Tensile stress-strain curves of LD/E-BA-MAH/Organoclay ternary nanocomposites with 5 wt % compatibilizer and 2 wt % organoclay loading....	194
Figure D.12	Tensile stress-strain curves of HD/E-MA-GMA/Organoclay ternary nanocomposites with 5 wt % compatibilizer and 2 wt % organoclay loading....	195
Figure D.13	Tensile stress-strain curves of HD/E-BA-MAH/Organoclay ternary nanocomposites with 5 wt % compatibilizer and 2 wt % organoclay loading....	195

Figure D.14 Tensile stress-strain curves of LIN/E-MA-GMA/Organoclay ternary nanocomposites with 5 wt % compatibilizer and 2 wt % organoclay loading....196

Figure D.15 Tensile stress-strain curves of LIN/E-BA-MAH/Organoclay ternary nanocomposites with 5 wt % compatibilizer and 2 wt % organoclay loading....196

NOMENCLATURE

A_0	Original, undeformed cross-sectional area, mm^2
b	Width of beam tested, mm
d	Depth of beam tested, mm
d	Plane spacing, Å
E	Young's Modulus, MPa
F	Tensile Load, N
L	Support span, mm
L_0	Initial gauge length, mm
ΔL	Change in sample length, mm
m	Slope of the tangent to the initial straight-line portion of the load deflection curve, N/mm
n	Order of diffraction
T	Thickness, mm
T_c	Crystallization temperature, $^{\circ}\text{C}$
T_g	Glass transition temperature, $^{\circ}\text{C}$
T_m	Melting temperature, $^{\circ}\text{C}$

Greek Letters

ϵ	Tensile strain, mm/mm
δ	Phase angle, °
λ	Wavelength, nm
σ	Tensile stress(nominal), MPa
θ	Scattering angle, °

Abbreviations

30B	Cloisite® 30B
ASTM	American Society for Testing and Materials
CEC	Cation Exchange Capacity
DSC	Differential Scanning Calorimetry
E-MA-GMA	Ethylene-Methyl Acrylate-Glycidyl Methacrylate
E-BA-MAH	Ethylene-Butyl Acrylate-Maleic Anhydride
GMA	Glycidyl Methacrylate
HD	High Density Polyethylene
HDPE	High Density Polyethylene
HT	Hydrogenated Tallow
LD	Low Density Polyethylene
LDPE	Low Density Polyethylene
LIN	Linear Low Density Polyethylene
LLDPE	Linear Low Density Polyethylene
MAH	Maleic Anhydride
MFI	Melt Flow Index
MMT	Montmorillonite
NF8	Nanofil® 8
PE	Polyethylene
PLSN	Polymer Layered Silicate Nanocomposites
SEM	Scanning Electron Microscopy
T	Tallow
TEM	Transmission Electron Microscopy
XRD	X-Ray Diffraction

CHAPTER 1

INTRODUCTION

Nanocomposites are a special class of polymer matrix composites, containing fillers, at least one dimension of which is in the nanometer (10^{-9}) range [1]. Due to the structural properties gained by well dispersion of the nanosized fillers, nanocomposites possess highly improved mechanical, thermal, physical, and barrier properties when compared to neat polymer and conventional composites [2].

Considering the inorganic fillers, due to their high aspect ratio, layered silicates are widely used in nanocomposites. In the case of well dispersion of the silicate layers throughout the polymer matrix, interaction of the filler and polymer increases significantly and improves material properties.

Montmorillonite is the most commonly used smectite clay in nanocomposites. The structure of montmorillonite consists of an octahedral alumina sheet between two tetrahedral silica sheets. The layer thickness of the crystal structure is approximately 1 nm, and the lateral dimensions of these layers are in the range of 30 nm to several microns or larger [3]. Montmorillonite is a quite hydrophilic material, thus it is incompatible with many hydrophobic polymers. So the layered silicates are not easily dispersed in most polymers. In order to solve this problem, a simple process, cation exchange process, is applied to make the clay organophilic.

Organically modified layered silicates have been widely studied recently as property enhancers for polymers. There are various studies that investigated improvement in mechanical [4-6], thermal [7-8], flame resistance [7-8], and barrier [9-10] properties of materials due to addition of layered silicates to polymers.

Several industrial and academic research studies have been done on polymer-layered silicate nanocomposites due to significant property enhancement in mechanical, flame resistance, thermal, and barrier properties of thermoplastics. Because of this property enhancement at very low filler content, PLSN systems have drawn tremendous attention.

Among the commercial thermoplastics, polyethylene (PE) is one of the most widely used one due to its low cost, versatility of attainable properties with modifications in its chain architecture and molecular weight. PE can be classified into three main categories according to the structure of its main chain. The three principal types of PE, which are commercially extensively used; low-density polyethylene (LDPE), high-density polyethylene (HDPE), and linear low-density polyethylene (LLDPE).

Incompatibility of organoclay and non-polar polyolefine's brings out the necessity of using a third material in nanocomposites, called the compatibilizer. Various authors emphasized the effects of the compatibilizer such as maleated polyethylene or maleated polypropylene on dispersion of organoclay in the polymer matrix [11-21].

In-situ intercalative polymerization, solution intercalation and melt intercalation methods are the three main methods of nanocomposite synthesis.

In 1988 Toyota filed the first US patent ((#4739007) of production of nylon-clay nanocomposites by in-situ intercalative polymerization method. Okada et al. achieved intercalation of monomers between the galleries of clay followed by in-situ polymerization. Several studies were done to produce polymer-clay nanocomposites by in-situ intercalative polymerization method, with polymer matrices such as epoxy [22], polystyrene [23], polyethylene [24, 25], PET [26], PMMA [27]. Nanocomposites prepared by this method have shown significantly improved properties, however the batch size obtained by this method in a laboratory is limited due to the small size reactors. Presence of additives in the system also lead to complicated reaction conditions thus making the production of these materials complicated in the large reactors used in the industry [3].

Solution intercalation method includes dissolving of polymer at first in a solvent, and then addition of modified clay to it in order to synthesize polymer-clay nanocomposites. The steps of this method are swelling of the clay layers by the solvent and then intercalation of the polymer chains into the expanded clay galleries by displacing the solvent molecules out of the gallery. The system is heated to evaporate all the solvent from clay galleries. Aranda et al. [28] obtained PEO/montmorillonite nanocomposites by dissolving PEO in a suitable solvent which also swells montmorillonite. Then various studies were done to obtain polymer-clay nanocomposites by this method with different polymer matrices: PE [29], poly (ethylene oxide) (PEO) [30] and poly-vinyl acetate (PVA) [31, 32].

In 1993, Giannelis et al. produced polymer-clay nanocomposites by melt compounding the polymer matrix and an organophilic clay in a twin-screw extruder. Both polymer and clay were either simultaneously or separately premixed and then fed to the twin-screw extruder. The heat and shear generated by the screw in the barrel of the extruder resulted in intercalation and exfoliation of the clay in the polymer matrix. In the literature some examples of usage of this method are: PE [33], PET [34], PP [35], and nylons [36]. Melt intercalation method is favored in industry owing to ease of processing, absence of organic solvents during processing and compatibility with several industrial processes such as extrusion and injection processes [37].

In the light of the research, in this thesis it was aimed to investigate the effects of three different types of polyethylenes: low density polyethylene (LDPE), high density polyethylene (HDPE) and linear low density polyethylene (LLDPE) and two types of organoclay Cloisite® 30B and Nanofil® 8, and two different types of elastomeric materials; ethylene-methyl acrylate- glycidyl methacrylate (E-MA-GMA), ethylene-butyl acrylate-maleic anhydride (E-BA-MAH) on the morphology, thermal, rheological and mechanical properties. Extrusion process was the melt blending method to produce the nanocomposites. All samples were prepared by a co-rotating twin screw extruder. Specimens for characterization tests were prepared via injection molding.

To observe the dispersion of clay particles in the polyethylene matrices X-ray diffraction, scanning electron microscopy and transmission electron microscopy

analyses were performed. The thermal behavior of the samples was investigated by using differential scanning calorimetry analysis, and rheological properties were determined with the melt flow index test. Mechanical properties of the specimens were evaluated according to the tensile tests.

CHAPTER 2

BACKGROUND INFORMATION

2.1 Nanocomposites

Nanotechnology is a science trying to improve the ability to work at the molecular level to create large materials that have unique properties that are not shared by conventional composites. Polymer nanocomposites are two-phase materials in which the polymers are reinforced by nanoscale fillers. Major differences in behavior between conventional composites and nanocomposites are due to the difference of the interface area per unit volume ratio. [38].

Improved mechanical properties, such as reduced gas and water permeability for barrier applications, increased thermal stability, flame resistance, elevated heat-distortion temperature, recyclability, and improved processability are some of the attractive properties of nanocomposites [39].

Nanocomposites are generally used in aerospace, automotive, housing, coating, telecommunication, electronic and packing industries due to their transparency, low density, reduced flammability, low permeability, and enhanced thermal and mechanical properties [40].

2.2 Polymer Layered Silicate Nanocomposites (PLSN)

Polymer layered silicate nanocomposites (PLSN) have attracted great interest both in academia and industry, because they usually exhibit significant

improvement in materials properties when compared with neat polymer or conventional composites. In the literature there are several studies on improvements of high moduli [41-44], tensile strength and heat resistance [45], decreased gas permeability [46-49] and flammability [8, 50]. In addition to these, there are also studies on the effects of preparation method and properties of these materials [51-59].

The degree of dispersion of the clay platelets through the polymer matrix determines the structure of nanocomposites. According to interaction between the clay and the polymer matrix, two main types of polymer–clay morphologies can be obtained: namely, intercalated and exfoliated. Figure 2.1 shows these nanocomposite structures.



Figure 2.1 Nanocomposite structures [60]

The intercalated structure results from penetration of a single polymer chain into the galleries between the silicate layers, resulting in formation of alternate layers of polymer. When the individual silicate layers are completely separated and dispersed randomly in a polymer matrix, an exfoliated structure occurs. The best property improvements are usually obtained with exfoliated nanocomposites [60].

After Toyota research group findings on improvement of material properties of Nylon-6/montmorillonite nanocomposite and obtaining well dispersed layered silicates by melt-mix polymers without the use of organic solvents by Vaia et al. [61] interest on polymer layered silicate nanocomposites increased.

Several other polymer nanocomposites have been investigated by many researchers. These include, polypropylene [62-75], polyethylene [76-90], polystyrene [91-102], poly(ethylene oxide) [103], polyamides [104-119], poly(ethylene terephthalate) [120-128], and polyurethane [129-131] etc.

2.3 Layered Silicates

Clays have been widely used as reinforcement materials for polymers. Two main characteristics of these materials are exploited in nanocomposite preparation: the very fine particles yield to very large specific surface areas, and the ability to modify their surface chemistry through the exchange reactions with organic and inorganic cations [132].

Clay minerals are not nanometer-sized themselves but can produce nanometer-sized fillers. Due to the stacked structure of 1 nm thick silicate layers with variable interlayer distance, clay minerals are called as layered silicates [133].

The commonly used layered silicates in preparation of polymer layered silicate nanocomposites belong to the phyllosilicates family [60]. In the structure of 2:1 layered family, two tetrahedrally coordinated silicon atoms are fused to an edge-shared central octahedral sheet of either aluminum or magnesium hydroxide. The oxygen atoms of the octahedral sheet also belong to the tetrahedral sheets [134].

The layer thickness of the crystal structure is around 1 nm, and the lateral dimensions of these layers are between 30 nm to several microns. Stacking of

the layers results in regular Van der Waals gap between the layers called interlayer or gallery. Structure of 2:1 phyllosilicates is given in Figure 2.2.

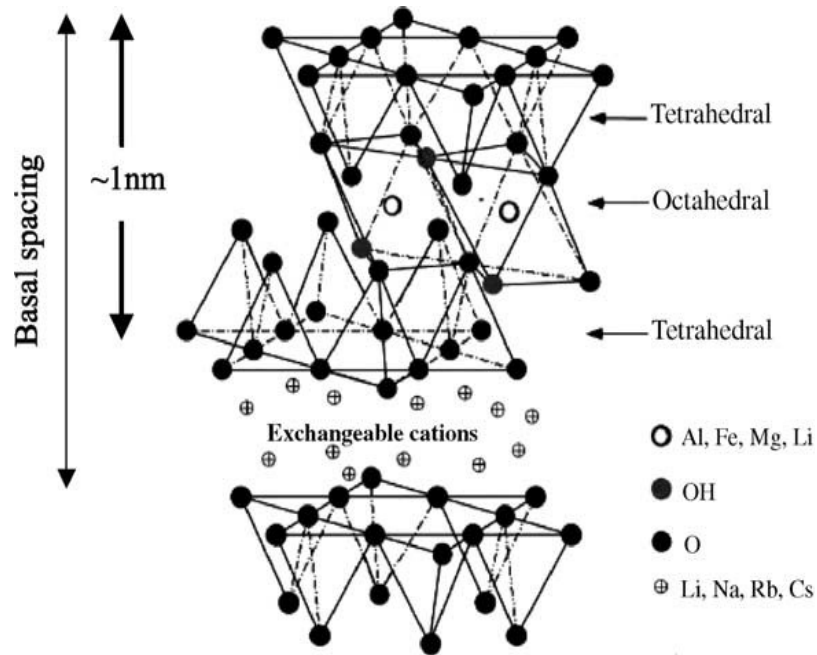


Figure 2.2 2:1 Layered phyllosilicates structure [60]

Montmorillonite is a naturally-occurring 2:1 phyllosilicate. Its chemical structure consists of an octahedral alumina sheet between two tetrahedral silica sheets. In general, the alumina sheet has some replacement of the aluminum cations by magnesium cations which results in a net negative charge to the layers. This negative charge is balanced by having hydrated Na^+ , Li^+ , Mg^{+2} , Ca^{+2} , K^+ cations situated in the galleries between the aluminosilicate layers [135].

Considering the structure of MMT, the silicate layers are planar, stiff, about 1 nm in thickness with high lateral dimensions. This results in obtaining very high aspect ratios in MMT [136].

An important distinction in clay mineral properties is the capacity of certain clays to change volume by adsorbing water molecules from other polar ions into their structures, that is named as swelling property. Clays are divided into swelling and non-swelling type of materials, and swelling types are called smectites. Among the smectite clays, montmorillonite is the most suitable as the basis for nanoclay [137].

2.4 Cation Exchange Process of Layered Silicates

Enhancement of properties of nanocomposites depends on the dispersion level of organoclay layers through the polymer matrix. However, it is not easy to obtain these structures due to the miscibility of filler and polymer matrix. Pure layered silicates generally contain hydrated sodium or potassium ions. In this pristine state, layered silicates are miscible only with hydrophilic polymers, such as poly(ethylene oxide) (PEO), or poly(vinyl alcohol) (PVA) [60]. In order to make these layered silicates miscible with other polymer matrices, their hydrophilic silicate surface must be converted to organophilic. After this reaction, intercalation of many polymer matrices is possible. Figure 2.3 shows the schematic of cation exchange process.

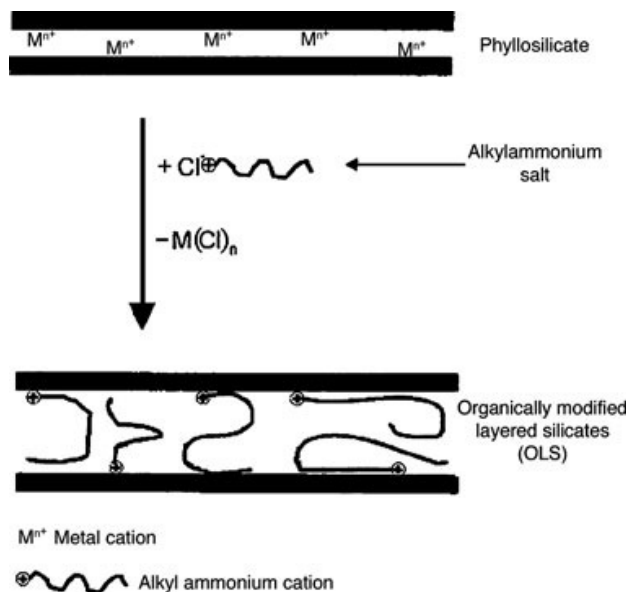


Figure 2.3 Cation Exchange Process [138]

The ability of a layered silicate to change its surface from hydrophilic to organophilic one is defined in terms of “cation exchange capacity” that is measured in milliequivalents per 100 g of air-dried clay. [139].

According to charge density of the clay and the onium ion surfactant, different arrangements of the onium ions as monolayer, lateral bilayer, pseudo-trimolecular layer, and inclined paraffin structure, are possible as seen in Figure 2.4 [42].

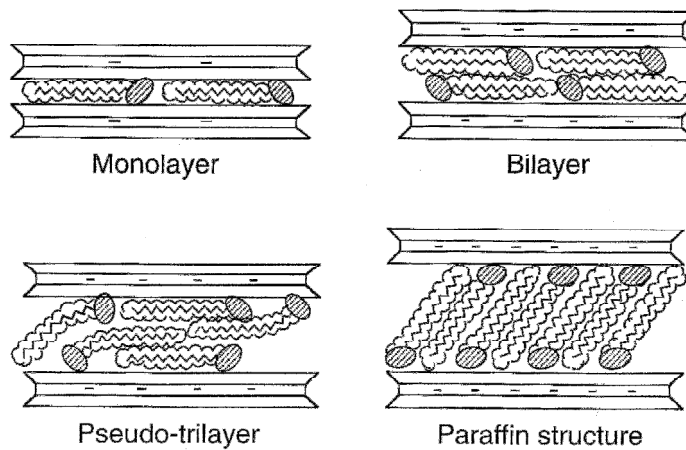


Figure 2.4 Possible types of arrangements of alkylammonium ions in the galleries of layered silicates [42]

2.5 Polymer Layered Silicate Nanocomposite Structures

The structures of the polymer layered silicate nanocomposites depend on the nature of the components used, synthesizing methods, and strength of the interfacial interactions between the nanoclay and the polymer, and the clay loading. There are mainly three morphology types of composites: phase separated composites (microcomposite), intercalated nanocomposites, and exfoliated nanocomposites. Figure 2.5 shows the types of nanocomposite structures.

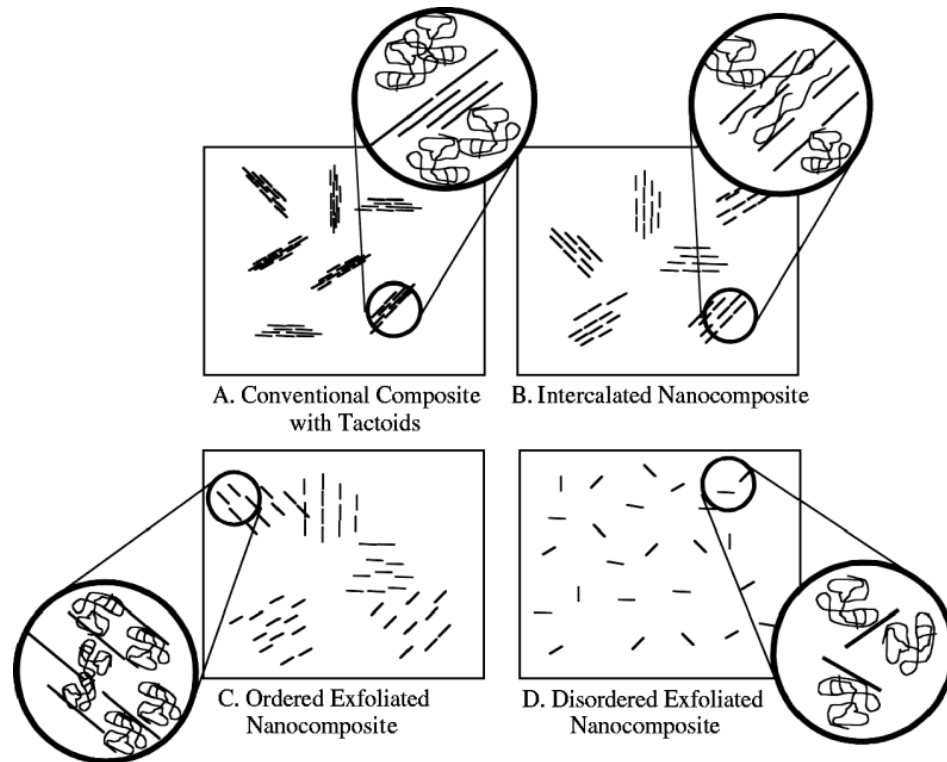


Figure 2.5 Morphological structures of nanocomposites [140]

If the polymer and clay are not compatible, and the clay platelets remain as large stacks without any polymer chains entering the region between the clay platelets the resulted structure is the “phase separated microcomposite”.

In the intercalated nanocomposites, polymer chains enter the clay gallery, but the platelets still remain as a stack and well ordered multilayer. In this type of nanocomposite a repeat distance is expanded, but only to a limited extent [140].

In an exfoliated nanocomposite, the individual clay layers are completely separated throughout the polymer matrix. This structure can be obtained if both the polymer and the clay layers have polar groups that have favorable interaction, and the greatest property enhancement in polymer layered silicate nanocomposites systems is obtained with exfoliated nanocomposite structures.

2.6 Synthesis Methods of PLSN

In-situ intercalative polymerization method, solution intercalation method and melt intercalation method are three main processes used for preparing polymer layered silicate nanocomposites.

In-situ intercalative polymerization method, involves mechanical mixing of the layered silicate mineral with the liquid monomer. The layered silicate is swollen within the liquid monomer and polymerization occurs within the interlayers of the clay. This process promotes the expansion of basal spacing of clay. Polymerization can be initiated by heat or a suitable initiator [141].

In solution intercalation method, a solvent is used to disperse the organoclay and the polymer. It includes intercalation of the polymer chains into the expanded clay galleries and removal of the solvent molecules out of the gallery. Finally, the system is heated to evaporate the solvent. The layers of the clay are dispersed enough during the process and do not collapse back.

In melt intercalation method, the layered silicate is mixed with the polymer matrix in the molten state. If the layer surfaces are compatible enough with the polymer matrix, the polymer can easily enter into the layered silicates as shown in Figure 2.6 and form either intercalated or exfoliated nanocomposites.

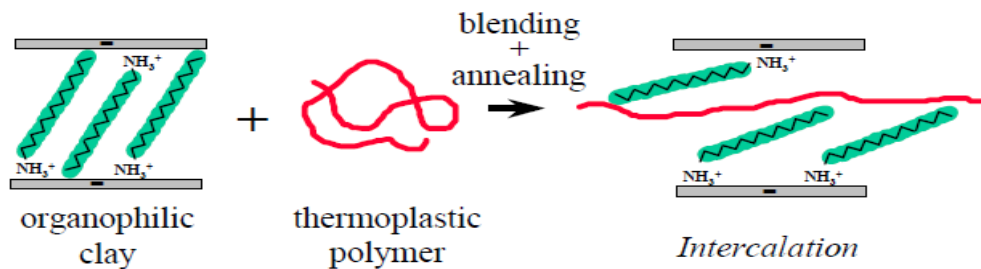


Figure 2.6 Melt Intercalation Method [141]

Extrusion process is generally used for obtaining melt intercalated nanocomposites. The heat and the shear generated by the screws of the extruder help to disperse the layered silicates throughout the polymer matrix. The mechanism of clay platelet dispersion during melt blending is shown in Figure 2.7.

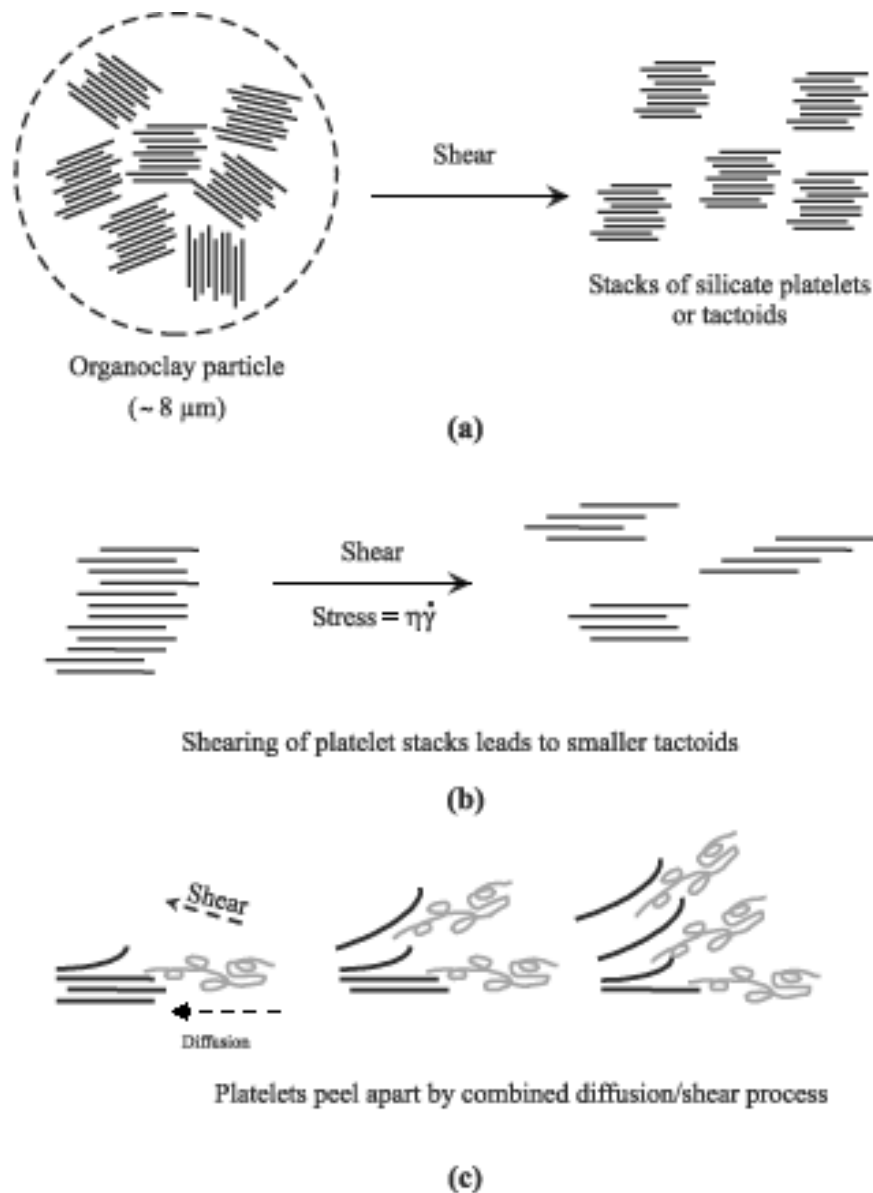


Figure 2.7 Schematic of dispersion of clay platelets during melt blending [60]

Melt intercalation method is relatively easier than the other two methods and environmentally friendly due to the absence of organic solvents and compatible with various industrial processes such as extrusion and injection [37].

2.7 Polymer Organoclay Interaction

In order to obtain significant property enhancement in polymer – organoclay nanocomposites, the layers of clay should disperse as single platelets throughout the polymer matrix. Dispersion of clay as single layers in the polymer matrix prevents stress concentration. To obtain such dispersion of clay platelets, the polymer should first penetrate between the clay platelets. This intercalation is possible if both the polymer and the clay layers have strong interfacial interaction [3].

Due to the nonpolar, hydrophobic structures of polyolefines, they can not make strong interaction with polar, hydrophilic layered silicates during melt compounding process. Thus, homogeneous dispersion of the silicate layers in the matrix and intercalation and/or exfoliation can not be achieved. According the research on nanocomposites, it is known that modification of clay increases the intercalation of polymer into the clay galleries, since the modifier of clay opens the galleries to some extent. However, this does not favor the intercalation of non-polar polymers like polyethylene (PE) and polypropylene (PP), because the long alkyl tail of modifier displays only a limited compatibility with the polymer chains [142]. A third component, compatibilizer, is necessary to enhance the intercalation of nonpolar polymer throughout the silicate layers [4]. In order to increase the polymer clay interaction, generally maleic anhydride grafted polyethylene and maleic anhydride grafted polypropylene are used as the third component, compatibilizer, to increase the miscibility of the polymer and the clay.

In this study, terpolymer of Ethylene – Methyl Acrylate – Glycidyl Methacrylate (E-MA-GMA), and terpolymer of Ethylene – nButyl Acrylate – Maleic Anhydride (E-BA-MAH) were used as compatibilizers in order to increase the polymer clay

interaction. These compatibilizers contain the functional groups: methacrylate (MA), glycidyl methacrylate (GMA) and maleic anhydride (MAH) in their structures.

Glycidyl methacrylate monomer contains both epoxy and acrylic groups that can react with a variety of monomers. There is also a possibility of the glycidyl methacrylate, to react with the hydroxyl groups that may be present on the organophilic clay. Moreover, acrylic group imparts thermal stability, flexibility and polarity. Increasing the polarity of the compatibilizer also increases the interaction of polymer matrix and the layered silicates. Also, the bulky nature of the compatibilizer increases the d-spacing of the layers and allows the polymer matrix to enter the galleries. Due to the epoxy functionality, crosslinking reactions with amines, carboxylic acids, anhydrides and hydroxyl containing polymers can be obtained. Both acrylic and epoxy functionality provide several benefits to polymer systems such as; improved impact resistance, improved strength, better acid resistance (epoxide reactions only), improved water and heat resistance, and improved thermoplastic polymer blend compatibility [143].

Maleic anhydride increases adhesion onto polar substrates and allows the creation of chemical bonds. Chemical reaction occurs between the hydroxyl groups of the organoclay and the maleic anhydride groups of maleated polyethylene. By the help of this reaction, maleated polyethylene can move into the clay galleries and expand the distance between the layers.

2.8 Polyethylene

Polyethylene is a general name for a large family of semicrystalline polymers. PE resins are linear polymers with ethylene molecules as the main backbone. These resins are produced either through radical polymerization reactions at high pressures or through catalytic polymerization reactions. Figure 2.8 shows the repeating unit and space filling model of polyethylene.

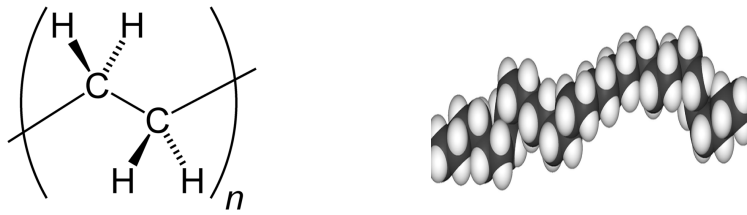


Figure 2.8 PE repeating unit and space filling model [144]

Historically, the classification of polyethylene resins has been developed in conjunction with the discovery of new catalysts for ethylene polymerization, as well as new polymerization processes and applications. The classification is based on two parameters: the resin density and its melt index [145]. At present, various types of polyethylenes are classified based mainly on their molecular weight, density, and branching.

The mechanical properties of PE depend significantly on properties such as the extent and type of branching, the crystal structure, and the molecular weight. The melting point and glass transition temperature depend on these variables and vary significantly with the type of polyethylene [146].

The three principal types of PE classified according to the architecture of their main chain, that are used extensively in industry are, low-density polyethylene (LDPE), high-density polyethylene (HDPE), and linear low-density polyethylene (LLDPE).

Figure 2.9 shows the chemical structure of LDPE, HDPE, LLDPE.

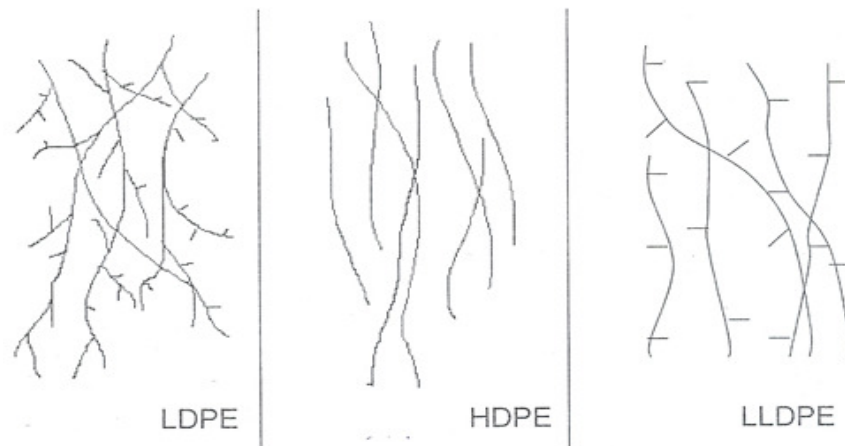


Figure 2.9 Chemical architecture of LDPE, HDPE, LLDPE

2.8.1 Low Density Polyethylene

Low-density polyethylene is a thermoplastic made from petroleum. It was the first grade of polyethylene, produced in 1933 by Imperial Chemical Industries (ICI) using a high pressure process via free radical polymerization. It continues to be one of the most used thermoplastics in industry [147].

LDPE has a density range of 0.910-0.940 g/cm³. It has a high degree of short and long chain branching. It has weak intermolecular forces, since the instantaneous-dipole induced-dipole attraction is less. This results in a low tensile strength and high ductility. The physical properties of LDPE depend on the molecular weight, the molecular weight distribution, as well as the frequency and distribution of long- and short-chain branching [145].

2.8.2 High Density Polyethylene

High density polyethylene is defined as a product of ethylene polymerization with a density of 0.940 g/cm³ or higher. It has little branching, giving it stronger

intermolecular forces and tensile strength than LDPE. The difference in strength exceeds the difference in density, giving HDPE a higher specific strength. It is also harder and more opaque and can withstand higher temperatures. The lack of branching is ensured by an appropriate choice of catalyst (e.g., Ziegler-Natta catalysts) and reaction conditions. HDPE can be produced by chromium/silica catalysts, Ziegler-Natta catalysts or metallocene catalysts [145].

The properties of HDPE that have the strongest influence on its mechanical behavior are molecular weight, MWD, orientation, morphology, and the degree of branching, which determines resin crystallinity and density.

HDPE's crystallinity is generally 40 to 80%. When the branching degree in HDPE increases, its crystallinity and the thickness of its crystalline lamellae decrease.

HDPE is used in products and packaging - bottles, pails, tubes, caps, uses where injection molding of complex shapes is required but low load is applied. HDPE by itself is a safe plastic material on account of its chemical inertness and no toxicity.

2.8.3 Linear Low Density Polyethylene

Linear low-density polyethylene defined by a density range of 0.915-0.925 g/cm³, is a substantially linear polymer (polyethylene), with significant numbers of short branches, commonly made by copolymerization of ethylene with longer-chain olefins. LLDPE differs structurally from conventional LDPE due to the absence of long chain branching. The linearity of LLDPE results from different manufacturing processes. In general, LLDPE is produced at lower temperatures and pressures by copolymerization of ethylene and such higher alpha olefins as butene, hexene, or octene.

The degree of LLDPE crystallinity depends primarily on the α -olefin content in the copolymer (the branching degree of a resin) and is usually below 40-45% [145]. LLDPE has higher tensile strength than LDPE. It exhibits higher impact and puncture resistances than LDPE. Although various applications are available, LLDPE is used predominantly in packaging film, due to its toughness, flexibility,

and relative transparency. It is also used for cable covering, toys, lids, and containers [148].

2.9 Polymer Processing Methods to Produce Nanocomposites

Polymer nanocomposites can be produced with basic polymer processing methods as extrusion and injection molding.

2.9.1 Extrusion Process

Extrusion is one of the most widely used ways of processing of polymers. This technique includes converting thermoplastic materials in powdered or granular form into a continuous melt, which is shaped into items by forcing it through a die [149]. The solid feeds are mainly in the form of pellets, flakes, powder beads, or reground material [150].

Single screw, Figure 2.10, or twin screw extruders, Figure 2. 11, are used in industry according to the process conditions and properties of raw materials. Twin-screw type extruders are the most common among the multiscrew extruders [151]. Considering both types of extruders, with twin-screw it is possible to obtain lower melt temperatures and better mixing of raw materials. Twin-screw extruder does not subject the polymer to very high shear as in the single-screw extruder [154]

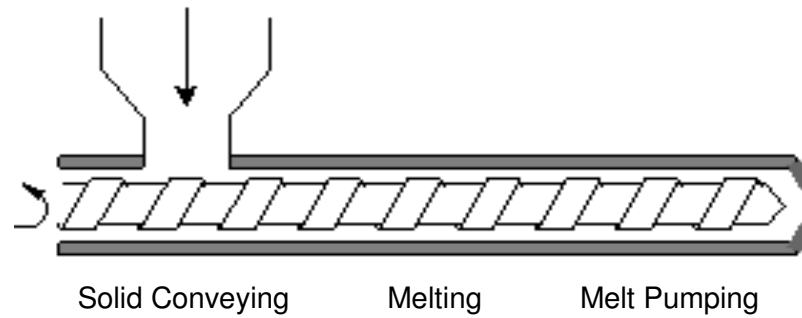


Figure 2. 10 Single Screw Extruder [153]

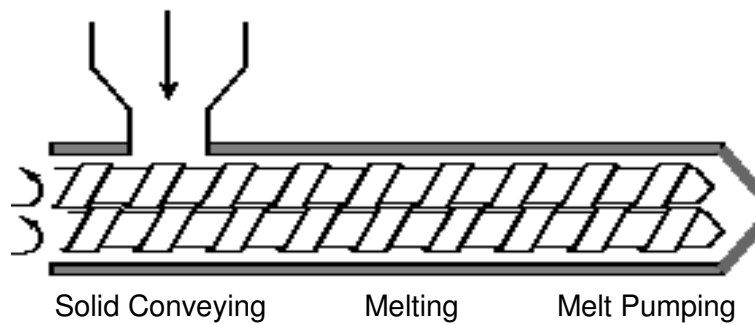


Figure 2.11 Twin Screw Extruder [153]

There are several types of twin screw extruders, with vast differences in design, principle of operation, and field of applications; such as co-rotating, counter rotating, intermeshing, non-intermeshing, etc. [155].

Co-rotating twin screw extruders in which both screws rotate in the same direction, are generally used in applications where mixing and compounding need to be accomplished in addition to the molding of the plastic melt. They are highly capable of dispersing small agglomerates such as carbon black or clay [156].

2.9.2 Injection Molding Process

Injection molding process is a widely used process to produce finished forms of samples with variable dimensions. It is a major processing technique for converting thermoplastic and thermosetting materials into all types of products [155].

The injection unit may be screw fed or ram fed. The ram fed injection molding machine uses a hydraulically operated plunger to push the material through a heated region. In addition to the material properties, the injection molding process itself has a large influence on the final properties of the material, since the polymer chains undergo orientation in the flow direction during the melt-filling phase of the injection cycle [156].

Three steps of injection molding process are: melting of polymer pellets, injection of molten material into mold under high pressure and holding the melt in cold mold until the polymer melt solidifies, finally opening the mold and ejection of the product sample. Melt temperature, mold temperature, pressure during process cycle, duration of each process step are the process parameters of the injection molding [157].

2.10 Previous Studies

Wang et al. [12] prepared maleated polyethylene/clay nanocomposites by melt compounding method. They investigated the effects of the MAH grafting level and organic modifier of clay on the morphology of LLDPE/clay nanocomposites. It was concluded that maleic anhydride grafting level of polyethylene should be higher than 0.1 wt % and organic modifiers should contain higher methylene groups in order to obtain better exfoliation of LLDPE/clay nanocomposites.

Gopakumar et al. [14] studied the influence of clay exfoliation on the physical properties of MMT/PE composites. They prepared conventional composites and nanocomposites of two different montmorillonite clays. HDPE and 1 wt % maleic anhydride grafted polyethylene by melt compounding method and concluded that it was necessary to modify both the montmorillonite clay and polyethylene in order to prepare polyethylene nanocomposites with higher interfacial interaction.

Kato et al. [15] prepared different compositions of nanocomposites by melt compounding with maleic anhydride grafted polyethylene, organophilic clay and polyethylene. Silicate layers were exfoliated and dispersed which led to better mechanical and gas barrier properties.

Morawiec et al. [20] prepared nanocomposites based on LDPE, containing 3 or 6 wt. % of organo-modified montmorillonite clay and maleic anhydride grafted low density polyethylene as the compatibilizer by melt blending. According to this study, it was concluded that the mechanical performance of the system did not only depend on the exfoliation of clay and the clay content, but it was also affected by the presence of a significant amount of compatibilizer. The results showed that maleic anhydride grafted polyethylene promoted the exfoliation of the clay and its adhesion to LDPE and moreover it toughened the polymer matrix.

Marini et al. [158] studied the effects of ethylene-vinyl acetate (EVA) as compatibilizer on the mechanical properties, and permeability characteristics of HDPE/Clay nanocomposites. They obtained intercalated nanocomposites with each type of nanocomposites. In both cases, the organoclay was inside the EVA phase and at the interface of HDPE/EVA, forming a two-phase morphology.

Hemati and Garmabi [159] studied compatibilized LDPE/LLDPE/nanoclay nanocomposites by using a lab-scale co-rotating twin screw extruder. Tensile properties indicated that all the prepared nanocomposites exhibited a significant improvement in elastic modulus and toughness compared to pristine LDPE/LLDPE blends of the same composition. Thermal stability of nanocomposites in the air and nitrogen atmosphere was improved. Partially exfoliated and intercalated structures were observed for the nanocomposites prepared by different orders of mixing.

Picard et al. [160] investigated the influence of the compatibilizer polarity and molar mass on the morphology and the gas barrier properties of polyethylene/clay nanocomposites. Nanocomposites having 5 wt % organo-modified clay (Nanofil 15) and 20 wt % interfacial agent were prepared by melt blending. It was observed that the amount of large and dense filler aggregates was considerably reduced by introduction of an interfacial agent. High degree of clay delamination was obtained with the compatibilizers having high molar mass. The gas barrier properties could not be directly related to the clay dispersion state but resulted also from the matrix/clay interfacial interactions.

Minkova and Filippi [161] studied the morphology, thermal properties, and microhardness of compatibilized polyethylene/clay nanocomposites. They prepared ethylene glycidyl methacrylate copolymer (EGMA)/clay and ethylene-acrylic ester-glycidyl methacrylate terpolymer (EAGMA)/clay nanocomposites with different clay concentrations. The results showed that EGMA and EAGMA are effective compatibilizers for PE and organoclays Cloisite 20A and Cloisite 30B.

Minkova et al. [162] prepared polymer clay nanocomposites based on blends of PE/PE-g-MA and investigated the morphology, thermal properties, microhardness and transparency of the nanocomposites. They discussed the influence of the degree of exfoliation and intercalation on the material characteristics. They showed that addition of the compatibilizer increased the degree of exfoliation and intercalation and thus improved the properties of the polymer nanocomposites.

Andersson and Wessleén [163] studied degradation of different polyethylenes, LDPE, LLDPE, and HDPE, during extrusion coating processing. They concluded that degradation of polyethylene taking place in the extruder barrel, in addition to thermo mechanical degradation, is dependant on the amount of oxygen present in the melt, and might be controlled by antioxidants, which interact with the formed radicals, and slows down the degradation. The molecular architecture of the polyethylene had an influence on the predominating degradation products.

Kwon et al. [164] studied the mechanical properties and complex melt viscosity of unfilled and the calcite (calcium carbonate: CaCO_3) filled high density polyethylene (HDPE), low density polyethylene (LDPE), and linear low density polyethylene (LLDPE) composites. The tensile strength and the complex melt viscosity of the 50 wt % calcite filled polyethylene composites were higher than those of unfilled ones, exhibiting that the reinforcing effect of calcium carbonate.

CHAPTER 3

EXPERIMENTAL SECTION

Ternary nanocomposites of three different PE/compatibilizer/organoclay types were prepared in the present study. In this section, the raw materials, equipment and the procedures used to perform the experiments are explained in detail.

3.1 Materials

3.1.1 Polymer Matrix

Three different kinds of polyethylenes were used as the polymer matrix: Low density polyethylene (LDPE), High density polyethylene (HDPE), Linear low density polyethylene (LLDPE).

LDPE

Low density polyethylene, Petilen I22-19T, was purchased from Petkim Petrokimya Holding A.Ş, İzmir, Turkey. It is sold in the form of pellets in 25 kg bags. Properties of LDPE are given in Table 3.1.

Table 3.1 Properties of LDPE

Properties	Unit	Value	Test Method
Melt Flow Rate (2,16 kg, 190 °C)	g/10 min	17-29	ASTM D -1238
Density , 23 °C	g/cm ³	0.917- 0.921	ASTM D - 1505

HDPE

High density polyethylene was purchased from Petkim Petrokimya Holding A.Ş, İzmir, Turkey. The trade name of the HDPE used is Petilen I 668 and it is sold in the form of pellets in 25 kg bags. Properties of HDPE obtained from the company are given in Table 3.2.

Table 3.2 Properties of HDPE

Properties	Unit	Value	Test Method
Melt Flow Rate (2,16 kg, 190 °C)	g/10 min	4.4 – 6.5	ASTM D -1238
Density , 23 °C	g/cm ³	0.966- 0.970	ASTM D - 1505
Tensile Strength			
- at yield	MPa	28.9	ASTM D- 638
- at break	MPa	23.5	ASTM D- 638

LLDPE

Linear low density polyethylene (Lanufene LLI- 2420) was purchased from Ras Lanuf Oil and Gas Processing Company, Libya. It is sold in the form of pellets in

25 kg bags. Properties of LLDPE obtained from the company are given in Table 3.3.

Table 3.3 Properties of LLDPE

Properties	Unit	Value	Test Method
Melt Flow Rate (2,16 kg, 190 °C)	g/10 min	20	ASTM D - 1238
Density , 23 °C	g/cm ³	0.924	ASTM D - 1505
Ultimate Tensile Strength	MPa	11	ASTM D- 638
Elongation at break	%	450	ASTM D- 638

3.1.2 Compatibilizers

Two different types of elastomeric materials; Lotader[®] AX 8900, ethylene- methyl acrylate- glycidyl methacrylate (E-MA-GMA) and Lotader[®] 2210, ethylene-butyl acrylate-maleic anhydride (E-BA-MAH) were purchased from Arkema Chemicals, France. These polymers are highly compatible with thermoplastics including polyethylene due to their reactivity and flow characteristics. In addition to these, both terpolymer have high thermal stability during processing.

Terpolymer E-MA-GMA contains reactive group glycidyl methacrylate monomer. This contains both acrylic and epoxy groups which enable the polymer to react with substances such as hydroxyl containing materials, carboxylic acids (COOH), and amines.

Chemical structure and properties of the terpolymer ethylene methyl acrylate-glycidyl methacrylate are given in Figure 3.1 and Table 3.4.

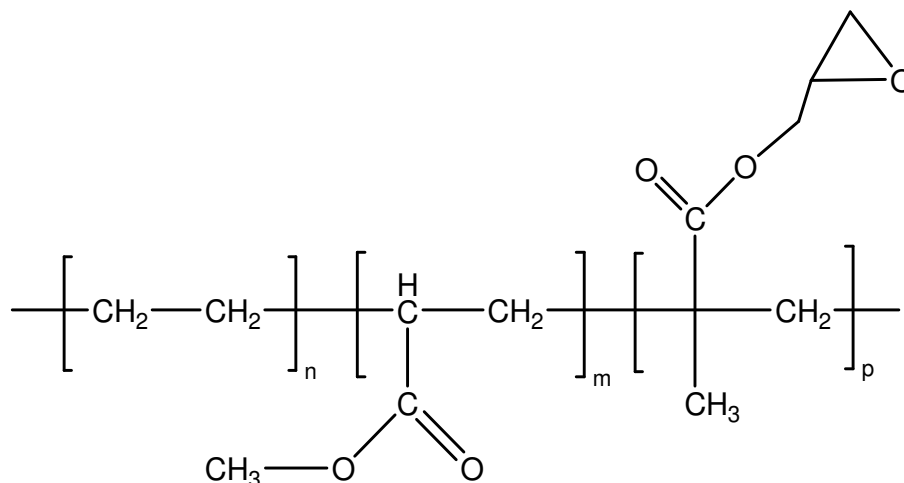


Figure 3.1 Chemical structure of E-MA-GMA; Lotader® AX 8900

Table 3.4 Properties of E-MA-GMA

Type of Polymer	E-MA-GMA	
	Unit	Value
Methyl Acrylate Content	wt %	25
Glycidyl Methacrylate Content	wt%	8
Melt Index (190°C, 2.1kg, ASTM 1238)	g/10min.	6
Melting Point (DSC)	°C	60
Tensile Strength at Break (ASTM D638)	MPa	4
Elongation at Break (ASTM D638)	%	1100
Hardness Shore A (ASTM D2240)	-	70

Chemical structure and properties of terpolymer ethylene-butyl acrylate-maleic anhydride are given in Figure 3.2 and Table 3.5.

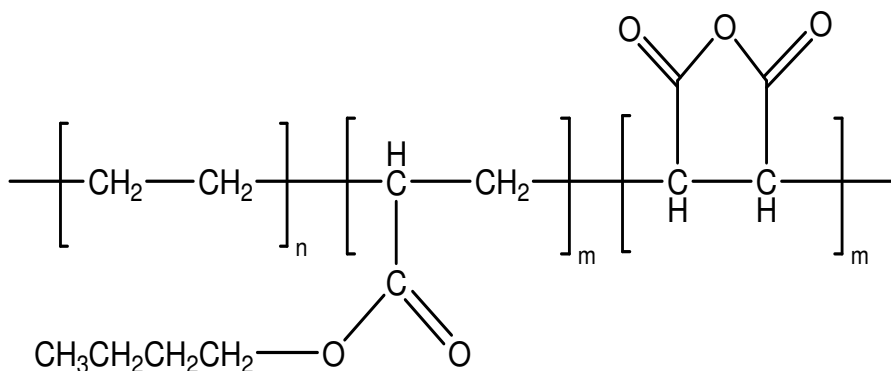


Figure 3.2 Chemical structure of E-BA-MAH; Lotader® 2210

Table 3.5 Properties of E-BA-MAH

Type of Polymer	E-BA-MAH	
	Unit	Value
Butyl Acrylate Content	wt %	8
Maleic Anhydride Content	wt%	2.6
Melt Index (190°C, 2.1kg, ASTM 1238)	g/10min.	3
Melting Point (DSC)	°C	107
Tensile Strength at Break (ASTM D638)	MPa	12
Elongation at Break (ASTM D638)	%	600
Hardness Shore D (ASTM D2240)	-	46

E-BA-MAH contains maleic anhydride (MAH) monomer, instead of GMA monomer, as the reactive group. The acrylic ester group of this terpolymer decreases the crystallinity. The reactive group, MAH, increases adhesion onto polar substrates and helps formation of chemical bonds with substrates such as metals, polymers, and metallized products.

3.1.3 Organoclays

Two different natural montmorillonites modified with a quaternary ammonium salt were used in this study as the organoclays. These organoclays, namely Cloisite® 30B and Nanofil® 8, were purchased from Southern Clay Products, and Süd-Chemie, respectively. These organoclays are used as fillers for plastics to improve various physical properties, such as mechanical, thermal, and barrier properties.

Cloisite® 30B

Cloisite® 30B is treated with methyl, tallow, bis-2-hydroxyethyl, quaternary ammonium by manufacturer. The anion of this clay is chloride ion. The chemical structure of organic modifier is shown in Figure 3.3.

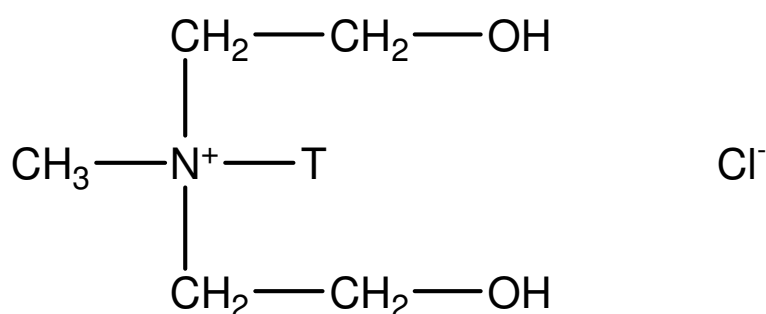


Figure 3.3 Chemical structure of organic modifier (MT2EtOH) and anion (Cl⁻) of Cloisite® 30B

MT2EtOH: methyl, tallow, bis-2-hydroxyethyl, quaternary ammonium

T : tallow (~65% C18; ~30% C16; ~5% C14)

The physical properties of Cloisite® 30B are given in Table 3.6.

Table 3.6 Typical physical properties of Cloisite® 30B

Properties	Cloisite® 30B
Organic Modifier	MT2EtOH
Modifier Concentration	90 meq/100g clay
% Moisture	< 2%
% Weight Loss on Ignition	30%
<u>Typical Dry Particle Sizes:</u> (microns, by volume)	10% less than: 2μ 50% less than: 6μ 90% less than: 13μ
Color	Off white
Specific Gravity, g/cc	1.98
d- spacing (d ₀₀₁) (X-Ray)	18.5 Å

Nanofil® 8

Nanofil® 8 is treated with dimethyl, (dihydrogenated tallow) alkyl quaternary ammonium (2M2HT) by manufacturer. The anion of this clay is also chloride ion. The chemical structure of organic modifier 2M2HT is shown in Figure 3.4.

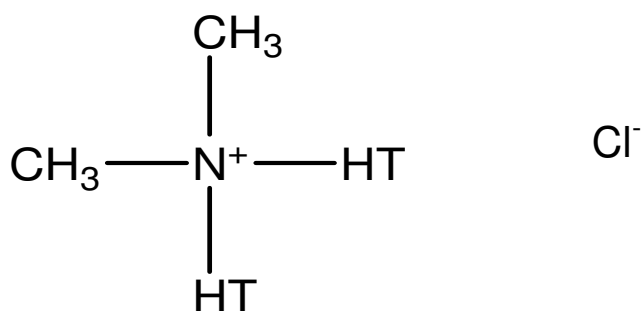


Figure 3.4 Chemical structure of organic modifier (2M2HT) and anion (Cl⁻) of Nanofil® 8

2M : Dimethyl

HT : Hydrogenated Tallow (Alkyl chain), (~65% C18; ~30% C16; ~5% C14)

The physical properties of Nanofil® 8 obtained from the manufacturer are given in Table 3.7.

Table 3.7 Typical physical properties of Nanofil® 8

Properties	Nanofil® 8
Product form	Powder
Organic Modifier	2M2HT
Modifier Concentration	125 meq/100g clay
% Moisture	1,6
% Weight Loss on Ignition	43%
Median Particle Size	5 μm
Color	Off white
Bulk Density (g/l)	270
d- spacing (d_{001}) (X-Ray)	35 Å

3.2 Experimental Work

This study includes mainly four different stages. These stages are; drying of materials, production of nanocomposites by melt mixing process, sample preparation with injection molding process and performing the characterization experiments. Flowchart of experimental procedure and characterization of the nanocomposites is shown in Figure 3.5.

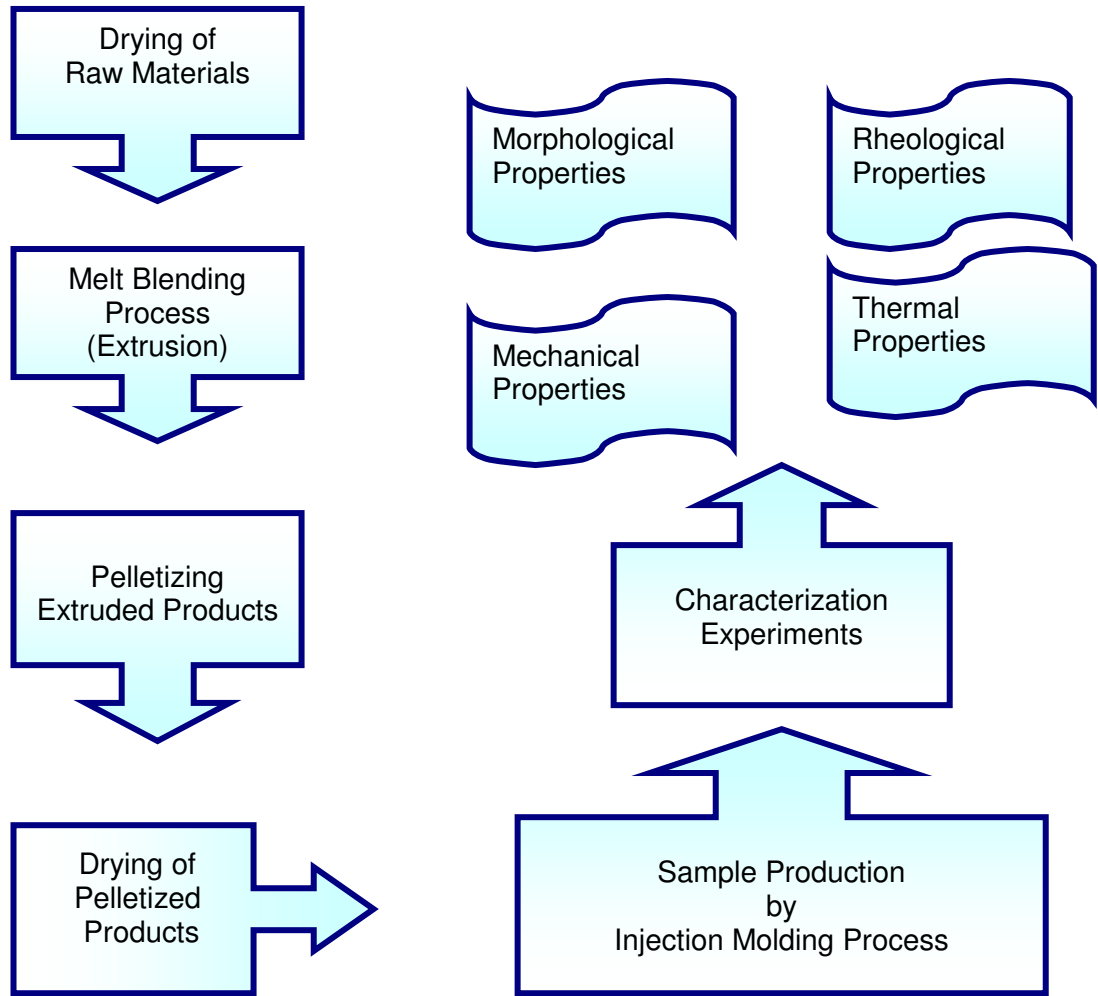


Figure 3.5 Flowchart of the experimental work

3.2.1 Drying Conditions

Before melt blending process and injection molding process, the raw materials and samples were dried in order to get rid of the moisture. Drying conditions were determined by considering the melting point of raw materials. Table 3.8 shows the drying conditions applied during the experimental work.

Table 3.8 Drying conditions

Materials	Drying Temperature (°C)	Duration (h)
Before Extrusion Process		
LDPE, HDPE, LLDPE	-	-
E-MA-GMA	40	12-16
E-BA-MAH	40	12-16
Cloisite® 30B	110	12-16
Nanofil® 8	110	12-16
Before Injection Molding Process		
All extruded samples	100	8

3.2.2 Melt Blending Process

Polyethylene (PE) -Montmorillonite (MMT) nanocomposites were prepared by melt compounding in a co-rotating twin-screw extruder (Thermoprism TSE 16 TC, L/D = 25) shown in Figure 3.6. The screw diameter, barrel length and die length of extruder are 16, 384 and 16 mm, respectively. Screw configuration of the extruder is given in Figure 3.7.



Figure 3.6 Thermo Prism TSE 16 TC twin screw extruder

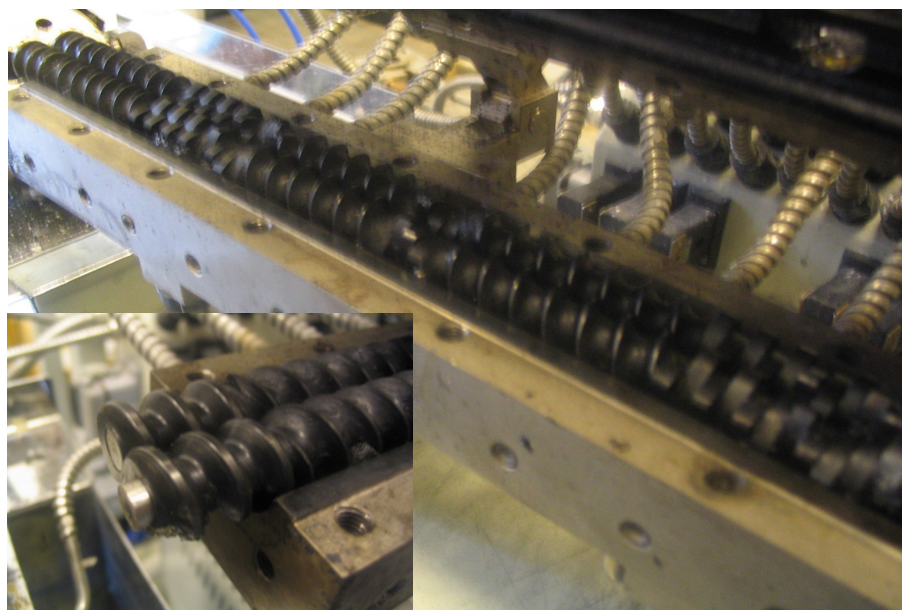


Figure 3.7 Screw configuration of Thermo Prism TSE 16 TC twin screw extruder

Extrusion process temperature profile was determined according to the melt flow index test and rheological analysis of the polymer matrices; LDPE, HDPE, LLDPE. It was aimed to obtain similar flow properties of these matrices during melt compounding.

During the extrusion process, temperature profile of the hopper, the mixing zones and the die, the screw speed, and the total flow rate of feed to extruder barrel were constant in all the experiments for each polyethylene type. Temperature profiles for the hopper, the three mixing zones and the die were the same: Extrusion process temperature for LDPE, HDPE and LLDPE were 160, 235 and 180 °C, respectively.

The screw speed and total flow rate of feed were kept constant at 200 rpm and ~ 25 g/min throughout the experiments. The molten product obtained from the extruder barrel was cooled by passing through a water bath, whose temperature was continuously controlled. At the end of the water bath, an air fan was placed in order to remove the water from the product surface and finally the product was collected in plastics bags after passing through the pelletizer.

Before and after extrusion process, the raw materials and samples were dried in order to get rid of the moisture.

3.2.2.1 Sample Compositions

To investigate the effects of the polyethylene type, compatibilizer and organoclay type on the properties of nanocomposites several compositions were prepared as shown in Tables 3.9-3.11.

Not only ternary nanocomposites of PE/Compatibilizer/Organoclay were obtained by melt compounding method, but also pure polyethylene, binary nanocomposites of PE/Organoclay and PE/Compatibilizer blends were prepared with the same process conditions in order to compare their properties with the properties of ternary nanocomposites.

Table 3.9 LDPE matrix sample compositions

SAMPLE	PE Content wt %	Compatibilizer Content wt %	Organoclay Content wt %
LDPE	100	-	-
LD/E-MA-GMA 5 %	95	5	-
LD/E-MA-GMA 10 %	90	10	-
LD/E-BA-MAH 5 %	95	5	-
LD/E-BA-MAH 10 %	90	10	-
LD/30B 2%	98	-	2
LD/30B 4%	96	-	4
LD/30B 6%	94	-	6
LD/E-MA-GMA/30B	93	5	2
LD/E-BA-MAH/30B	93	5	2
LD/NF8 2%	98	-	2
LD/NF8 4%	96	-	4
LD/NF8 6%	94	-	6
LD/E-MA-GMA/NF8	93	5	2
LD/E-BA-MAH/NF8	93	5	2

Table 3.10 HDPE matrix sample compositions

SAMPLE	PE Content wt %	Compatibilizer Content wt %	Organoclay Content wt %
HDPE	100	-	-
HD/E-MA-GMA 5 %	95	5	-
HD/E-MA-GMA 10 %	90	10	-
HD/E-BA-MAH 5 %	95	5	-
HD/E-BA-MAH 10 %	90	10	-
HD/30B 2%	98	-	2
HD/30B 4%	96	-	4
HD/30B 6%	94	-	6
HD/E-MA-GMA/30B	93	5	2
HD/E-BA-MAH/30B	93	5	2
HD/NF8 2%	98	-	2
HD/NF8 4%	96	-	4
HD/NF8 6%	94	-	6
HD/E-MA-GMA/NF8	93	5	2
HD/E-BA-MAH/NF8	93	5	2

Table 3.11 LLDPE matrix sample compositions

SAMPLE	PE Content wt %	Compatibilizer Content wt %	Organoclay Content wt %
LLDPE	100	-	-
LIN/E-MA-GMA 5 %	95	5	-
LIN/E-MA-GMA 10 %	90	10	-
LIN/E-BA-MAH 5 %	95	5	-
LIN/E-BA-MAH 10 %	90	10	-
LIN/30B 2%	98	-	2
LIN/30B 4%	96	-	4
LIN/30B 6%	94	-	6
LIN/E-MA-GMA/30B	93	5	2
LIN/E-BA-MAH/30B	93	5	2
LIN/NF8 2%	98	-	2
LIN/NF8 4%	96	-	4
LIN/NF8 6%	94	-	6
LIN/E-MA-GMA/NF8	93	5	2
LIN/E-BA-MAH/NF8	93	5	2

3.2.3 Injection Molding

The specimens for characterization tests were prepared by injection molding using a laboratory scale injection-molding machine, DSM Micro 10 cc Injection Molding Machine, shown in Figure 3.8. During molding; barrel temperatures were 160, 235 and 180 °C for LDPE, HDPE and LLDPE, respectively. Mold temperature (30°C) and injection pressure (12 bars) were identical for the preparation of each sample. Figure 3.9 shows the samples obtained.

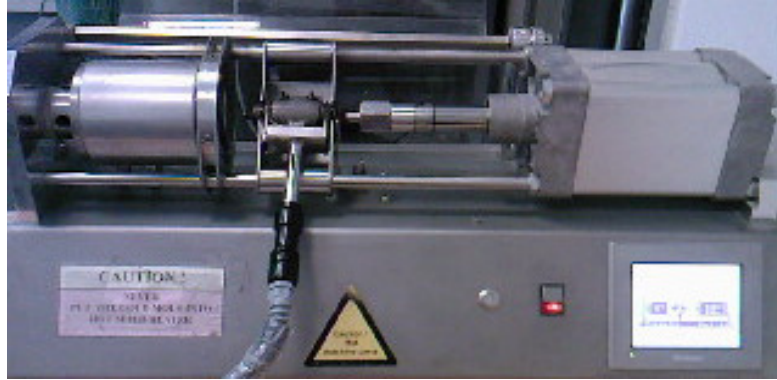


Figure 3.8 DSM Micro 10 cc Injection Molding Machine



Figure 3.9 A photograph of injected molded HDPE

3.3 Characterization Experiments

In order to investigate the effects of the polymer matrix, compatibilizer and organoclay type on the final properties of the nanocomposites, morphological , rheological, thermal and mechanical analyses were applied to samples.

Morphology of the nanocomposites was investigated by XRD, SEM and TEM analyses. Capillary rheometer analysis and MFI tests were carried out to

investigate the flow characteristics. Melting point and crystallinity of the nanocomposites were studied with DSC analysis. Mechanical behavior of the nanocomposites was evaluated by measuring tensile properties (tensile strength, Young's modulus, elongation at break).

3.3.1 Morphological Characterization

3.3.1.1 X-Ray Diffraction (XRD) Analysis

X-ray diffraction (XRD) patterns of organoclays and nanocomposites were obtained by using RIGAKU D/MAX 2200/PC X-Ray diffractometer (METE-METU) that generates a voltage of 40kV and current 40 mA from Cu K α radiation source ($\lambda = 1.5418$). The diffraction angle 2θ was scanned from 1° to 10° with scanning rate of $1^\circ/\text{min}$ and a step size of 0.01° . To calculate the distance between the silicate layers Bragg's equation was used:

$$n\lambda = 2d \sin \theta \quad (3.1)$$

where, n is degree of diffraction, λ is wavelength, θ is the measured diffraction angle, and d is the interlayer spacing.

X-Ray analysis of organoclays were done in powder form. Tensile bars obtained by injection molding were used for XRD analysis.

3.3.1.2 Scanning Electron Microscopy (SEM) Analysis

Scanning electron microscopy (SEM) analysis was performed by a JEOL JSM-6400 low voltage scanning electron microscope at the METE-METU department. In this technique, a fine beam of electrons is scanned across the surface of an opaque specimen to which a light conducting film (gold, platinum, silver) has been applied by high vacuum evaporation. The fractured surfaces were obtained

by using liquid nitrogen for all the samples shown in Figure 3.10. Before SEM photographs were taken, the fractured surfaces were coated with a thin layer of gold in order to obtain a conductive surface. SEM photographs were taken for each specimen at x250 and x3000 magnifications.



Figure 3.10 A photograph of specimen in liquid nitrogen

3.3.1.3 Transmission Electron Microscopy (TEM) Analysis

Morphological characterization of the samples was made also by TEM analysis. TEM gives a qualitative understanding of the polymer clay interaction, distribution of the various phases, and views of the defect structure through direct visualization at atomic dimensions.

Ultra thin sections of ≤ 100 nm in thickness were cryogenically cut with a diamond knife at a temperature of -100 °C for ternary nanocomposites of PE/Compatibilizer/Organoclay. All samples were trimmed parallel to the molding direction. Prepared samples were examined by a FEI Tecnai™ G² Transmission

Electron Microscope at an acceleration rate of 80 kV at the METU Central Laboratory.

3.3.2 Rheological Characterization

In order to determine the melt compounding process temperatures for different polyethylene types, melt flow index test and capillary rheometer analysis were applied to pure LDPE, HDPE and LLDPE. Effects of compatibilizer and organoclay types on flow properties on nanocomposites were investigated by melt flow index test.

3.3.2.1 Melt Flow Index Test

Melt flow index (MFI) test was performed according to ASTM D1238-79 using an Omega Melt Flow Indexer shown in Figure 3.11. In order to determine the extrusion process conditions, the MFI measurements of neat polyethylenes were carried out in the range of 160 °C - 270 °C with a load of 2.16 kg. The weight of sample passing through the die in 10 min, was determined for all the polyethylene types. The results were recorded in grams/10 min.

MFI measurements for rheological characterization of all samples produced were made at previously determined process temperatures; LDPE: 160 °C; HDPE: 235 °C; LLDPE: 180 °C, with a load of 2.16 kg. The results were also recorded in grams/10 min. To obtain a more accurate result at least five measurements were done on each sample type.



Figure 3.11 Omega Melt Flow Indexer

3.3.2.2 Capillary Rheometer Analysis

The apparent viscosity of raw materials, LDPE, HDPE and LLDPE were obtained by Capillary Rheometer analyses performed with the Dynisco, LCR-7001 equipment at the METU Central laboratory. The measurements were made at different temperatures for each polyethylene type. The analyses temperatures were determined according to MFI test results of pure polyethylenes. The analysis temperatures were as follows:

LDPE : 160 ° C ; HDPE: 235 ° C ; LLDPE: 180 ° C.

3.3.4 Thermal Characterization

3.3.4.1 Differential Scanning Calorimetry (DSC) Analysis

Differential scanning calorimetry analysis was performed by using a differential scanning calorimeter DSC-60 Shimadzu at the CHE-METU department.

Measurements were carried out in the temperature range of 30 °C to 200 °C with a heating rate of 10 °C/min under nitrogen atmosphere. Melting points of samples and the degree of crystallinity were determined with these analyses.

3.3.5 Mechanical Characterization

3.3.5.1 Tensile tests

In order to observe the mechanical property enhancement of nanocomposites tensile tests were performed on all the materials prepared. Tensile test results give the force required to break a specimen and the extent to which the specimen elongates to that breaking point. Tensile tests were performed at room temperature according to ASTM D638-3 with Shimadzu AG-IS 100 kN test machine at CHE-METU department. Figure 3.12 shows the test machine. Gauge length, crosshead speed and strain rate were 30 mm, 15 mm/min, and 0.5 1/min, respectively.



Figure 3.12 Shimadzu AG-IS 100 kN test machine

Dog bone type of injection molded sample shown in Figure 3.13 was used for tensile tests. Dimensions of samples are given in Table 3. 12.

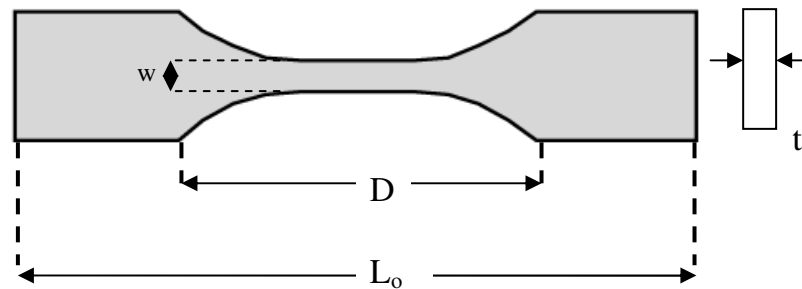


Figure 3.13 Dog bone shape of the tensile test specimen

Table 3.12 Dimensions of the tensile test samples

Designation	Dimension
Distance between grips, D	30 mm
Overall length, L _o	74 mm
Thickness, t	2.1 mm
Width of narrow section, W	4 mm

At least five samples were used for each composition set and the average values of test results and standard deviation values were calculated. At the end of the tests, tensile strength (MPa), tensile modulus (MPa) and elongation at break values (%) of each composition were measured from stress- strain diagrams using the following equations:

$$\text{Stress } \sigma = \frac{F}{A_0} \quad ; \text{ Strain: } \varepsilon = \frac{\Delta L}{L_0} \quad (3.2)$$

where, F is the force (N), and A_0 is the original cross-section area of the gage region (mm^2), ΔL is the change in gage length (mm), and L_0 is the original gage length of the specimen (mm).

Young's modulus is the ratio of the stress to strain in the elastic region of the stress-strain curve which is given in the Equation 3.3

$$E = \frac{\sigma}{\varepsilon} \quad (3.3)$$

CHAPTER 4

RESULTS AND DISCUSSION

4.1 Determination of Process Parameters

4.1.1 Determination of Nanocomposite Production Temperature

In order to determine the extrusion process temperature to produce LDPE, HDPE and LLDPE nanocomposites, melt flow index tests and capillary rheometer analysis were applied to each pristine polyethylene at different temperatures. It was aimed to determine the temperatures at which the three polyethylenes would exhibit similar flow properties during extrusion and injection molding processes.

According to the data sheets obtained from producers of polyethylenes, the MFI values were: 17-29 ; 4.4-6.5 and 20 g/10 min for LDPE, HDPE and LLDPE. Thus, MFI of LDPE and LLDPE should be decreased and MFI of HDPE should be increased to obtain similar flow conditions. In order to achieve this, LDPE and LLDPE should be processed at lower temperatures and HDPE should be processed at a higher temperature than 190 °C. In order to determine the process temperature, initially melt flow tests were carried out in the temperature range of 160 °C - 270 °C with a load of 2.16 kg. The results were recorded as grams/10 min. Figure 4.1 shows the MFI values of pristine polyethylenes.

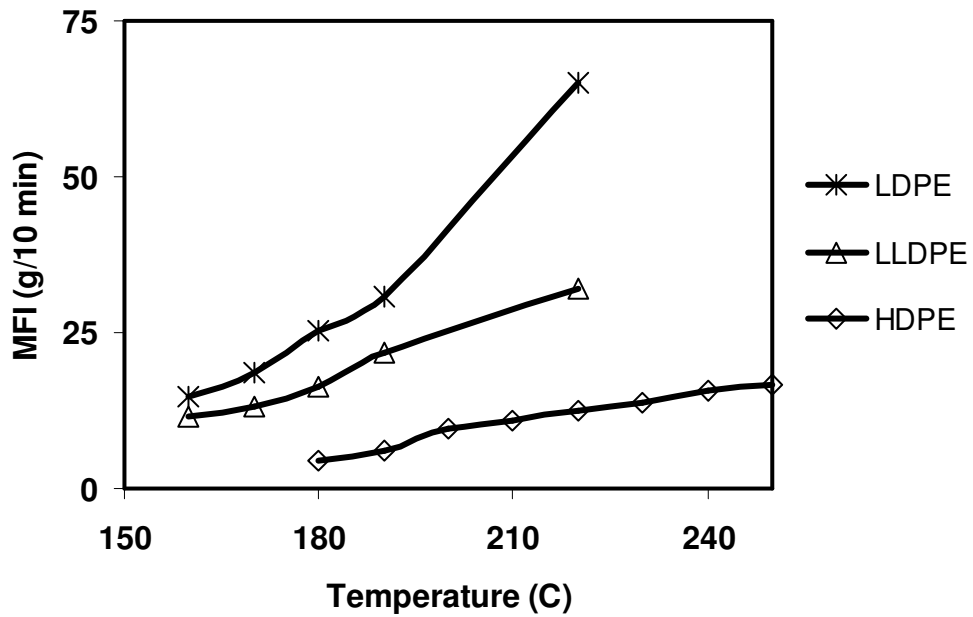


Figure 4.1 MFI values of pristine LDPE, HDPE, LLDPE

MFI values of LDPE, LLDPE and HDPE were found to be around 15 g/10min at temperatures 160, 180 and 235 °C, respectively.

Capillary rheometer analyses temperatures were decided according to the results of MFI tests. Apparent viscosity of each polyethylene at different shear rates was determined with this analysis. The analysis temperatures were:

LDPE : 160 °C; LLDPE:180 °C; HDPE: 235 °C

Figure 4.2 shows the results of the analysis, for the selected temperatures.

The objective was to obtain the temperatures such that each polyethylene would have the same apparent viscosity at shear rate at approximately 100 1/s. This is confirmed in Figure 4.2. At selected temperatures polyethylenes will have similar flow properties during melt blending process.

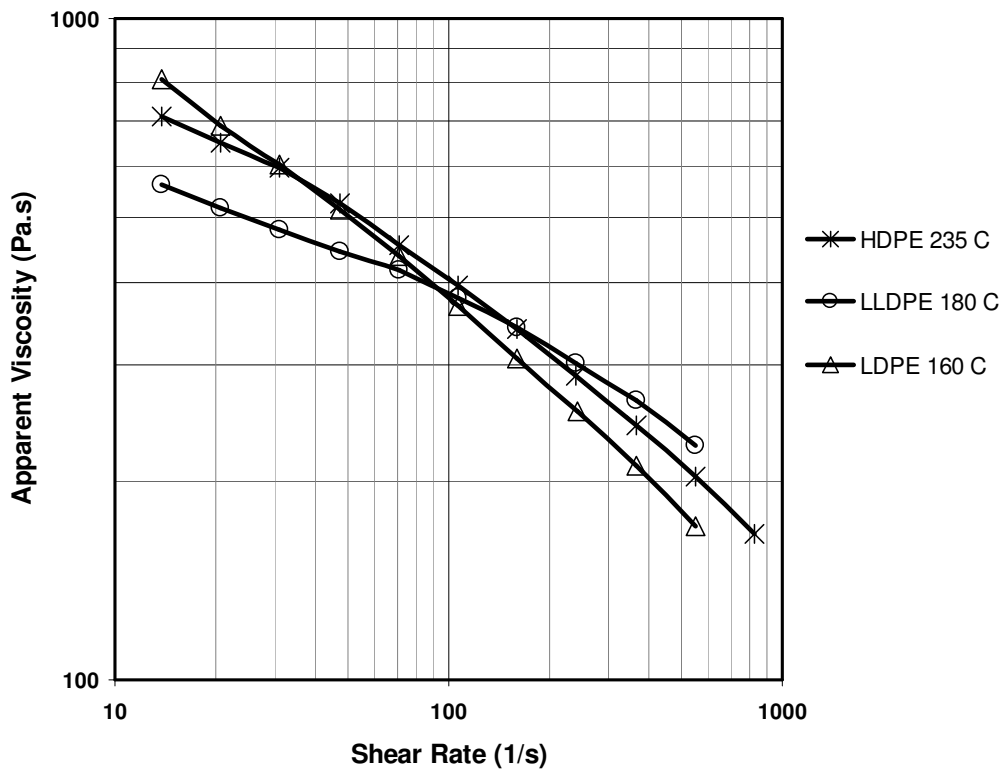


Figure 4.2 Apparent viscosity of pristine polyethylenes at different temperatures

Considering the MFI values and apparent viscosity of polyethylene types, melt mixing temperatures for LDPE, HDPE and LLDPE were selected as 160, 235 and 180 °C, respectively.

4.1.2 Determination of Number of Extrusion Passes

In order to determine the number of extrusion passes that would be applied in the rest of the study, XRD analyses and tensile tests were applied to ternary nanocomposites of LDPE/E-MA-GMA/30B which were obtained by extruding the materials once or twice. Process temperature was 160 °C, the feed rate and screw speed were 25 g/min and 200 rpm, respectively.

Table 4.1 shows the XRD analysis of once and twice extruded LDPE/E-MA-GMA/30B samples.

Table 4.1 XRD results of LDPE/E-MA-GMA/30B samples

		2 θ	d – spacing(Å)
30B	d1	5.02	17.6
Extrusion Once	d1	2.08	42.5
	d2	6.0	14.7
Extrusion Twice	d1	2.1	42.1
	d2	5.98	14.8

According to XRD results, basal spacing of samples that were extruded once or twice were almost the same as observed in Figure 4.3.

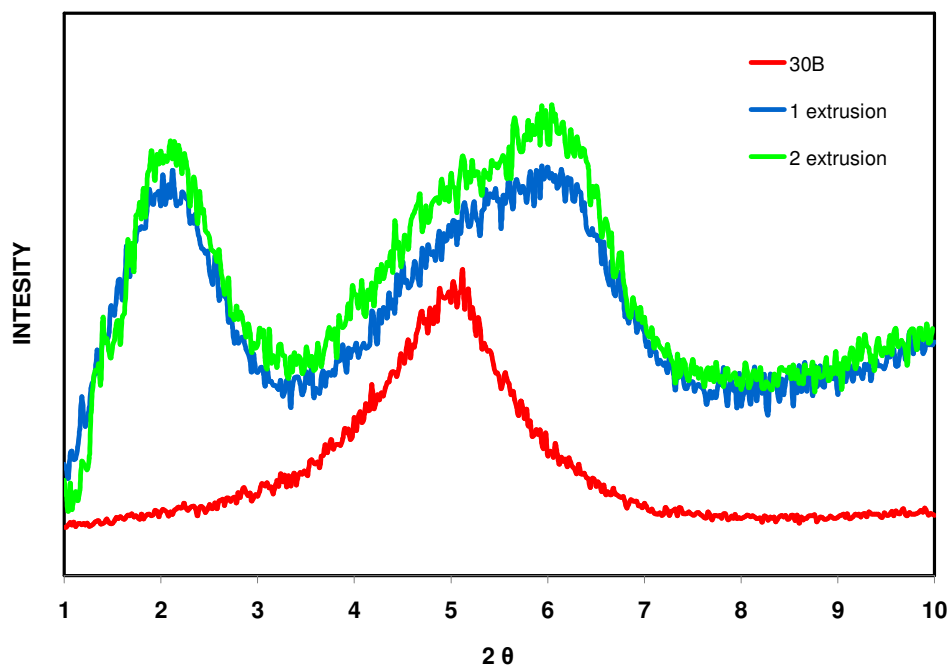


Figure 4.3 XRD analyses of LDPE/E-MA-GMA/30B samples

Tensile test results of both types of samples also support the XRD results. Tensile strength and strain at break values of the samples are given in Table 4.2.

Table 4.2 Tensile test results of LDPE/E-MA-GMA/30B samples

	Tensile Strength MPa	Strain at Break %
Extrusion Once	14.4 ± 0.2	78.8 ± 0.5
Extrusion Twice	14.5 ± 0.2	77.1 ± 0.3

Since there were no significant differences between the XRD results and tensile test results of samples that were extruded once or twice, the extrusion mixing was carried out once in the rest of the study.

4.2 Morphological Analysis

Morphological characterization of nanocomposites were done by XRD, TEM and SEM analyses.

4.2.1 XRD Analysis

XRD analysis is used in most nanocomposite research studies to determine the dispersion of the organoclay platelets through the polymer matrix. This analysis gives information on the structure of the nanocomposites. It is possible to identify intercalated and/or exfoliated structures according to the position, shape and intensity of the basal reflections from the silicate layers of the organoclay. The

interlayer spacing (d-spacing) of the silicate layers are calculated at the peak positions of the XRD patterns according to Bragg's law.

In phase separated composites, no change in basal spacing occurs. The reason is that, the polymer matrix does not exist in the clay galleries.

When intercalation occurs, polymer matrix flows into the clay platelets and thus the platelets are periodically arranged. Due to this structure, a reflection from the clay platelets is observed. When more polymer chains enter the clay galleries, interlayer spacing also increases. This structure is observed from the XRD pattern as a shift of the clay peak to lower angles. In addition to this, periodicity of the clay platelets decreases due to the separation of the platelets and in the XRD pattern reduction in intensity of clay peak is observed.

In exfoliated nanocomposites, the polymer matrix enters the clay galleries and pushes them far away from each other resulting in random dispersion of clay platelets. Due to this, no clay peak is observed in the XRD pattern. However, lack of organoclay peak in XRD pattern does not always mean the complete delamination of clay platelets. An immiscible or disordered sample, may also give a XRD pattern without any peaks. Thus in order to support the exfoliation, additional morphological analysis should be performed.

4.2.1.1 XRD Analysis Results of Organoclays

XRD analysis were performed on all the samples in the angle 2θ range of 1-10 °. Organoclay Cloisite® 30B (30B) has one diffraction peak (d_1) at $2\theta = 5.02$ with basal spacing of 17.6 Å. Organoclay Nanofil® 8 has three diffraction peaks at $2\theta = 2.56$, $2\theta = 4.78$ and $2\theta = 7.3$ with basal spacing of $d_1 = 34.5$, $d_2 = 18.5$, $d_3 = 12.1$ Å, respectively. The interlayer spacing results of organoclays are in accordance with the data obtained from manufacturers. It is thought that d_3 is due to the unmodified clay platelets, since the original d spacing of unmodified clay is approximately 12 Å. Similarly, d_2 may be due to partially modified clay. The diffraction patterns of pure organoclays and neat polyethylene types are given in the Appendix, Figures A1-A5.

4.2.1.2 XRD Analysis Results of LDPE Matrix Nanocomposites

XRD analysis of neat LDPE, LD/Organoclay binary nanocomposites and LD/Compatibilizer/Organoclay ternary nanocomposites were performed in order to determine the level of clay dispersion in the polymer matrix. Ternary LDPE nanocomposites contained 5 wt % compatibilizer, 2 wt % organoclay and 93 wt % LDPE.

4.2.1.2.1 LDPE Matrix Nanocomposites Containing Organoclay Cloisite® 30B

Figure 4.4 shows the XRD patterns of neat 30B, and binary nanocomposites of LD/30B containing 2, 4 and 6 wt % organoclay. Table 4.3 gives the basal spacing data of LDPE matrix nanocomposites containing organoclay Cloisite® 30B with LDPE matrix.

Considering the binary nanocomposites of LDPE and organoclay Cloisite® 30B, in Figure 4.4, increase in the interlayer spacing of clay platelets was not observed. On the other hand, the peak of diffraction pattern was slightly shifted to the right side, meaning slight decrease in the basal spacing of clay galleries.

Table 4.3 Basal spacing data of nanocomposites containing organoclay Cloisite® 30B with LDPE matrix

Sample	d_1 d-spacing (Å)	d_2 d-spacing (Å)
LD	-	-
30B	17.6	-
LD/30B %2	16.3	-
LD/30B %4	16.4	-
LD/30B %6	16.4	-
LD/E-MA-GMA/30B	36.5	15.0
LD/E-BA-MAH/30B	29.3	14.6

Interlayer spacings of 2 wt %, 4 wt % and 6 wt % Cloisite® 30 containing binary nanocomposites are 16.3, 16.4 and 16.4 Å, respectively. During the melt blending process, clay platelets may be stacked and this may have resulted in decrease of the interlayer spacing. As seen in Figure 4.4, increase in the clay content resulted in increase in intensity of diffraction peaks due to the high concentration of ordered clay platelets. It can be concluded that neither intercalation nor exfoliation were observed in binary nanocomposites of LD/30B.

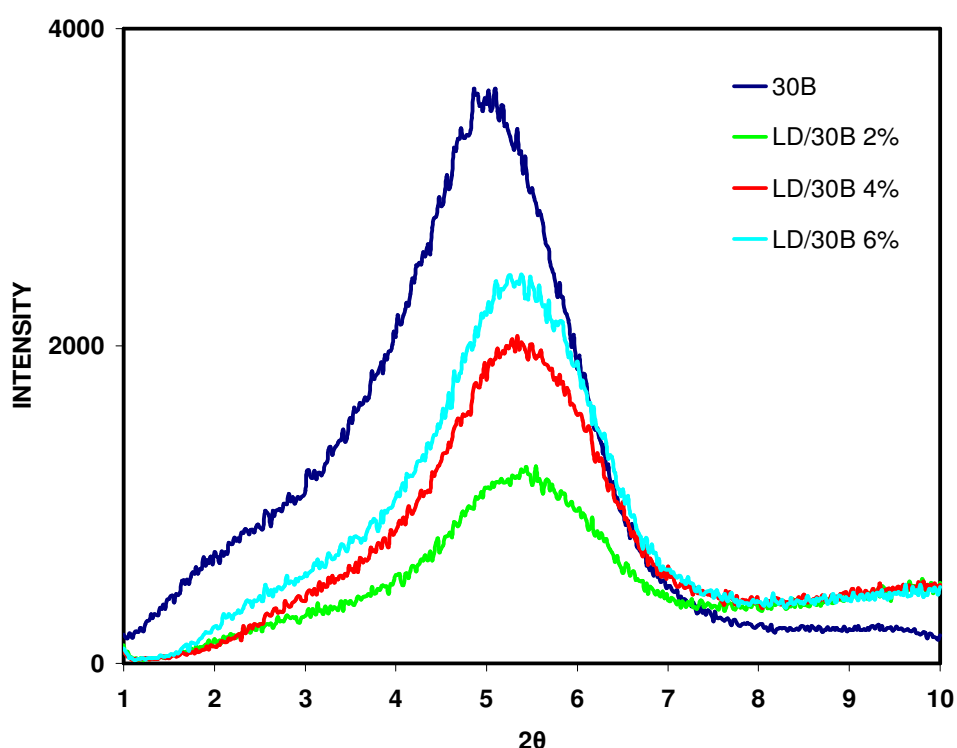


Figure 4.4 XRD patterns for binary nanocomposites of LD/30B

Both Cloisite® 30B and Nanofil® 8 are organically modified clays. They contain long alkyl chains in their structure that promote the increase of the basal spacing of layered silicates. However, it was not sufficient to obtain intercalated or completely dispersed structures in binary nanocomposites.

Figure 4.5 shows the XRD patterns of neat 30B, LD/30B containing 2 wt % organoclay, ternary nanocomposites of LD/ E-MA-GMA/ 30B and LD/ E-BA-MAH/ 30B containing 2 wt % organoclay and 5 wt % compatibilizer. Addition of 5 wt % compatibilizer, E-MA-GMA and E-BA-MAH, to binary nanocomposites resulted in significant change in morphology as seen in Figure 4.5.

According to the XRD patterns, characteristic diffraction peaks were shifted to lower angles and resulted in increase of basal spacing of clay galleries. This indicates the intercalation of the LDPE into clay galleries. Weak peaks were observed at $2\theta = 2.42$ and $2\theta = 3.02$, resulting in basal spacing of 36.5 and 29.3 Å for ternary nanocomposites of LD/E-MA-GMA/30B and LD/E-BA-MAH/30B, respectively.

In the XRD patterns of both ternary nanocomposites, secondary peaks were also observed at higher angles indicating smaller basal spacing values than the basal spacing of pure organoclay. These secondary peaks are due to unintercalated organoclay structure. During extrusion process, the alkyl chains of organoclay may be rearranged and electrostatic interaction between the organic modifier of clay and the negative charge of silicate surface may be lost. Due to the loss of this interaction, basal spacing of clay layers may decrease [165]. Diffraction peaks of ternary nanocomposites were broader than the characteristic diffraction peak of neat organoclay. This is due to the several intercalated structures with different interlayer spacing that were formed during the melt blending process.

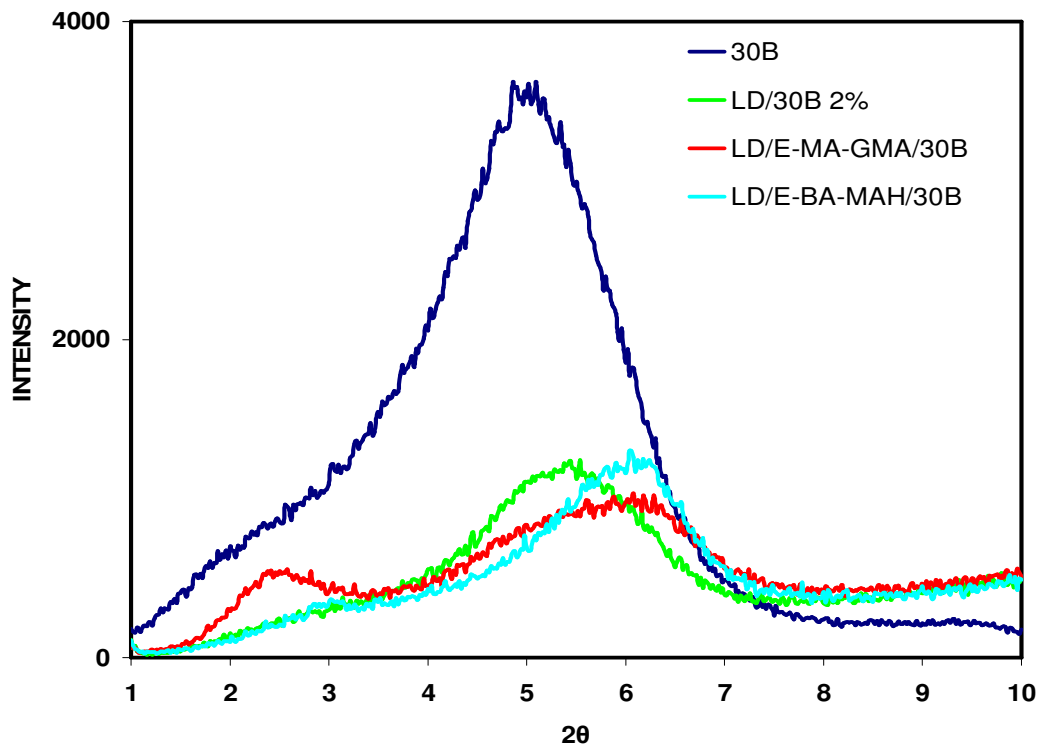


Figure 4.5 XRD patterns for ternary nanocomposites of LD/Compatibilizer/30B

Organoclay Cloisite 30B contains hydroxyl (OH⁻) groups in its structure. There may be reaction between the hydroxyl groups and functional groups of compatibilizers (GMA, MAH) used that enhance the interaction of the compatibilizer and organoclay. E-MA-GMA and E-BA-MAH are both polyethylene based polymers. They are highly miscible with PE matrix.

Considering the chemical structures of E-MA-GMA and E-BA-MAH, they both have bulky functional groups. This feature also promotes the dispersion of clay platelets by decreasing the interaction of clay platelets and increasing the intercalation of polymer matrix. One important feature of these compatibilizers is that, they have polar structure which increases the interaction of organoclay and the PE. This property enhances the possibility of intercalation and exfoliation [3].

4.2.1.2.2 LDPE Matrix Nanocomposites Containing Organoclay Nanofil® 8

Three different binary LD/ Nanofil 8 nanocomposites were prepared to discuss the effects of clay content on morphological properties of nanocomposites. These were 2 wt %, 4 wt % and 6 wt % organoclay containing binary nanocomposites. Ternary nanocomposites of LD/E-MA-GMA / Nanofil® 8 and LD/E-BA-MAH/ Nanofil® 8 contained 2 wt % organoclay and 5 wt % compatibilizer. XRD analysis results are given in Table 4.4 and X-Ray diffraction patterns are given in Figures 4.6-4.7. Organoclay Nanofil® 8 has three characteristic diffraction peaks at 2.56, 4.78 and 7.3° corresponding the d-spacing's of 34.5, 18.5 and 12.1 Å.

Table 4.4 Basal spacing data of nanocomposites containing organoclay Nanofil® 8 with LDPE matrix

Sample	d ₁ d-spacing (Å)	d ₂ d-spacing (Å)	d ₃ d-spacing (Å)
NF8	34.5	18.5	12.1
LD/NF8 %2	33.7	18.0	12.3
LD/NF8 %4	33.5	18.0	12.3
LD/NF8 %6	32.7	17.9	12.3
LD/E-MA-GMA/NF8	37.1	19.4	13.2
LD/E-BA-MAH/NF8	35.9	18.6	12.7

Figure 4.6 shows the XRD patterns of binary nanocomposites of LD/NF8 containing 2, 4 and 6 wt % organoclay. According to the X-Ray diffraction patterns of binary nanocomposites of LD/NF8, place of XRD reflection peaks did not change in all the compositions. First peak d₁, was observed at 2.62°, 2.64° and 2.70° in 2 wt %, 4 wt % and 6 wt % organoclay containing nanocomposites. Very slight shift of diffraction peak to right side occurred. It can be concluded that intercalation was not achieved in binary nanocomposites of LD/NF8. Increase in

the clay content resulted in increase of the intensity of the peaks due to the increase in the number of ordered clay galleries.

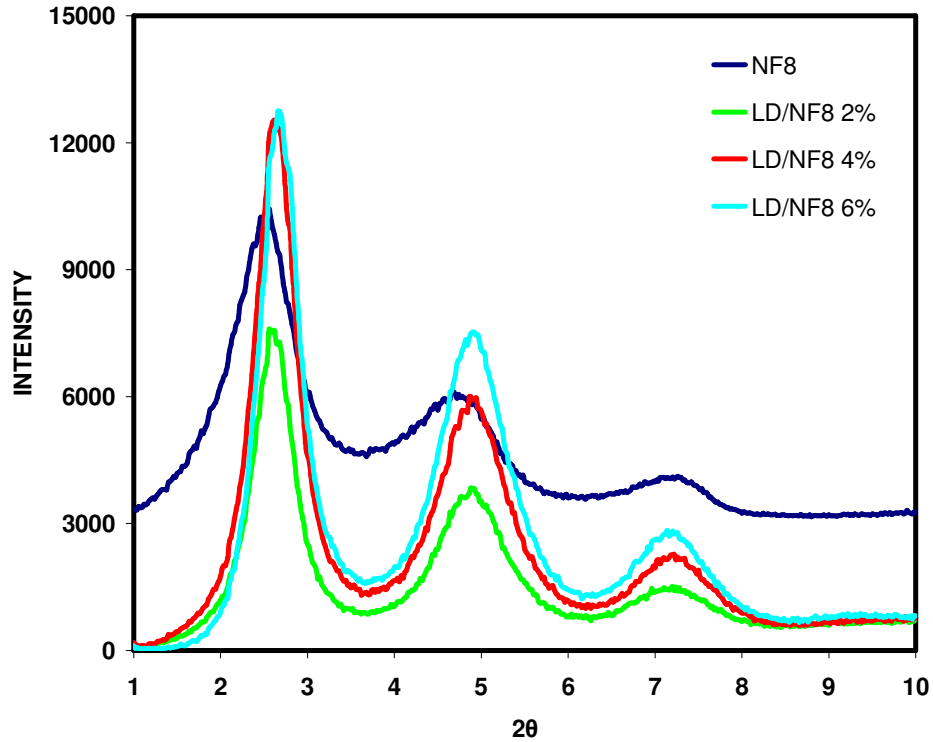


Figure 4.6 XRD patterns for binary nanocomposites of LD/NF8

A third component is necessary to increase the interaction the of polymer matrix and organoclay. Compatibility of this third component with both polymer matrix and organoclay is an important factor to obtain intercalated/exfoliated structures.

Figure 4.7 shows the XRD patterns of neat NF8, LD/NF8 containing 2 wt % organoclay, ternary nanocomposites of LD/ E-MA-GMA/ NF8 and LD/ E-BA-MAH/ NF8 containing 2 wt % organoclay and 5 wt % compatibilizer. It is seen that addition of 5 wt % compatibilizer enhanced the intercalation of polymer matrix into the organoclay galleries. Diffraction peak d_1 shifted to the left side, to lower angles, in both ternary nanocomposites. Basal spacing, d_1 , of organoclay platelets were, 37.1 and 35.9 Å for LD/E-MA-GMA/NF8 and LD/E-BA-MAH/NF8,

respectively. Secondary diffraction peak and tertiary diffraction peaks of LD/E-MA-GMA/NF8 shifted to lower angles of 4.56° and 6.72° with basal spacings of 19.4 \AA and 13.2 \AA , respectively. Intensity of ternary nanocomposites with E-MA-GMA decreased significantly indicating the decrease of ordered clay platelets.

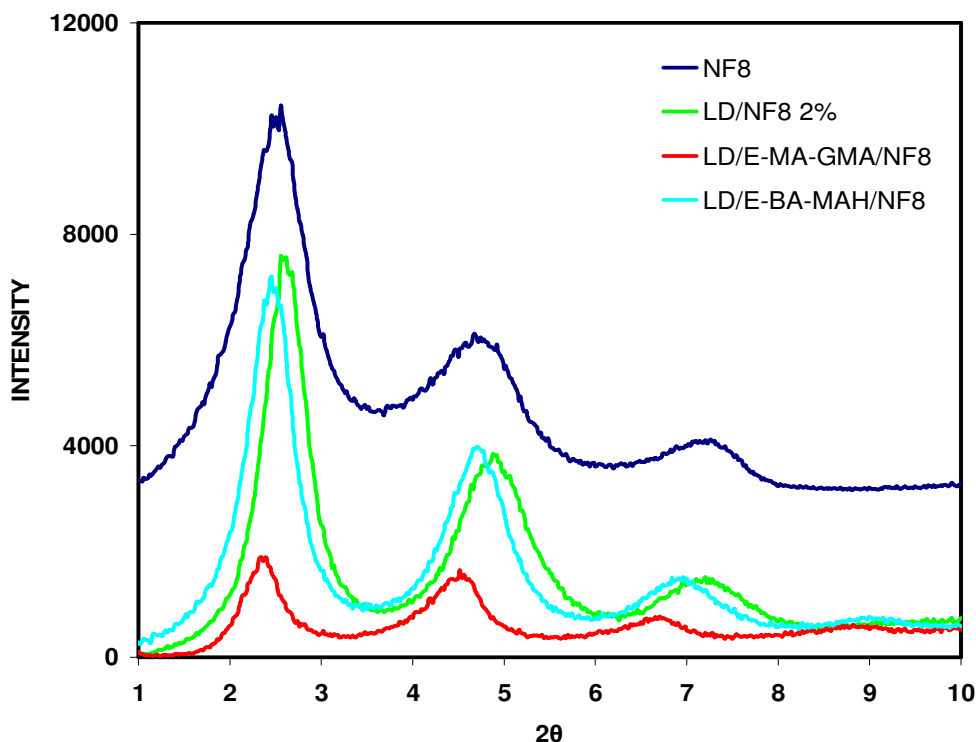


Figure 4.7 XRD patterns for ternary nanocomposites of LD/Compatibilizer/NF8

Considering the nanocomposites containing 5 wt % E-BA-MAH, partially intercalation was achieved. First diffraction peak slightly shifted to the left side and resulted in 4.1 % increase in the basal spacing of clay galleries.

4.2.1.3 XRD Analysis Results of HDPE Matrix Nanocomposites

HDPE was the second polymer matrix that was used to produce nanocomposites. XRD analyses of neat HDPE, HD/Organoclay binary nanocomposites and HD/Compatibilizer/Organoclay ternary nanocomposites

were performed. Binary nanocomposites contained 2 wt %, 4 wt % and 6 wt % organoclay. Ternary nanocomposites contained 2 wt % organoclay and 5 wt % compatibilizer.

4.2.1.3.1 HDPE Matrix Nanocomposites Containing Organoclay Cloisite® 30B

Neat HDPE X-Ray diffraction pattern did not have reflection peak due to the lack of organoclay. XRD analysis results of organoclay Cloisite® 30B containing samples are given in Table 4.5.

Table 4.5 Basal spacing data of nanocomposites containing organoclay Cloisite® 30B with HDPE matrix

Sample	d_1 d-spacing (Å)	d_2 d-spacing (Å)
HD	-	-
30B	17.6	-
HD/30B %2	14.5	-
HD/30B %4	14.5	-
HD/30B %6	14.5	-
HD/E-MA-GMA/30B	43.7	14.6
HD/E-BA-MAH/30B	37.4	14.4

Figure 4.8 shows the XRD patterns of neat 30B, binary nanocomposites of HD/30B containing 2, 4 and 6 wt % organoclay.

Considering the binary compositions of HDPE/30B, intercalation of polymer matrix is not observed in X-Ray diffraction patterns as shown in Figure 4.8. Peak position of characteristic peak of Cloisite® 30B shifted to the higher angles with

melt mixing. It was not possible to disperse the stacked organoclay layers with the extrusion process.

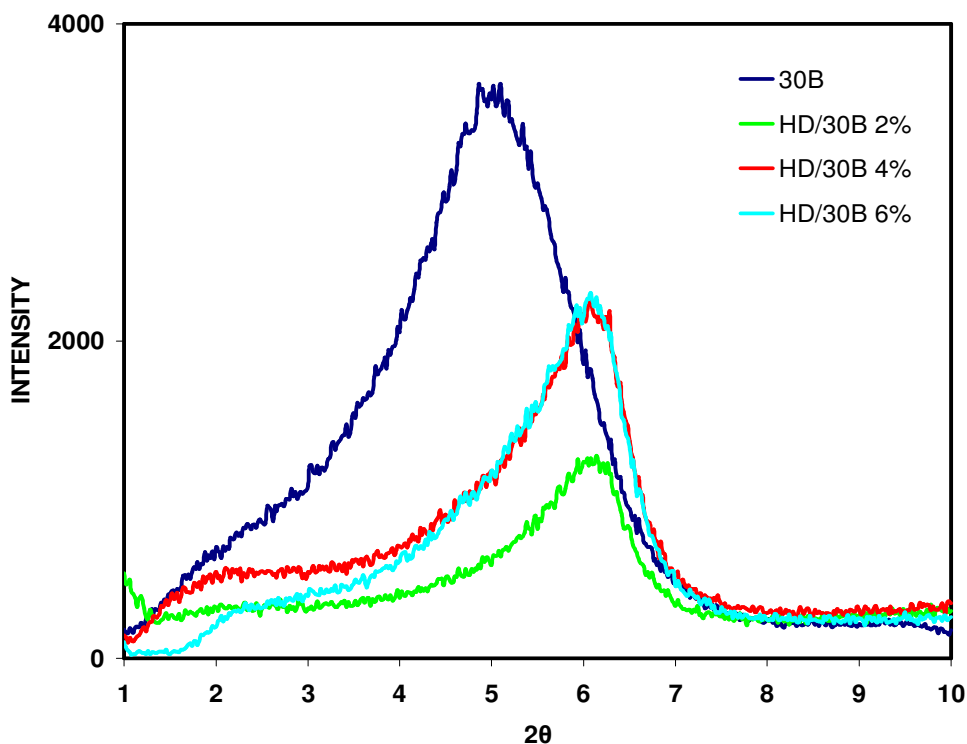


Figure 4.8 XRD patterns for binary nanocomposites of HD/30B

Diffraction peaks of all the binary compositions were observed approximately at 6.08° indicating basal spacing of 14.5 \AA which was smaller than the neat organoclay interlayer spacing. The reason for collapsing interlayer distance of organoclays was that, during preparation of samples for analysis, injection molding process was applied at 12 bars. During injection molding stacking of organoclay galleries might have occurred.

Figure 4.9 shows the XRD patterns of neat 30B, HD/30B containing 2 wt % organoclay, ternary nanocomposites of HD/ E-MA-GMA/ 30B and HD/ E-BA-MAH/ 30B containing 2 wt % organoclay and 5 wt % compatibilizer. Both

compatibilizers had a significant effect on dispersion of silicate layers in the HDPE matrix.

HD/E-MA-GMA/30B nanocomposites showed a weak peak at 2.02° indicating interlayer spacing of 43.7 \AA . Intercalation of polymer matrix into clay galleries was achieved by addition of 5 wt % of E-MA-GMA to system. At 6.06° another diffraction peak was also observed with interlayer spacing of 14.6 \AA . This peak indicates that, there were unintercalated and collapsed structures in the polymer matrix.

In the case of HD/E-BA-MAH/30B nanocomposites, intercalation of HDPE was also achieved. X-Ray diffraction peak was at 2.32° with the basal spacing of 37.4 \AA . E-BA-MAH was also a good choice for increasing the interaction of organoclay 30B with HDPE matrix. It was compatible with both the clay and the polymer. Secondary diffraction peak was also seen in the X-Ray diffraction pattern of HD/E-BA-MAH/30B. Some of the organoclay kept its original stacking structure.

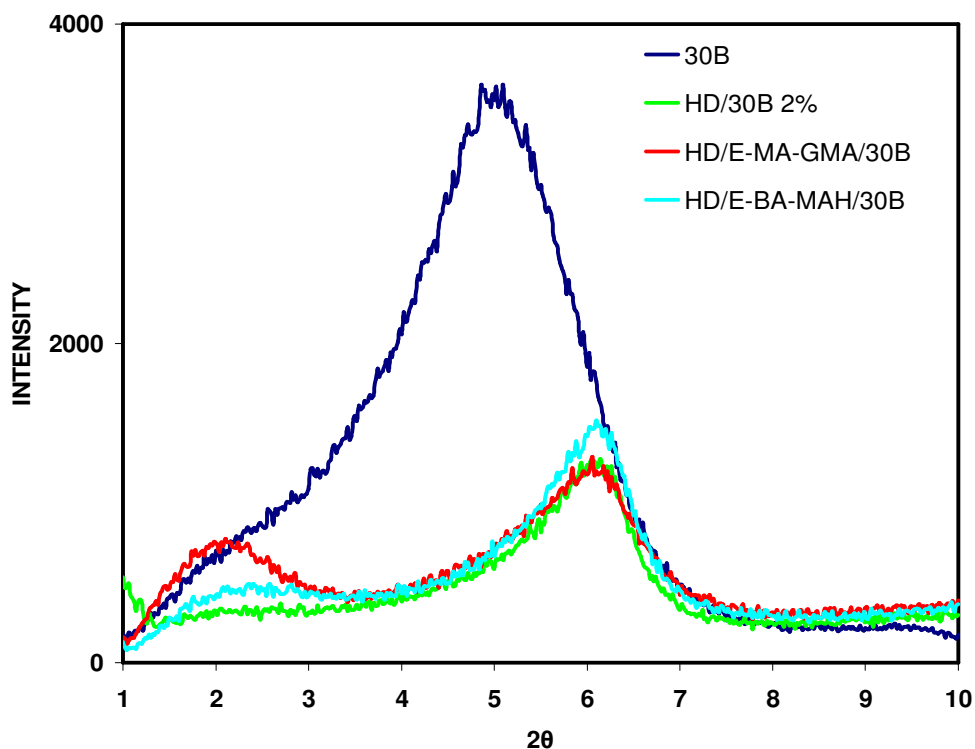


Figure 4.9 XRD patterns for ternary nanocomposites of HD/Compatibilizer/30B

X-Ray diffraction peaks of HDPE ternary nanocomposites with organoclay 30B, are broad, not sharp peaks. Thus, it was concluded that partially intercalation was achieved with addition of both compatibilizer types. Reactive and polar structures of compatibilizers enhanced the intercalation. However, complete delamination (exfoliation) of clay platelets was not obtained.

4.2.1.3.2 HDPE Matrix Nanocomposites Containing Organoclay Nanofil® 8

XRD analyses results of HDPE matrix nanocomposites with organoclay Nanofil® 8 are given in Table 4.6. XRD patterns of these nanocomposites can be found in Figures 4.10 - 4.11.

Table 4.6 Basal spacing data of nanocomposites containing organoclay Nanofil® 8 with HDPE matrix

Sample	d_1 d-spacing (Å)	d_2 d-spacing (Å)	d_3 d-spacing (Å)
NF8	34.5	18.5	12.1
HD/NF8 %2	26.9	13.1	-
HD/NF8 %4	26.9	12.8	-
HD/NF8 %6	27.1	12.6	-
HD/E-MA-GMA/NF8	37.8	20.0	13.5
HD/E-BA-MAH/NF8	34.2	17.2	-

Normally, characteristic XRD pattern of neat Nanofil® 8 has three different reflection peaks. Figure 4.10 shows the XRD patterns of neat NF8, and binary nanocomposites of HD/NF8 containing 2, 4 and 6 wt % organoclay. Considering the binary compositions of HD/NF8, only two peak positions were observed in

XRD patterns. Peak positions of 2 wt % organoclay containing nanocomposites were, 3.28° and 6.74° with basal spacings 26.9 Å and 13.1 Å; peak positions of 4 wt % organoclay containing nanocomposites were 3.28°, 6.88° with basal spacings 26.9 Å and 12.8 Å; peak positions of 6 wt % organoclay containing nanocomposites were, 3.26° and 7.0° with basal spacings 27.1 Å and 12.6 Å. It was seen that, the d_1 peaks were shifted to right resulting in decrease in interlayer distance. This may be due to injection molding, during which the clay galleries may have been stacked more. The second diffraction peaks were lost in all types, indicating partial intercalation of polymer matrix into clay galleries. The tertiary peaks were shifted to left, smaller angles, representative of partially intercalated structure.

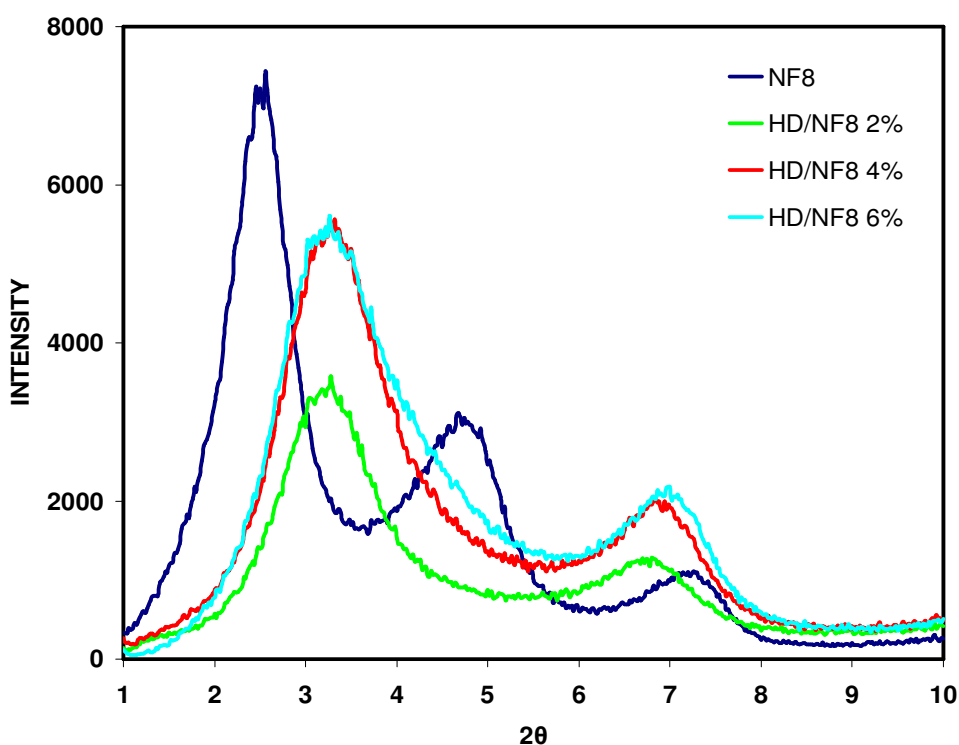


Figure 4.10 XRD patterns for binary nanocomposites of HD/NF8

Considering the ternary nanocomposites of HD/Compatibilizer/Nanofil® 8, different morphological structures were obtained. Figure 4.11 shows the XRD

patterns of neat NF8, HD/NF8 containing 2 wt % organoclay, ternary nanocomposites of HD/ E-MA-GMA/ NF8 and HD/ E-BA-MAH/ NF8 containing 2 wt % organoclay and 5 wt % compatibilizer. Three diffraction peaks were observed in XRD patterns of HD/E-MA-GMA/ Nanofil® 8, nanocomposites. Peak positions were shifted slightly to left, smaller angles, indicating that intercalation of polymer matrix was achieved. Basal spacings d_1 , d_2 and d_3 were 37.8, 20.0 and 13.5 Å, respectively. On the other hand, HD/E-BA-MAH/ Nanofil® 8, nanocomposites had two diffraction peaks d_1 and d_2 . The first peak was at 2.58° and the second was at 5.14°. Basal spacings were, 34.2 and 17.2 Å. The place of the first peak was not changed. However, its intensity decreased indicating partial exfoliation. The second peak was a broad peak which indicates several basal spacing values, and intercalation of the polymer matrix. Third diffraction peak disappeared due to partial delamination of the clay platelets.

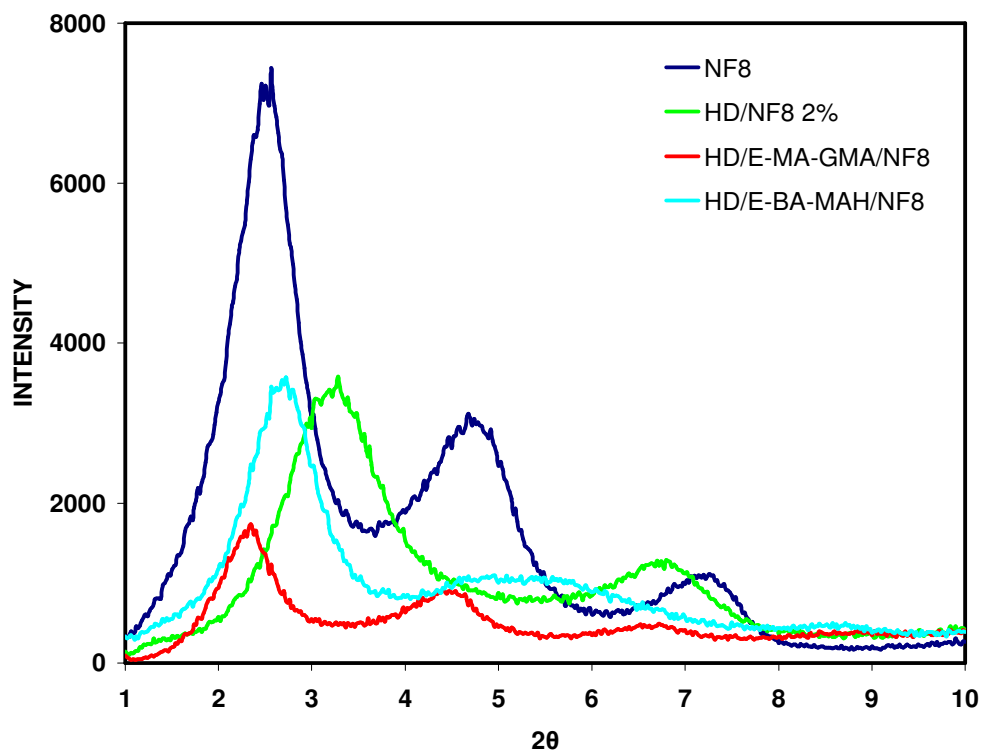


Figure 4.11 XRD patterns for ternary nanocomposites of HD/Compatibilizer/NF8

4.2.1.4 XRD Analysis Results of LLDPE Matrix Nanocomposites

Samples of neat LLDPE (LIN), LLDPE/Organoclay and LLDPE/Compatibilizer/Organoclay compositions were analyzed by XRD in order to investigate the structure of nanocomposites prepared. Compositions of the samples were the same as those of LDPE and HDPE nanocomposites. Binary compositions contained 2 wt%, 4 wt % and 6 wt % organoclay and ternary nanocomposites contained 2 wt % organoclay and 5 wt % compatibilizer.

4.2.1.4.1 LLDPE Matrix Nanocomposites Containing Organoclay Cloisite® 30B

XRD analysis results of the binary and ternary nanocomposites containing Cloisite® 30B are given in Table 4.7. No increases in the basal spacing of binary compositions were observed in XRD patterns. Slight shift of peak position to higher angles, meaning decrease in the interlayer distance, was due to the applied pressure during injection molding process. Since extrusion and injection molding process temperature was not so high, degradation of organoclay was not probable.

Table 4.7 Basal spacing data of nanocomposites containing organoclay Cloisite® 30B with LLDPE matrix

Sample	d_1 d-spacing (Å)	d_2 d-spacing (Å)
LIN	-	-
30B	17.6	-
LIN/30B %2	15.8	-
LIN/30B %4	15.7	-
LIN/30B %6	16.5	-
LIN/E-MA-GMA/30B	39.8	14.9
LIN/E-BA-MAH/30B	38.1	15.0

Figure 4.12 shows the XRD patterns of neat 30B, binary nanocomposites of LIN/30B containing 2, 4 and 6 wt % organoclay. It was observed that diffraction peaks of binary nanocomposites were broadened peaks with less intensity with respect to neat organoclay. This feature is a characteristic of highly disordered organoclay platelets. Broadened peaks and decrease in peak heights of binary nanocomposites, indicate decrease in the number of layers of individual clay particles that constitute the intercalated structures. There were also shoulders at small values of 2θ , in the binary composites indicating some intercalation.

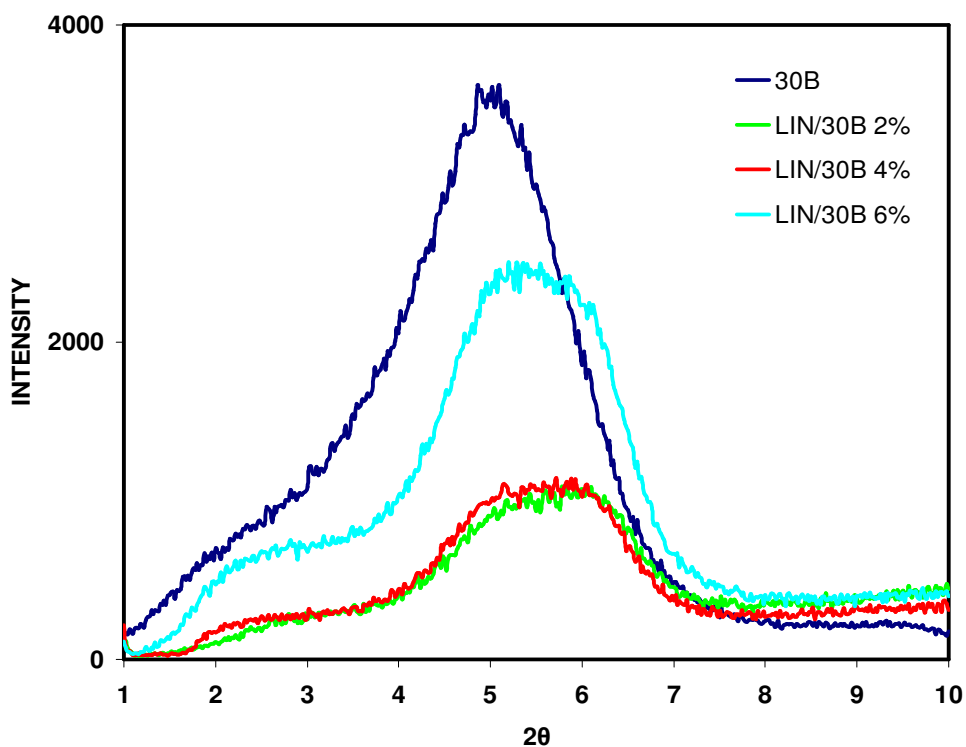


Figure 4.12 XRD patterns for binary nanocomposites of LIN/30B

Figure 4.13 shows the XRD patterns of neat 30B, LIN/30B containing 2 wt % organoclay, ternary nanocomposites of LIN/ E-MA-GMA/ 30B and LIN/ E-BA-MAH/ 30B containing 2 wt % organoclay and 5 wt % compatibilizer. Significant effect of compatibilizer on dispersion of organoclay in polymer matrix was also observed in ternary nanocomposites of LLDPE. As explained previously, melt

blending of LLDPE with organoclay was not sufficient to obtain complete delamination of clay. A third component, compatible with polymer matrix and organoclay is necessary to increase the interaction of polymer and organoclay.

Addition of 5 wt % E-MA-GMA and E-BA-MAH to binary compositions resulted in shift of the characteristic peak of organoclay to lower angles indicating the intercalation of polymer into clay galleries. Two different diffraction peaks were observed in diffraction patterns of LIN/ E-MA-GMA/ Cloisite® 30B and LIN/ E-BA-MAH/ Cloisite® 30B nanocomposites. First diffraction peaks were at 2.32° and 2.22° with basal spacing of 38.1 Å and 39.8 Å for LIN/ E-BA-MAH/ Cloisite® 30B and LIN/ E-MA-GMA/ Cloisite® 30B, respectively. Secondary diffraction peaks were observed at approximately 6° with basal spacing of 15Å. Both peaks were broad indicating several clay galleries with different interlayer spacing. It was concluded that partial intercalation was achieved in ternary nanocomposites of LLDPE containing organoclay Cloisite® 30B.

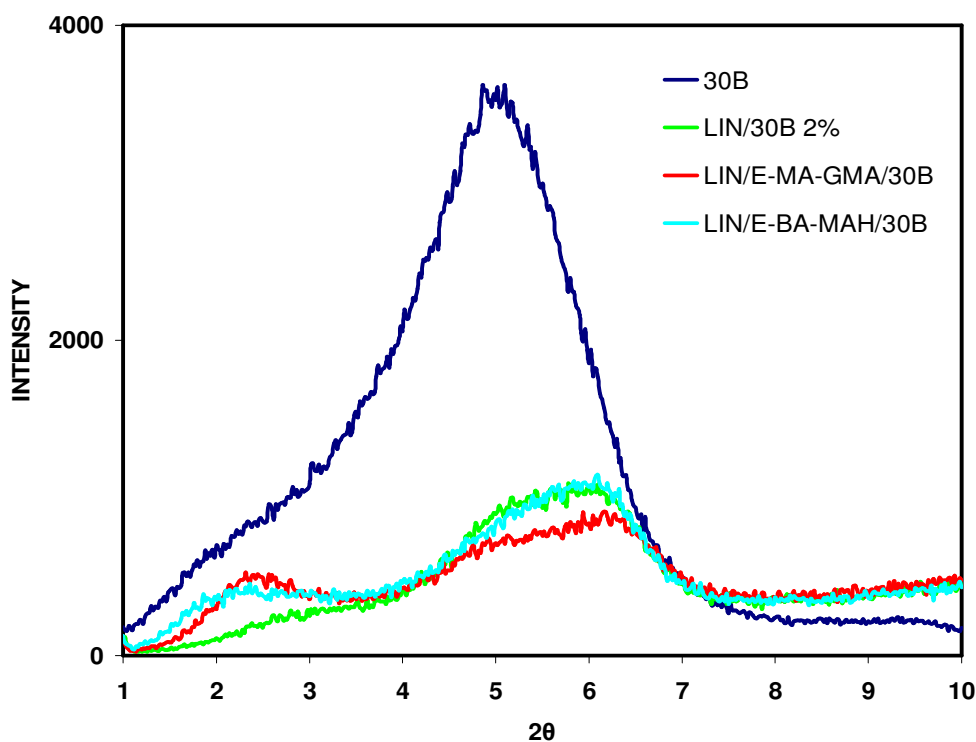


Figure 4.13 XRD patterns for ternary nanocomposites of LIN/Compatibilizer/30B

4.2.1.4.2 LLDPE Matrix Nanocomposites Containing Organoclay Nanofil® 8

Binary and ternary nanocomposites of LLDPE with organoclay Nanofil® 8 were produced with the same compositions as LLDPE/ Cloisite® 30B. XRD analysis results of LLDPE matrix nanocomposites containing Nanofil® 8 are given in Table 4.8.

Table 4.8 Basal spacing data of nanocomposites containing organoclay Nanofil® 8 with LLDPE matrix

Sample	d_1 d-spacing (Å)	d_2 d-spacing (Å)	d_3 d-spacing (Å)
NF8	34.5	18.5	12.1
LIN/NF8 %2	34.0	18.6	13.0
LIN/NF8 %4	34.0	18.5	12.8
LIN/NF8 %6	33.5	18.0	12.6
LIN/E-MA-GMA/NF8	41.7	20.5	13.6
LIN/E-BA-MAH/NF8	37.1	19.2	13.1

Figure 4.14 shows the XRD patterns of binary nanocomposites of LIN/NF8 containing 2, 4 and 6 wt % organoclay. Primary, secondary and tertiary diffraction peaks were observed in all the binary nanocomposites as seen in Figure 4.14. It is observed that the basal spacing of organoclay did not change in 2 wt %, 4 wt % and 6 wt % organoclay containing nanocomposites, and d_1 , d_2 and d_3 were calculated as 34, 18.5 and 13 Å, respectively. Intercalation was not observed in binary compositions. In addition to this, increase in clay content resulted in increase of the peak intensity due to the increased number of ordered clay layers.

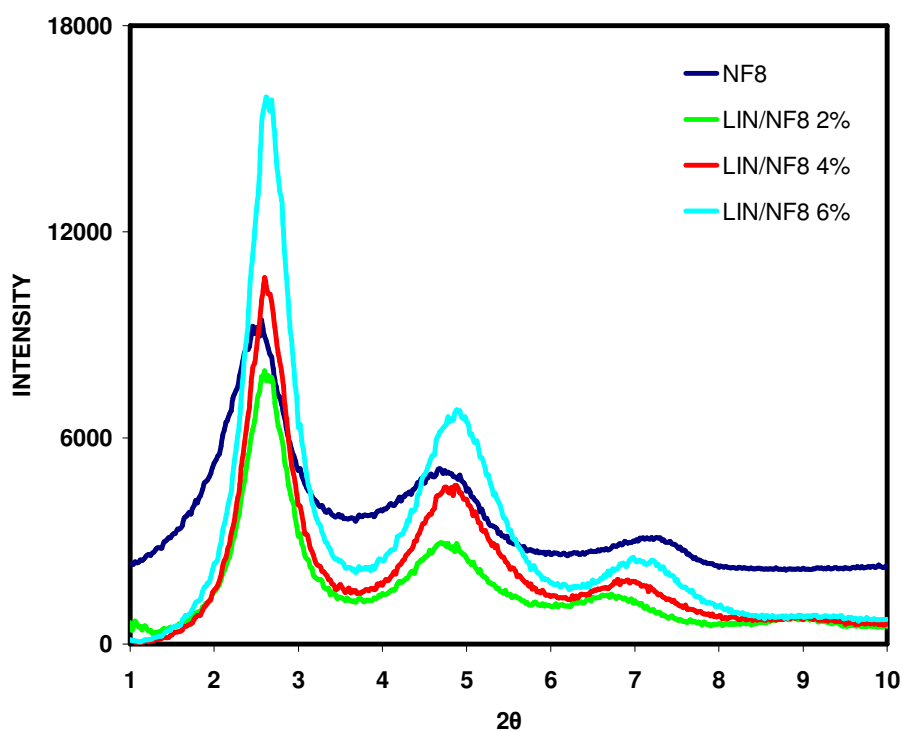


Figure 4.14 XRD patterns for binary nanocomposites of LIN/NF8

Although intercalation was not achieved in binary compositions, usage of compatibilizer had positive effect in obtaining dispersion of clay platelets. Figure 4.15 shows the XRD patterns of neat NF8, binary nanocomposite of LIN/NF8 containing 2 wt % organoclay and ternary nanocomposites of LIN/ E-MA-GMA/ NF8 and LIN/ E-BA-MAH/ NF8 containing 2 wt % organoclay and 5 wt % compatibilizer. Usage of compatibilizer enhanced the increase of basal spacing of clay galleries by shifting the peak position to lower angles.

Three diffraction peaks were observed in both types of ternary nanocomposites. Primary diffraction peaks were observed at 2.12° and 2.38° with basal spacings 41.7 and 37.1 Å for LIN/E-MA-GMA/ Nanofil® 8 and LIN/E-BA-MAH/ Nanofil® 8 nanocomposites, respectively. It is seen from Figure 4.15, that the intensity of the peaks of LD/NF8 decreases, indicating change of large silicate agglomerates into small tactoids as a result of applied shear during extrusion process. Decrease in intensity of peaks was due to formation of several intercalated or partial exfoliated structures.

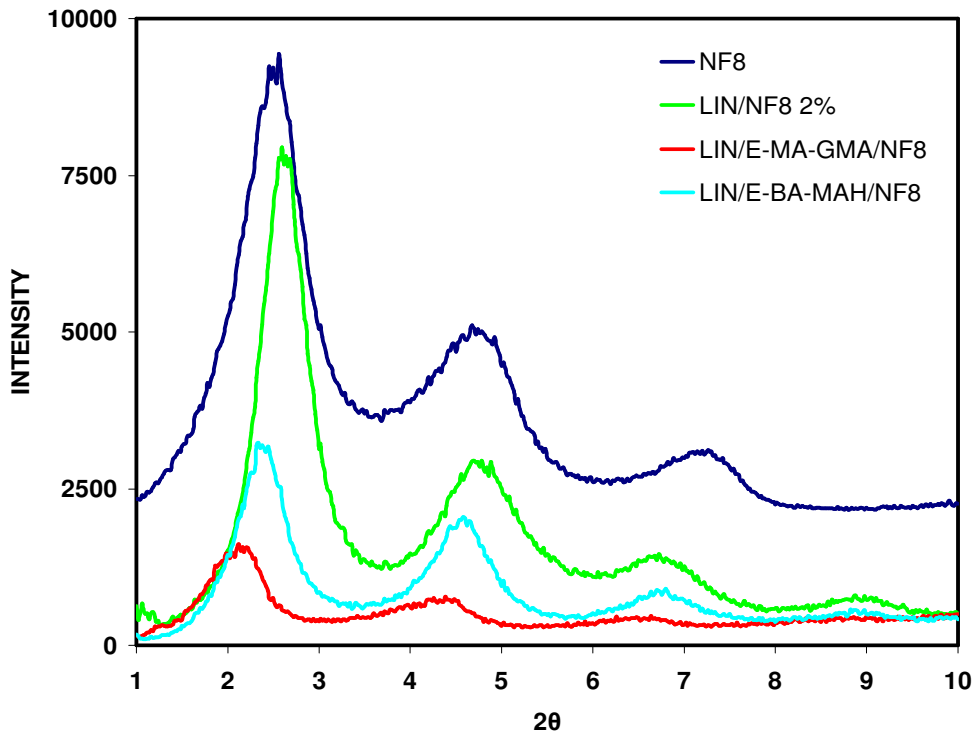


Figure 4.15 XRD patterns for ternary nanocomposites of LIN/Compatibilizer/NF8

Table 4.9 summarizes the data on % increase in basal spacing of ternary nanocomposites of LDPE, HDPE and LLDPE.

Table 4.9 Basal spacing data (Δd_1 %) of ternary nanocomposites of LDPE, HDPE and LLDPE containing 2 wt % organoclay and 5 wt % compatibilizer

	LDPE		HDPE		LLDPE	
	E-MA-GMA	E-BA-MAH	E-MA-GMA	E-BA-MAH	E-MA-GMA	E-BA-MAH
30B	107.4	66.5	148.3	112.5	126.1	116.5
NF8	7.5	4.1	9.6	-	20.9	7.5

Considering the organoclay type, significant increase in basal spacing was achieved with Cloisite® 30B. On the other, hand slight increase in basal spacing of Nanofil® 8 was observed in ternary nanocomposites.

Considering the initial interlayer distances of organoclays, initial basal spacing of Nanofil 8 is higher than the basal spacing of Cloisite® 30B. However, no significant change was observed in the distance between the clay platelets of nanocomposites with Nanofil® 8. It may be thought that, larger initial d-spacing might enhance exfoliation due to reduction of interaction between clay galleries and easier diffusion of polymer chains might take place inside the clay galleries . However, this was not achieved for any type of ternary nanocomposites of LDPE, HDPE and LLDPE with organoclay Nanofil® 8. Results of morphological characterization showed that among the factors affecting clay dispersion, polymer-organoclay interaction is an important issue and compatibility of polymer matrix and the clay surface modifier is essential to obtain an intercalated/exfoliated nanocomposite.

Both compatibilizers were highly compatible with all polyethylene types and organoclay types. However, considering the percentage increase of interlayer spacing of organoclays, E-MA-GMA was found to be more compatible. It is possible that reactions may occur between the functional groups (GMA, MAH) of the compatibilizers and the hydroxyl groups of the montmorillonite. It is known that the epoxy group is more reactive than the anhydride group supporting these observations. Interaction of organoclay and polymer significantly enhance clay dispersion.

Among all the ternary nanocomposites, the highest increase in interlayer spacing was observed as 148.3 % for HDPE/E-MA-GMA/30B nanocomposites. This is due to high compatibility of HDPE and organoclay 30B in the presence of E-MA-GMA.

Considering the structures of PE types, LDPE is highly branched and HDPE has no branched structure. LLDPE has small but regular branches. Results of XRD analysis showed that among the ternary nanocomposites containing the same organoclay and compatibilizer, the highest increase in basal spacing was

obtained in HDPE matrix nanocomposites and the least increase in basal spacing was obtained in LDPE matrix nanocomposites. It was concluded that chain structure is also an important factor affecting the clay dispersion. Intercalation of highly branched polymer chains was less with respect to intercalation of unbranched polymer chains. Unbranched chain structure may enhance the flow of polymer matrix into clay galleries easily during melt blending.

With hydroxyl (-OH) groups on its organic modifier, Cloisite® 30B, has less hydrophobic surface than Nanofil® 8. In addition, to this, 30B has a polar structure. It is more probable for it to interact with polar compatibilizers. Thus, Cloisite® 30B would be more compatible with the compatibilizers than Nanofil® 8. Considering the type of compatibilizers, 30B is more compatible with the one that contains the epoxy group. Epoxy is more reactive than the MAH. Results of XRD analysis support this phenomena, since the percentage increase in basal spacing is significantly higher in the ternary nanocomposites containing Cloisite® 30B than the nanocomposites containing Nanofil® 8. Thus, the degree of dispersion of clay Cloisite® 30B aggregates in LDPE, HDPE and LLDPE should be higher than the degree of dispersion of Nanofil® 8 aggregates in LDPE, HDPE and LLDPE . This high degree of dispersion of Cloisite® 30B in nanocomposites is due to the reactions of OH groups of 30B with epoxy and MAH groups of the compatibilizers and existence of attractive interactions via hydrogen bonding.

Vaia et al. (1995) suggested that external force that is applied on clay agglomerates depends on melt viscosity of polymer, shear rate, surface area of clay, and surface tension between molten polymer and clay, melt temperature, interlayer spacing of clay, chain structure of polymers, and surfactant modifiers on the clay surface. According to the results of their study, they concluded that compatibility of the polymer matrix and organoclay, chemistry of the clay treatment, and chemistry of compatibilizer are also important factors in dispersion of clay. The shear applied during extrusion can only reduce the size of tactoid particles or the size of intercalated clay stacks when the chemical compatibility of polymer and organoclay is not strong enough. These results also supported by the results of this thesis.

4.2.2 TEM Analysis

Transmission electron microscopy analysis is a complementary analysis to observe the morphology of nanocomposites. TEM analyses were applied on twelve different compositions of ternary nanocomposites of LDPE, HDPE and LLDPE which are given in Table 4.9, in order to investigate the dispersion of silicate layers through the polymer matrices.

Sample preparation for TEM analysis is a very important factor that affects the quality of the TEM analysis results. In order to obtain clear image of the morphology very thin cross-sections are necessary. Thus, the sample should be microtomed cryogenically. Sample preparation and heating of the sample by the high energy electron beam might have an effect on the morphology of the nanocomposites.

4.2.2.1 TEM Analysis Results of Nanocomposites with LDPE Matrix

Figures 4.16 through 4.19 show the TEM micrographs of ternary nanocomposites of LD/E-MA-GMA/30B, LD/E-BA-MAH/30B, LD/E-MA-GMA/NF8 and LD/E-BA-MAH/NF8, respectively. The dark lines represent the silicate layers and gray/white areas are the polymer/compatibilizer matrix. According to the XRD analyses, intercalation of LDPE was achieved in all the four different ternary nanocomposites. TEM images also supported the results of XRD analyses, since intercalated structures were detected. In addition to this, partial exfoliation of silicate layers was also detected in TEM micrographs of LDPE. However, in XRD analysis full exfoliation was not observed. Tactoids representing the stacked clay galleries were also detected. These are the dark parallel lines groups seen in the TEM images.

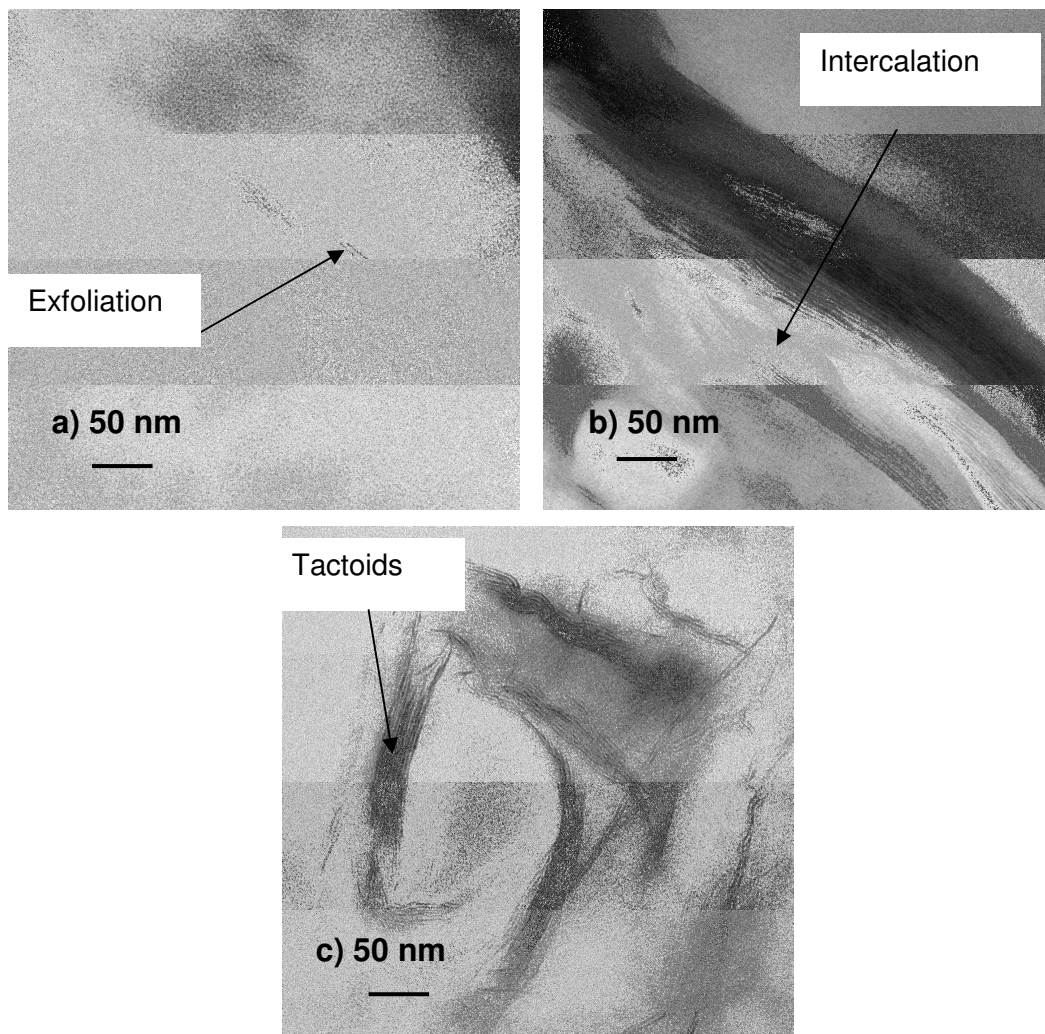


Figure 4.16 TEM micrographs of LD/E-MA-GMA/30B nanocomposite

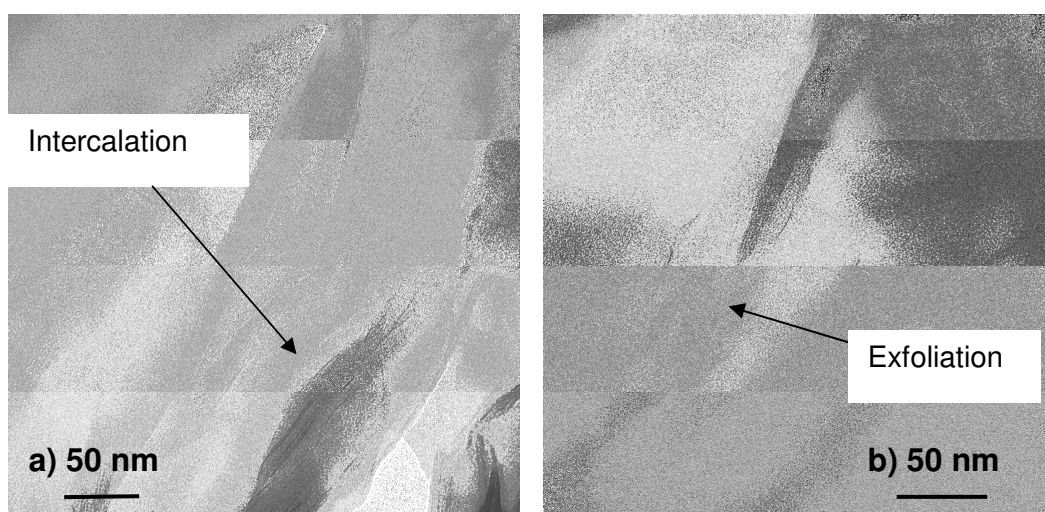


Figure 4.17 TEM micrographs of LD/E-BA-MAH/30B nanocomposite

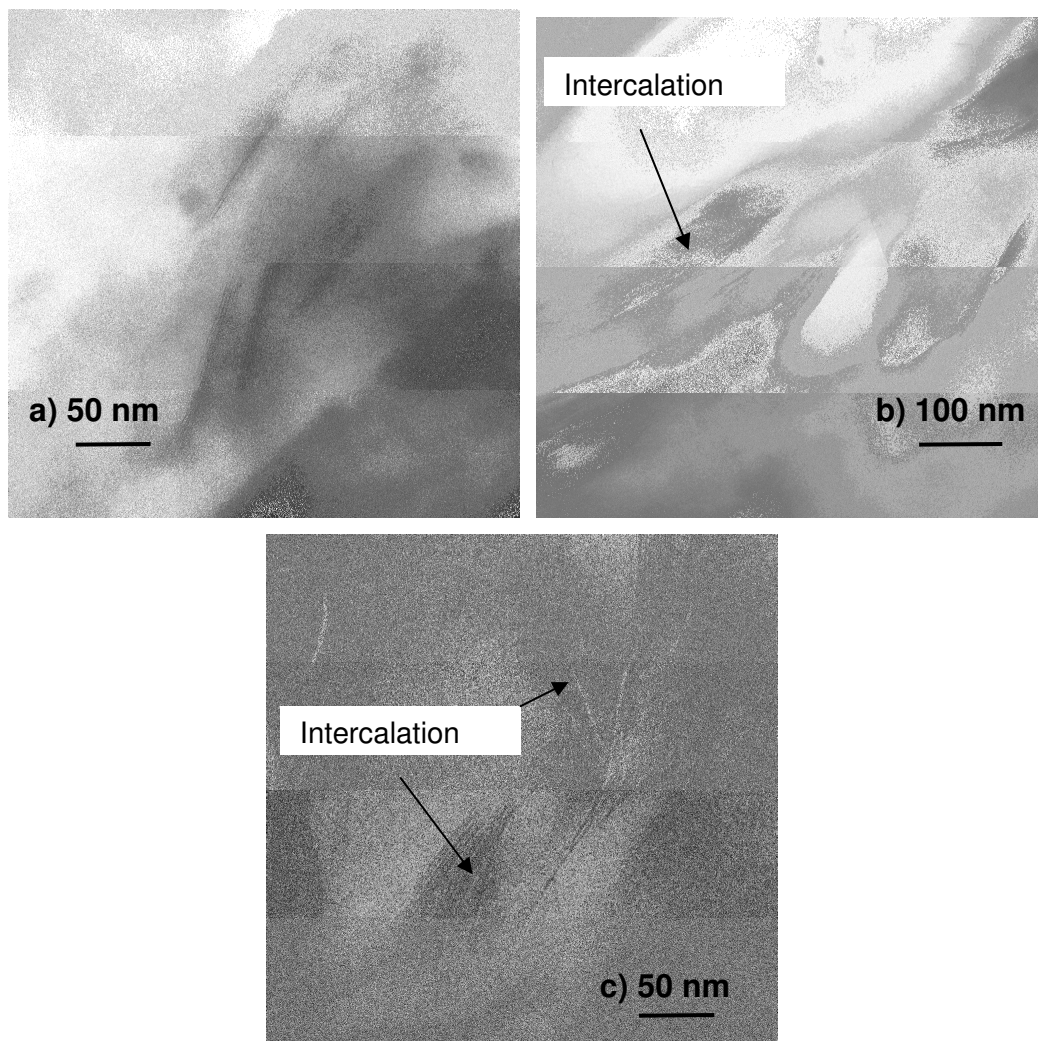


Figure 4.18 TEM micrographs of LD/E-MA-GMA/NF8 nanocomposite

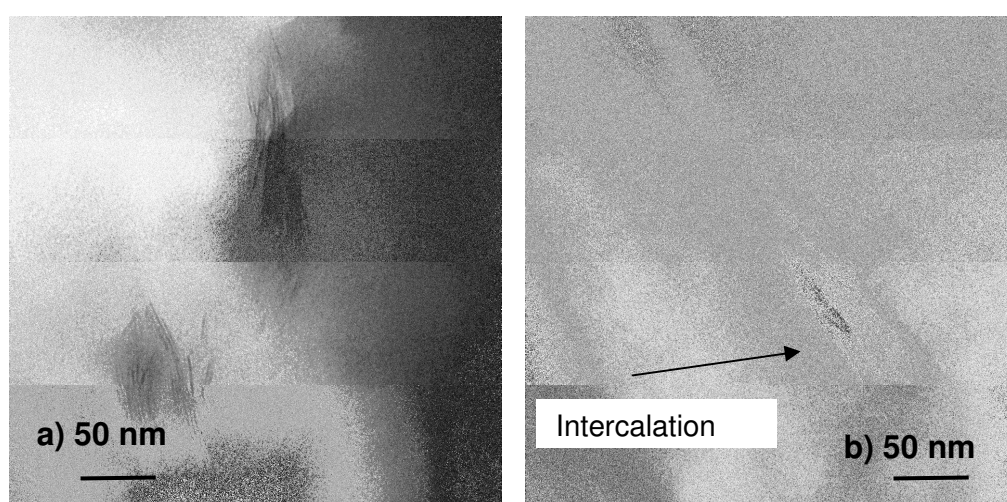


Figure 4.19 TEM micrographs of LD/E-BA-MAH/NF8 nanocomposite

4.2.2.2 TEM Analysis Results of Nanocomposites with HDPE Matrix

Figures 4.20 and 4.21 show the ternary nanocomposites of HDPE with organoclay 30B. In these figures, both intercalated and exfoliated structures are observed. Partial exfoliation and delamination of silicate layers are also detected in systems containing E-MA-GMA and E-BA-MAH compatibilizers. The dark areas are the agglomerates that might have formed due to clustering. XRD analysis results showed that better dispersion of organoclay was achieved in HDPE/Compatibilizer/30B nanocomposites in comparison to LDPE and LLDPE nanocomposites. TEM analysis results are also consistent with the XRD analysis. Compatibilizers had a significant effect on dispersion of silicate layers in the polymer matrix.

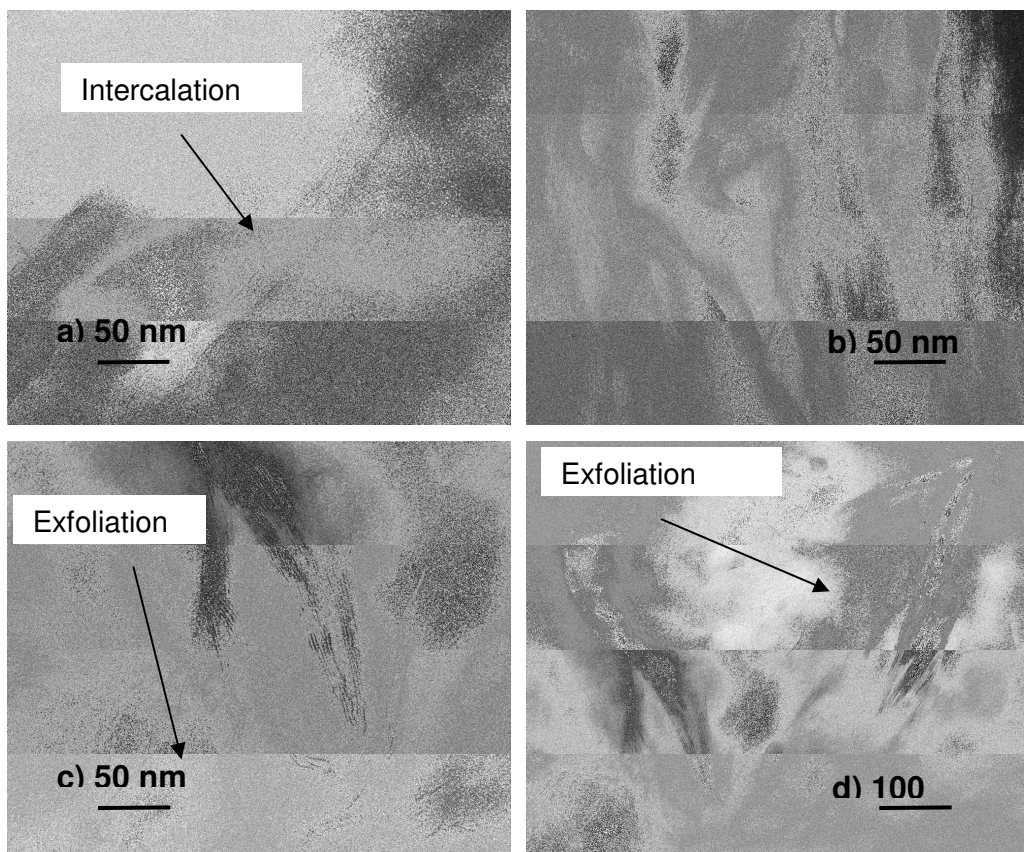


Figure 4.20 TEM micrographs of HD/E-MA-GMA/30B nanocomposite

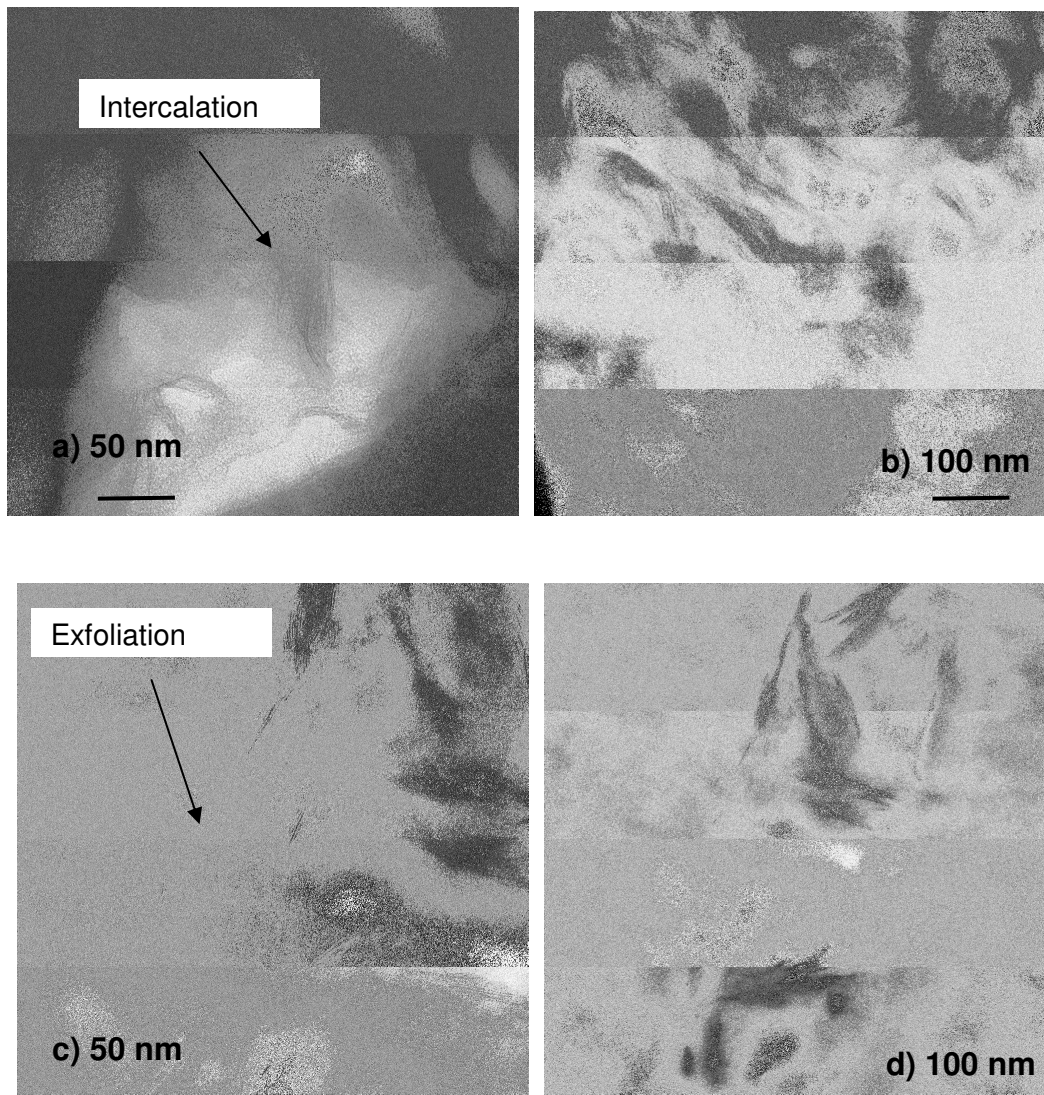


Figure 4.21 TEM micrographs of HD/ E-BA-MAH /30B nanocomposite

Figures 4.22 and 4.23 shows the TEM images of ternary nanocomposites of HD/Compatibilizer/NF8. Dispersion of silicate layers are observed in these micrographs. As seen in figures, in addition to the intercalated structure, exfoliated morphology is also detected with the compatibilizer E-MA-GMA and organoclay NF8. However, with compatibilizer E-BA-MAH, delamination of silicate layers is not detected; only intercalated structure is observed.

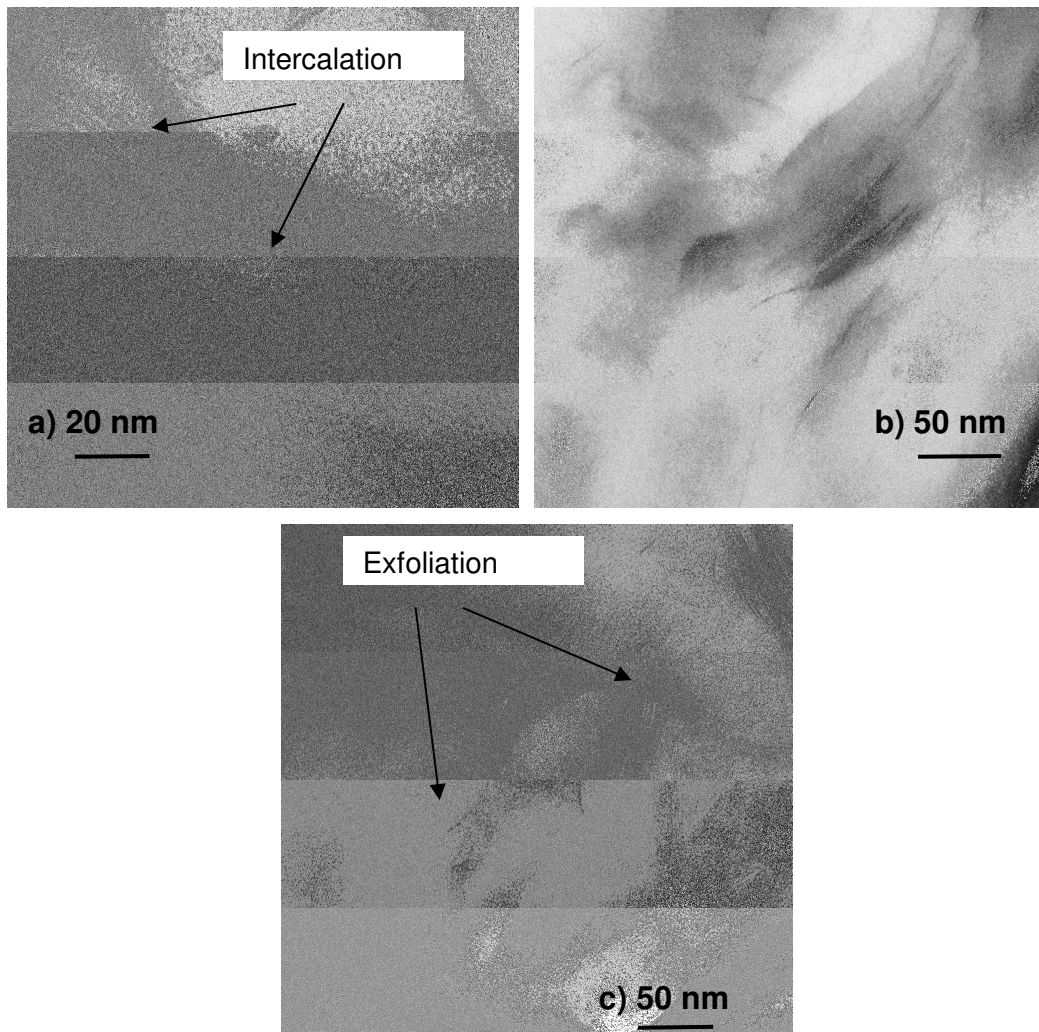


Figure 4.22 TEM micrographs of HD/ E-MA-GMA /NF8 nanocomposite

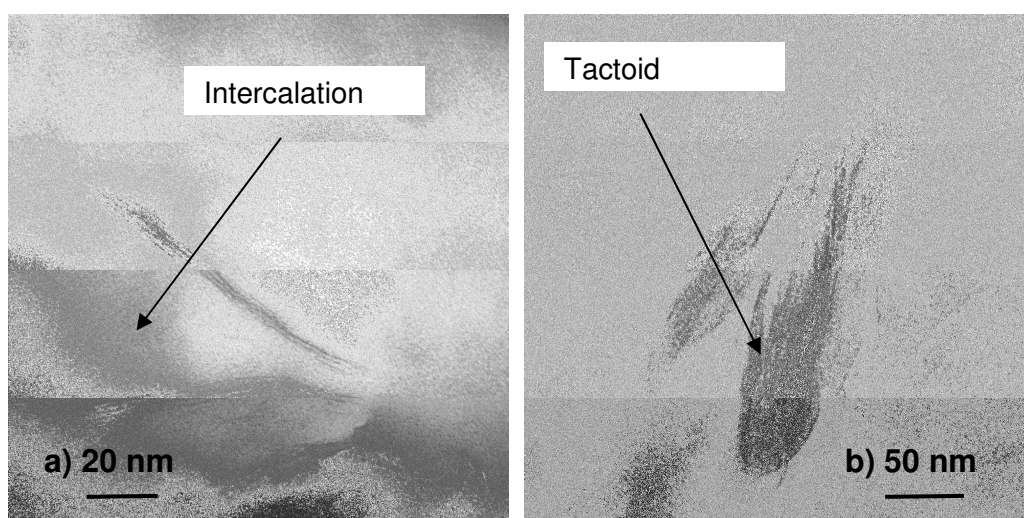


Figure 4.23 TEM micrographs of HD/ E-BA-MAH /NF8 nanocomposite

4.2.2.3 TEM Analysis Results of Nanocomposites with LLDPE Matrix

Figures 4.24 through 4.27 show the TEM micrographs of LLDPE/Compatibilizer/Organoclay nanocomposites. The XRD analysis indicated that the increase in the basal spacing of LLDPE based ternary nanocomposites was lower than that of HDPE based nanocomposites, but higher than that of LDPE based nanocomposites. TEM images support the results of XRD. Good dispersion of clay platelets in LLDPE was achieved in this study. Both intercalated and partially exfoliated structures were detected in TEM micrographs with both compatibilizers and both organoclays. Detection of individual silicate layers was also possible in the TEM images.

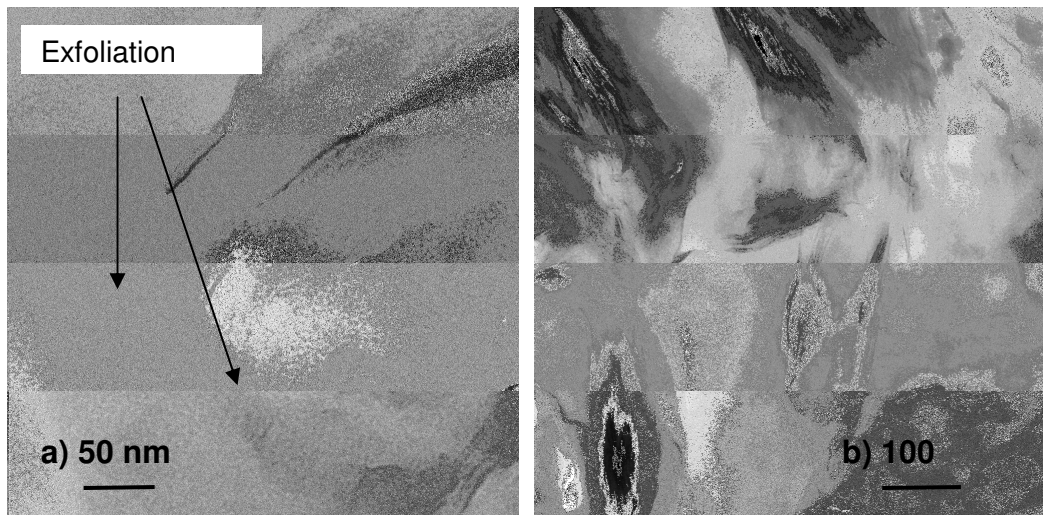


Figure 4.24 TEM micrographs of LIN/E-MA-GMA/30B nanocomposite

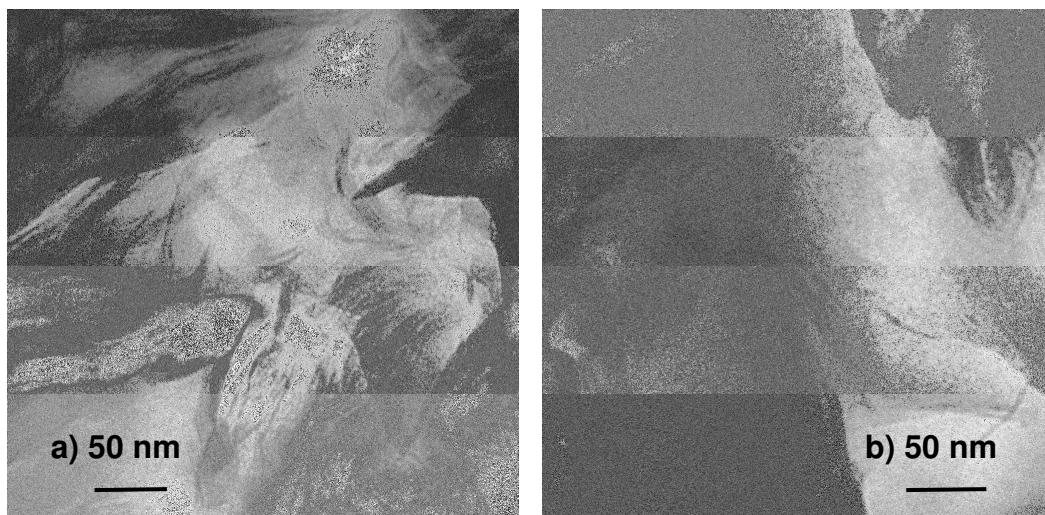


Figure 4.25 TEM micrographs of LIN/ E-BA-MAH /30B nanocomposite

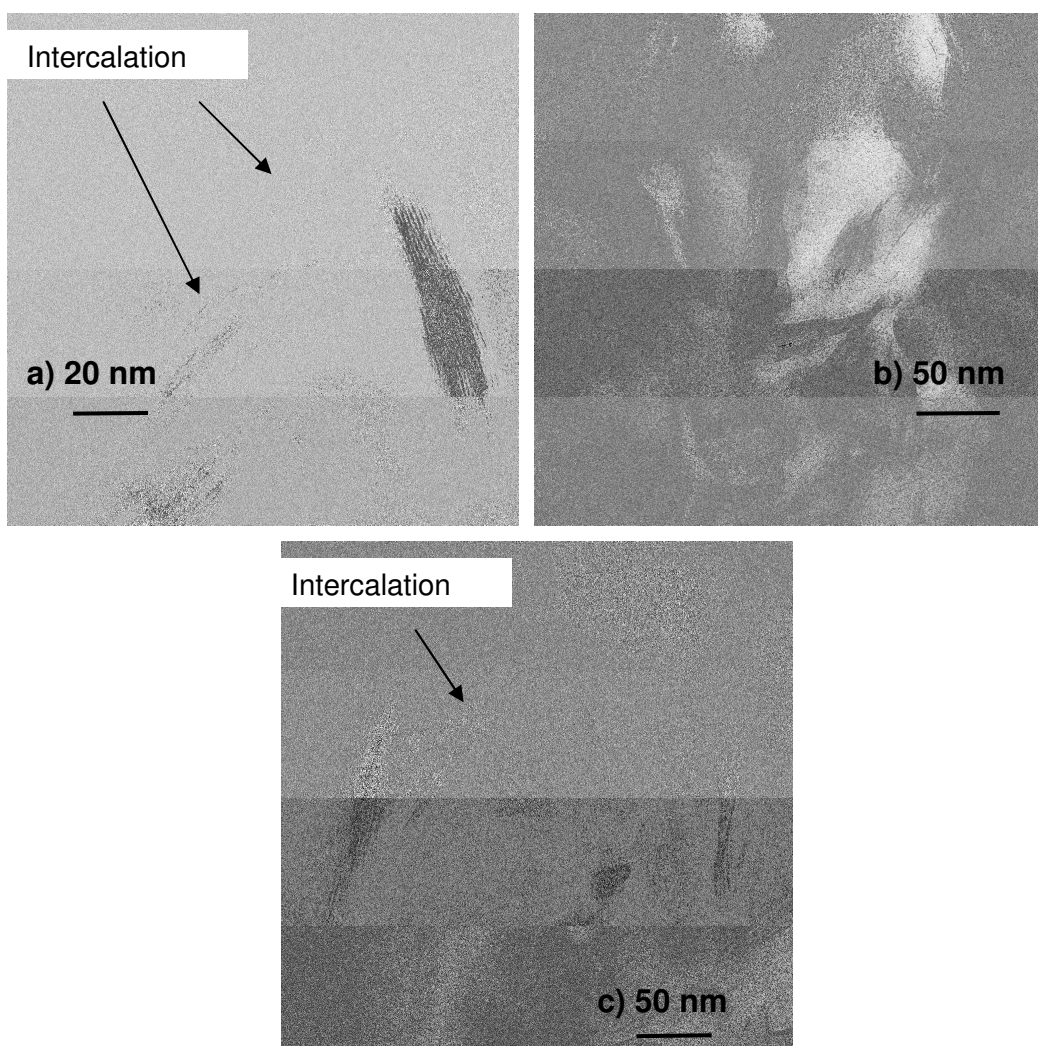


Figure 4.26 TEM micrographs of LIN/ E-MA-GMA /NF8 nanocomposite

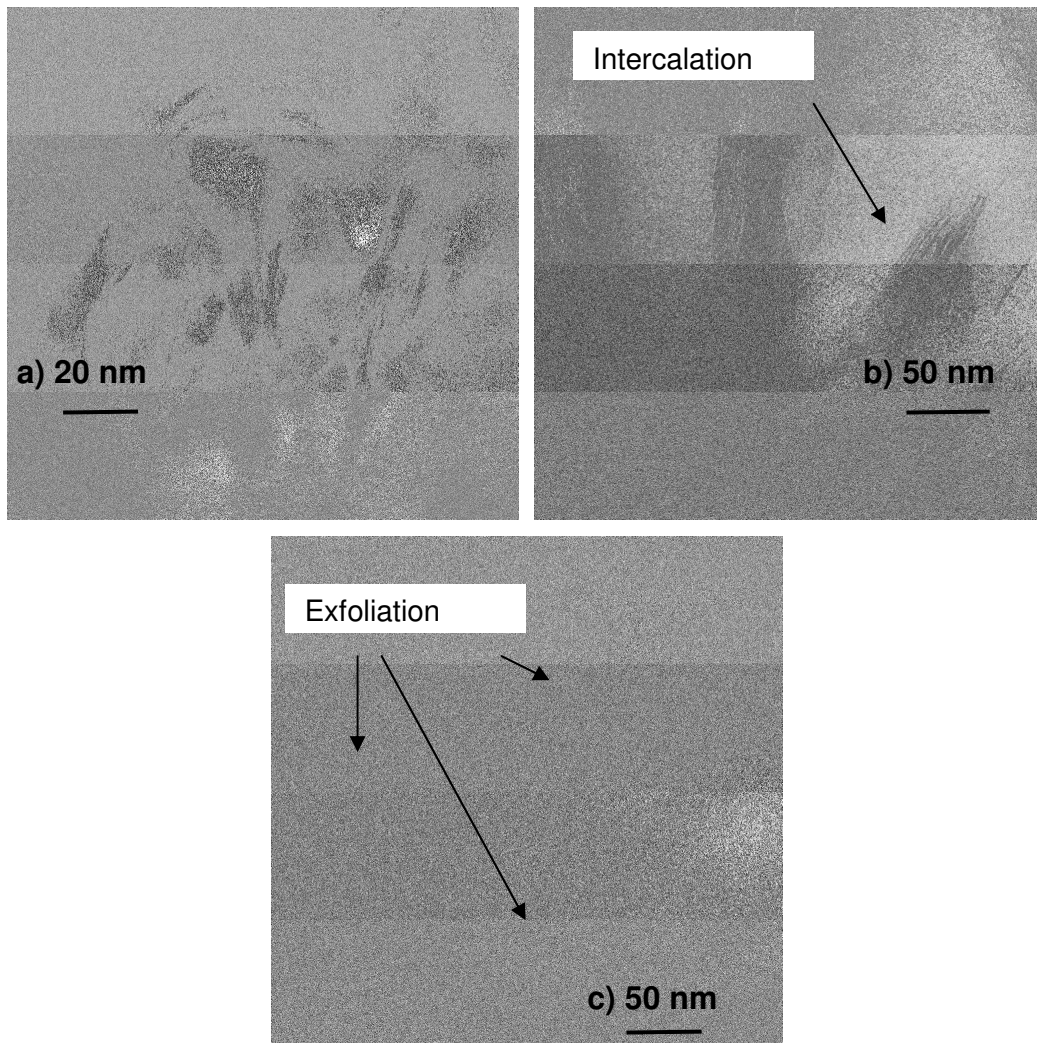


Figure 4.27 TEM micrographs of LIN/ E-BA-MAH /NF8 nanocomposite

According to the TEM analysis results, it can be concluded that XRD analysis was not sufficient to decide on the level of dispersion of clay in the polymer matrices. TEM analysis gave the opportunity to conclude on the morphology of the nanocomposite samples. Both intercalated and partially exfoliated structures were obtained in the ternary nanocomposites of LDPE, HDPE and LLDPE. The results were consistent with the XRD analysis.

4.2.3 SEM Analysis

In addition to XRD and TEM analyses, SEM analyses were also applied to fractured surfaces of neat LDPE, HDPE, LLDPE, blends of PE/Compatibilizer, binary nanocomposites of PE/Organoclay and ternary nanocomposites of PE/Compatibilizer/Organoclay to observe the morphology, namely dispersion of the organoclay and effects of adding compatibilizer to the materials investigated. The fractured surfaces were obtained by using liquid nitrogen for all the samples. In each PE matrix type, samples prepared contained the same composition of raw materials. PE/Compatibilizer blends contained 5 wt % compatibilizer, PE/Organoclay binary nanocomposites contained 2 wt % organoclay and PE/Compatibilizer/Organoclay ternary nanocomposites contained 2 wt % organoclay and 5 wt % compatibilizer. SEM micrographs of all the samples are presented here with magnifications of x250 and x3000.

4.2.3.1 SEM Analysis Results of Samples with LDPE Matrix

Figure 4.28 shows the micrographs of neat LDPE. Smooth surfaces with few crack propagation lines are observed in these micrographs. Figures 4.29 and 4.30 show the fractured surfaces of LD/E-MA-GMA and LD/E-BA-MAH blends, respectively. Interpenetrated and continuous structures were obtained indicating that both compatibilizers are miscible with LDPE. In addition to this, introducing 5 wt % compatibilizer to pure matrix made crack propagation lines coarser. Considering the effects of E-MA-GMA and E-BA-MAH on morphology of neat LDPE, no significant difference was seen in the micrographs of the two blends.

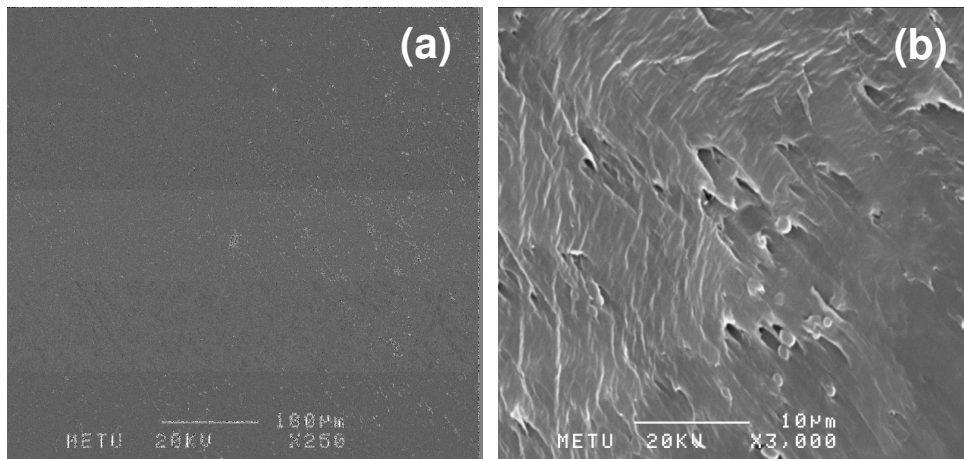


Figure 4.28 SEM micrographs of pure LDPE (a) x250 magnification , (b) x3000 magnification

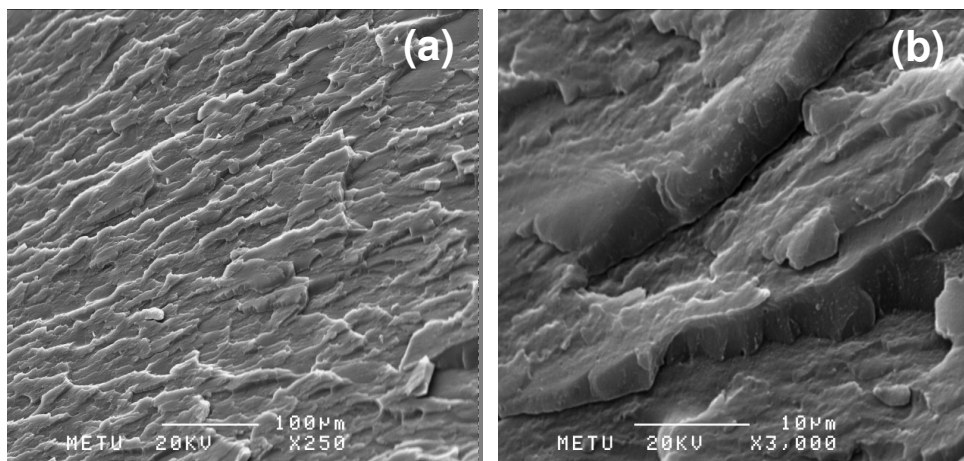


Figure 4.29 SEM micrographs of LD/E-MA-GMA blend (a) x250 magnification (b) x3000 magnification

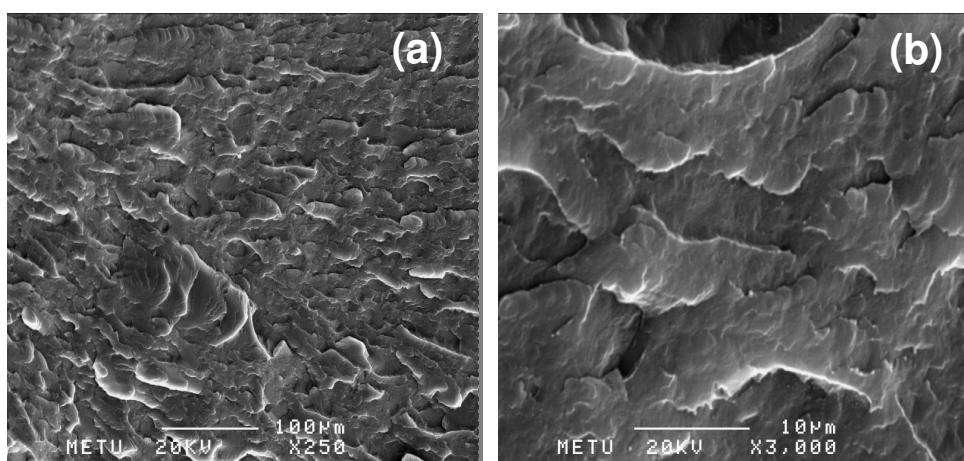


Figure 4.30 SEM micrographs of LD/E-BA-MAH blend (a) x250 magnification (b) x3000 magnification

Figures 4.31 and 4.32 show the micrographs of binary compositions containing 2 wt % organoclay of LD/ Cloisite® 30B and LD/ Nanofil® 8, respectively. It is seen that, smooth, featureless surface of pure LDPE disappeared with organoclay addition. The fractured surface of LD/ Cloisite® 30B is not homogeneous. It contains both tortuous and straight crack propagation lines. As crack propagation lines become shorter and closer, this tortuous structure prevents the continuity of the crack propagation. This feature results in endurance to impact stresses. On the other hand, long straight propagation lines mean that, there are no significant barriers to stop the crack propagation and less energy is enough to fracture the sample.

As seen in Figure 4.32, more straight crack propagation lines are observed in binary compositions of LD/Nanofil® 8 in comparison to LD/Cloisite® 30B. It is also observed from the images that homogeneous dispersion of organoclays was not achieved in binary compositions of LD/Organoclay. Several clay agglomerates are easily detected on the surfaces of both binary composites. These clay agglomerates behave as stress concentrators and may result in low mechanical properties.

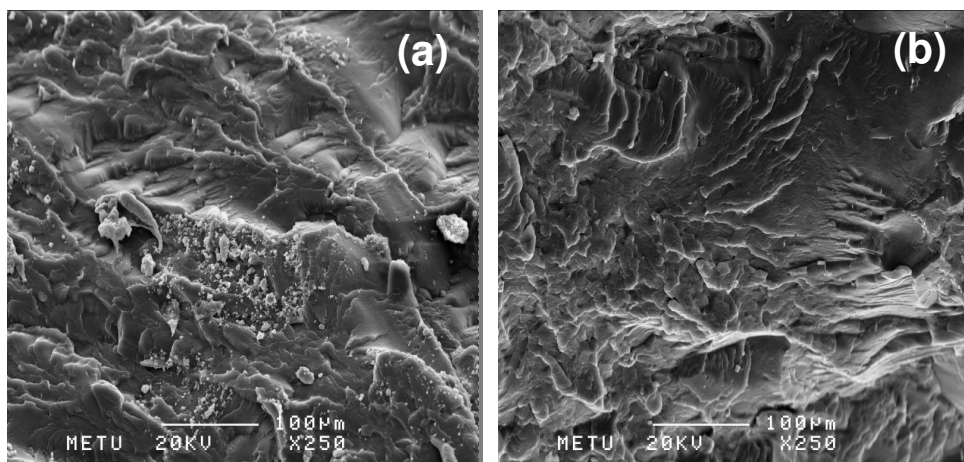


Figure 4.31 SEM micrographs of LD/30B binary nanocomposite (a) x250 magnification (b) x3000 magnification

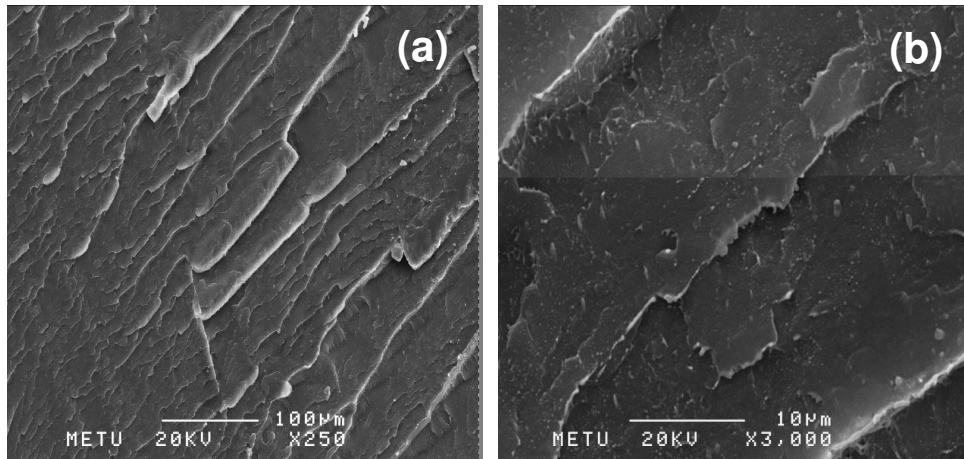


Figure 4.32 SEM micrographs of LD/NF8 binary nanocomposite (a) x250 magnification (b) x3000 magnification

Figures 4.33 and 4.34 show the fractured surfaces of LD/E-MA-GMA/30B and LD/E-BA-MAH/30B ternary nanocomposites, respectively. Comparing these images with binary nanocomposites of LD/30B (Figure 4.31), it is observed that addition of compatibilizer E-MA-GMA resulted in smoother surface, due to better dispersion of organoclay through the polymer matrix. The surface became smooth and homogeneous view is observed. Also, crack propagation lines are smaller and closer.

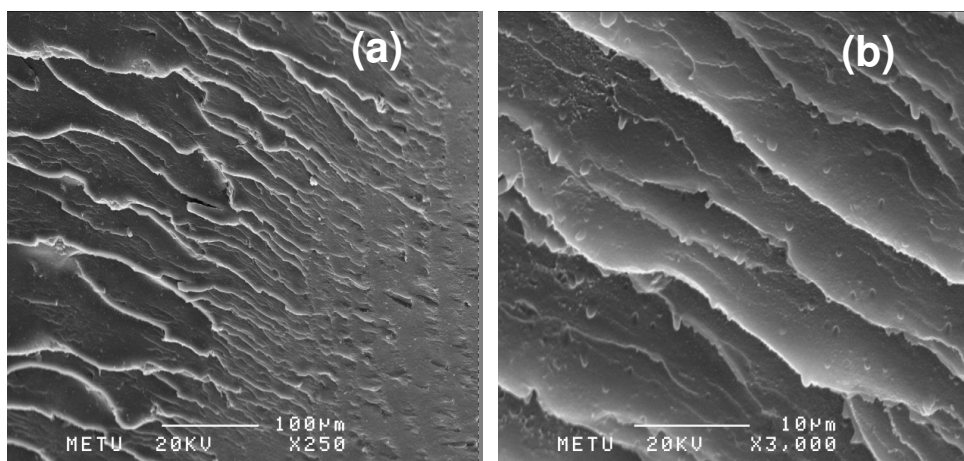


Figure 4.33 SEM micrographs of LD/ E-MA-GMA/30B ternary nanocomposite (a) x250 magnification (b) x3000 magnification

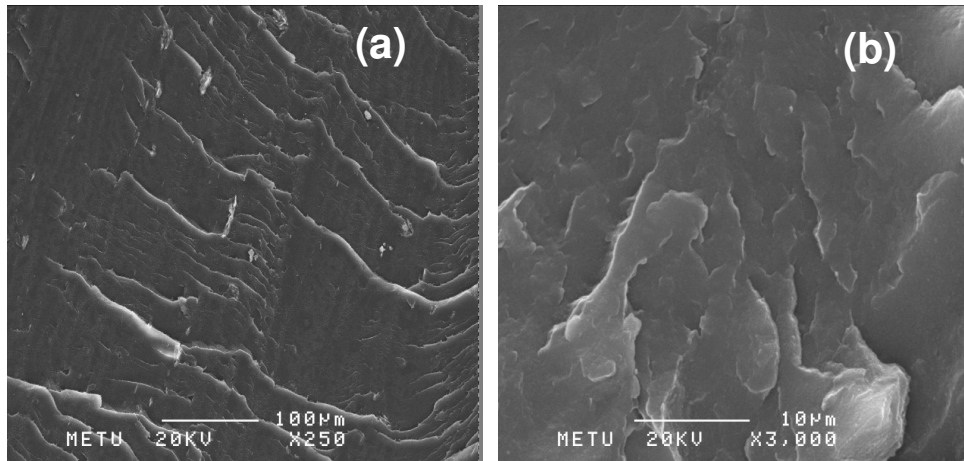


Figure 4.34 SEM micrographs of LD/ E-BA-MAH/30B ternary nanocomposite (a) x250 magnification (b) x3000 magnification

Figures 4.35 and 4.36 belong to the ternary nanocomposites containing Nanofil® 8 and compatibilizers E-MA-GMA and E-BA-MAH, respectively. The surfaces shown in Figures 4.35 and 4.36, became more tortuous by introducing 5 wt % compatibilizer to LD/NF8 (Figure 4.32) composition. Also, straight propagation lines disappeared and short zigzagged lines appeared.

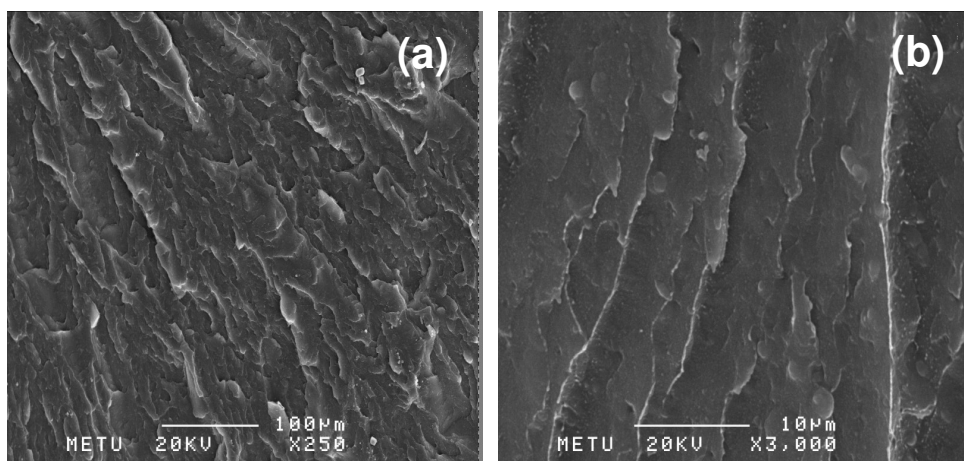


Figure 4.35 SEM micrographs of LD/ E-MA-GMA/NF8 ternary nanocomposite (a) x250 magnification (b) x3000 magnification

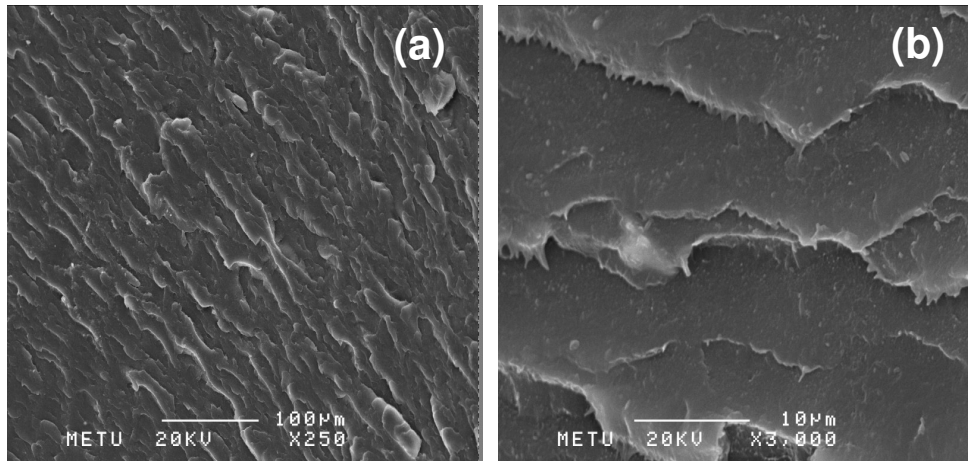


Figure 4.36 SEM micrographs of LD/ E-BA-MAH/NF8 ternary nanocomposite (a) x250 magnification (b) x3000 magnification

4.2.3.2 SEM Analysis Results of Samples with HDPE Matrix

Figure 4.37 shows the SEM micrograph of pure HDPE. The fractured surface of HDPE is also smooth and homogeneous. Straight long crack propagation lines are observed. There are no barriers to stop the crack on the surface.

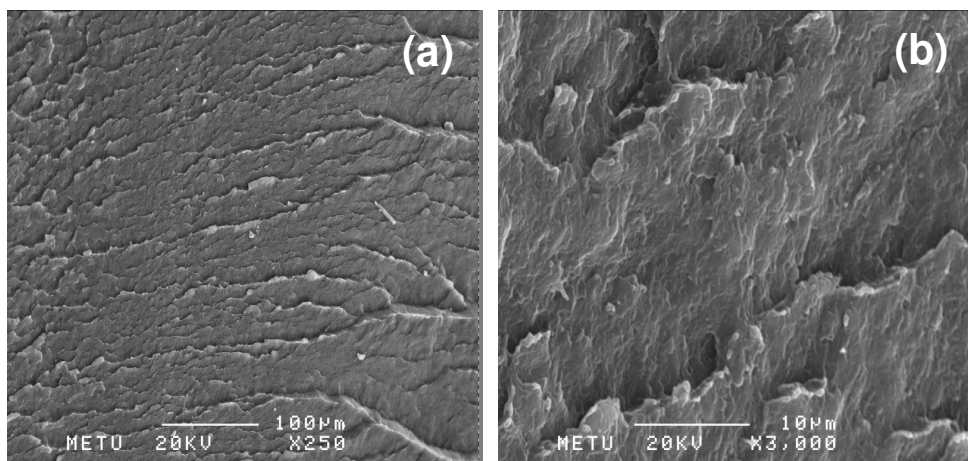


Figure 4.37 SEM micrographs of pure HDPE (a) x250 magnification , (b) x3000 magnification

Figures 4.38 and 4.39 show the fractured surfaces of HD/Compatibilizer blends containing 5 wt % compatibilizer. Homogeneous structures are observed with addition of both E-MA-GMA and E-BA-MAH to HDPE. Lines are interpenetrated and no phase separation is observed indicating that both compatibilizers are miscible with HDPE.

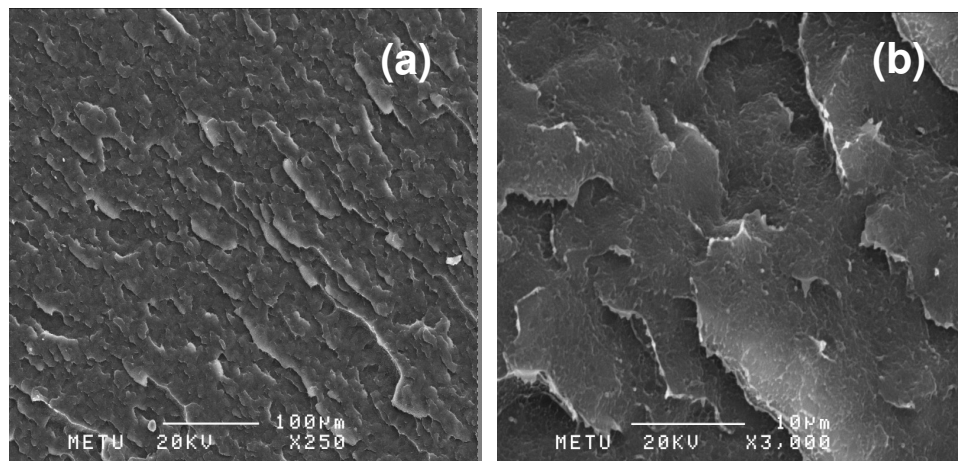


Figure 4.38 SEM micrographs of HD/E-MA-GMA blend (a) x250 magnification (b) x3000 magnification

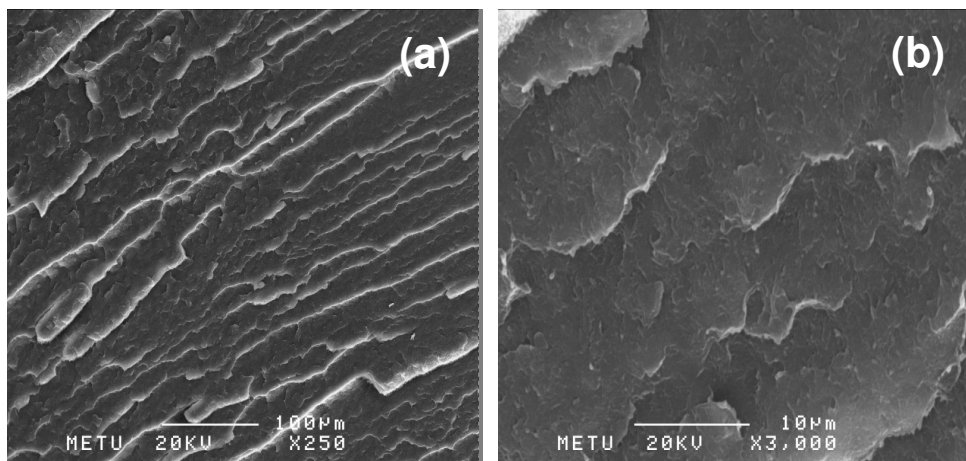


Figure 4.39 SEM micrographs of HD/E-BA-MAH blend (a) x250 magnification (b) x3000 magnification

Figures 4.40 and 4.41 represent the fractured surfaces of binary nanocomposites of HD/30B and HD/NF8 containing 2 wt % organoclay. Addition of organoclay resulted in change of the morphology of the surfaces. Smooth surface of the neat polymer disappeared. Tortuous structure and smaller crack propagation lines are observed. Homogeneous distribution of organoclay through the polymer matrix is observed in images with X3000 magnification.

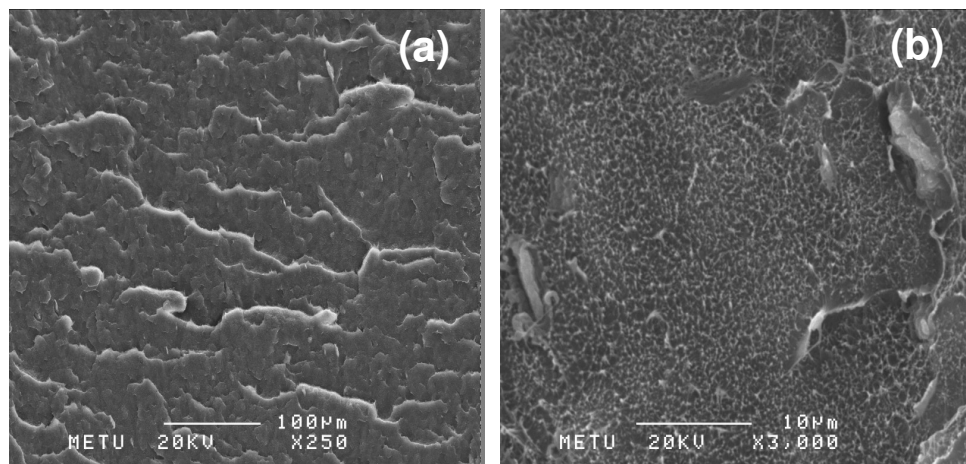


Figure 4.40 SEM micrographs of HDPE/30B binary nanocomposite (a) x250 magnification (b) x3000 magnification

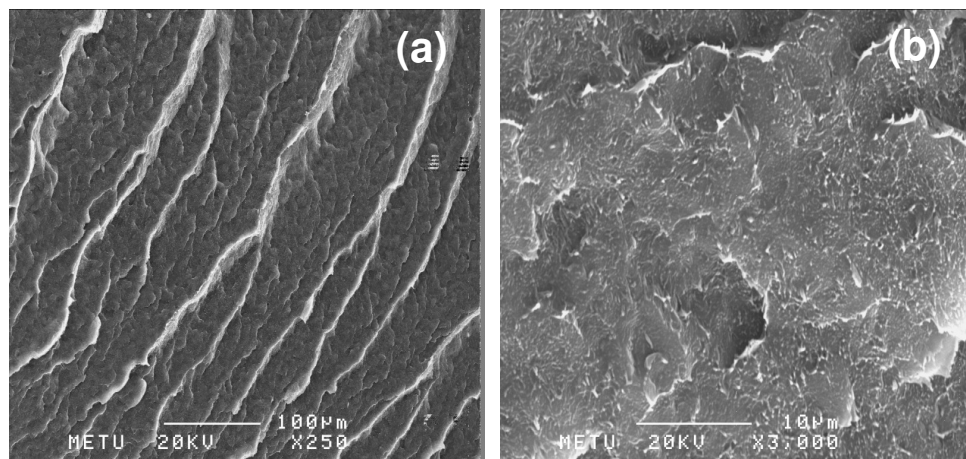


Figure 4.41 SEM micrographs of HDPE/NF8 binary nanocomposite (a) x250 magnification (b) x3000 magnification

Addition of compatibilizer to binary systems of HD/Organoclay resulted in significant change in the morphology of fractured surfaces. Figures 4.42 through 4.45 show the morphology of ternary nanocomposites HD/E-MA-GMA/30B and HD/E-BA-MAH/30B, HD/E-MA-GMA/NF8 and HD/E-BA-MAH/NF8, respectively.

Featureless surface of neat HDPE is destroyed and crack propagation lines are not long and straight. It is seen that, several shorter, closer, nonlinear, circular lines exist on the surface, indicating good dispersion of organoclay in the polymer matrix. These nonlinear lines grow until they interfere with each other. At the interface the stress fields interact and they prevent crack propagation by reducing the applied stress by distributing it around the interface [166].

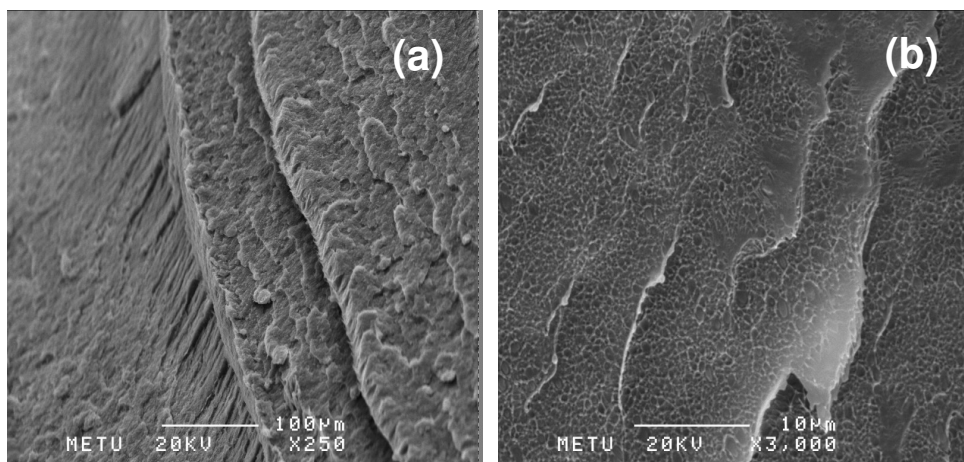


Figure 4.42 SEM micrographs of HDPE/ E-MA-GMA/30B ternary nanocomposite (a) x250 magnification (b) x3000 magnification

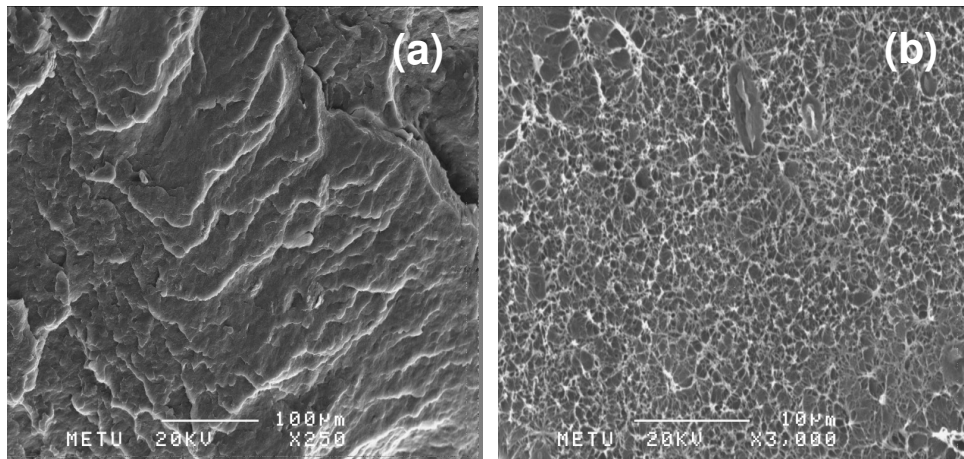


Figure 4.43 SEM micrographs of HDPE/ E-BA-MAH/30B ternary nanocomposite (a) x250 magnification (b) x3000 magnification

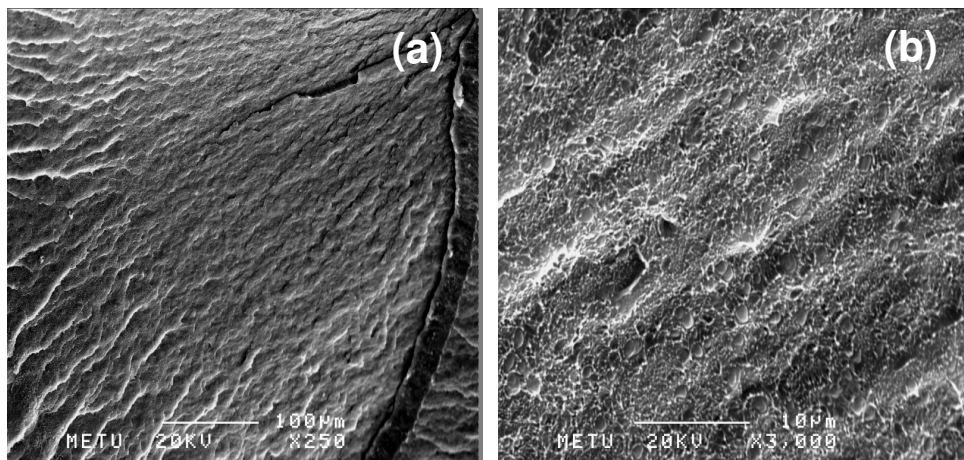


Figure 4.44 SEM micrographs of HDPE/ E-MA-GMA/NF8 ternary nanocomposite (a) x250 magnification (b) x3000 magnification

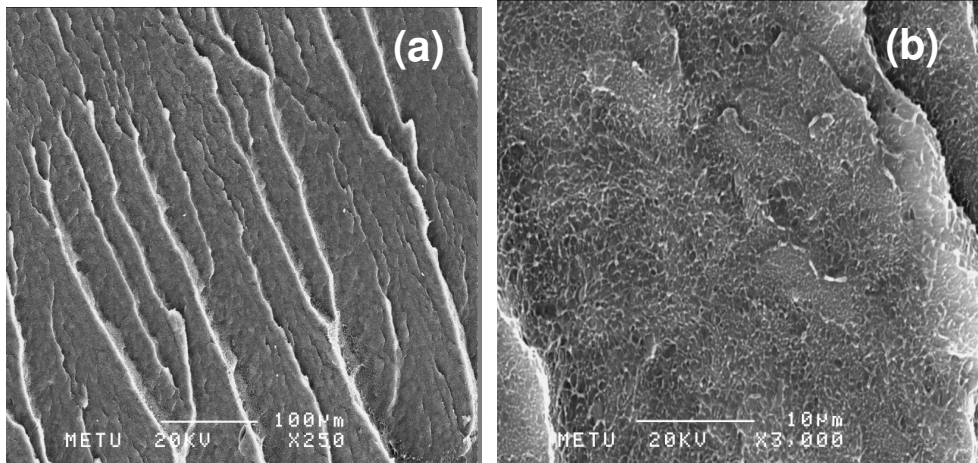


Figure 4.45 SEM micrographs of HDPE/ E-BA-MAH/NF8 ternary nanocomposite (a) x250 magnification (b) x3000 magnification

It can be concluded that E-MA-GMA and E-BA-MAH are both miscible with HDPE. They had remarkable effects on improving the interaction between the HDPE and organoclays 30B and NF8, enhancing the organoclay distribution through the polymer matrix. These results also support the XRD and TEM analyses results.

4.2.3.3 SEM Analysis Results of Samples with LLDPE Matrix

Figure 4.46 shows the fractured surface of neat LLDPE. Similar to LDPE and HPE, neat LLDPE exhibits smooth and homogeneous surface.

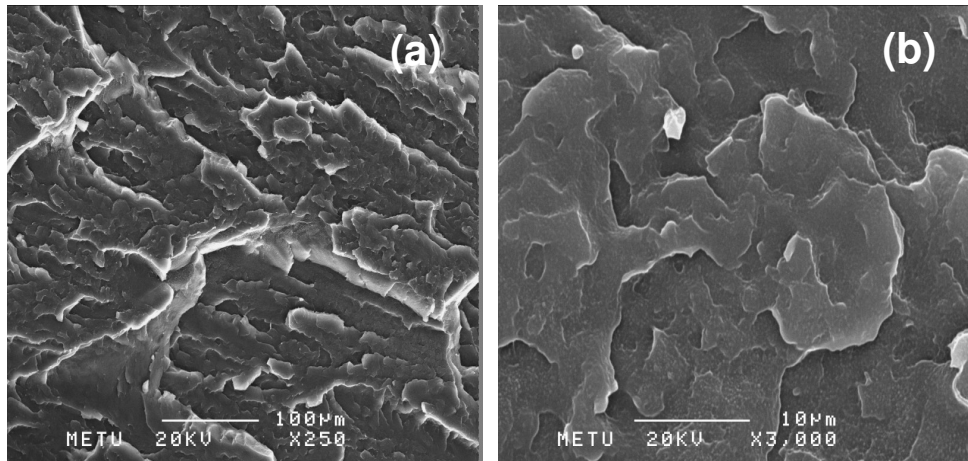


Figure 4.46 SEM micrographs of pure LLDPE (a) x250 magnification , (b) x3000 magnification

Figures 4.47 and 4.48 represent the fractured surfaces of blends of LIN/E-MA-GMA and LIN/E-BA-MAH containing 5 wt % compatibilizer. Both compatibilizers had similar effects on morphology. Long and straight crack propagation lines are detected. Smoothness of neat LLDPE did not disappear indicating that compatibilizers are miscible with LLDPE.

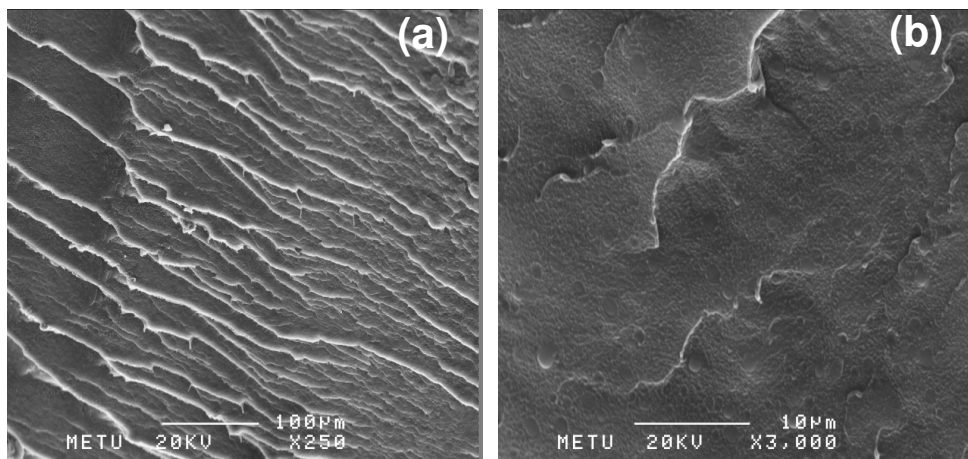


Figure 4.47 SEM micrographs of LIN/E-MA-GMA blend (a) x250 magnification (b) x3000 magnification

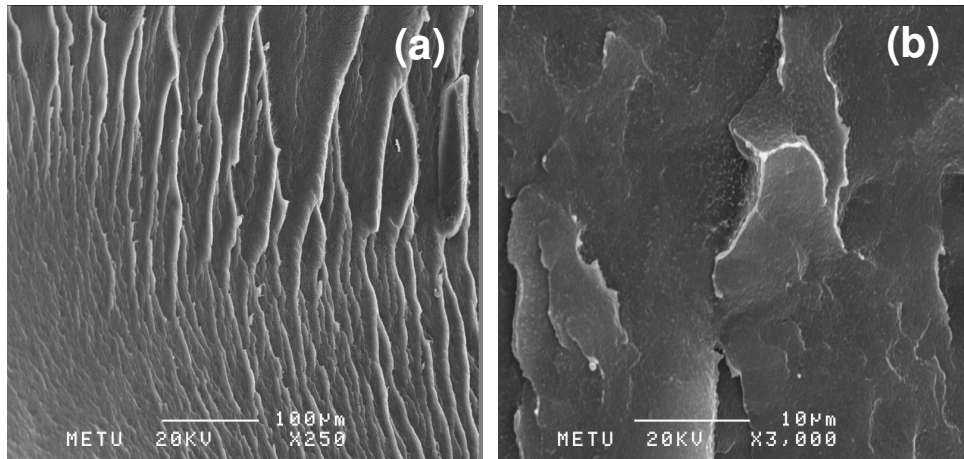


Figure 4.48 SEM micrographs of LIN/E-BA-MAH blend (a) x250 magnification (b) x3000 magnification

Considering the binary compositions of LIN/30B and LIN/NF8 seen in Figures 4.49 and 4.50, respectively, addition of 2 wt % organoclay to neat LLDPE resulted in more tortuous surface. Several crack propagation lines occurred at different magnifications. Homogeneity of surface also disappeared due to the dispersion of organoclays. Agglomerates of organoclay are detected in the images.

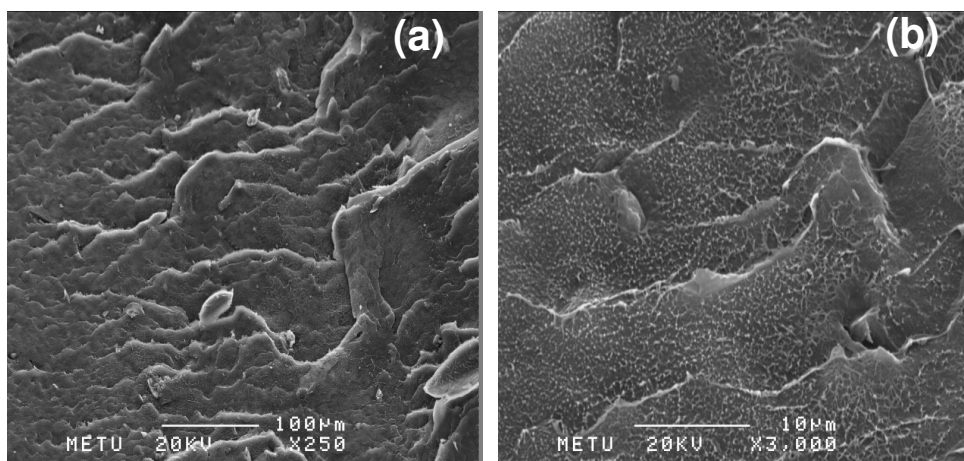


Figure 4.49 SEM micrographs of LIN/30B binary nanocomposite (a) x250 magnification (b) x3000 magnification

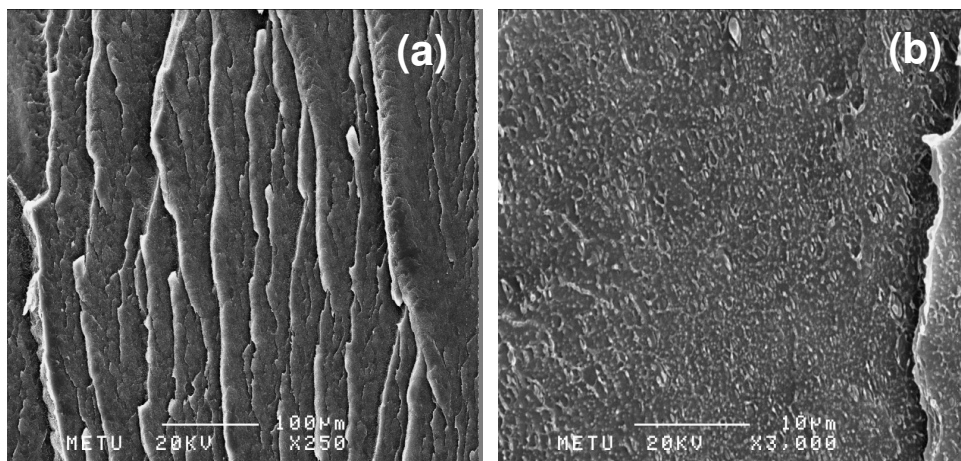


Figure 4.50 SEM micrographs of LIN/NF8 binary nanocomposite (a) x250 magnification (b) x3000 magnification

Similar discussion as in the previous section on ternary nanocomposites of HDPE, is also valid for the ternary nanocomposites of LLDPE. Addition of 5 wt % compatibilizer to binary compositions of LIN/Organoclay had significant effects on dispersion of organoclay as seen in Figures 4.51 through 4.54. Spider weblike structures including short, close, circular, non linear crack propagation lines are observed in all the ternary nanocomposite types of LLDPE. Compatibilizers E-MA-GMA and E-BA-MAH are miscible with LLDPE, and they increased the dispersion of organoclays 30B and NF8 in the polymer matrix.

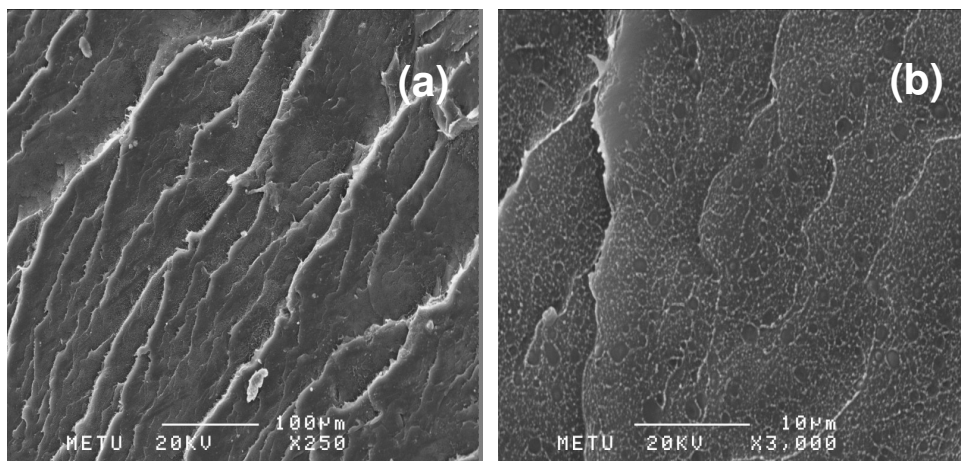


Figure 4.51 SEM micrographs of LIN/ E-MA-GMA/30B ternary nanocomposite (a) x250 magnification (b) x3000 magnification

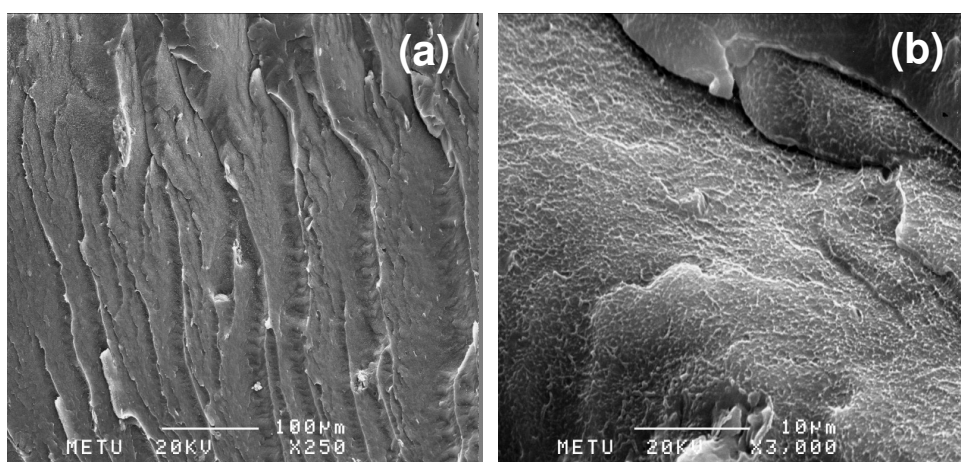


Figure 4.52 SEM micrographs of LIN/ E-BA-MAH/30B ternary nanocomposite (a) x250 magnification (b) x3000 magnification

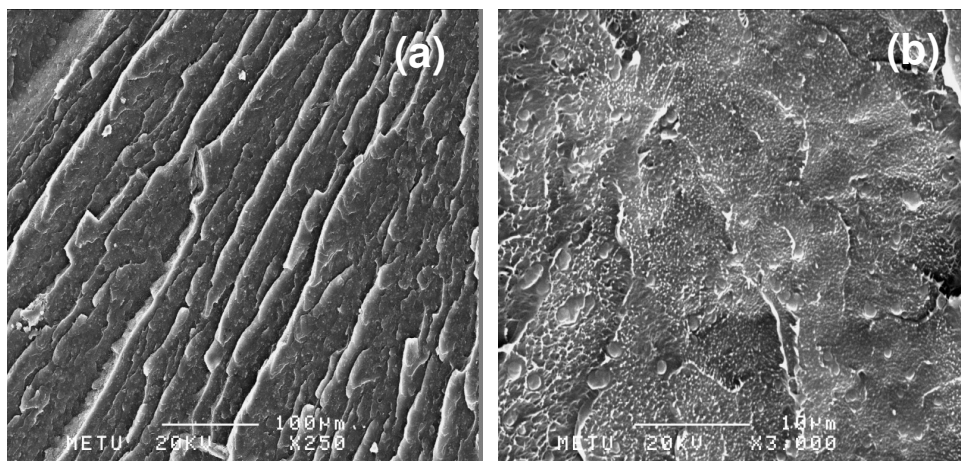


Figure 4.53 SEM micrographs of LIN/E-MA-GMA/NF8 ternary nanocomposite (a) x250 magnification (b) x3000 magnification

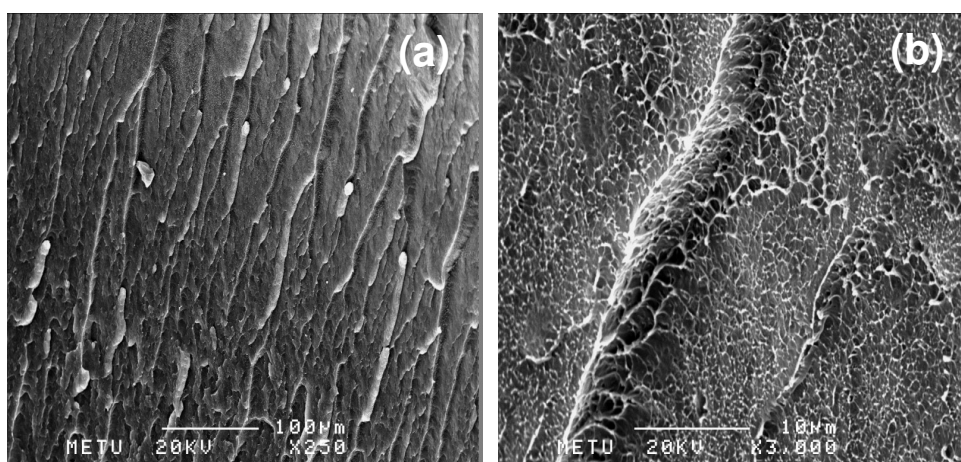


Figure 4.54 SEM micrographs of LIN/E-BA-MAH/NF8 ternary nanocomposite (a) x250 magnification (b) x3000 magnification

4.3 Flow Properties

4.3.1 MFI Test Results

Effects of organoclay and compatibilizer on flow properties were investigated by melt flow index tests that were applied at temperatures 160 °C, 235°C and 180°C to LDPE, HDPE and LLDPE matrix samples, respectively with a load of 2.16 kg. Table 4.10-a shows the melt flow index values of neat polyethylenes at 190 °C. MFI results of neat compatibilizers at selected process temperatures are given in Table 4.10-b. These results are consistent with the data given in technical data sheets of each polymer matrix. According to these results, melt blending temperatures were determined. For LDPE and LLDPE process temperature lower than 190 °C, for HDPE process temperature higher than 190 °C was selected to have equal MFI values of the neat resins.

Table 4.10-a MFI test results of neat polyethylenes at 190 °C

Sample	MFI (g/10min) @190 °C
LDPE	30.84 ± 0.05
HDPE	6.2 ± 0.08
LLDPE	21.87 ± 0.11

Table 4.10-b MFI test results of neat compatibilizers at 160 °C, 180 °C and 235 °C

Sample	MFI (g/10min) @160 °C	MFI (g/10min) @180 °C	MFI (g/10min) @235 °C
E-MA-GMA	3.46 ± 0.034	3.96 ± 0.087	6.64 ± 0.317
E-BA-MAH	1.36 ± 0.061	2.42 ± 0.086	18.6 ± 1.08

4.3.1.1 MFI Test Results of Samples with LDPE Matrix

Tables 4.11 through 4.13 give the MFI test results of LDPE/Compatibilizer blends, LDPE/Organoclay compositions and LDPE/Compatibilizer/Organoclay compositions at 160 °C. Addition of E-MA-GMA or E-BA-MAH compatibilizers to neat LDPE resulted in decrease of MFI values. Increase in compatibilizer content also resulted in lower MFI values in comparison to that of neat LDPE. LDPE has a non-polar structure. On the other hand both compatibilizers have more polar structures. Due to the non-polar structure, LDPE can easily flow through the MFI equipment barrel. However, addition of a polar compatibilizer to non-polar polymer results in a polar polymer blend. This increase in polarity might result in sticking of the polymer blend on the barrel walls and increase the viscosity and decrease the MFI value. In addition to this, increase in the compatibilizer content increases the polarity, thus adhesion of the polymer blend on the walls.

Table 4.11 MFI test results of LDPE/Compatibilizer blends at 160 °C

Sample	Compatibilizer wt %	MFI (g/10 min)
LDPE	-	14.72 ± 0.09
LD/E-MA-GMA	5	14.10 ± 0.21
LD/E-MA-GMA	10	13.32 ± 0.16
LD/E-BA-MAH	5	13.26 ± 0.13
LD/E-BA-MAH	10	13.16 ± 0.10

Considering the LD/Organoclay binary compositions in Table 4.12, it is observed that addition of organoclay to LDPE resulted in decrease of MFI value, i.e. increase in viscosity. Organoclay behaved as filler. Moreover, dispersion of organoclay layers in polymer matrix prevented the flow of the LDPE chains. Increase in organoclay content increased the viscosity, and thus decreased the MFI value as expected.

As mentioned above, good dispersion of organoclay is an important factor affecting the flow characteristics of polymers. Good dispersion of organoclay results in higher viscosity, i.e. lower melt flow index value. Table 4.13 shows that remarkable decrease in MFI values of LDPE/Organoclay compositions containing 2 wt % organoclay took place after addition of 5 wt % compatibilizer to LDPE/Organoclay system. Based on the flow characterization test results it is concluded that addition of compatibilizer increased the dispersion of organoclay through polymer matrix according to the flow characterization test results.

Table 4.12 MFI test results of LDPE/Organoclay nanocomposites at 160 °C

Sample	Organoclay wt %	MFI (g/10 min)
LDPE	-	14.72 ± 0.09
LD/30B 2%	2	13.79 ± 0.05
LD/30B 4%	4	13.81 ± 0.06
LD/30B 6%	6	13.31 ± 0.08
LD/NF8 2%	2	14.47 ± 0.13
LD/NF8 4%	4	13.69 ± 0.04
LD/NF8 6%	6	13.53 ± 0.07

Table 4.13 MFI test results of LDPE/Compatibilizer/Organoclay nanocomposites at 160 °C

Sample	Compatibilizer wt %	Organoclay wt %	MFI (g/10 min)
LDPE	-	-	14.72 ± 0.09
LD/E-MA-GMA/30B	5	2	12.74 ± 0.11
LD/E-BA-MAH/30B	5	2	12.53 ± 0.08
LD/E-MA-GMA/NF8	5	2	11.54 ± 0.09
LD/E-BA-MAH/NF8	5	2	11.47 ± 0.05

4.3.1.2 MFI Test Results of Samples with HDPE Matrix

Tables 4.14 through 4.16 display MFI test results of HDPE/Compatibilizer blends, HDPE/Organoclay Nanocomposites and LD/Compatibilizer/Organoclay nanocomposites at 235 °C. The same discussions made on LDPE in the previous section are valid for HDPE containing samples. Addition of compatibilizer resulted in lower MFI values due to the sticking of the polar polymer blend to metal barrel wall. Addition of organoclay also decreased the MFI value due to the filler effect, and thus increased the viscosity of the polymer. Both compatibilizers, E-MA-GMA and E-BA-MAH are compatible with HDPE and organoclays 30B and NF8, thus good dispersion of clay platelets was achieved and this prevented the flow of the polymer resulting in lower MFI values in the ternary nanocomposites in comparison to binary blends and binary composites.

Table 4.14 MFI test results of HDPE/Compatibilizer blends at 235 °C

Sample	Compatibilizer wt %	MFI (g/10 min)
HDPE	-	13.55 ± 0.14
HD/E-MA-GMA	5	9.21 ± 0.04
HD/E-MA-GMA	10	9.07 ± 0.04
HD/E-BA-MAH	5	10.27 ± 0.05
HD/E-BA-MAH	10	10.39 ± 0.04

Table 4.15 MFI test results of HDPE/Organoclay nanocomposites at 235 °C

Sample	Organoclay wt %	MFI (g/10 min)
HDPE	-	13.55 ± 0.14
HD/30B 2%	2	12.47 ± 0.08
HD/30B 4%	4	12.29 ± 0.09
HD/30B 6%	6	12.04 ± 0.03
HD/NF8 2%	2	13.10 ± 0.04
HD/NF8 4%	4	12.84 ± 0.05
HD/NF8 6%	6	12.68 ± 0.03

Table 4.16 MFI test results of HDPE/Compatibilizer/Organoclay nanocomposites at 235 °C

Sample	Compatibilizer wt %	Organoclay wt %	MFI (g/10 min)
HDPE	-	-	13.55 ± 0.14
HD/E-MA-GMA/30B	5	2	10.78 ± 0.05
HD/E-BA-MAH/30B	5	2	11.29 ± 0.11
HD/E-MA-GMA/NF8	5	2	10.12 ± 0.04
HD/E-BA-MAH/NF8	5	2	11.14 ± 0.06

4.3.1.3 MFI Test Results of Samples with LLDPE Matrix

MFI values of LLDPE/Compatibilizer blends, LLDPE/Organoclay binary compositions and LLDPE/Compatibilizer/Organoclay ternary Nanocomposites are given in Tables 4.17-4.19, respectively. The tests were carried out at 180 °C.

Expected effect of compatibilizers are also seen in LIN/E-MA-GMA and LIN/E-BA-MAH blends. MFI value of LLDPE decreased with the introduction of polar compatibilizers. Increase in the compatibilizer contents resulted in increase in the viscosity, i.e. decrease in MFI values.

Organoclay addition to polymer decreased the MFI value. Increase in clay content also increased the viscosity due to the filler effect.

Effects of dispersion of organoclay on flow properties are also observed in ternary composites with LLDPE matrix. Lower MFI values are recorded for the ternary nanocomposites due to the same reasons as explained in the previous section.

Table 4.17 MFI test results of LLDPE/Compatibilizer blends at 180 °C

Sample	Compatibilizer wt %	MFI (g/10 min)
LINPE	-	17.57 ± 0.08
LIN/E-MA-GMA	5	15.91 ± 0.05
LIN/E-MA-GMA	10	15.17 ± 0.14
LIN/E-BA-MAH	5	15.67 ± 0.16
LIN/E-BA-MAH	10	14.90 ± 0.09

Table 4.18 MFI test results of LLDPE/Organoclay nanocomposites at 180 °C

Sample	Organoclay wt %	MFI (g/10 min)
LINPE	-	17.57 ± 0.08
LIN/30B 2%	2	17.50 ± 0.18
LIN/30B 4%	4	17.12 ± 0.03
LIN/30B 6%	6	17.00 ± 0.18
LIN/NF8 2%	2	17.26 ± 0.19
LIN/NF8 4%	4	17.23 ± 0.08
LIN/NF8 6%	6	16.54 ± 0.11

Table 4.19 MFI test results of LLDPE/Compatibilizer/Organoclay nanocomposites at 180 °C

Sample	Compatibilizer wt %	Organoclay wt %	MFI (g/10 min)
LINPE	-	-	17.57 ± 0.08
LIN/E-MA-GMA/30B	5	2	16.49 ± 0.19
LIN/E-BA-MAH/30B	5	2	15.48 ± 0.08
LIN/E-MA-GMA/NF8	5	2	16.24 ± 0.29
LIN/E-BA-MAH/NF8	5	2	14.13 ± 0.15

4.4 Thermal Characterization

4.4.1 DSC Analysis Test Results

Thermal characterization of samples was done by differential scanning calorimetry analysis. DSC is a rapid analysis method for determination of polymer crystallinity that is based on the heat required to melt (fusion) the polymer. Percent crystallinity is calculated by normalizing the observed heat of fusion to that of a 100 % crystalline sample of the same polymer.

The thermogram of the samples obtained are given in Appendix B, Figures B.1 through B.27. Melting point and % crystallinity data of LDPE; HDPE and LLDPE based samples are listed in Tables 4.20 through 4.22, respectively.

Polymer crystallinity has significant effects on polymer properties such as hardness, tensile strength, modulus, and melting point. Figure 4.55 is a representative diagram for a mixed crystalline-amorphous polymer.

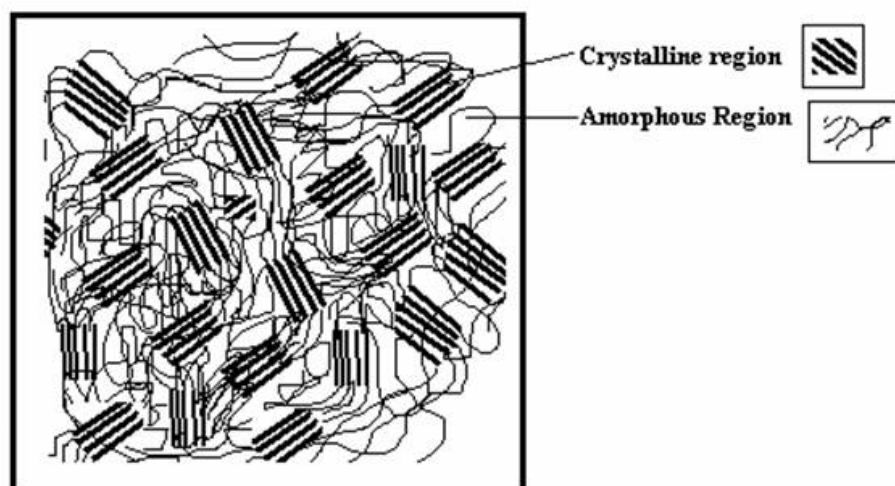


Figure 4.55 Schematic of amorphous-crystalline polymer structure [167]

Polymer crystallinity of the samples were calculated by using the following formula;

$$\% \text{ crystallinity} = \Delta H_f / (\Delta H_{f_0} \times (1-w)) \times 100 \quad (4.1)$$

where ΔH_f is the heat of fusion measured, ΔH_{f_0} is the heat of fusion of 100 % crystalline polymer and w is the weight fraction of clay. The value of the heat of fusion, ΔH_{f_0} , for 100 % crystalline LDPE and HDPE was taken as 293.1 J/g and 276.7 J/g for LLDPE [173].

Considering the neat PE types, HDPE had higher percent crystallinity due to the presence of few branches in its structure. On the other hand, LDPE had lower crystallinity, in comparison to HDPE since its highly branched chemical structure resulted in mainly amorphous structure.

Table 4.20 DSC analysis results of samples with LDPE matrix

Sample	Melt Peak Temperature (°C)	Enthalpy ΔH_f (J/g)	Crystallinity (%)
LDPE	104.4	67.8	23.1
LD/E-MA-GMA %5	106.3	59.1	21.2
LD/E-BA-MAH %5	105.3	64.3	23.1
LD/30B %2	106.4	61.7	21.5
LD/NF8 %2	105.3	63.1	22.0
LD/E-MA-GMA/30B	105.1	63.5	23.3
LD/E-BA-MAH/30B	104.4	72.3	26.5
LD/E-MA-GMA/NF8	104.8	63.4	23.3
LD/E-BA-MAH/NF8	105.4	56.9	20.9

Table 4.21 DSC analysis results of samples with HDPE matrix

Sample	Melt Peak Temperature (°C)	Enthalpy ΔH_f (J/g)	Crystallinity (%)
HDPE	131.9	159.6	54.5
HD/E-MA-GMA %5	132.9	145.1	52.1
HD/E-BA-MAH %5	133.8	148.5	53.4
HD/30B %2	134.3	142.7	49.7
HD/NF8 %2	133.8	159.3	55.5
HD/E-MA-GMA/30B	134.3	134.0	49.2
HD/E-BA-MAH/30B	133.2	145.7	53.5
HD/E-MA-GMA/NF8	136.8	145.7	53.5
HD/E-BA-MAH/NF8	134.4	141.6	51.9

Table 4.22 DSC analysis results of samples with LLDPE matrix

Sample	Melt Peak Temperature (°C)	Enthalpy ΔH_f (J/g)	Crystallinity (%)
LLDPE	124.0	81.5	29.5
LIN/E-MA-GMA %5	124.0	70.7	26.9
LIN/E-BA-MAH %5	124.5	66.7	25.4
LIN/30B %2	124.4	74.4	27.4
LIN/NF8 %2	124.8	68.4	25.2
LIN/E-MA-GMA/30B	124.5	59.6	23.2
LIN/E-BA-MAH/30B	124.7	62.7	24.4
LIN/E-MA-GMA/NF8	124.4	74.2	28.8
LIN/E-BA-MAH/NF8	123.8	70.0	27.2

According to the results given in Tables 4.20–4.22, addition of either 5 wt % compatibilizer or 2 wt % organoclay to LDPE, HDPE and LLDPE did not

significantly influence the melting temperature and the enthalpy of fusion of the polymer matrices. Considering the ternary nanocomposites of polyethylenes, decrease in degree of crystallization was seen. This was an evidence of better dispersion of nanoscale organoclays through polymer matrices that organoclays prevented the alignment of polyethylene chains and prevented the crystals to be formed.

4.5 Mechanical Characterization

Tensile tests were done on neat polyethylenes, PE/Compatibilizer binary blends, PE/Organoclay binary nanocomposites and PE/Compatibilizer/Organoclay ternary nanocomposites. In each set of samples, using the stress-strain curves, tensile strength, Young's modulus and elongation at break values were obtained for five samples, and the average values and standard deviation of the results are reported. The effects of compatibilizer type, organoclay type and polymer matrix type on the mechanical properties of samples are shown in the following section. Mechanical test results are tabulated in Appendix C.

4.5.1 Tensile Test Results

4.5.1.1 Tensile Test Results of PE/Compatibilizer Blends

Stress-strain curves give information about the response of the polymer to an applied stress. Representative tensile stress-strain curves of neat LDPE, HDPE and LLDPE are given in Figures 4.56 -4.58. The differences in structure of polyethylene types resulted in different responses to applied tensile stress. LDPE has highly branched structure, on the other hand HDPE has very few branches, and LLDPE has short branches in its structure. Degree of crystallinity of these polymer types increases in the order of LDPE, LLDPE and HDPE.

The stress-strain curves all PE types showed elastic behavior in the low strain region. In the elastic region, stress is proportional to strain and the deformation is completely reversible. Elastic modulus of the polymer is determined from the slope of the initial parts of this region. Beyond the elastic region, yield occurs in ductile polymers. Yield point is either the end of the elastic region or the top of the following curve before the plastic region.

After yield, cold drawing and strain hardening occurred in HDPE and LLDPE. LDPE did not show cold drawing in its stress-strain curves. The process of neck formation and its extension is called as “cold drawing”. During the test, polymer chains disentangle and align relatively parallel to the direction of applied stress. During this period cold drawing takes place.

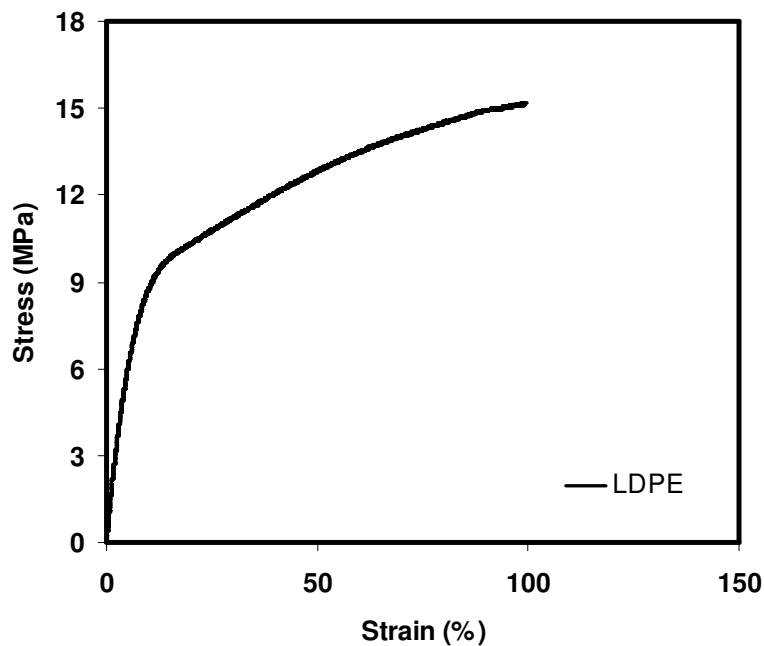


Figure 4. 56 Tensile stress-strain curve of neat LDPE

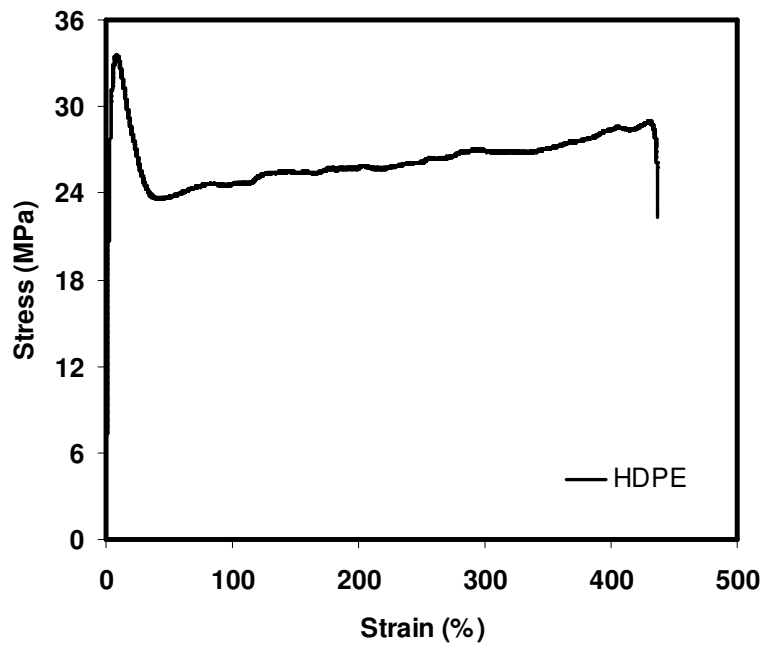


Figure 4. 57 Tensile stress-strain curve of neat HDPE

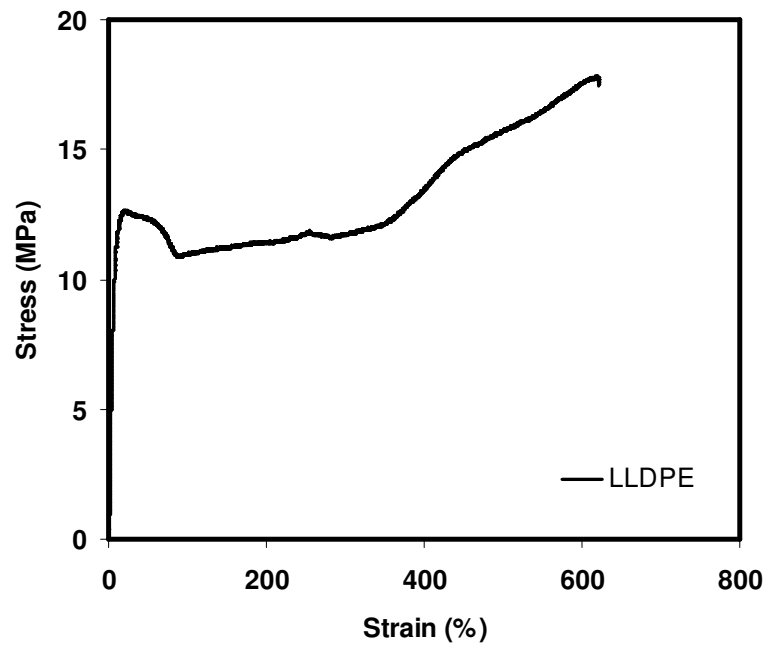


Figure 4. 58 Tensile stress-strain curve of neat LLDPE

As seen in the Figures 4.56-4.58, there is an increase in the final part of the curves. This is due to the strain hardening. Strain hardening occurs as a result of chain orientation in extension of polymers. Chains of polymer are reorganized parallel to the applied stress direction in the cold drawn regions of polymer. Due to the directional structure of molecules and nature of covalent bonding, an oriented structure is remarkably stronger and stiffer than an isotropic structure. Thus, the material in the neck is able to support much more stress than outside the neck. Finally, when no additional chain alignment is possible, failure occurs.

Representative stress-strain diagrams of PE/Compatibilizer blends, PE/Organoclay binary composites and PE/Compatibilizer/Organoclay ternary composites are given in Appendix D. The stress-strain curves of the samples prepared with any PE type, are similar to the stress-strain curve of mentioned neat PE type.

Figures 4.59 through 4.67 show the tensile test results of binary blends of PE/E-MA-GMA and PE/E-BA-MAH containing 5 wt % and 10 wt % compatibilizer. It was recorded from technical specification sheets of compatibilizers, that tensile strength of E-MA-GMA and E-BA-MAH is 4 MPa and 12 MPa, respectively.

Tensile strength of neat LDPE, HDPE and LLDPE is 15.1 MPa, 33.7 MPa and 15.9 MPa, respectively. Young's modulus values are, 166.6 MPa, 1131.7 MPa and 230.4 MPa for LDPE, HDPE and LLDPE, respectively. Finally, % elongation at break values of neat polymers are 121.4 %, 455,7 % and 624.3 % for LDPE, HDPE and LLDPE, respectively.

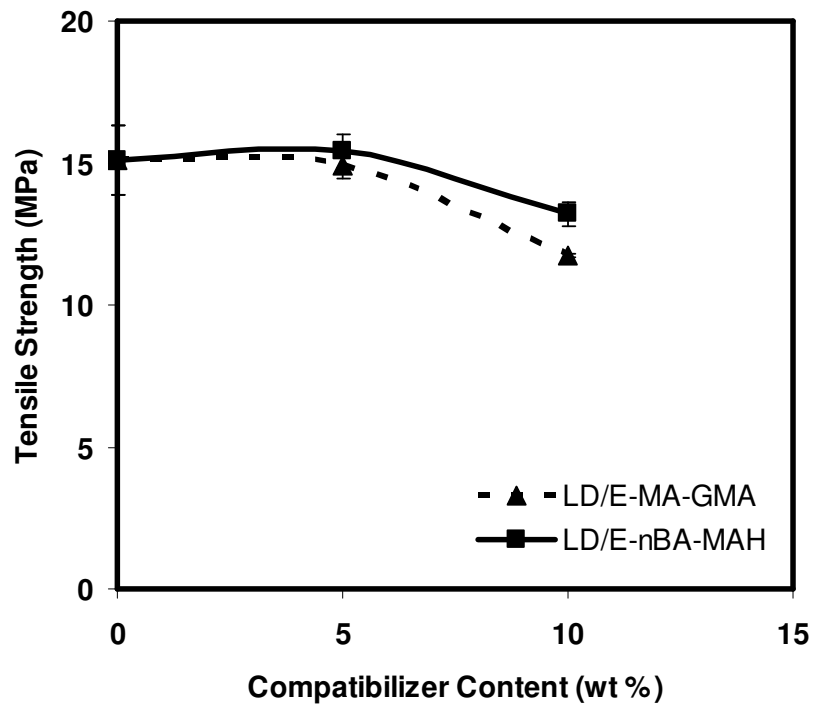


Figure 4.59 Effect of compatibilizer content on tensile strength of LD/Compatibilizer blends

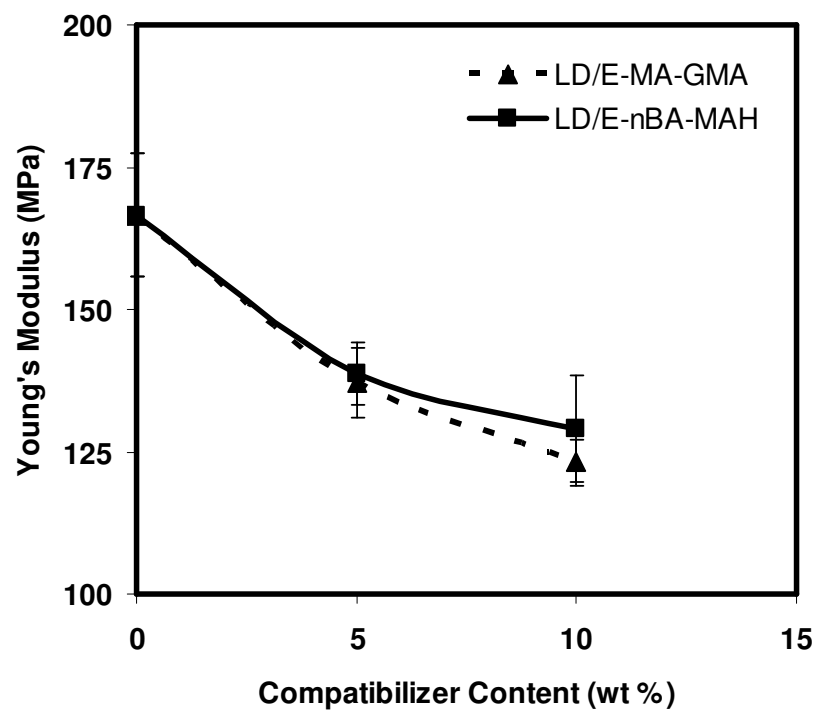


Figure 4.60 Effect of compatibilizer content on Young's Modulus of LD/Compatibilizer blends

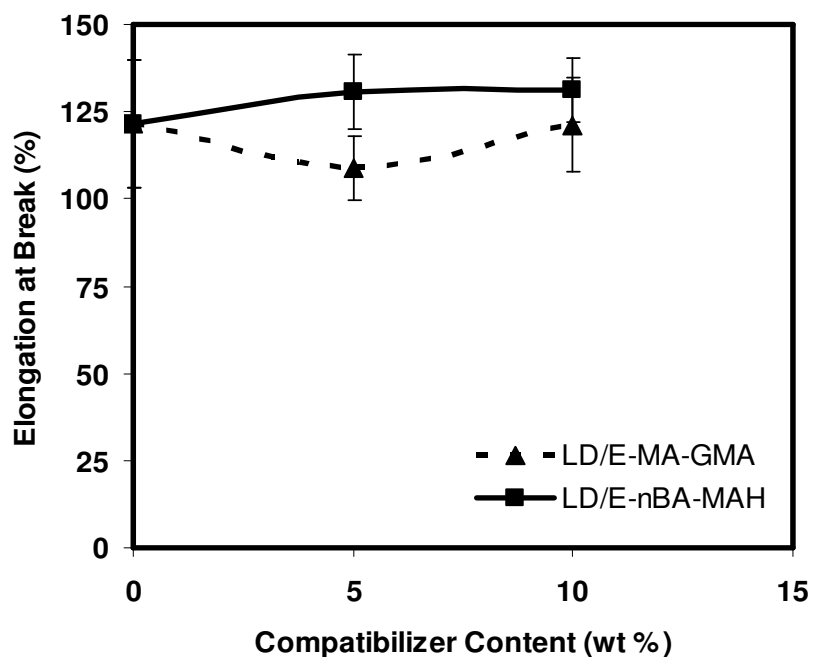


Figure 4.61 Effect of compatibilizer content on % elongation at break of LD/Compatibilizer blends

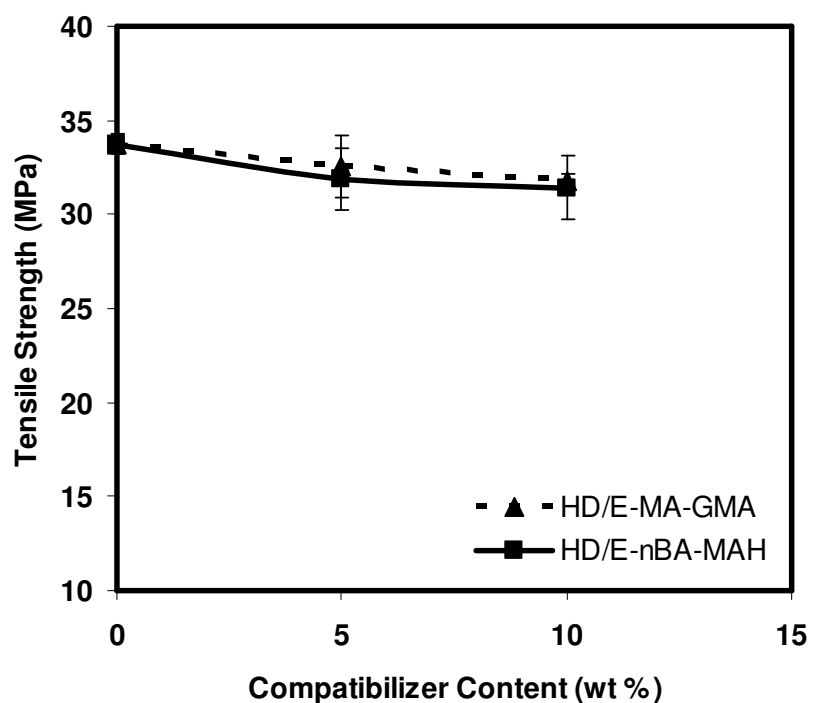


Figure 4.62 Effect of compatibilizer content on tensile strength of HD/Compatibilizer blends

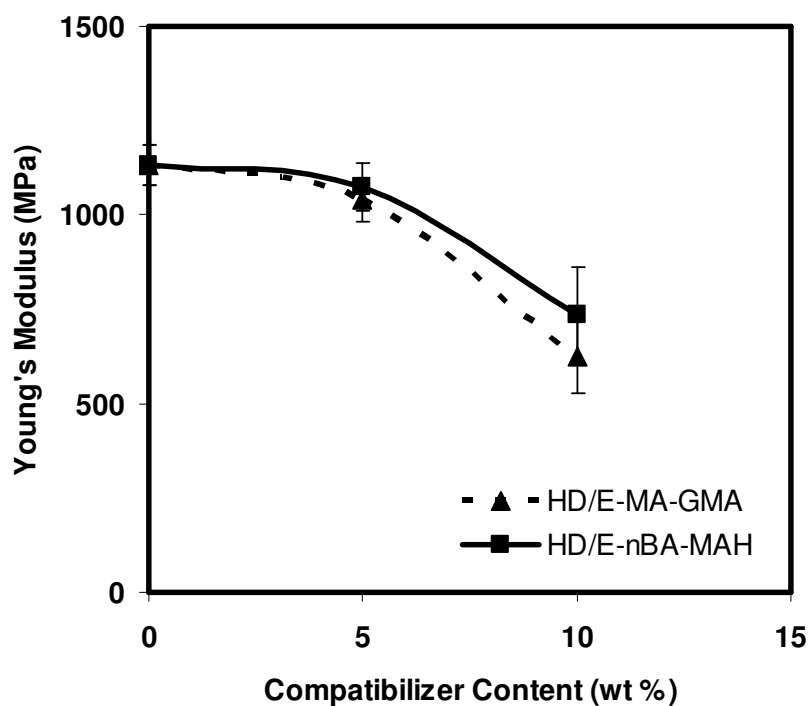


Figure 4.63 Effect of compatibilizer content on Young's Modulus of HD/Compatibilizer blends

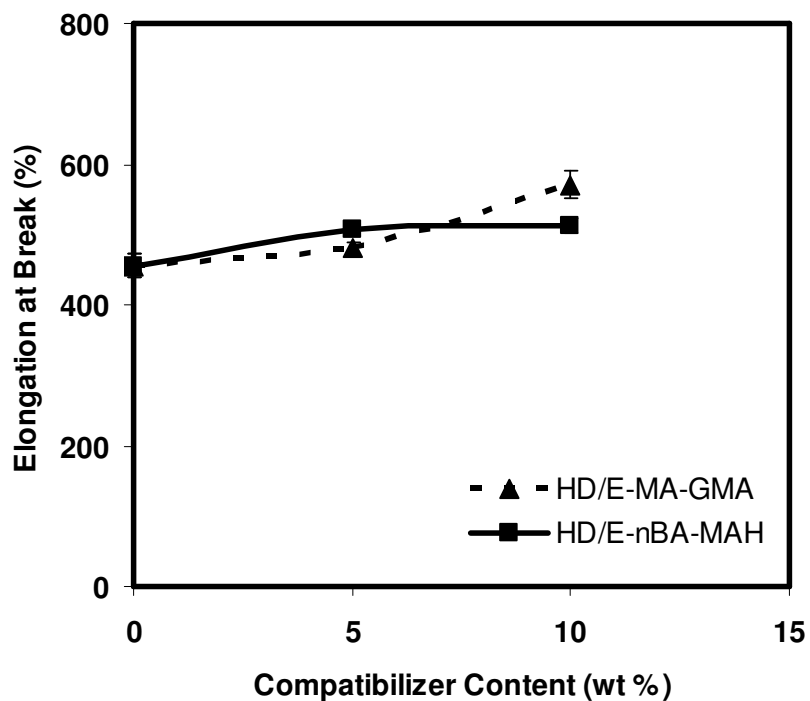


Figure 4.64 Effect of compatibilizer content on % elongation at break of HD/Compatibilizer blends

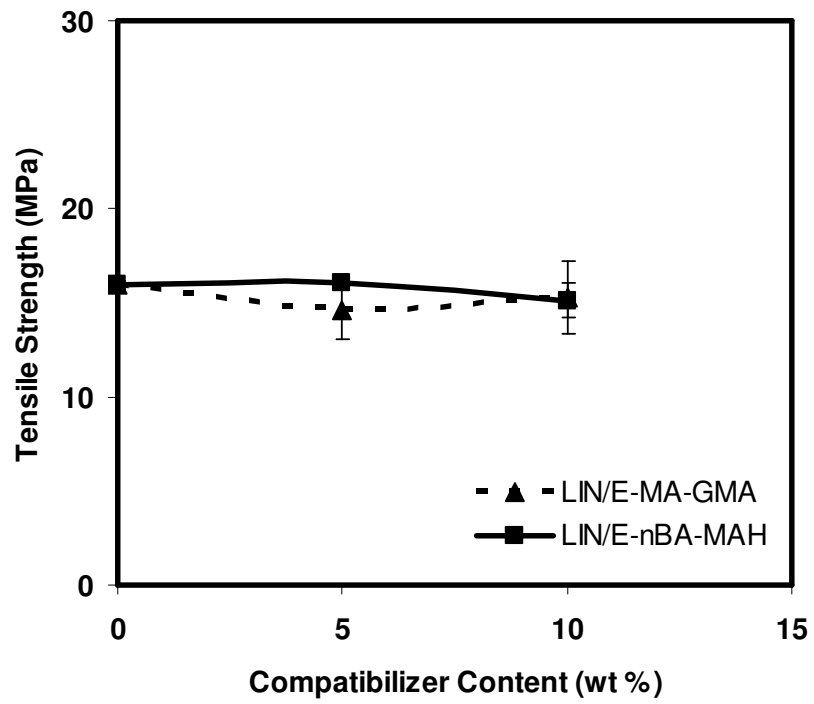


Figure 4.65 Effect of compatibilizer content on tensile strength of LIN/Compatibilizer blends

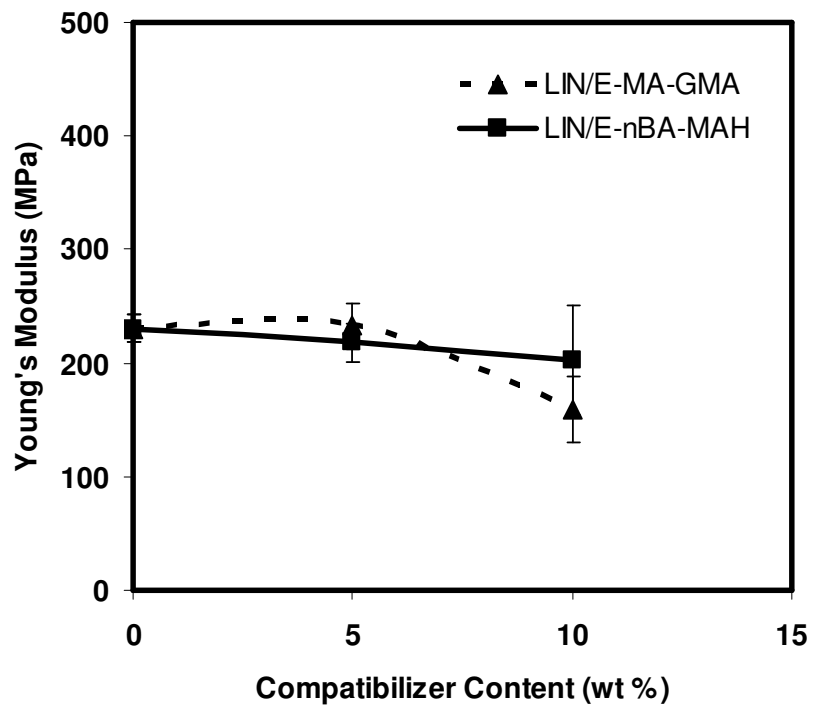


Figure 4.66 Effect of compatibilizer content on Young's Modulus of LIN/Compatibilizer blends

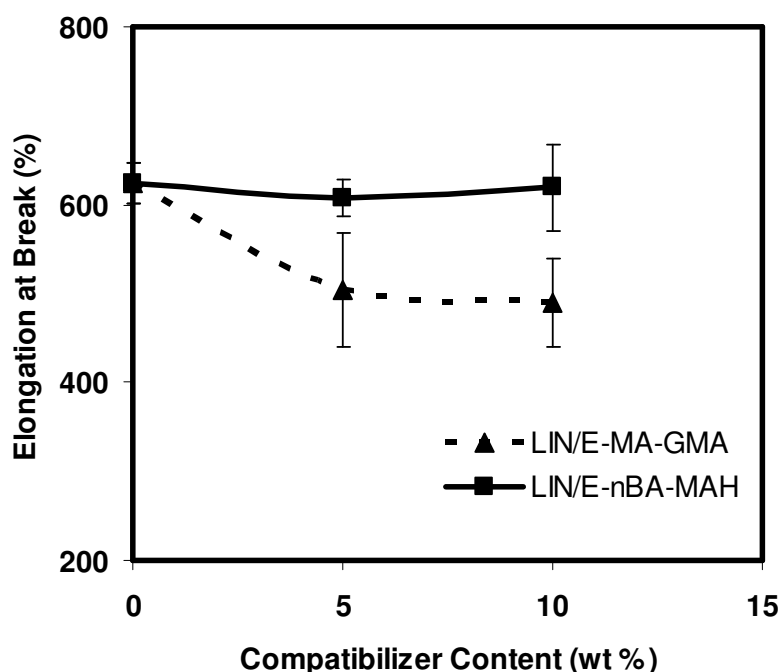


Figure 4.67 Effect of compatibilizer content on % elongation at break of LIN/Compatibilizer blends

Table 4.23 shows the change of mechanical properties of PE/Compatibilizer blends with 5 wt % and 10 wt % compatibilizer content. Tensile strengths and modulus of the blends were lower than those of polyethylene matrices. In addition to this, increase in compatibilizer content resulted in drastic decrease in tensile strength and especially in Young's modulus of polymer matrices.

For all types of PE, owing to the dilution effect, increase in E-MA-GMA or E-BA-MAH content resulted in decrease in both tensile strength and Young's modulus of the samples, since tensile strength and Young's modulus of E-MA-GMA and E-BA-MAH are lower than those of neat polyethylenes. Considering the elongation at break values of binary blends of PE/Compatibilizer it was not easy to make conclusion on effect of compatibilizer. The strain at break values increased in some cases showing the compatibility between the polyethylenes and compatibilizers. For HDPE, at each composition strain at break values were increased. Compatibilizers E-MA-GMA and E-BA-MAH are high density polyethylene based polymers thus, they are more compatible with HDPE.

Table 4.23 Change of tensile properties of binary blends of LDPE, HDPE and LLDPE containing 5 wt % and 10 wt % compatibilizer

	LDPE		HDPE		LLDPE	
	E-MA-GMA	E-BA-MAH	E-MA-GMA	E-BA-MAH	E-MA-GMA	E-BA-MAH
Tensile Strength Δ % (5 wt %)	-1.39	-12.5	-3.6	-5.5	-8.2	0.6
Tensile Strength Δ % (10 wt %)	-22.3	2.12	-5.9	-6.9	-4.0	-5.01
Young's Modulus Δ % (5 wt %)	-17.7	-16.8	-8.1	-5.2	0.9	-5.2
Young's Modulus Δ % (10 wt %)	-26.1	-22.6	-44.8	-35.2	-30.9	-11.9
Elongation at Break Δ % (5 wt %)	-10.47	7.59	5.5	11.2	-19.4	-2.7
Elongation at Break Δ % (10 wt %)	-0.22	8.03	25.1	12.5	-21.6	-0.8

4.5.1.2 Tensile Test Results of PE/Organoclay Binary Nanocomposites

Binary compositions of PE and organoclays 30B and NF8 were prepared with 2 wt %, 4 wt% and 6 wt % organoclay content. Stress-strain behavior of binary nanocomposites are shown in Appendix D.

Figures 4.68-4.70 show the effect of organoclay content on tensile strength, Young's modulus and percent elongation of LDPE. Considering the LD/30B compositions, higher clay content resulted in decrease in tensile strength. Considering the LD/NF8 compositions tensile strength decreased at 2 wt % NF8 loading. However, an increase occurred at 4 wt % loading. However, further increase in organoclay content decreased the strength 9 %. Reason for the decrease in tensile strength is the weak interaction of LDPE matrix and the silicate layers of organoclay.

Considering the Young's modulus, generally, increase in organoclay content had a tendency to increase the elastic modulus. With 2 wt % clay content Young's modulus decreased in both 30B and NF8 containing samples. Additional clay loading increased the modulus of LDPE.

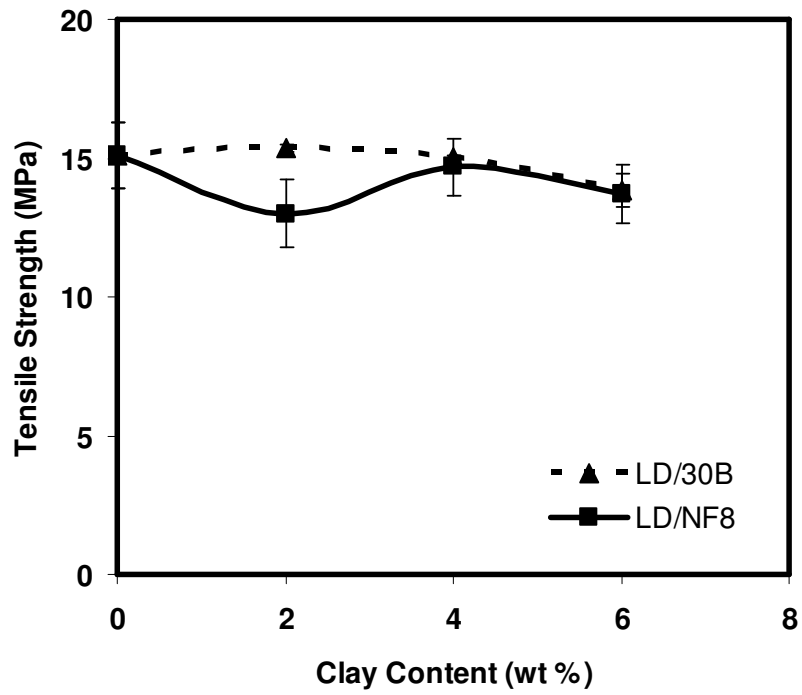


Figure 4.68 Effect of organoclay content on tensile strength of LD/Organoclay binary nanocomposites

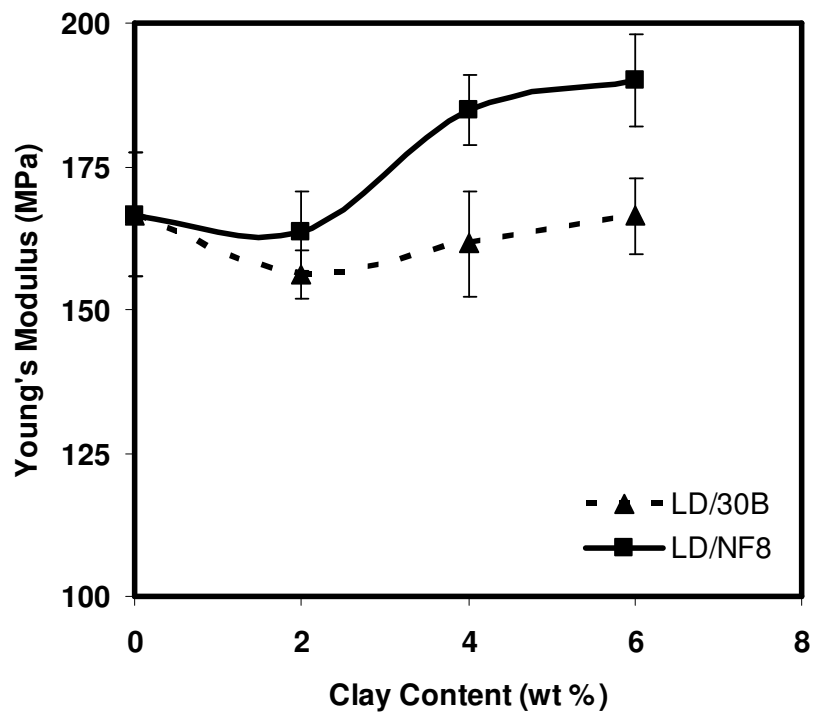


Figure 4.69 Effect of organoclay content on Young's Modulus of LD/Organoclay binary nanocomposites

As seen in Figure 4.70, increase in organoclay content leads to continuous decrease in elongation at break values. During melt blending it was not possible to disperse the agglomerates of organoclay. Thus, the interaction of polymer matrix and organoclay could not be increased to a sufficient level that affects the mechanical properties positively. The agglomerates behave as stress concentrators and lead to early fracture of polymer.

Also, it is known that the clay agglomerates can not extend as much as the matrix can. This is also effective in decreasing the elongation at break values of the nanocomposites.

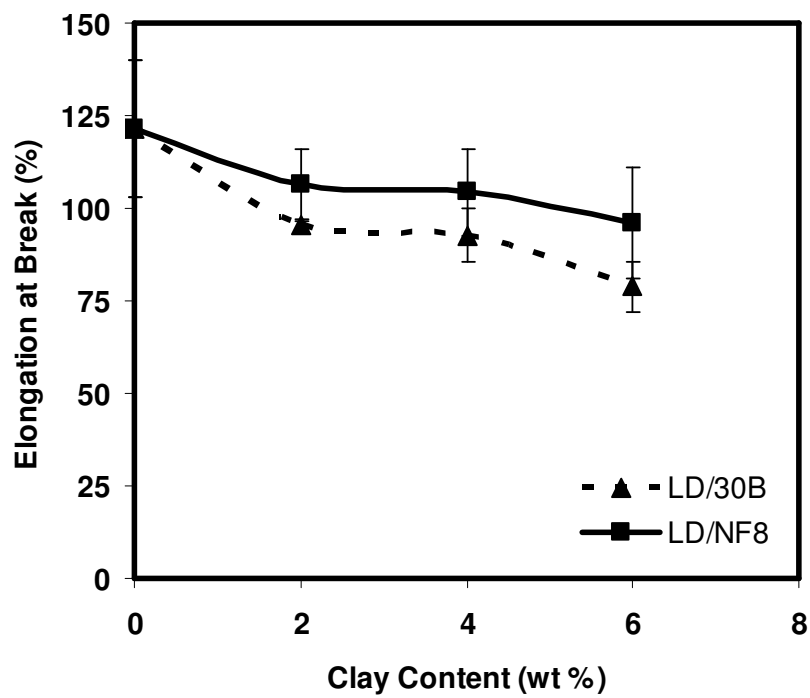


Figure 4.70 Effect of organoclay content on % elongation at break of LD/Organoclay binary nanocomposites

Figures 4.71-4.73 show the tensile strength, Young's modulus and elongation at break values of HDPE with respect to loading of organoclays 30B and NF8. At 2 wt % organoclay loading, slight decrease in tensile strength occurred for the composite HD/30B. Increase in organoclay content resulted in slightly higher tensile strength. Change in tensile strength for HD/NF8 nanocomposites was more remarkable.

Young's modulus did not change significantly at 2 wt % organoclay loading in both 30B and NF8 composites with HDPE matrix. However, increase in organoclay content resulted in opposite trend for each organoclay type. Young's modulus decreased with increasing 30B content. On the other hand, modulus increased with increasing NF8 content.

Considering the effect of organoclay content on percent elongation of HDPE, beyond 4 wt % organoclay loading, significant decrease is observed. At higher concentrations of organoclay it is not easy to obtain well dispersion of organoclay layers during melt blending process. Due to the agglomerates of organoclays elongation at break values decreases.

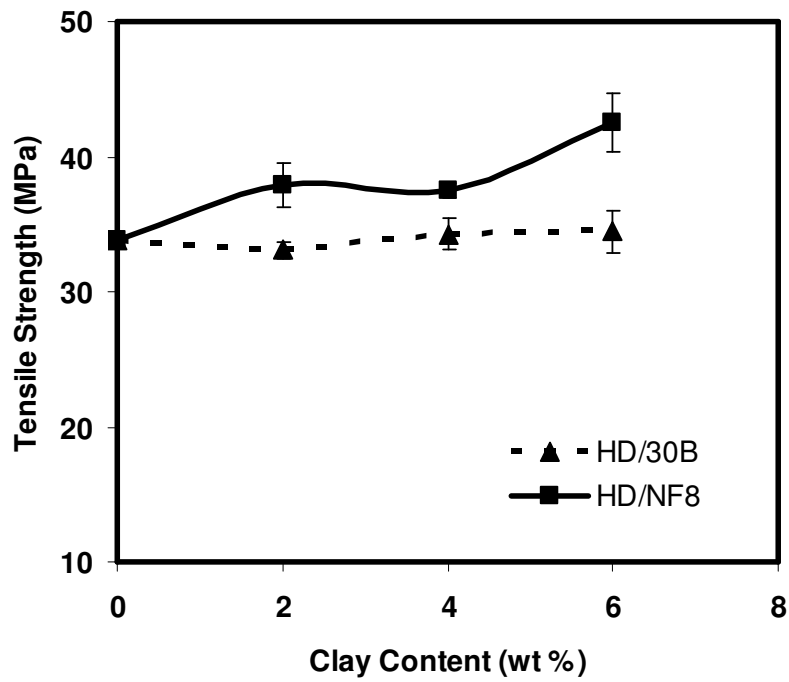


Figure 4.71 Effect of organoclay content on tensile strength of HD/Organoclay binary nanocomposites

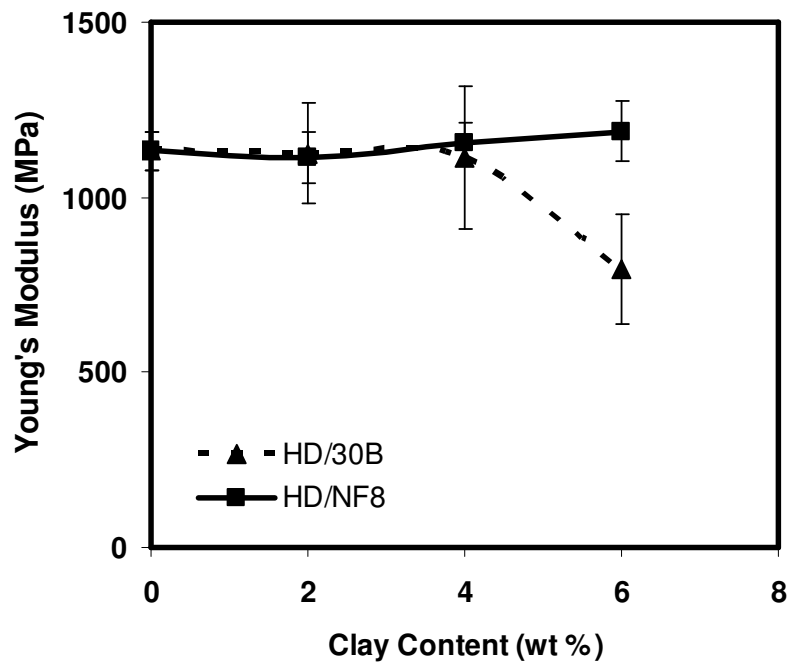


Figure 4.72 Effect of organoclay content on Young's Modulus of HD/Organoclay binary nanocomposites

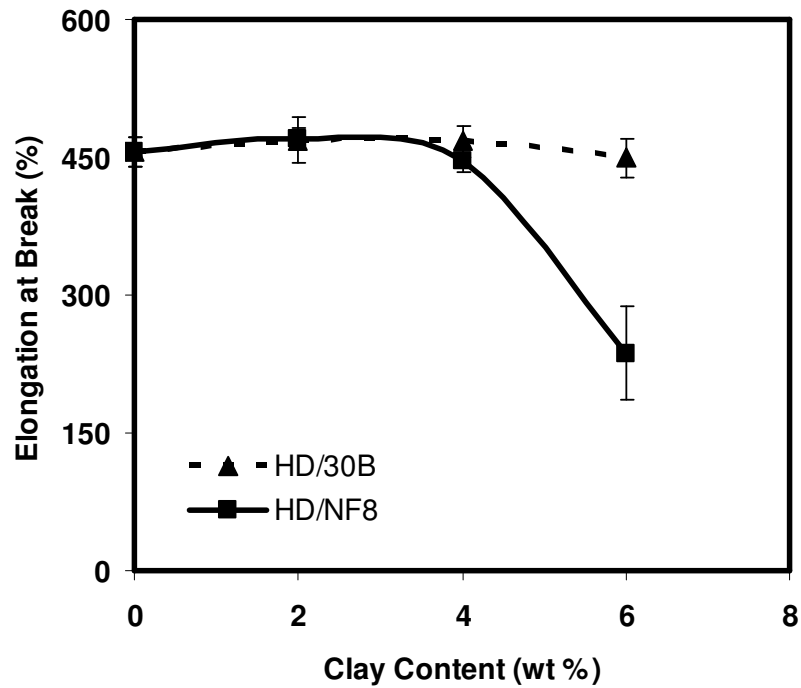


Figure 4.73 Effect of organoclay content on % elongation at break of HD/Organoclay binary nanocomposites

Figures 4.74-4.76 show the effects of organoclay content on tensile properties of LLDPE. Addition of organoclay resulted in decreasing tensile strength at each composition for both 30B and NF8. Young's modulus of the samples increased by 14.5 % and 47.5 % with 2 wt % 30B and NF8 loading, respectively. For nanocomposites containing 30B, modulus decreased beyond 4 wt % loading. However, for NF8, decrease in modulus was observed after 2 wt % loading. At all compositions, Young's modulus values were higher than of the neat LLDPE. Showing that addition of organoclay increased the stiffness of LLDPE.

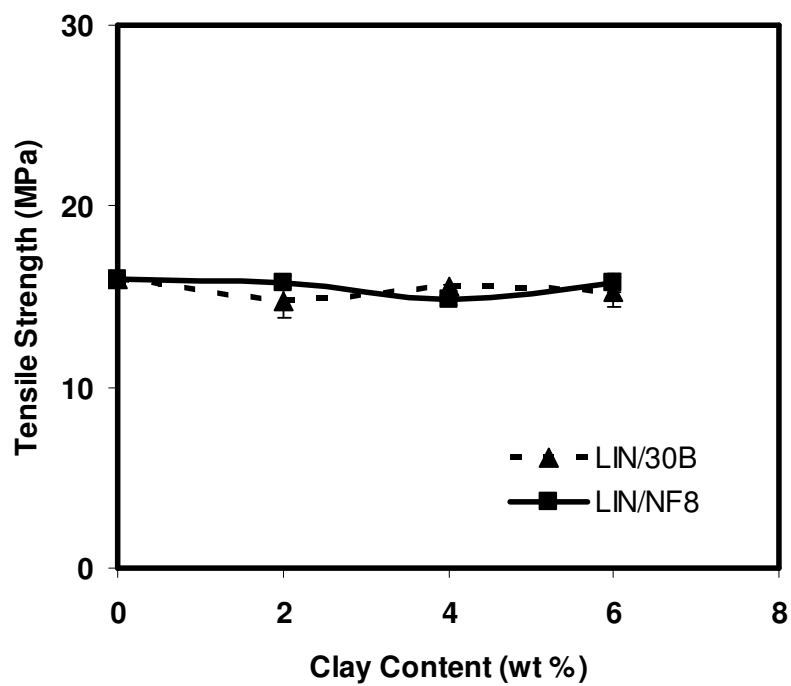


Figure 4.74 Effect of organoclay content on tensile strength of LIN/Organoclay binary nanocomposites

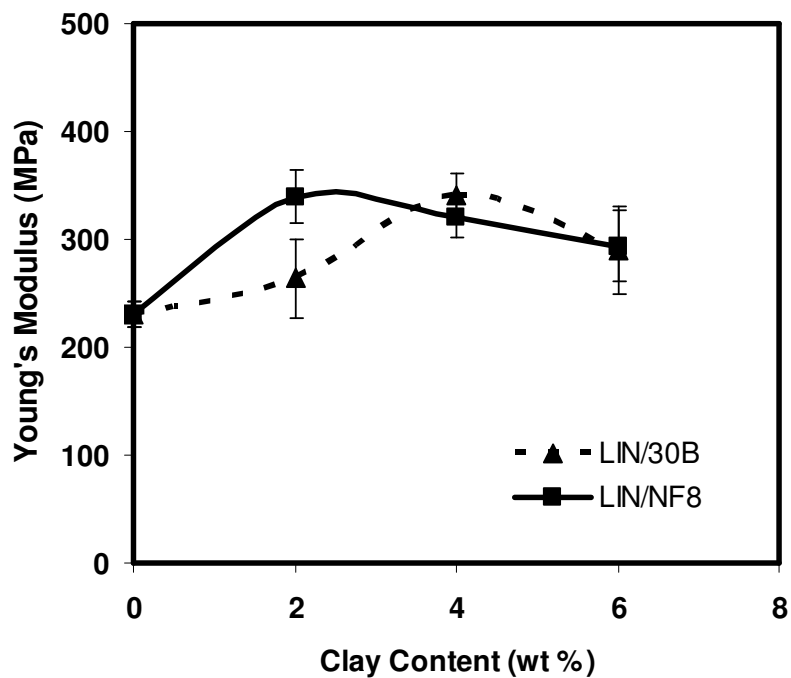


Figure 4.75 Effect of organoclay content on Young's Modulus of LIN/Organoclay binary nanocomposites

Effect of organoclay content on deformation of LLDPE was similar to the results observed with LDPE and HDPE. Increase in organoclay content resulted in significant decrease in elongation at break values of LLDPE/Organoclay binary nanocomposites.

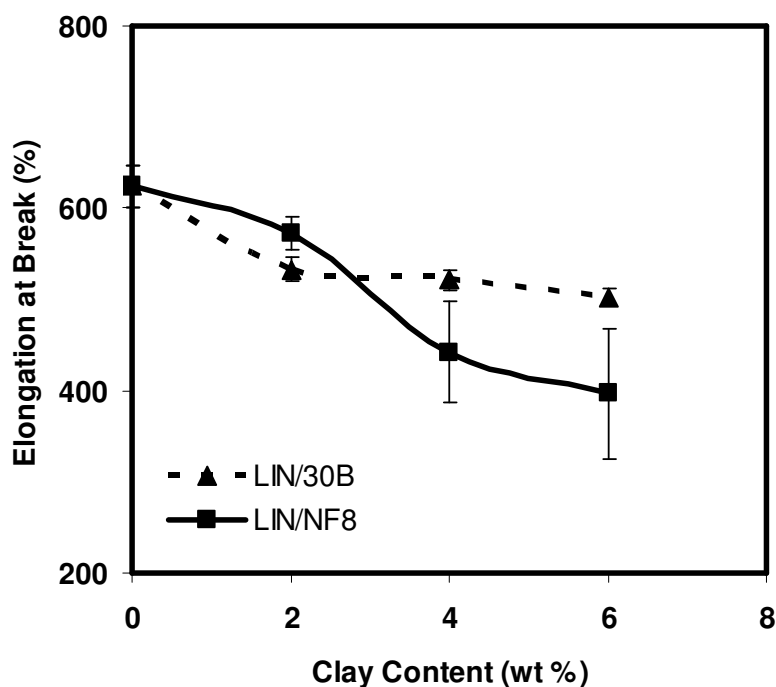


Figure 4.76 Effect of organoclay content on % elongation at break of LIN/Organoclay binary nanocomposites

Table 4.24 summarizes the change of tensile properties of binary nanocomposites with 2 wt % organoclay content. Improvement in mechanical properties was not achieved with binary compositions of PE/Organoclay. Generally tensile strength of matrices decreased with addition of 2 wt % organoclay due to weak interaction between the organoclays and polymer matrices. No significant change in Young's modulus was seen in LDPE and HDPE matrix compositions. On the other hand improvement was seen in LLDPE matrix compositions with 2 wt % organoclay loading. Increasing organoclay content resulted in decrease of material tensile properties as seen in Figures that

are given above. Thus, organoclay content of ternary nanocomposites was selected as 2 wt %.

Table 4.24 Change of tensile properties of binary nanocomposites of LDPE, HDPE and LLDPE with 2 wt % organoclay content.

2 wt % Organoclay	LDPE		HDPE		LLDPE	
	30B	NF8	30B	NF8	30B	NF8
Tensile Strength (MPa)	1.66	-13.8	-1.9	12.1	-7.7	-0.9
Young's Modulus (MPa)	-6.32	-1.74	-0.6	-1.6	14.5	47.5
Elongation at Break (%)	-21.3	-13.2	2.8	3.3	-14.6	-8.4

4.5.1.3 Tensile Test Results of PE/Compatibilizer/Organoclay Ternary Nanocomposites

Representative stress–strain behavior of ternary nanocomposites of polyethylenes are given in Appendix D.

Figures 4.77 -4.79 show the mechanical properties of ternary nanocomposites with LDPE matrix. In the figures, first bars belong to LDPE, second bars belong to LD/Compatibilizer blends, third and fourth bars belong to ternary nanocomposites of LD/Compatibilizer/30B and LD/Compatibilizer/NF8, respectively.

Addition of 5 wt % E-MA-GMA decreased tensile strength by 1.4 %. On the other hand, E-BA-MAH exhibited the opposite effect. A slight increase of, 2.1 %, was observed in the tensile strength value. For LDPE, ultimate strength occurred at break. This value highly depends on the interaction of the polymer matrix and the filler introduced. Tensile strength decreases with addition of rigid particulate fillers if good adhesion can not be obtained at the interface of polymer and fillers.

Considering the ternary LDPE matrix nanocomposites, increase in tensile strength was obtained in all types of ternary nanocomposites. Addition of compatibilizer increased the interaction of the polymer and the silicate layers by enhancing the organoclay dispersion through the matrix. For samples containing E-MA-GMA, 4.6 % increase and 2.7 % increase in tensile strength were obtained with organoclays 30B and NF8, respectively. For samples containing E-BA-MAH, 6.7 % and 5.5 % increase in tensile strength were recorded for 30B and NF8 containing nanocomposites.

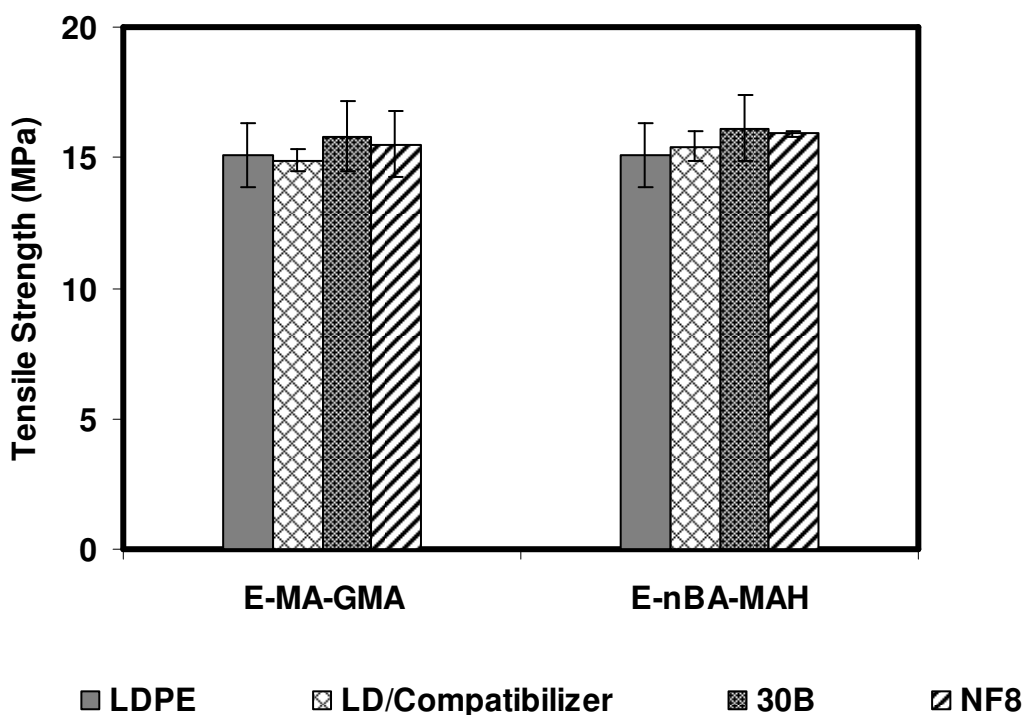


Figure 4.77 Tensile strength values of LD/Compatibilizer/Organoclay ternary nanocomposites with 5 wt % compatibilizer and 2 wt % organoclay loading

Young's Modulus of ternary nanocomposites of LDPE are given in Figure 4.78. Young's Modulus gives information on stiffness of a material at the beginning of the tensile test. Improvement of modulus was obtained with ternary nanocomposite systems. Young's Modulus value decreased 6.3 % and 1.4 % with addition of 2 wt % organoclay 30B and NF8 to LDPE, respectively. Melt blending of E-MA-GMA with the binary system increased the modulus by 4.7 % and 8.2 % for the ternary nanocomposites containing 30B and NF8, respectively. Introducing 5 wt % E-BA-MAH to binary systems also increased the modulus by 2.1% and 6.7 % for the nanocomposites containing 30B and NF8, respectively.

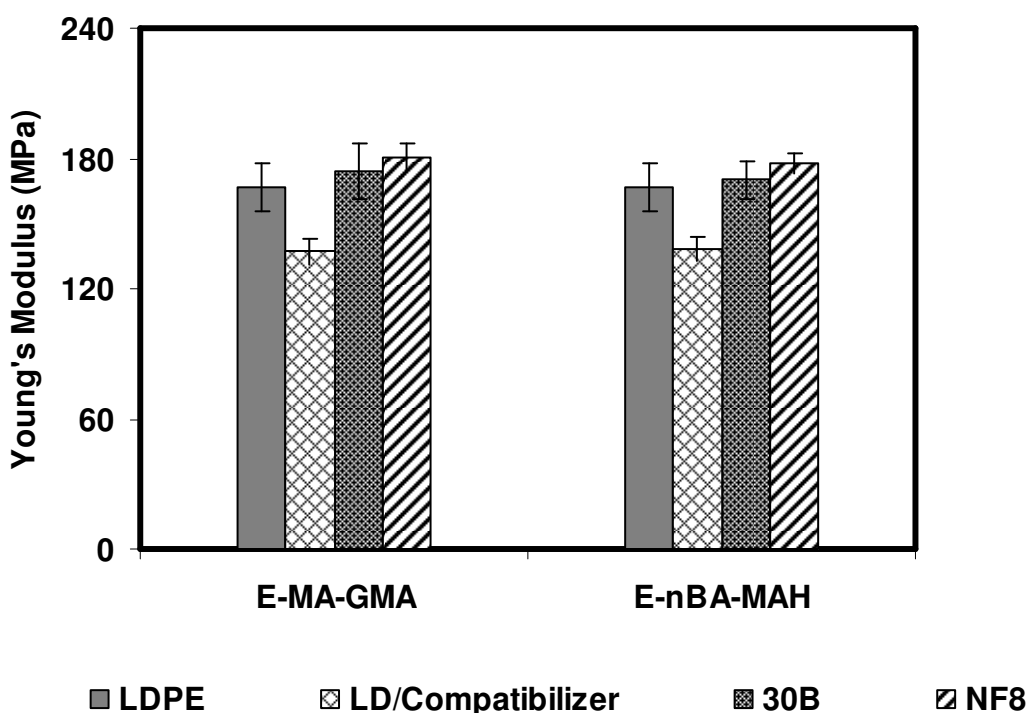


Figure 4.78 Young's Modulus values of LD/Compatibilizer/Organoclay ternary nanocomposites with 5 wt % compatibilizer and 2 wt % organoclay loading

The increase in modulus strongly depends on the dispersion of the silicate layers in the polymer matrix as well as the improved interaction between polymer and organoclay. Improvement occurs due to the strong interaction between the

polymer matrix and dispersed silicate layers, thus to formation of bonding of the hydroxyl groups of the organoclay and functional groups of the compatibilizers, GMA and MAH. These possible reactions increase the adhesion between the polymer matrix and the clay. The possibility of transferring the applied stress from polymer to organoclay increases, and owing to this reason higher Young's Modulus values are obtained.

The tensile test results for LD/Compatibilizer/Organoclay nanocomposites are consistent with the XRD and TEM analysis. Increase in basal spacing of ternary nanocomposites were obtained with XRD analysis, and TEM images showed intercalated and partially exfoliated structures. Among LDPE nanocomposites, highest increase in tensile strength is obtained in LD/E-MA-GMA/30B as 6.7 %, and highest Young's Modulus is obtained in LD/E-BA-MAH/NF8 nanocomposite as 8.2 %.

Strain at break values of ternary nanocomposites of LDPE are given in Figure 4.79. In all the compositions, decrease in strain at break values are recorded. This is due to the inextensibility of clay. Lowest strain at break value was with a decrease of 32.6 % for LD/E-MA-GMA/30B nanocomposites.

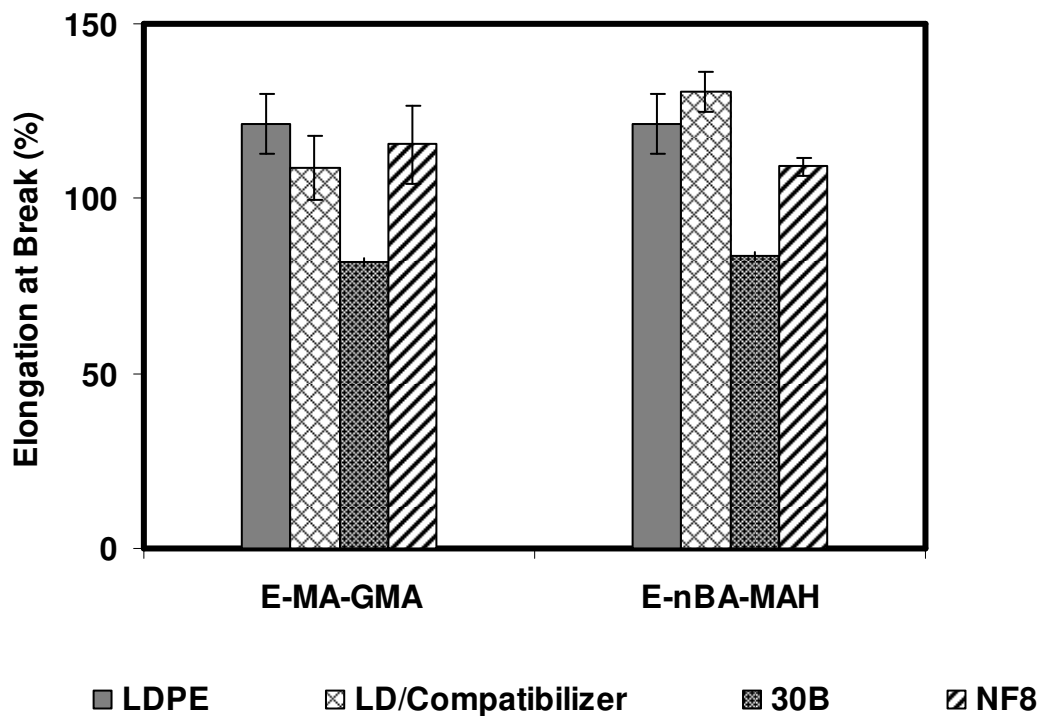


Figure 4.79 % Elongation at break values of LD/Compatibilizer/Organoclay ternary nanocomposites with 5 wt % compatibilizer and 2wt % organoclay loading

The tensile properties of HDPE/Compatibilizer/Organoclay nanocomposites are shown in Figures 4.80-4.82. Improvement in tensile properties was achieved by melt blending of HDPE with 2 wt % organoclay and 5 wt % compatibilizer.

As seen in Figures 4.80 and 4.81, tensile strength and Young's modulus of binary blends of both HD/E-MA-GMA and HD/E-BA-MAH with 5 wt % compatibilizer content, are lower than those of the neat HDPE, due to the dilution effect of the compatibilizer in the system. Compatibilizers have lower Young's modulus and tensile strength than the neat HDPE.

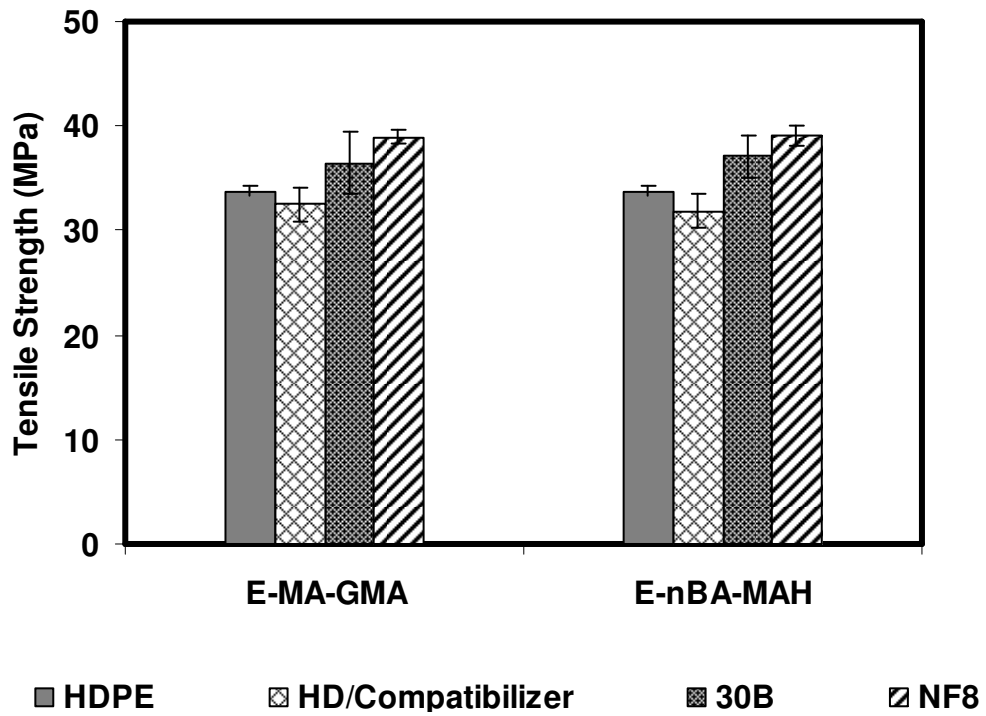


Figure 4.80 Tensile strength values of HD/Compatibilizer/Organoclay ternary nanocomposites with 5 wt % compatibilizer and 2 wt % organoclay loading

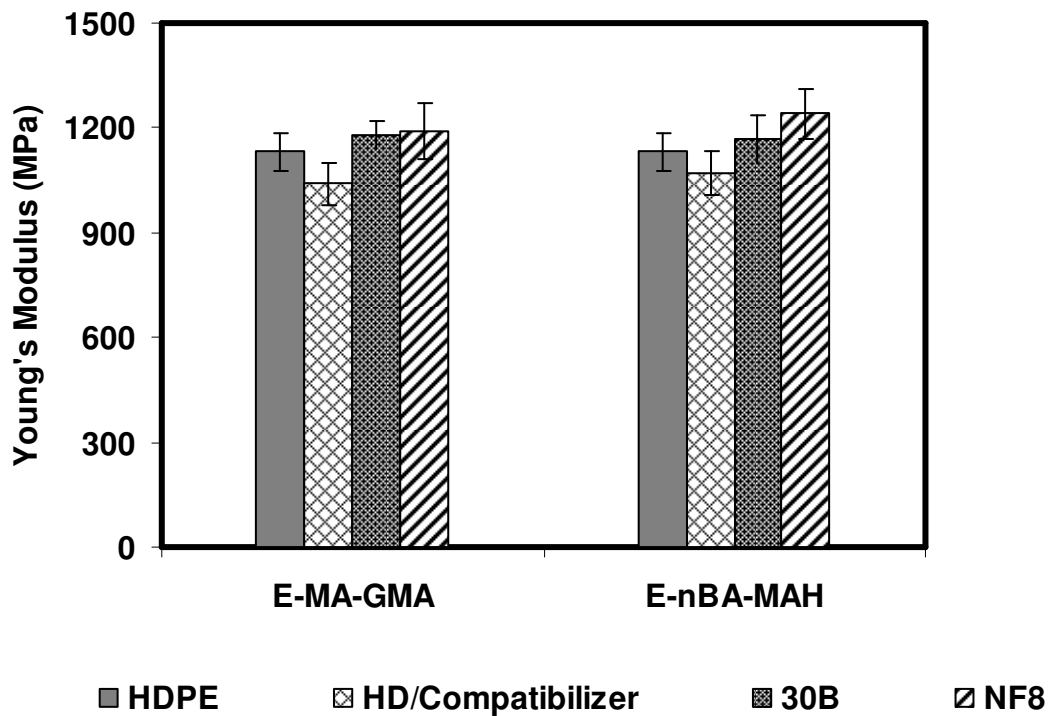


Figure 4.81 Young's Modulus values of HD/Compatibilizer/Organoclay ternary nanocomposites with 5 wt % compatibilizer and 2 wt % organoclay loading

Among the HD/E-MA-GMA/Organoclay nanocomposites highest improvement in tensile strength was obtained with organoclay NF8 with an increase of 15.5 %. The increase in Young's modulus was 4.2 % and 5.1 % for organoclays 30B and NF8, respectively.

Considering the effect of compatibilizer E-BA-MAH on mechanical properties of ternary nanocomposites higher values were obtained in HD/E-BA-MAH/NF8 nanocomposites. Tensile strength increased by 15.9 % and Young's Modulus increased by 9.6 % with respect to the tensile strength of neat HDPE. Increase in modulus was due to the high interaction at the interface of polymer matrix and organoclay.

In general, no significant change was observed in elongation at break values of HD/Compatibilizer/Organoclay nanocomposites as seen in Figure 4.82. Slight increase in elongation at break value was observed for HD/Compatibilizer/Organoclay nanocomposites except for the HD/E-BA-MAH/NF8 composition. For HD/E-BA-MAH/NF8 nanocomposites 7.8 % decrease in elongation at break value was observed.

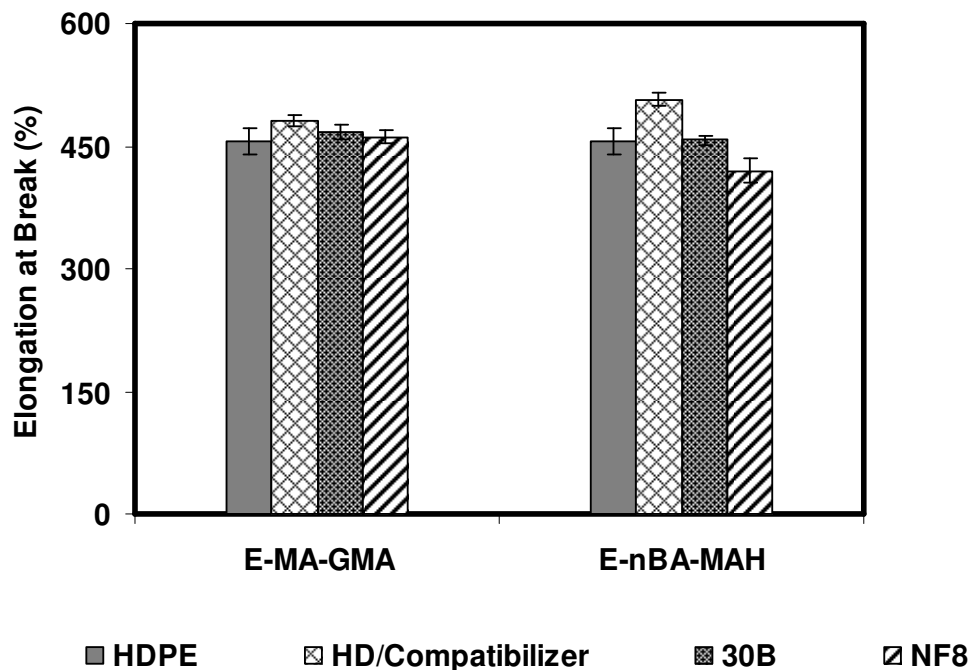


Figure 4.82 % Elongation at break values of HD/Compatibilizer/Organoclay ternary nanocomposites with 5 wt % compatibilizer and 2 wt% organoclay loading

Figures 4.83–4.85 show the tensile properties of LLDPE /Compatibilizer/Organoclay ternary nanocomposites. In the binary nanocomposites of LLDPE/Organoclay analyzed earlier, tensile strength values were 14.71 MPa and 15.8 MPa with 7.7 % decrease and 0.9 % decrease for 2 wt % loading of 30B and NF8, respectively.

Introducing a compatible polymer to this system led to enhancement of mechanical properties. The maximum increase in tensile strength and Young’s modulus in LLDPE containing nanocomposites was obtained in LIN/E-MA-GMA/30B nanocomposites as 17.9 MPa and 255.9 MPa with 12.9 % increase in tensile strength and 11.1 % increase in Young’s Modulus. The lowest increase in tensile strength was obtained with LIN/E-BA-MAH/NF8 nanocomposite with 3.6 % increase. In addition to this, 2.1 % decrease in modulus was observed for this nanocomposite.

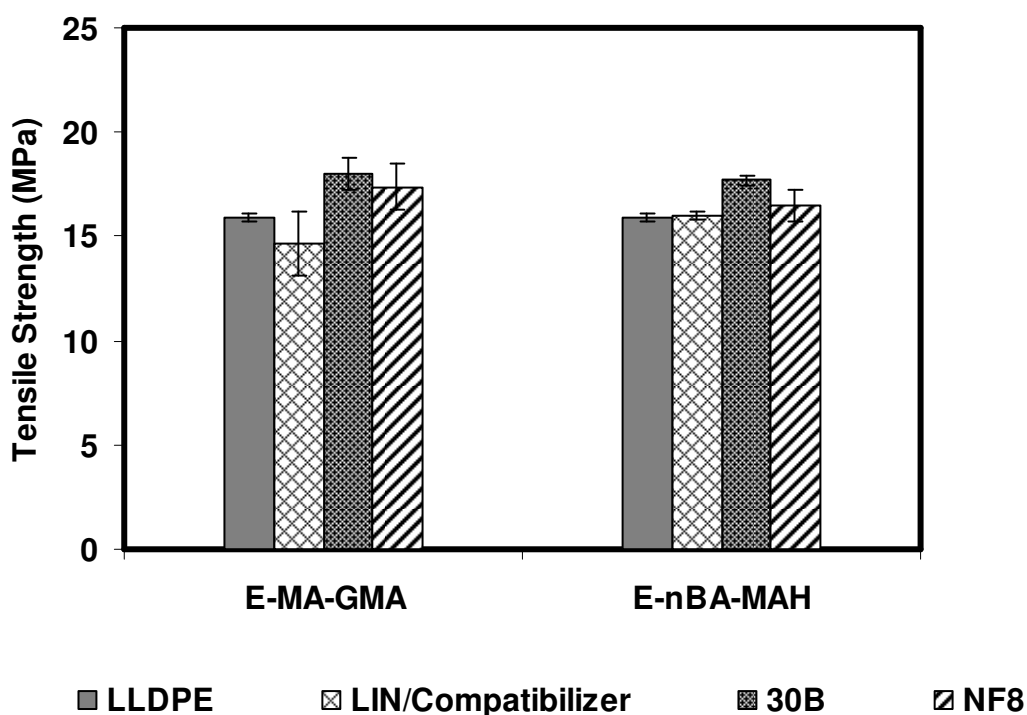


Figure 4.83 Tensile strength values of LIN/Compatibilizer/Organoclay ternary nanocomposites with 5 wt % compatibilizer and 2 wt % organoclay loading

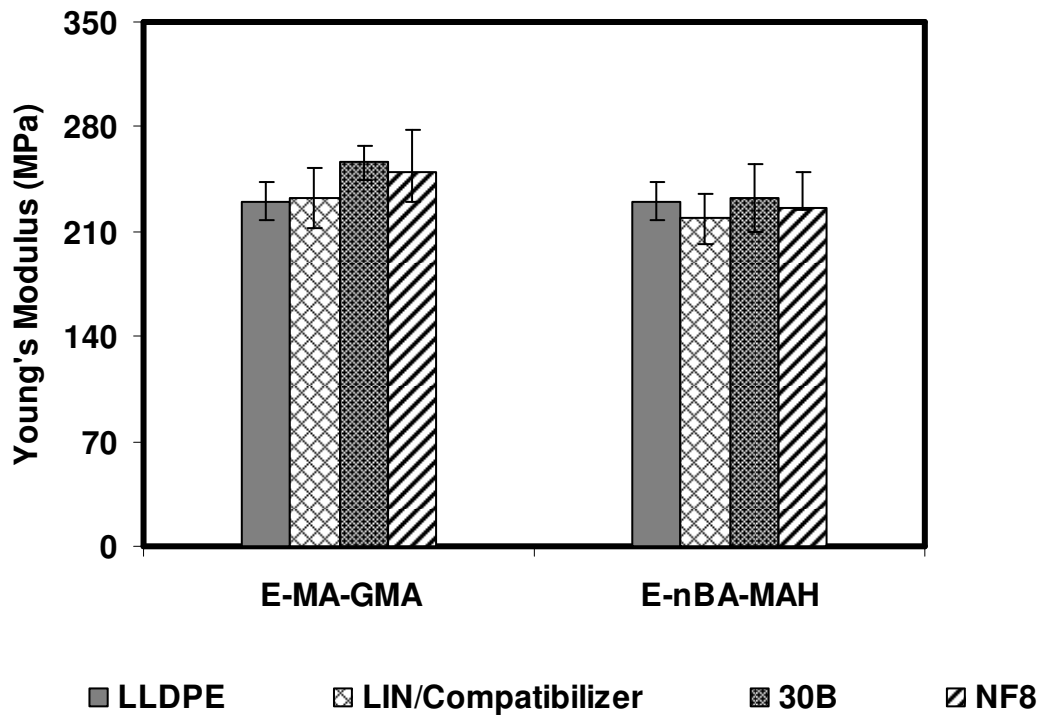


Figure 4.84 Young's Modulus values of LIN/Compatibilizer/Organoclay ternary nanocomposites with 5 wt % compatibilizer and 2 wt % organoclay loading

Strain at break values of LLDPE based ternary nanocomposites are shown in Figure 4.85. Decrease in % elongation at break was observed in all types of ternary nanocomposites with LLDPE matrix with respect to neat LLDPE.

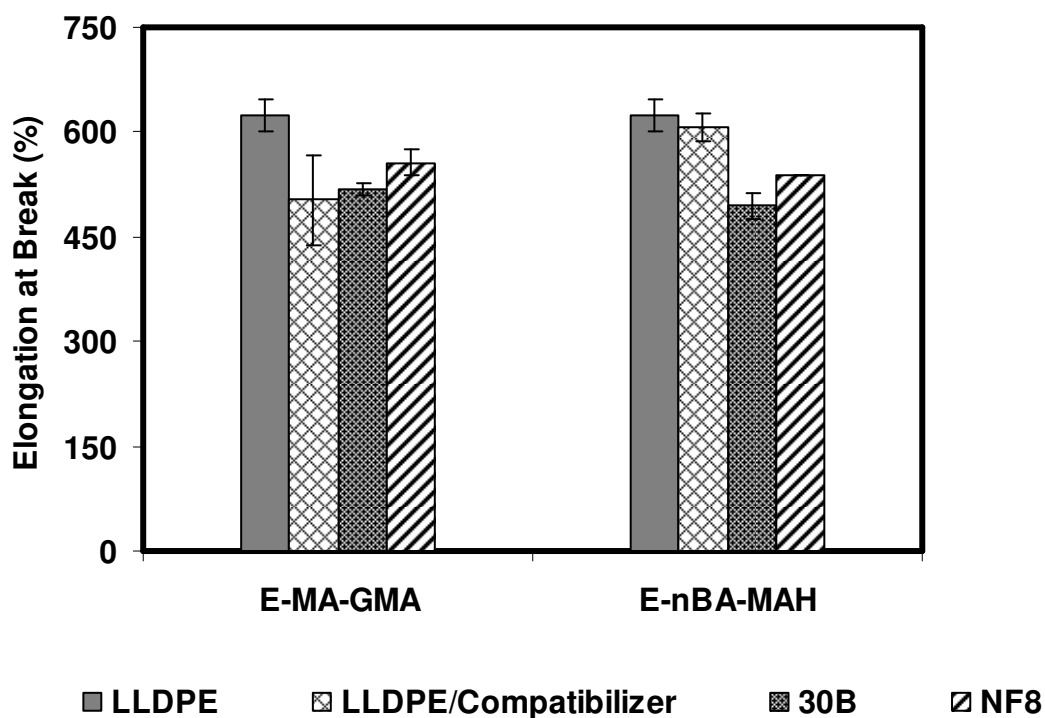


Figure 4.85 % Elongation at break values of LIN/Compatibilizer/Organoclay ternary nanocomposites with 5 wt % compatibilizer and 2 wt% organoclay loading

Table 4.25 gives the % change in tensile properties of all types of ternary nanocomposites prepared in this study with respect to the matrix polymers. Considering the types of polymer matrix, with HD polyethylene higher improvement in tensile strength was obtained. In all PE types, the highest tensile strength was obtained with HD/E-BA/NF8 nanocomposites. The second highest improvement in tensile strength was obtained with LLDPE. Considering the Young's Modulus, maximum increase was obtained in LLDPE/E-MA-GMA/30B and HD/E-BA-MAH/NF8. According to the results, the compatibility of the system changed as HDPE >LLDPE > LDPE. Results of XRD analysis are also in consistent with these mechanical test results. HDPE and LLDPE containing nanocomposites exhibited higher basal spacing of silicate layers in XRD analysis

Table 4.25 Comparison of tensile properties of ternary nanocomposites of LDPE, HDPE and LLDPE containing 2 wt % organoclay and 5 wt % compatibilizer with the matrix polymers

Sample	Tensile Strength Δ %	Young's Modulus Δ %	Elongation at Break Δ %
LD/E-MA GMA/30B	4.6	4.3	-32.6
LD/E-BA-MAH/30B	6.7	2.0	-31.0
LD/E-MA-GMA/NF8	2.7	8.2	-5.0
LD/E-BA-MAH/NF8	5.5	6.7	-10.1
HD/E-MA GMA/30B	8.0	4.2	2.4
HD/E-BA-MAH/30B	9.8	3.2	0.3
HD/E-MA-GMA/NF8	15.5	5.1	1.2
HD/E-BA-MAH/NF8	15.9	9.5	-7.8
LIN/E-MA GMA/30B	12.9	11.1	-17.1
LIN/E-BA-MAH/30B	11.1	1.0	-20.7
LIN/E-MA-GMA/NF8	8.9	8.2	-10.8
LIN/E-BA-MAH/NF8	3.6	-2.1	-13.7

CHAPTER 5

CONCLUSIONS

In the binary nanocomposites containing 2 wt % organoclay good dispersion of silicate layers was not achieved. A decrease in the basal spacing of clay galleries was also observed in some of the samples. This decrease in the basal spacing is thought to be due to the injection pressure effect during the sample preparation. Remarkable increase in basal spacing of silicate layers was obtained with organoclay 30B and organoclay NF8 in the presence of compatibilizers. Complete exfoliation was not achieved in any type of ternary nanocomposites. However, intercalation and partial exfoliation was achieved in ternary nanocomposites of LDPE, HDPE and LLDPE. Considering the compatibilizer type, E-MA-GMA was more compatible than E-BA-MAH with all three types of polymer matrices and both organoclays. Higher increase in basal spacing was seen by introducing E-MA-GMA to the material systems.

Among the ternary nanocomposites containing the same organoclay and compatibilizer, the highest increase in basal spacing was obtained in HDPE matrix based nanocomposites, and the least increase in basal spacing was seen in LDPE matrix based nanocomposites. It was concluded that the chain structure is an important factor affecting the clay dispersion. Intercalation of highly branched polymer chains was hindered in comparison to intercalation of unbranched polymer chains. Unbranched chain structure enhanced the intercalation of polymer chains into clay galleries during melt mixing. Maximum increase in basal spacing was 148.3 % for HD/E-MA-GMA/30B nanocomposites.

TEM analysis supported the results of XRD analysis. Intercalated and partially exfoliated structures were observed in TEM images of ternary nanocomposites of LDPE, HDPE and LLDPE.

Homogeneous structures were observed in SEM images of PE/Compatibilizer blends indicating that the compatibilizers used were miscible with all the PE types. Addition of organoclay to polymers resulted in change of smooth homogeneous surface of polyethylenes to tortuous surfaces with several crack propagation lines. Compatibilizers had significant effect on dispersion of organoclay through polyethylene matrices. Short, close, circular, nonlinear crack propagation lines were observed in all the ternary nanocomposites indicating good dispersion of organoclay through the polymer matrices.

Lower MFI values were obtained by addition of compatibilizer to polymer matrices due to the dilution effect. Each type of compatibilizers have lower MFI values than the neat polyethylenes at test temperatures. In addition to this polar structures of compatibilizers increased the adhesion of the polymer blends to the metal walls of the test apparatus. Addition of organoclay also decreased the MFI value due to the filler effect increasing the viscosity of polymer. Rigid nanoclays prevented the motion of the polyethylene chains through the barrel of test equipment. According to the MFI test results both compatibilizers, E-MA-GMA and E-BA-MAH were compatible with LDPE, HDPE and LLDPE, as well as with the organoclays 30B and NF8. They enhanced the dispersion of organoclay platelets and thus increased the viscosity resulting in lower MFI values in all the ternary nanocomposites.

Melting temperature and enthalpy of fusion of the polymer matrices did not change remarkably by addition of the compatibilizers and organoclays. Organoclays acted as filler and reduced the degree of crystallinity of polyethylenes by preventing the alignment of the chains of matrices. Considering the ternary nanocomposites, dispersion of organoclays through polymer matrices reduced the degree of crystallinity.

Compatibilizer had an important effect on dispersion of organoclay in polymer matrix. Due to the good dispersion of silicate layers, interaction of polymer and silicate layer increased and this led to improvement in tensile properties. Both compatibilizers had functional groups in their structures (GMA and MAH) that might react with the hydroxyl groups on the organoclay. This strong interaction led to increase in tensile properties such as the tensile strength and modulus.

This effect was higher for E-MA-GMA owing to the higher reactivity of GMA group in comparison to MAH group.

Organoclay 30B has hydroxyl groups in its structure. These hydroxyl groups also promoted the reaction possibility with reactive groups of compatibilizers.

In binary nanocomposites of PE/Organoclay, increase in organoclay content resulted in lower mechanical properties such as low tensile strength and elongation at break values due to the agglomerates of organoclays. At high concentrations of organoclays it was not possible to disperse the organoclay agglomerates, and they behaved as stress concentrators during tensile tests.

Effect of compatibilizer on property enhancement was observed also in mechanical test results. Increase in tensile strength and Young's modulus achieved in each type of ternary nanocomposites. HDPE matrix nanocomposites had the highest improvement in mechanical properties. Lack of long chain branching resulted in partial exfoliation and intercalation, and increase in tensile properties in HDPE based ternary nanocomposites. LLDPE based nanocomposites exhibit second highest mechanical properties owing to regular short chain branching of LLDPE.

The results show that E-MA-GMA and E-BA-MAH are effective compatibilizers for LDPE, HDPE and LLDPE. Addition of compatibilizer to binary nanocomposite systems increased the dispersion of silicate layers and thus the interfacial bonding strength of organoclay and polymer matrices. This mechanism improved the mechanical properties of all the polyethylene types.

REFERENCES

1. Alexandre M. and Dubois P., 2000. "Polymer-layered Silicate Nanocomposites: Preparation, Properties and Uses of a New Class of Materials", *Materials Science and Engineering*, 28, 1-63.
2. Giannelis E.P., 1996. "Polymer Layered Silicate Nanocomposites" , *Advanced Materials*,8, 29-35.
3. Bafna A. A., 2004. " Polyethylene-Clay Nanocomposites: Processing-Structure-Property Relationship", Ph. D. Thesis, University of Cincinnati, Ohio, USA.
4. Hambir S., Bulakh N., Kodgire P., Kalgaonkar R., and Jog J. 2001. "PP/clay nanocomposites: a study of crystallization and dynamic mechanical behavior", *Journal of Polymer Science, Polymer Physics*, 39, 446-450.
5. Fornes T., Yoon P., Keskkula H., and Paul D. 2001. "Nylon 6 nanocomposites: the effect of matrix molecular weight", *Polymer*, 42, 9929-9940.
6. Oya A., Kurokawa Y., and Yasuda H., 2000. "Factors controlling mechanical properties of clay mineral/polypropylene nanocomposites", *Journal of Material Science*, 35, 1045-1050.
7. Beyer G., and Eupen K., 2001. "Nanocomposites of layered silicate and EVA copolymer – new synthesis route and flame retardancy", *Journal of Applied Polymer Science*, 52, 1123- 1130.
8. Gilman J., 1999. "Flammability and thermal stability studies of polymer layered silicate (clay) nanocomposites", *Applied Clay Science*, 15, 31-49.

9. Kojima Y., Usuki A., Kawasumi M., Okada A., Kurauchi T., and Kamigaito O. 1993. "Sorption of water in nylon 6-clay hybrid", *Journal of Applied Polymer Science*, 49, 1259- 1264.
10. Messermith P., and Giannelis E., 1995 "Synthesis and barrier properties of poly(epsilon-caprolactone)-layered silicate nanocomposites", *Journal of Polymer Science, Polymer Chemistry*, 33, 1047-1057.
11. Hambir S., Bulakh N., and Jog J.P., 2002. "Polypropylene / Clay Nanocomposites: Effect of Compatibilizer on the Thermal, Crystallization and Dynamic Behavior", *Polymer Engineering and Science*, 42 No.9, 1800-1807.
12. Wang K. H., Choi M. H., Koo C. M., Choi Y.S., and Chung I. J., 2001. "Synthesis and Characterization of Maleated Polyethylene / Clay Nanocomposites", *Polymer*, vol.42, 9819-9826.
13. Li X., 2002. "Effect of Blending Sequence on the Microstructure and Properties of PBT/EVA-g-MAH / Organoclay Ternary Nanocomposites". *Polymer Engineering and Science*, 42, No.11,2156-2164,
14. Gopakumar T.G., Lee J.A., Kontopoulou M., and Parent J.S., 2002. "Influence of Clay Exfoliation on the Physical Properties of Montmorillonite / Polyethylene Composites", *Polymer*, 43, 5483-5491.
15. Kato M., Okamoto H., Hasegawa N., Tsukigase A. and Usuki A., 2003. "Preparation and Properties of Polyethylene-Clay Hybrids", *Polymer Engineering and Science*, vol.43 No.6, 1312-1316.
16. Liang G., Xu J., Bao S., and Xu W., 2004. "Polyethylene/Maleic Anhydride Grafted Polyethylene/Organic-Montmorillonite Nanocomposites.I. Preparation, Microstructure, and Mechanical Properties", *Journal of Applied Polymer Science*, vol.91, 3974-3980.

17. Zhang J., and Wilkie C.A., 2003. "Preparation and Flammability of Polyethylene-Clay Nanocomposites", *Polymer Degradation and Stability*, 80, 163-169.
18. Hotta S., and Paul D.R., 2004. "Nanocomposites Formed From Linear Low Density Polyethylene and Organoclays", *Polymer*, vol.45, 7639-7654.
19. Zhai H., Xu W., Guo H., Zhou Z., Shen S., and Song Q., 2004. "Preparation and Characterization of PE and PE-g-MAH/montmorillonite Nanocomposites", *European Polymer Journal*, vol. 40, No: 11, 2539-2545.
20. Morawiec J., Pawlak A., Slouf M., Galeski A., Piorkowska E., and Krasnikowa N., 2005. "Preparation and Properties of Compatibilized LDPE/Organo-modified Montmorillonite Nanocomposites", *European Polymer Journal*, 41, 1115-1122.
21. Zhong Y., and Kee D.D., 2005. "Morphology and Properties of Layered Silicate-Polyethylene Nanocomposite Blown Films", *Polymer Engineering and Science*, 469-477.
22. Beker O., Varley L., and Simon G. 2002. "Morphology, thermal relaxations and mechanical properties of layered silicate nanocomposites based upon high functionality epoxy resins", *Polymer*, 43, 4365-4373.
23. Okamoto M., Morita S., and Kokata T. 2001. "Dispersed structure and ionic conductivity of smectic clay/polymer nanocomposites", *Polymer*, 42, 2685-2688.
24. Gopakumar T., Lee J., Kontopoulou M., and Parent J. 2002. "Influence of clay exfoliation on the physical properties of montmorillonite/polyethylene composites", *Polymer*, 43, 5483-5491.
25. Jin Y. , Park H., Im S., and Kwak S., 2002. "Polyethylene/clay nanocomposites by insitu exfoliation of montmorillonite during Ziegler-Natta polymerization of ethylene", *Macromol. Rapid. Commun.*, 23, 135-140.

26. Sekelik D., Stepanov E., Schiraldi D., Hiltner A., and Baer E., 1999. "Oxygen barrier properties of crystallized and talc-filled poly(ethylene terephthalate)", *J. Polym. Sci., Polym Phys.*, 37, 847-857.
27. Okamoto M., Morita S., Taguchi, H. Kim Y., Kataka T., and Tateyama H., 2000. "Synthesis and structure of smectic clay/poly(methyl methacrylate) and clay/polystyrene nanocomposites via in situ intercalative polymerization", *Polymer*, 41, 3887-3890.
28. Aranda P., and Ruiz-Hitzky E., 1992 "Poly(ethylene oxide) – silicate intercalation materials", *Chem. Mater.*, 4, 1395-1403.
29. Jeon H., Jung H., Lee S., and Hudson S., 1998. "Morphology of polymer/silicate nanocomposites", *Polymer Bulletin*, 41, 107-113.
30. Choi H., Kim S., Hyun Y., and Jhon M., 2001. "Preparation and Rheological Characteristics of Solvent-Cast Poly(ethylene-oxide)/Montmorillonite Nanocomposites", *Macromol. Rapid Commun.*, 22, 320.
31. Strawhecker K., and Manias E. 2000 "Structure and properties of poly(vinly alcohol)/Na⁺ montmorillonite nanocomposites", *Chem. Mater.*, 12, 2943-2949.
32. Jin Y., Park H., Im S., and Kwak S. 2002. "PE/clay nanocomposites by insitu exfoliation of montmorillonite during Ziegler-Natta polymerization of ethylene", *Macromol. Rapid. Commun.*, 23, 135-140.
- 33 Wang. K., Choi M., Koo C., Choi Y., and Chung I. 2001. "Synthesis and characterization of maleated polyethylene/clay nanocomposites", *Polymer*, 42, 9819-9826.
34. Davis C., Mathias L., Gilman J., Schiraldi D., Shields J., Trulove P., Sutto T., and Delong H. 2002. "Effects of melt-processing conditions on the quality of poly(ethylene terephthalate) montmorillonite clay nanocomposites", *J. Polym. Sci., Polym. Phys.*, 40, 2661-2666.

35. Usuki A., Kato M., Okada A., and Kurauchi T. 1997. "Synthesis of polypropyleneclay hybrid", *J. Appl. Polym. Sci.*, 63, 137-138.
36. Fornes. T., Yoon P., Keskkula H., and Paul D. 2001., "Nylon 6 nanocomposites: the effect of matrix molecular weight", *Polymer*, 42, 9929-9940.
37. Hasegawa, N., Okamoto, H., Kato, M., and Usuki, A., 2000. "Preparation and Mechanical Properties of Polypropylene-Clay Hybrids Based on Modified Polypropylene and Organophilic Clay", *Journal of Applied Polymer Science*, vol. 78, 1918-1922.
38. Luo J. and Daniel I.M., 2003. "Characterization and modeling of mechanical behavior of polymer/clay nanocomposites", *Composites Science and Technology*, vol.63, 1607-1616,
39. Fried J.R., 2003. "Polymer Science and Technology", 2 nd. Edition, Prentice Hall PTR.
40. Zanetti, M., Lomakin S., and Camino G., 2000. "Polymer-Layered Silicate Nanocomposites.", *Macromolecular Materials and Engineering*, 279: p. 1-9.
41. Giannelis EP, Krishnamoorti R, and Manias E. 1999. "Polymer-silicate nanocomposites: model systems for confined polymers and polymer brushes". *Adv Polym Sci*;138:107-47.
42. LeBaron PC, Wang Z, and Pinnavaia TJ. 1999. "Polymer-layered silicate nanocomposites: an overview". *Applied Clay Science*;15: 11-29.
43. Vaia RA, Price G, Ruth PN, Nguyen HT, and Lichtenhan J. 1999., "Polymer/layered silicate nanocomposites as high performance ablative materials". *Applied Clay Science*;15:67-92.
44. Biswas M, and Sinha Ray S. 2001., "Recent progress in synthesis and evaluation of polymer-montmorillonite nanocomposites". *Adv Polym Sci*;155:167-221.

45. Giannelis EP., 1998., "Polymer-layered silicate nanocomposites: synthesis, properties and applications", *Appl Organomet Chem* 12:675–80.
46. Xu R, Manias E, Snyder AJ, and Runt J. 2001. "New biomedical poly(urethane uera)-layered silicate nanocomposites". *Macromolecules*;34:337–9.
47. Bharadwaj RK. 2001. "Modeling the barrier properties of polymerlayered silicate nanocomposites". *Macromolecules*, 34: 1989–92.
48. Messersmith PB, and Giannelis EP. 1995. "Synthesis and barrier properties of poly(1 caprolactone)-layered silicate nanocomposites". *J Polym Sci, Part A: Polym Chem* 1995;33:1047–57.
49. Yano K, Usuki A, Okada A, Kurauchi T, and Kamigaito O. 1993. "Synthesis and properties of polyimide–clay hybrid. *J Polym Sci, Part A: Polym Chem*;31:2493–8.
50. Gilman JW, Jackson CL, Morgan AB, Harris Jr R, Manias E, Giannelis EP, Wuthenow M, Hilton D, and Phillips SH. 2000. "Flammability properties of polymer-layered silicate nanocomposites. Propylene and polystyrene nanocomposites." *Chem Mater*;12:1866–73.
51. Vaia RA, Jandt KD, Kramer EJ, and Giannelis EP. 1995. "Kinetics of polymer melts intercalation". *Macromolecules*;28: 8080–5.
52. Vaia RA, and Giannelis EP. 1997. "Lattice of polymer melt intercalation in organically modified layered silicates". *Macromolecules*, 30:7990–9.
53. Vaia RA, and Giannelis EP. 1997. "Polymer melts intercalation in organically-modified layered silicates: model predictions and experiment." *Macromolecules*;30:8000–9.

54. Ginsburg VV, Singh C, and Balazs AC. 2000. "Theoretical phase diagram of polymer/clay composites: the role of grafted organic modifier". *Macromolecules* 2000;33:1089–99.
55. Lee JY, Baljon ACR, Sogah DY, and Loring RF. 2000. "Molecular dynamics study of intercalation of diblock copolymer into layered silicates". *J Chem Phys* 112:9112–9.
56. Lee JY, Baljon ARC, Loring RF, and Panagiopoulos AZ. Simulation of polymer melt intercalation in layered nanocomposites. *J Chem Phys* 1998;109:10321–30.
57. Balazs AC, Singh C, and Zhulina E. 1998. "Modeling the interactions between the polymers and clay surfaces through self-consistent field theory." *Macromolecules*;31: 8370–81.
58. Balazs AC, Singh C, Zhulina E, and Lyatskaya Y. 1999. "Modeling the phase behavior of polymer–clay composites". *Acc Chem Res* 1999;32:651–7.
59. Manias E, Chen E, Krishnamoorti R, Genzer J, Kramer EJ, and Giannelis EP. 2000. "Intercalation kinetics of long polymers in 2 nm confinements." *Macromolecules* 2000;33:7955–66.
60. Ray S.S. and Okamoto M.,2003. "Polymer/layered Silicate Nanocomposites: A Review from Preparation to Processing", *Progress in Polymer Science*.
61. Vaia RA, Ishii H, and Giannelis EP. 1993. "Synthesis and properties of two-dimensional nanostructures by direct intercalation of polymer melts in layered silicates.", *Chem Mater* 1993;5: 1694–6.
62. Hassan, A., Imran, M., Wahit, M.U., and Balakrishnan, H. 2011. "Recent developments in PA6/PP nanocomposites", *Key Engineering Materials* 471-472, 7-19.

63. Naderi, G., Nekoomanesh, M., Mehtarani, R., and Eslami, H., 2011. "Preparation of a new polypropylene/clay nanocomposites via in situ polymerization", *E-Polymers*, art. no. 16
64. Ataefard, M., and Moradian, S., 2011. "Surface properties of polypropylene/organoclay nanocomposites", *Applied Surface Science* 257 (6), 2320-2326.
65. Ceccia, S., Bellucci, F., Monticelli, O., Frache, A., Traverso, G., and Casale, A., 2010. "The effect of annealing conditions on the intercalation and exfoliation of layered silicates in polymer nanocomposites", *Journal of Polymer Science, Part B: Polymer Physics* 48 (23), 2476-2483.
66. Somwangthanaroj, A., Ubankhlong, W., and Tanthapanichakoon, W., 2010. "Solid-state mechanical properties of polypropylene/nylon 6/clay nanocomposites", *Journal of Applied Polymer Science* 118 (1), 538-546.
67. Ali, M.A.-H., Elleithy, R., AlZahrani, S., and Chafidz, A. 2010. "Preparation of polypropylene-organoclay nanocomposites: Effect on thermal, morphological and viscoelastic properties", *Annual Technical Conference - ANTEC, Conference Proceedings* 1, 5-10.
68. Shroff Rama, M., Neppalli, R., Chellaswamy, R., and Swaminathan, S., 2010. "Exfoliation of clay layers in polypropylene matrix using potassium succinate-g-polypropylene as compatibilizer", *Composites Science and Technology* 70 (10), 1550-1556.
69. Kannan, M., Bhagawan, S.S., Jose, T., Thomas, S., and Joseph, K., 2010. "Preparation and characterization of nanoclay-filled polyurethane/ polypropylene blends", *Polymer Engineering and Science* 50 (9), 1878-1886.
70. Chiu, F.-C., Yen, H.-Z., and Chen, C.-C., 2010. "Phase morphology and physical properties of PP/HDPE/organoclay (nano) composites with and without a maleated EPDM as a compatibilizer", *Polymer Testing* 29 (6), 706-716.

71. Shafiee, M., Ahmad Ramazani, S.A., and Danaei, M., 2010. "Investigation of the gas barrier properties of PP/ciay nanocomposite films with EVA as a compatibiliser prepared by the melt intercalation method", *Polymer - Plastics Technology and Engineering* 49 (10), 991-995.
72. Zhang, X., Guo, J., Zhang, L., Yang, S., Zhang, J., and He, Y., 2010. "Rheological properties of polypropylene/ attapulgitite nanocomposite", *Journal of Nanoscience and Nanotechnology* 10 (8), 5277-5281.
73. Olewnik, E., Garman, K., and Czerwiński, W., 2010. "Thermal properties of new composites based on nanoclay, polyethylene and polypropylene", *Journal of Thermal Analysis and Calorimetry* 101 (1), 323-329.
74. Gaidukov, S., Maksimov, R.D., Kalnins, M., Zicans, J., and Krutohvastov, R., 2010. "Structure and mechanical properties of melt intercalated polypropylene-organomontmorillonite nanocomposites", *Composite Interfaces* 17 (5-7), 705-715.
75. Hao, C., Zhao, Y., He, A., Zhang, X., Wang, D., Ma, Q., and Xu, Y., 2010. "Investigation on the melt spinning fibers of PP/organoclay nanocomposites prepared by in-situ polymerization", *Journal of Applied Polymer Science* 116 (3), 1384-1391.
76. Coskunes, F.I., and Yilmazer, U., 2011. "Preparation and characterization of low density polyethylene/ethylene methyl acrylate glycidyl methacrylate/organoclay nanocomposites", *Journal of Applied Polymer Science* 120 (5), 3087-3097.
77. Dintcheva, N.T., Marino, R., and La Mantia, F.P., 2011. "Effect of the extensional flow on the properties of oriented nanocomposite films for twist wrapping", *Journal of Applied Polymer Science* 120 (5), 2772-2779.

78. Dadfar, A., S.M., Alemzadeh, I., Dadfar, R., and Vosoughi, M., 2011. "Studies on the oxygen barrier and mechanical properties of low density polyethylene/organoclay nanocomposite films in the presence of ethylene vinyl acetate copolymer as a new type of compatibilizer", *Materials and Design* 32 (4), 1806-1813.
79. Kim, J.-C., and Chang, J.-H., 2011. "Characterizations of ultrahigh molecular weight polyethylene nanocomposite films with organomica", *Polymer Engineering and Science* 51 (4), 679-686.
80. Borah, J.S., Karak, N., and Chaki, T.K., 2011. "Effect of organoclay platelets on morphology and properties of LLDPE/EMA blends", *Materials Science and Engineering A* 528 (6), 2820-2830.
81. Livi, S., Duchet-Rumeau, J., Pham, T.N., and Gérard, J.-F., 2011. "Synthesis and physical properties of new surfactants based on ionic liquids: Improvement of thermal stability and mechanical behaviour of high density polyethylene nanocomposites", *Journal of Colloid and Interface Science* 354 (2), 555-562.
82. Santamaría, P., Eguiazabal, J.I., and Nazabal, J., 2011. "Dispersion and mechanical properties of a nanocomposite with an organoclay in an ionomer-compatible LDPE matrix", *Journal of Applied Polymer Science* 119 (3), 1762-1770.
83. Maneshi, A., Soares, J.B.P., and Simon, L.C., 2011. "Polyethylene/clay nanocomposites made with metallocenes supported on different organoclays", *Macromolecular Chemistry and Physics* 212 (3), 216-228.
84. Shojaei, A., Behradfar, A., and Sheikh, N., 2011. "Effect of organoclay loading and electron beam irradiation on the physico-mechanical properties of low-density polyethylene/ethylene-vinyl acetate blend", *Polymers for Advanced Technologies*, Article in Press.
85. Tang, Y., Yang, C., Gao, P., Ye, L., Zhao, C., and Lin, W., 2011. "Polymer Engineering and Science 51 (1), 133-142.

86. Nour, M., Eid, A., El-Nagare, K., and Abdel Aziz, F., 2010. "Preparation and characterisation of polyethylene/clay nanocomposites as a flame retardant materials using ultrasonic technique", *Polymers and Polymer Composites* 18 (3), 159-166.
87. Wang K. H., Choi M. H., Koo C. M., Choi Y.S., and Chung I. J., 2001 "Synthesis and Characterization of Maleated Polyethylene / Clay Nanocomposites", *Polymer*, 42, 9819-9826.
88. Alexandre, M.; Dubois, P.; Sun, T.; Graces, J. M.; Jerome, R. 2002. *Polymer* 43, 2123.
89. Gopakumar T.G., Lee J.A., Kontopoulou M., Parent J.S., 2002. "Influence of Clay Exfoliation on the Physical Properties of Montmorillonite / Polyethylene Composites", *Polymer*, vol. 43, 5483-5491.
90. Bafna, A.; Beaucage, G.; Mirabella, F.; and Mehta, S., 2003. *Polymer*, 44, 1103.
91. Dunkerley, E., and Schmidt, D., 2010. "Effects of composition, orientation and temperature on the O₂ permeability of model polymer/clay nanocomposites", *Macromolecules* 43 (24), 10536-10544.
92. Zhu, B., Zha, W., Zhang, C., and Lee, L.J., 2010. "Polystyrene montmorillonite nanocomposite microcellular foam using supercritical carbon dioxide as blowing agent", *Annual Technical Conference - ANTEC, Conference Proceedings 2*, 1126-1130.
93. Yalçinkaya, S.E., Yildiz, N., Ak, M.S., and Çalimli, A., 2010. "Preparation of polystyrene/montmorillonite nanocomposites: Optimization by response surface methodology (RSM)", *Turkish Journal of Chemistry* 34 (4), 581-592.
94. Khoshniyat, A.R., Aalaie, J., Rahmatpour, A., and KhaBAbaie, G., 2010. "Investigation and preparation of high impact polystyrene nanocomposites", *AIP Conference Proceedings* 1217, 239-245.

95. Liu, S.-P., Huang, I.-J., Chang, K.-C., and Yeh, J.-M., 2010. "Mechanical properties of polystyrene-montmorillonite nanocomposites- prepared by melt intercalation", *Journal of Applied Polymer Science* 115 (1), 288-296.
96. Sedláková, Z., Pleštil, J., Baldrian, J., Šlouf, M., and Holub, P., 2009. "Polymer-clay nanocomposites prepared via in situ emulsion polymerization", *Polymer Bulletin* 63 (3), 365-384.
97. Nayak, S.K., and Mohanty, S., 2009. "Dynamic mechanical, rheological, and thermal properties of intercalated polystyrene/organomontmorillonite nanocomposites: Effect of clay modification on the mechanical and morphological behaviors", *Journal of Applied Polymer Science* 112 (2), 778-787.
98. Giannakas, A., Spanos, C.G., Kourkoumelis, N., Vaimakis, T., and Ladavos, A., 2009. "Structure and thermal stability of polystyrene/layered silicate nanocomposites", *Composite Interfaces* 16 (2-3), 237-247.
99. Kim, B.C., and Lee, B.J., 2008. "Silicate dispersion and rheological properties of high impact polystyrene/organoclay nanocomposites via in situ polymerization", *Korea Australia Rheology Journal* 20 (4), 227-233.
100. Giannakas, A., Spanos, C.G., Kourkoumelis, N., Vaimakis, T., and Ladavos, A., 2008. "Preparation, characterization and water barrier properties of PS/organo-montmorillonite nanocomposites", *European Polymer Journal* 44 (12), 3915-3921.
101. Yeniova C.E., and Yilmazer U., 2010. "Characteristics of Impact Modified Polystyrene/ Organoclay Nanocomposites", *Polymer Composites*, 31:1853–1861.
102. Ozden G., and Yilmazer U., 2006. "Polystyrene–Organoclay Nanocomposites Prepared by Melt Intercalation, In Situ, and Masterbatch Methods", *Polymer Composites* , 27:249–255.

103. Abraham, T.N., Ratna, D., Siengchin, S., and Karger-Kocsis, J., 2009. "Structure and properties of polyethylene oxide-organo clay nanocomposite prepared via melt mixing", *Polymer Engineering and Science* 49 (2), 379-390.
104. Taghizadeh, E., Naderi, G., and Razavi-Nouri, M., 2011. "Effects of organoclay on the mechanical properties and microstructure of PA6/ECO blend", *Polymer Testing* 30 (3), 327-334.
105. Yoo, Y., Spencer, M.W., and Paul, D.R., 2011. "Morphology and mechanical properties of glass fiber reinforced Nylon 6 nanocomposites", *Polymer* 52 (1), 180-190.
106. Scaffaro, R., Botta, L., Mistretta, M.C., and La Mantia, F.P., 2010. "Preparation and characterization of polyamide 6/polyethylene blend-clay nanocomposites in the presence of compatibilisers and stabilizing system", *Polymer Degradation and Stability* 95 (12), 2547-2554.
107. Cui, L., and Yeh, J.-T., 2010. "Nylon 6 crystal-phase transition in nylon 6/clay/poly(vinyl alcohol) nanocomposites", *Journal of Applied Polymer Science* 118 (3), 1683-1690.
108. Timmaraju, M.V., Gnanamoorthy, R., and Kannan, K., 2010. "Influence of organoclay on flexural fatigue behavior of polyamide 66/hectorite nanocomposites at laboratory condition", *Polymer Composites* 31 (11), 1977-1986.
109. Lim, S.-H., Yu, Z.-Z., and Mai, Y.-W., 2010. "Effects of loading rate and temperature on tensile yielding and deformation mechanisms of nylon 6-based nanocomposites", *Composites Science and Technology* 70 (13), 1994-2002.
110. Mert, M., and Yilmazer, U., 2010. "Polyamide 66 binary and ternary nanocomposites: Mechanical and morphological properties", *Journal of Applied Polymer Science* 118 (1), 209-217.

111. García-López, D., Fernández, J.F., Merino, J.C., Santarén, J., and Pastor, J.M., 2010. "Effect of organic modification of sepiolite for PA 6 polymer/organoclay nanocomposites", *Composites Science and Technology* 70 (10), 1429-1436.
112. Kim, E.S., Shim, J.H., Woo, J.Y., Yoo, K.S., and Yoon, J.S., 2010. "Effect of the silane modification of clay on the tensile properties of nylon 6/clay nanocomposites", *Journal of Applied Polymer Science* 117 (2), 809-816.
113. Leite, A.M.D., Maia, L.F., Pereira, O.D., Araújo, E.M., Lira, H.D.L., and de Castro, W.B., 2010. "Mechanical properties of nylon 6/Brazilian clay nanocomposites", *Journal of Alloys and Compounds* 495 (2), 596-597.
114. Goitisoló, I., Eguiazábal, J.I., and Nazabal, J., 2010. "Stiffening of polycarbonate by addition of a highly dispersed and fibrillated amorphous polyamide-based nanocomposite", *Macromolecular Materials and Engineering* 295 (3), 233-242.
115. Bourbigot, S., Samyn, F., Turf, T., and Duquesne, S., 2010. "Nanomorphology and reaction to fire of polyurethane and polyamide nanocomposites containing flame retardants", *Polymer Degradation and Stability* 95 (3), 320-326.
116. Lim, S.-H., Dasari, A., Wang, G.-T., Yu, Z.-Z., Mai, Y.-W., Yuan, Q., Liu, S., and Yong, M.S., 2010. "Impact fracture behaviour of nylon 6-based ternary nanocomposites", *Composites Part B: Engineering* 41 (1), 67-75.
117. Mert, M., and Yilmazer, U., 2009. "Comparison of Polyamiden66–Organoclay Binary and Ternary Nanocomposites", *Advances in Polymer Technology*, 28, No. 3, 155–164.
118. Mert, M., and Yilmazer, U., 2008. "Processing and Properties of Modified Polyamide 66-Organoclay Nanocomposites", *Journal of Applied Polymer Science*, Vol. 108, 3890–3900.

119. Isik I., and Yilmazer U., Bayram G., 2007. "Impact Modified Polyamide-6/Organoclay Nanocomposites: Processing and Characterization", *Polymer Composites*, 29:133–141.
120. Uribe-Calderon, J., and Kamal, M.R., 2010. "Melt compounding of poly(ethylene terephthalate)/clay nanocomposites: Comparison of different organoclays", *Annual Technical Conference - ANTEC, Conference Proceedings 1*, 576-580.
121. Tarverdi, K., and Sontikaew, S., 2009. "Processing of pet nanocomposites with different percentage of surfactants using twin screw extrusion technology", *Annual Technical Conference - ANTEC, Conference Proceedings 1*, 75-79.
122. Lee, S.J., Hahm, W.G., Kikutani, T., and Kim, B.C., 2009. "Effects of clay and POSS nanoparticles on the quiescent and shear-induced crystallization behavior of high molecular weight polyethylene terephthalate", *Polymer Engineering and Science* 49 (2), 317-323.
123. Frounchi, M., and Dourbash, A., 2009. "Oxygen barrier properties of poly(ethylene terephthalate) nanocomposite films", *Macromolecular Materials and Engineering* 294 (1), 68-74.
124. De Giraldo, A.L.F.M., Bizarria, M.T.M., Silva, A.A., Velasco, J.I., D'Ávila, M.A., and Mei, L.H.I., 2008. "Effects of extrusion conditions on the properties of recycled poly(ethylene terephthalate)/nanoclay nanocomposites prepared by a twin-screw extruder", *Journal of Applied Polymer Science* 108 (4), 2252-2259.
125. Kráčálik, M., Studenovský, M., Mikešová, J., Kovářová, J., and Sikora, A., Thomann, R., Friedrich, C., 2007. "Recycled PET-organoclay nanocomposites with enhanced processing properties and thermal stability", *Journal of Applied Polymer Science* 106 (3), 2092-2100.
126. Bizarria, M.T.M., Giraldo, A.L.F.D.M., De Carvalho, C.M., Velasco, J.I., D'Ávila, M.A., and Mei, L.H.I., 2007. "Morphology and thermomechanical properties of recycled PET-organoclay nanocomposites", *Journal of Applied Polymer Science* 104 (3), 1839-1844.

127. Yilmazer, U., and Alyamac, E., 2007. "Effect of impact modifier on the properties of poly (ethylene terephthalate)-organoclay nanocomposites", *Key Engineering Materials* 334-335 II, 649-652.
128. Kim, S.H., and Kim, S.C., 2007. "Synthesis and properties of poly(ethylene terephthalate)/ clay nanocomposites by in situ polymerization", *Journal of Applied Polymer Science* 103 (2), 1262-1271.
129. Barick, A.K., and Tripathy, D.K., 2010. "Effect of organoclay on thermal and dynamic mechanical properties of novel thermoplastic polyurethane nanocomposites prepared by melt intercalation technique", *Polymers for Advanced Technologies* 21 (12), 835-847.
130. Rama, M.S., and Swaminathan, S., 2010. "Influence of structure of organic modifiers and polyurethane on the clay dispersion in nanocomposites via in situ polymerization", *Journal of Applied Polymer Science* 118 (3), 1774-1786.
131. Dimitry, O.I.H., Abdeen, Z.I., Ismail, E.A., and Saad, A.L.G., 2010. "Preparation and properties of elastomeric polyurethane/organically modified montmorillonite nanocomposites", *Journal of Polymer Research* 17 (6), 801-813.
132. Zeng Q. H., Wang D.Z., Yu A.B. and Lu G.Q., 2002. "Synthesis of polymer-montmorillonite nanocomposites by in-situ intercalative polymerization", *Nanotechnology*, vol.13, 549-553.
133. Pinnavaia T.J. and Beall G.W., 2000. "Polymer-Clay Nanocomposites", John Wiley and Sons, Ltd., New York.
134. Manias E., Touny A., Wu L., Strawhecker K., Lu B., and Chung T.C., 2001. "Polypropylene/Montmorillonite Nanocomposites. Review of the Synthetic Routes and Materials Properties", *Chemistry of Materials*, 13, 3516-3523.
135. Fried J.R., 2003. "Polymer Science and Technology", 2 nd. Edition, Prentice Hall PTR.

136. Luo J. and Daniel I.M., 2003. "Characterization and modeling of mechanical behavior of polymer/clay nanocomposites", *Composites Science and Technology*, vol.63, 1607-1616.
137. Xanthos, M., 2005. "Functional Fillers for Plastics", Wiley-VCH Verlag GmbH & Co KGaA,
138. Nguyen Q.T., DONALD G. and Baird D.G., 2006. "Preparation of Polymer–Clay Nanocomposites and Their Properties", *Advances in Polymer Technology*, Vol. 25, No. 4, 270–285.
139. "Kirk-Othmer Encyclopedia of Chemical Technology", 4th ed., vol 6, John Wiley and Sons, Inc., New York, 1993.
140. Francesco C., Serena C., Elisa P., Andrea P., and Giacomo R., 2008. "Nanocomposites based on polyolefins and functional thermoplastic materials", *Polym Int* 57:805–836
141. Kornmann X., 2000. "Synthesis and Characterization of Thermoset-Clay Nanocomposites", Ph. D. Thesis, Lulea University of Technology, Sweden.
142. Fischer H., 2003. "Polymer Nanocomposites: From Fundamental Research to Specific applications" *Material Science and Engineering C*", vol. 23, 763-772.
143. The Dow Chemical Company, <http://www.dow.com>, last accessed April 2011.
144. <http://en.wikipedia.org/wiki/Polyethylene>, last accessed April 2011.
145. "Kirk-Othmer Encyclopedia of Chemical Technology", 4th ed., vol 17, John Wiley and Sons, Inc., New York, 1993
146. "Kirk-Othmer Encyclopedia of Chemical Technology", 4th ed., vol 8, John Wiley and Sons, Inc., New York, 1993.

147. LDPE, http://en.wikipedia.org/wiki/Low_density_polyethylene, last accessed April 2011.
148. LLDPE, http://en.wikipedia.org/wiki/Linear_low-density_polyethylene, last accessed April 2011.
149. Ebewele R.O., 2000. "Polymer Science and Technology", CRC Press LLC, U.S.A.
150. Kroschwitz J. I., 1990. "Concise Encyclopedia of Polymer Science and Engineering", Wiley-Interscience Publication, New York.
151. Rauwendaal C., 1998. "Understanding Extrusion", Hanser/Gardener Publications, Inc., Cincinnati,
152. Rodriguez F., 1996. "Principles of Polymer Systems", 4th edition, Taylor and Francis Publishers, USA.
153. Single screw extruder, <http://www.polymerprocessing.com>, last accessed April 2011.
154. Rauwendaal C. 1994. "Polymer Extrusion" , Third, revised edition, Hanser / Gardner Publications, Inc. Cincinnati.
155. Rubin I.I., 1990. "Handbook of Plastic Materials and Technology", John Wiley & Sons, Inc., New York.
156. Harper C.A., 2002. "Handbook of Plastics, Elastomers & Composites", 4 th Edition, McGraw - Hill, Inc.
157. Mazumdar S.K., 2002."Composites manufacturing: Materials, products and process engineering", CRC Press, New York.

158. Marini, J.; Branciforti, M. C.; Alves, R. M. V. 2010. "Effect of EVA as Compatibilizer on the Mechanical Properties, Permeability Characteristics, Lamellae Orientation, and Long Period of Blown Films of HDPE/Clay Nanocomposites", *J of Appl.Polymer Sci.* , 118, 3340.
159. Hemati, F.; and Garmabi,H. 2010. "Compatibilised Ldpe/Lldpe/Nanoclay Nanocomposites: I. Structural, Mechanical, And Thermal Properties" *Canadian J of Che Eng.*, 9999, 1-10
160. Picard, E.; Vermogen, A.; Ge´rard, J. F.; and Espuche, E. 2008. "Influence of the Compatibilizer Polarity and Molar Mass on the Morphology and the Gas Barrier Properties of Polyethylene/Clay Nanocomposites", *J of Polym. Sci. Part B. Polym. Phys*, 46, 2593.
161. Minkova, L.; and Filippi, S. 2010. "Polymer-Clay Nanocomposites Based on Blends of Various Types of Polyethylenes and PE-g-MA: Morphology, Thermal Properties, Microhardness, and Transparency", *Jour. Macr. Sci., Part B: Physics*, 49,1136.
162. Minkova, L.; Peneva, Y.; Valcheva, M.; Filippi, S.; M. Pracella, M.; Anguillesi, I.; Magagnini, P. 2010. " Morphology, Microhardness, and Flammability of Compatibilized Polyethylene/Clay NanocompositesL.", *Polym. Eng. Sci.* , 50, 1306.
163. Andersson, T.; and Wesslén, "Degradation Of LDPE LLDPE and HDPE In Film Extrusion"B. Department of Material Development, Sweden
164. Kwon, S.; Kima, K.J.; Kima, H.; and Kundua, P.P.; 2002. "Tensile property and interfacial dewetting in the calcite filled HDPE, LDPE, and LLDPE composites" *Polymer*, 43, 6901.
165. Yoon J. T., Jo W. H., Lee M. S., and Ko M.B, 2001. "Effects of Comonomers and Shear on the Melt Intercalation of Styrenics/Clay Nanocomposites", *Polymer*,vol. 42, 329-336.

166. Özden G., 2004. "Synthesis and Characterization of Polystyrene Clay Nanocomposites", M.Sc. Thesis, Middle East Technical University, Ankara, TURKEY.

167. Polymer Crystallinity, "[http:// www.engr.utk.edu/ mse/ Textiles/ Polymer % 20 Crystallinity.htm](http://www.engr.utk.edu/mse/Textiles/Polymer%20Crystallinity.htm)" , last accessed May 2011.

168. Isik I. 2007., "Impact Modified Polyamide-Organoclay Nanocomposites", Ph.D. Thesis, Middle East Technical University, Ankara.

APPENDIX A

XRD ANALYSIS

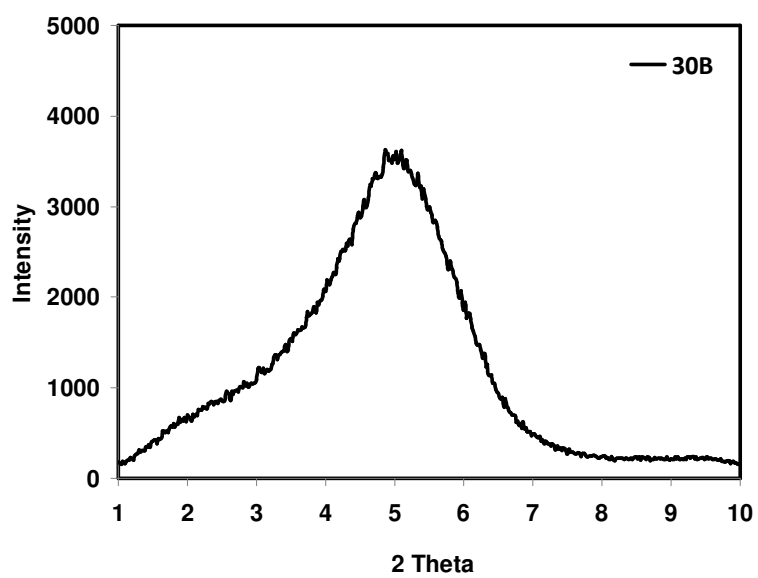


Figure A.1 X-Ray diffraction pattern of organoclay Cloisite 30B.

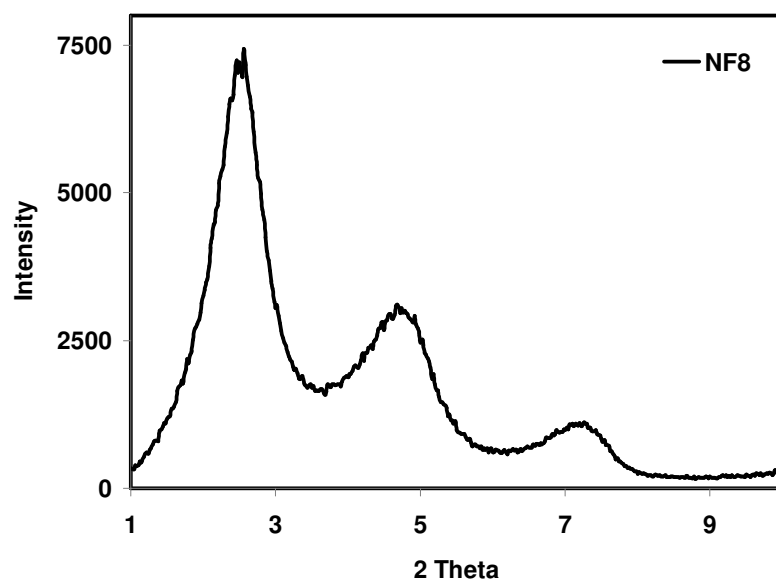


Figure A.2 X-Ray diffraction pattern of organoclay Nanofil 8.

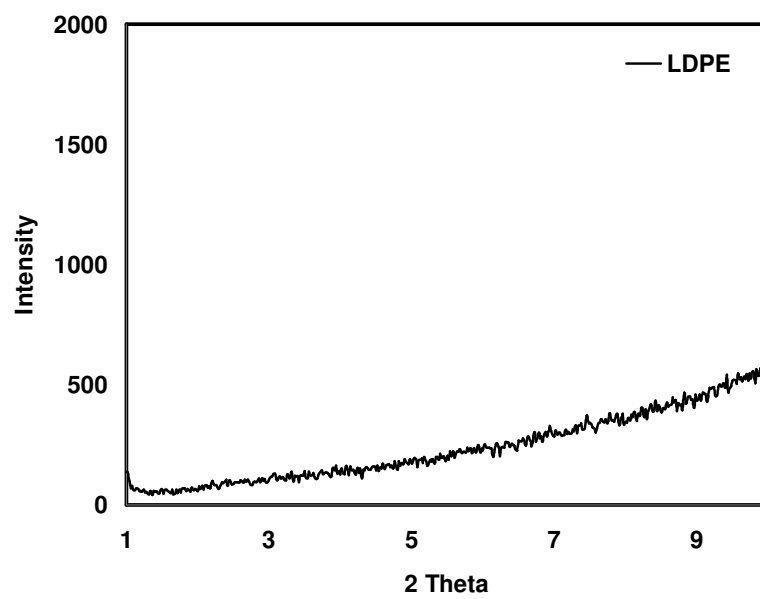


Figure A.3 X-Ray diffraction pattern of pure LDPE

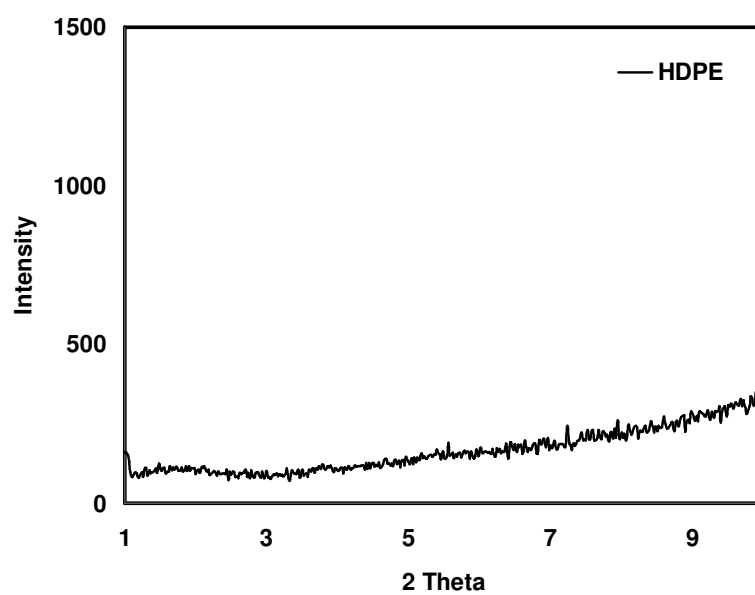


Figure A.4 X-Ray diffraction pattern of pure HDPE

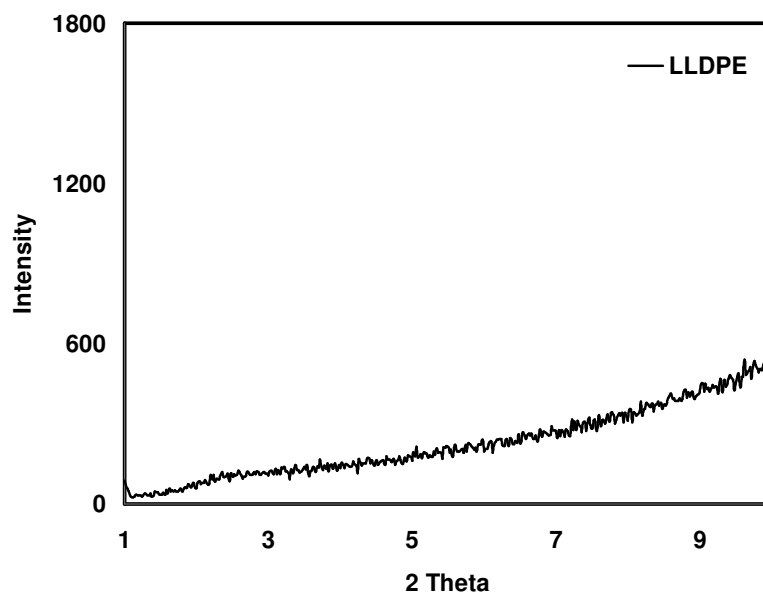


Figure A.5 X-Ray diffraction pattern of pure LLDPE

APPENDIX B

DSC ANALYSIS

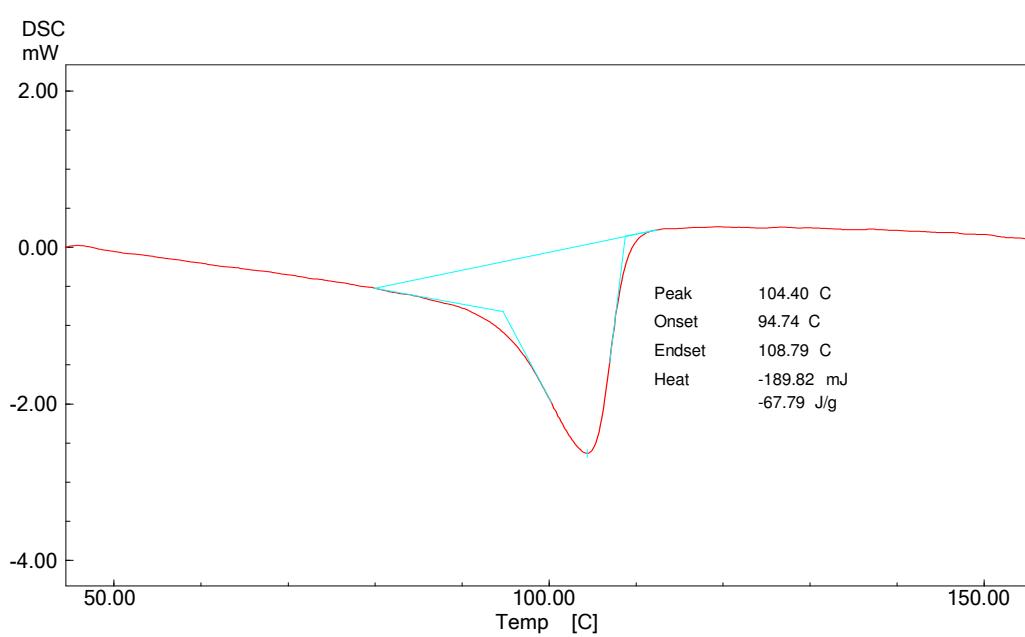


Figure B.1 DSC thermogram of neat LDPE

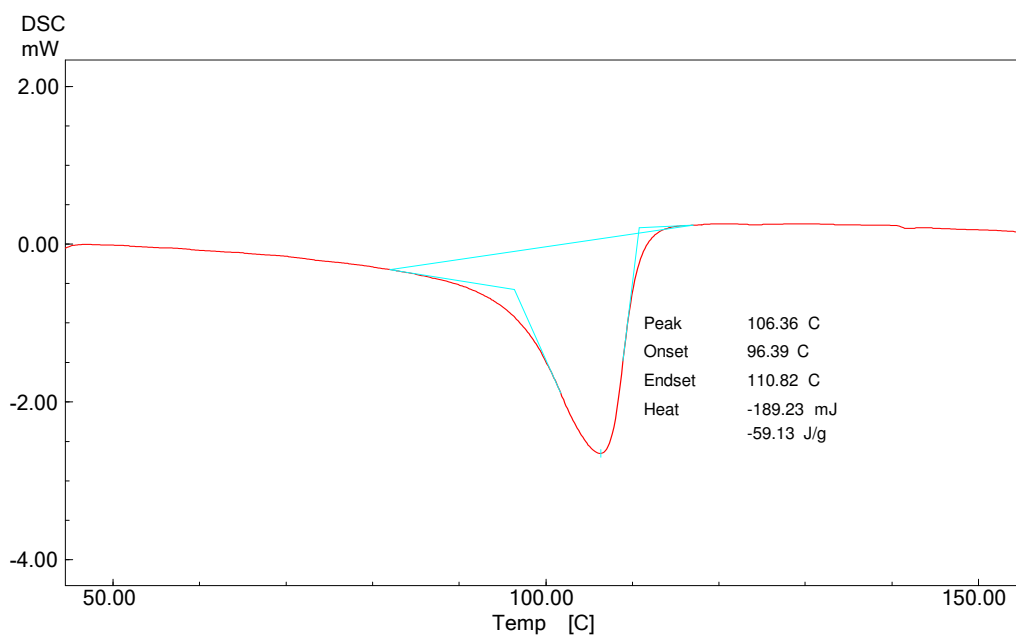


Figure B.2 DSC thermogram of LD/E-MA-GMA binary blend containing 5 wt % compatibilizer

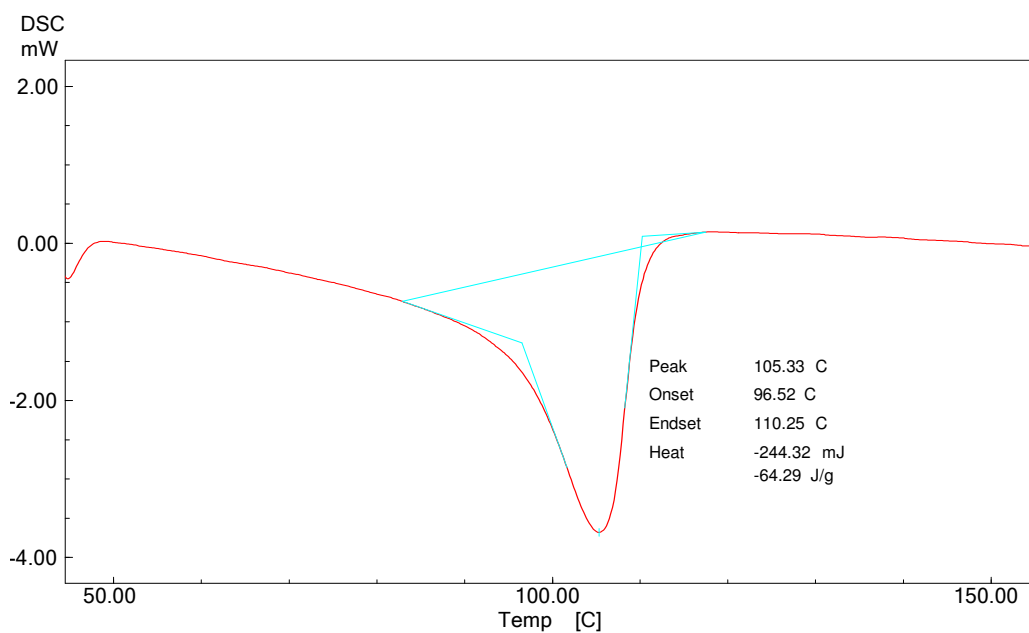


Figure B.3 DSC thermogram of LD/E-BA-MAH binary blend containing 5 wt % compatibilizer

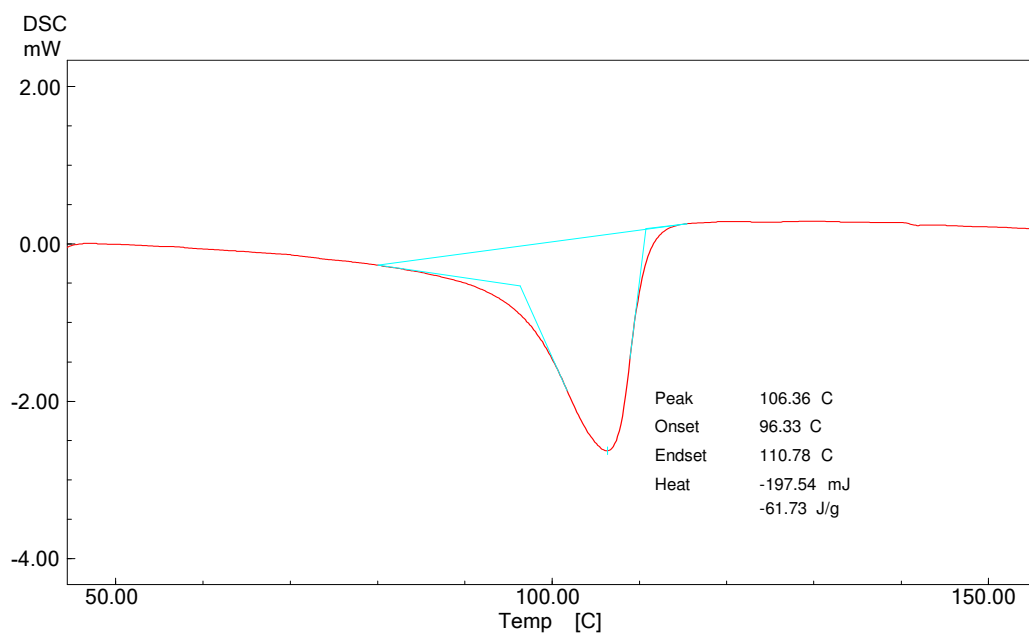


Figure B.4 DSC thermogram of LD/30B binary nanocomposite containing 2 wt % organoclay

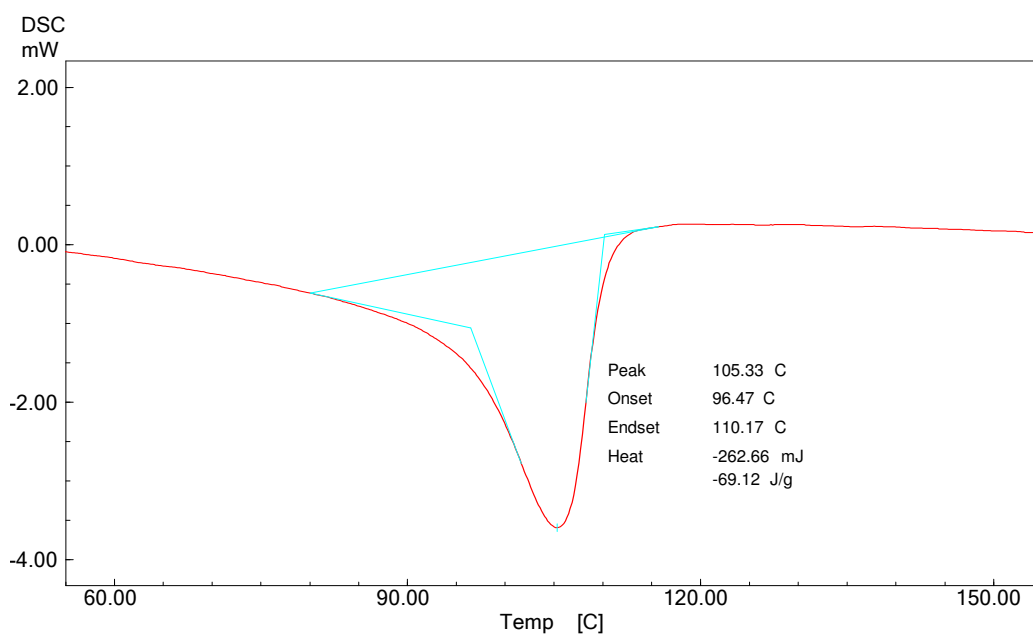


Figure B.5 DSC thermogram of LD/NF8 binary nanocomposite containing 2 wt % organoclay

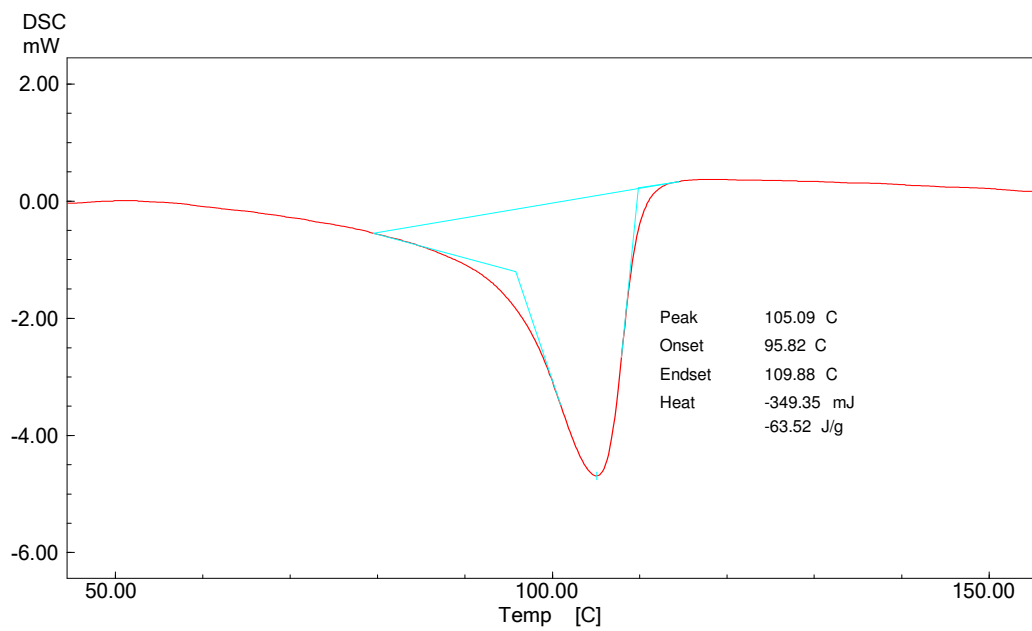


Figure B.6 DSC thermogram of LD/E-MA-GMA/30B ternary nanocomposite containing 5 wt % compatibilizer and 2 wt % organoclay

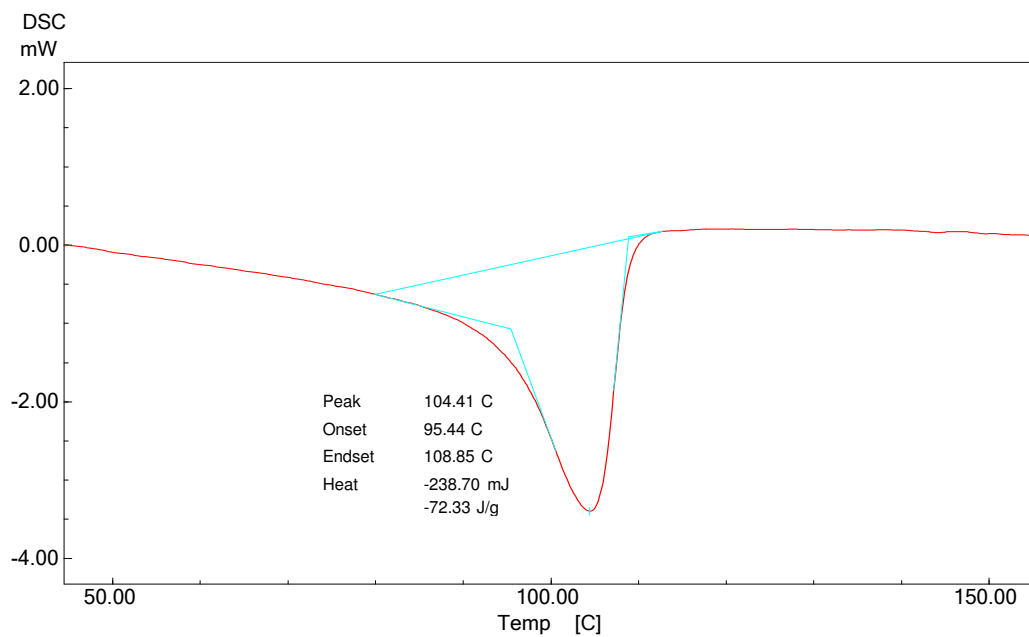


Figure B.7 DSC thermogram of LD/E-BA-MAH/30B ternary nanocomposite containing 5 wt % compatibilizer and 2 wt % organoclay

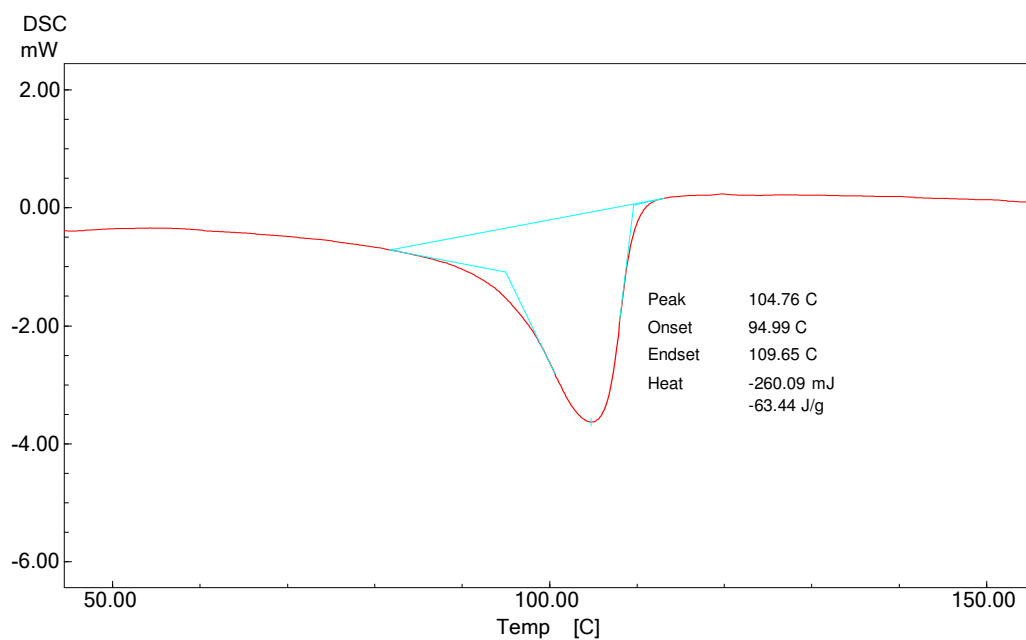


Figure B.8 DSC thermogram of LD/E-MA-GMA/NF8 ternary nanocomposite containing 5 wt % compatibilizer and 2 wt % organoclay

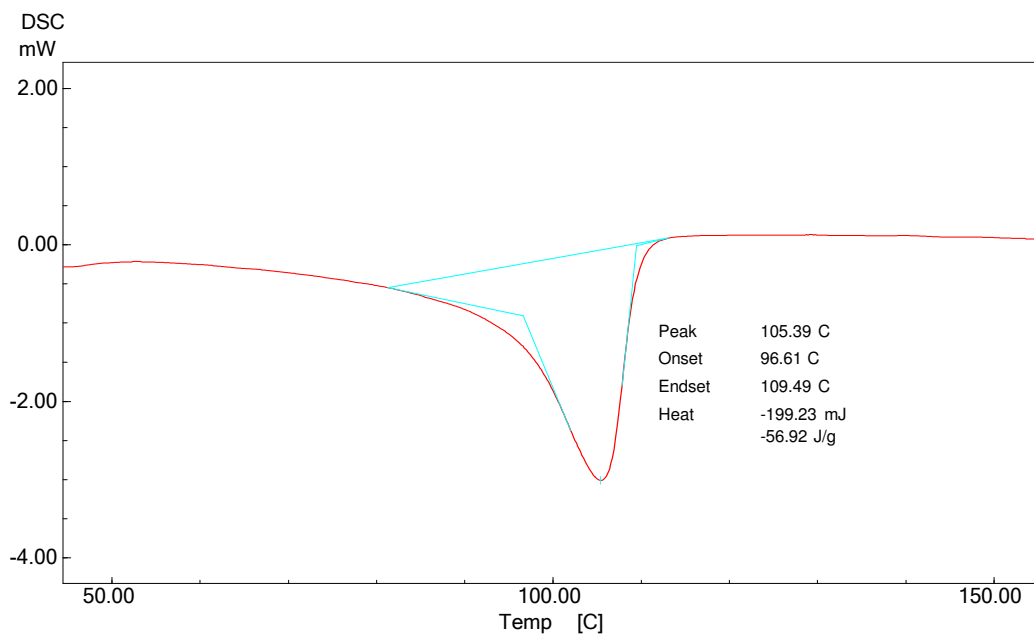


Figure B.9 DSC thermogram of LD/E-BA-MAH/NF8 ternary nanocomposite containing 5 wt % compatibilizer and 2 wt % organoclay

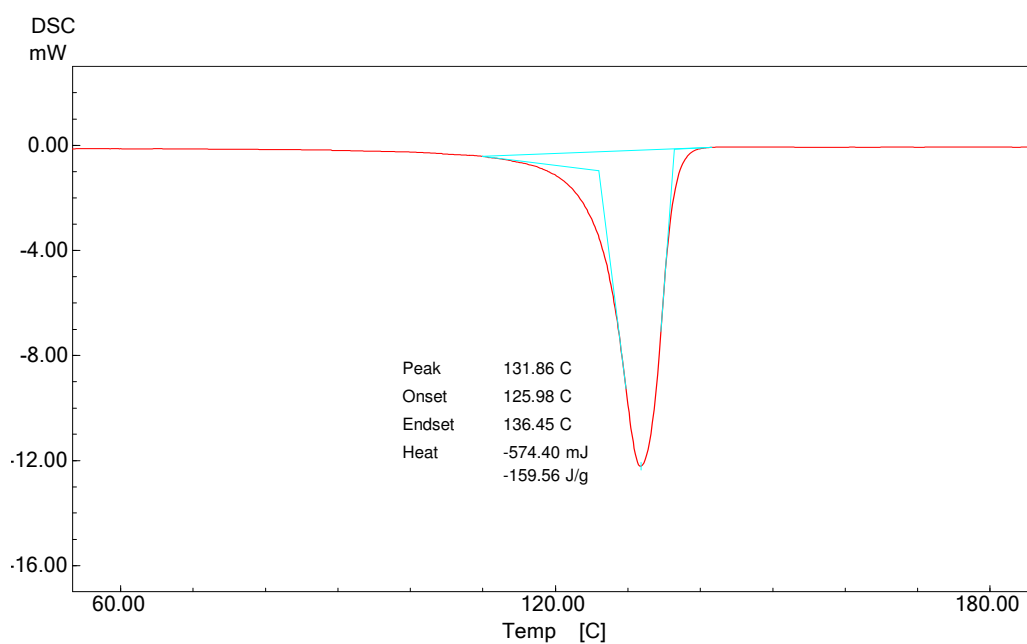


Figure B.10 DSC thermogram of neat HDPE

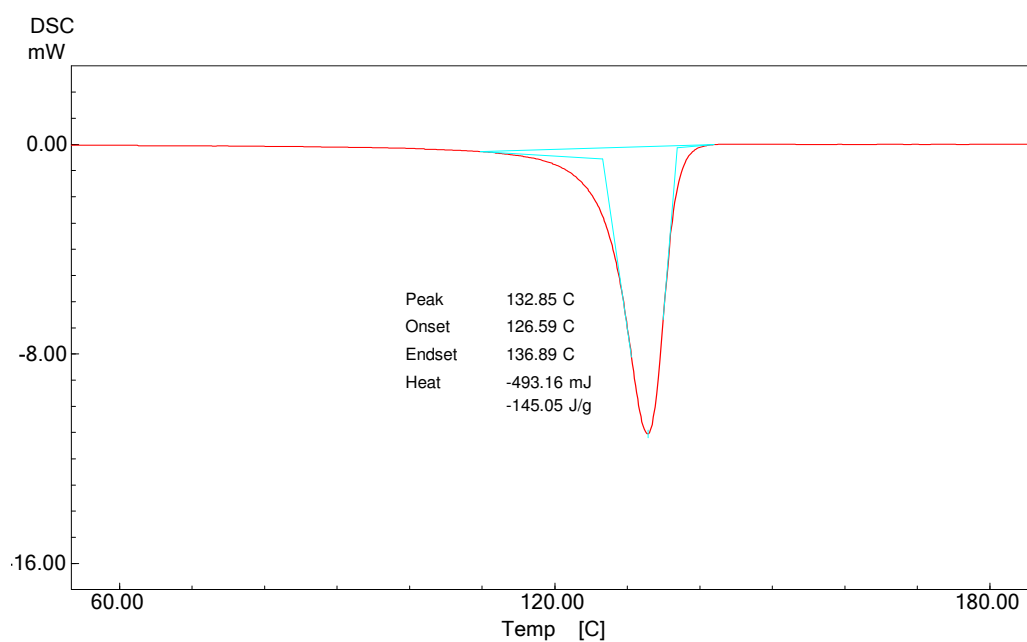


Figure B.11 DSC thermogram of HD/E-MA-GMA binary blend containing 5 wt % compatibilizer

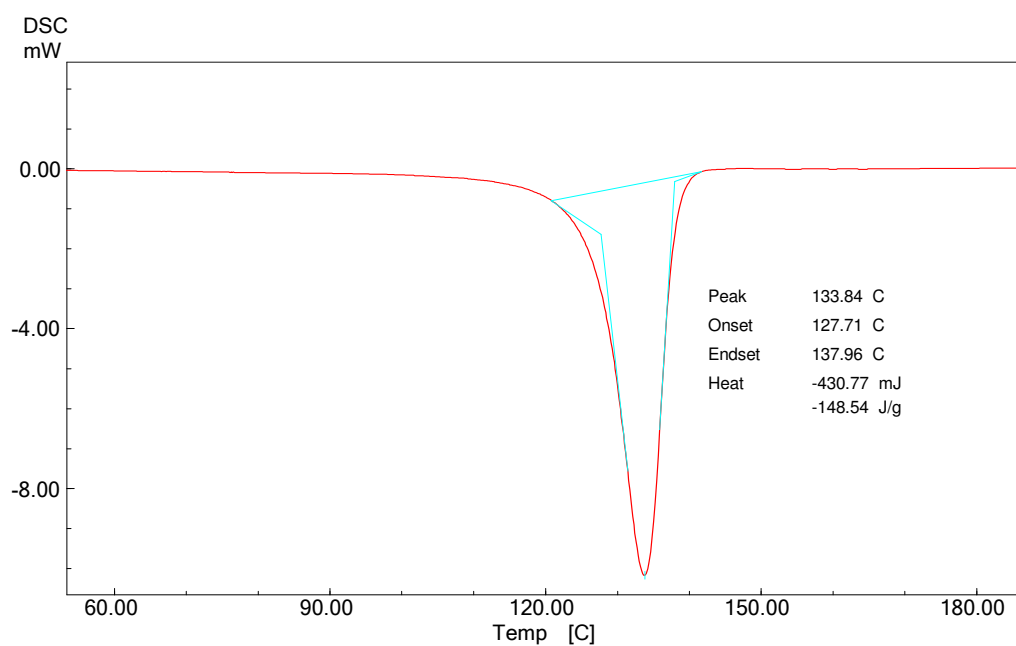


Figure B.12 DSC thermogram of HD/E-BA-MAH binary blend containing 5 wt % compatibilizer

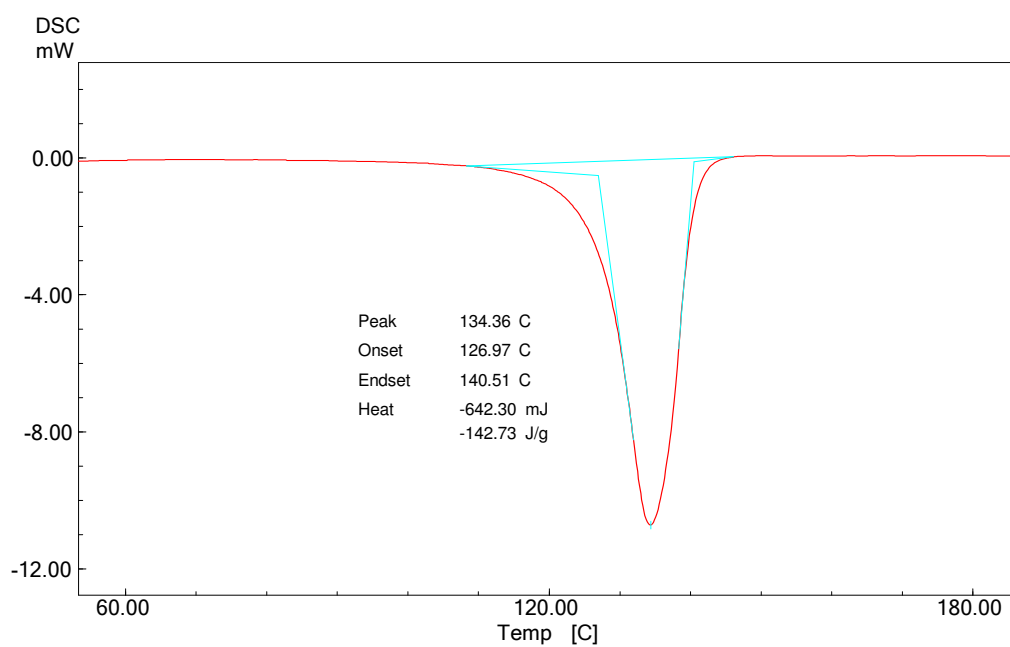


Figure B.13 DSC thermogram of HD/30B binary nanocomposite containing 2 wt % organoclay

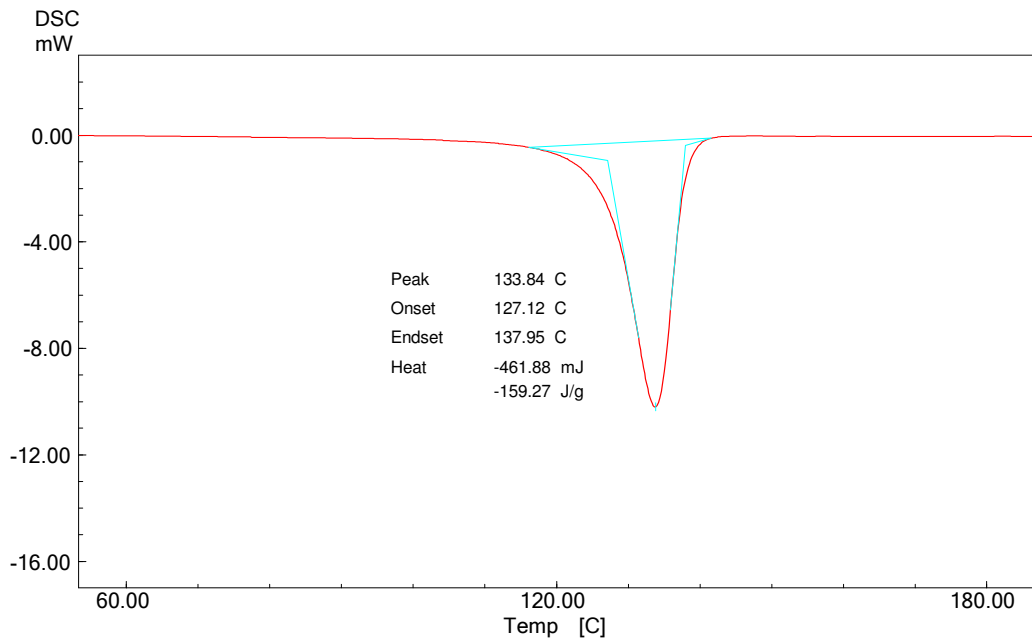


Figure B.14 DSC thermogram of HD/NF8 binary nanocomposite containing 2 wt % organoclay

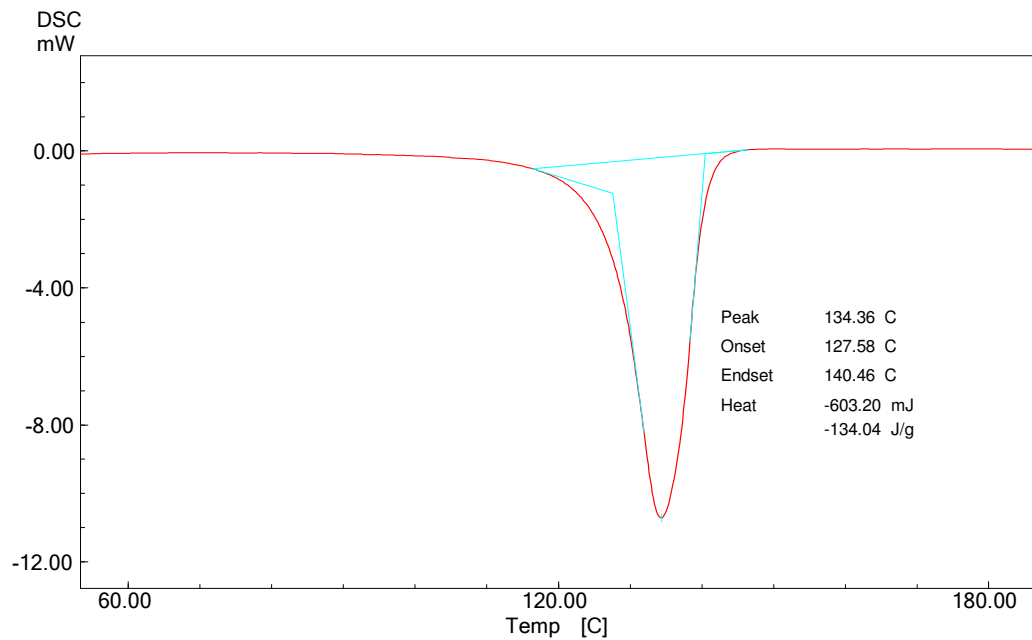


Figure B.15 DSC thermogram of HD/E-MA-GMA/30B ternary nanocomposite containing 5 wt % compatibilizer and 2 wt % organoclay

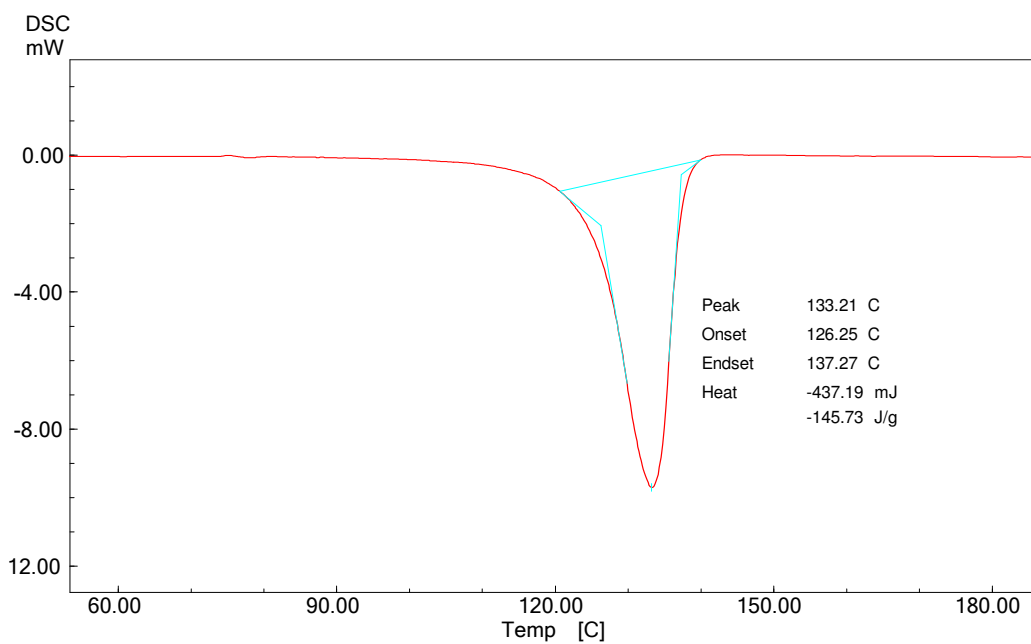


Figure B.16 DSC thermogram of HD/E-BA-MAH/30B ternary nanocomposite containing 5 wt % compatibilizer and 2 wt % organoclay

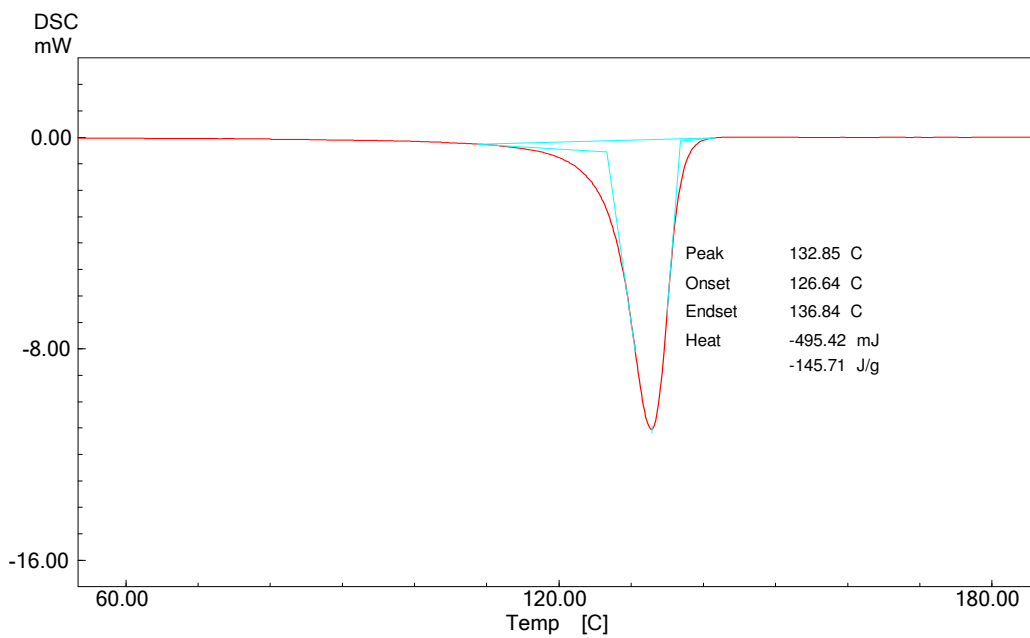


Figure B.17 DSC thermogram of HD/E-MA-GMA/NF8 ternary nanocomposite containing 5 wt % compatibilizer and 2 wt % organoclay

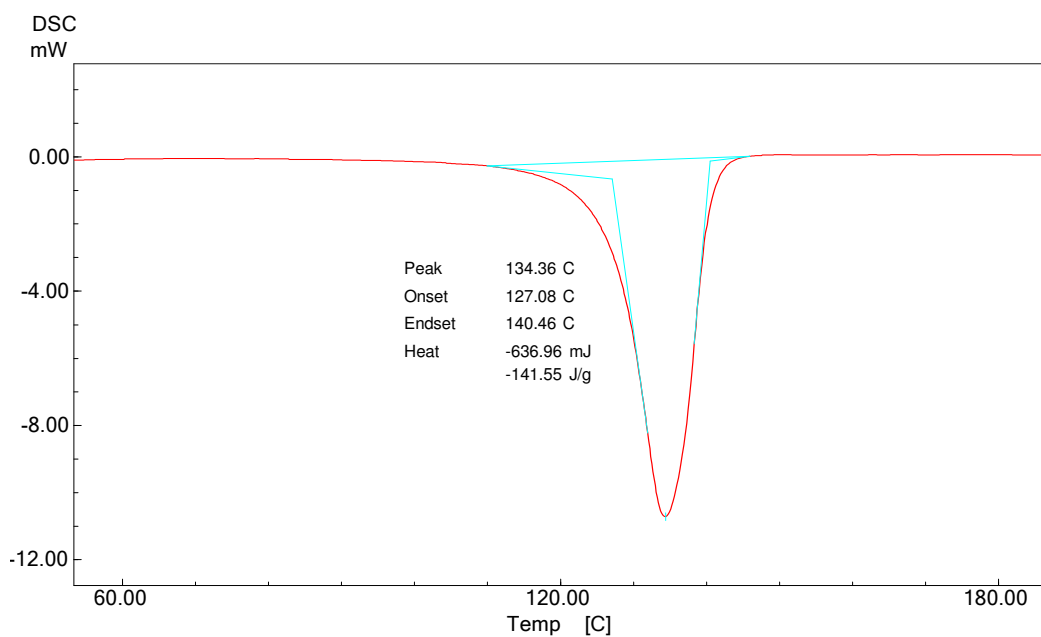


Figure B.18 DSC thermogram of HD/E-BA-MAH/NF8 ternary nanocomposite containing 5 wt % compatibilizer and 2 wt % organoclay

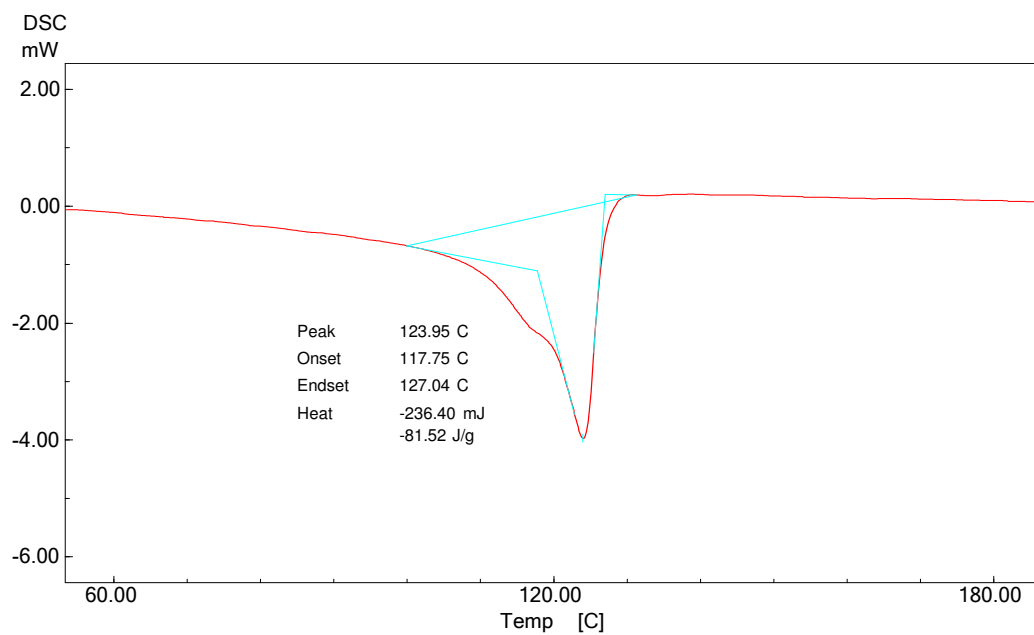


Figure B.19 DSC thermogram of neat LLDPE

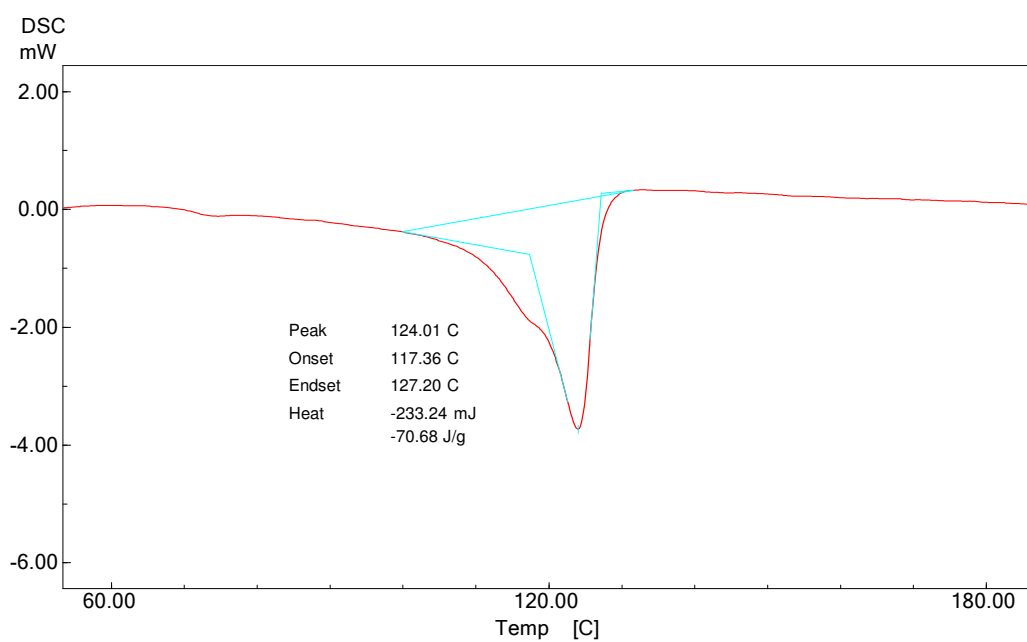


Figure B.20 DSC thermogram of LIN/E-MA-GMA binary blend containing 5 wt % compatibilizer

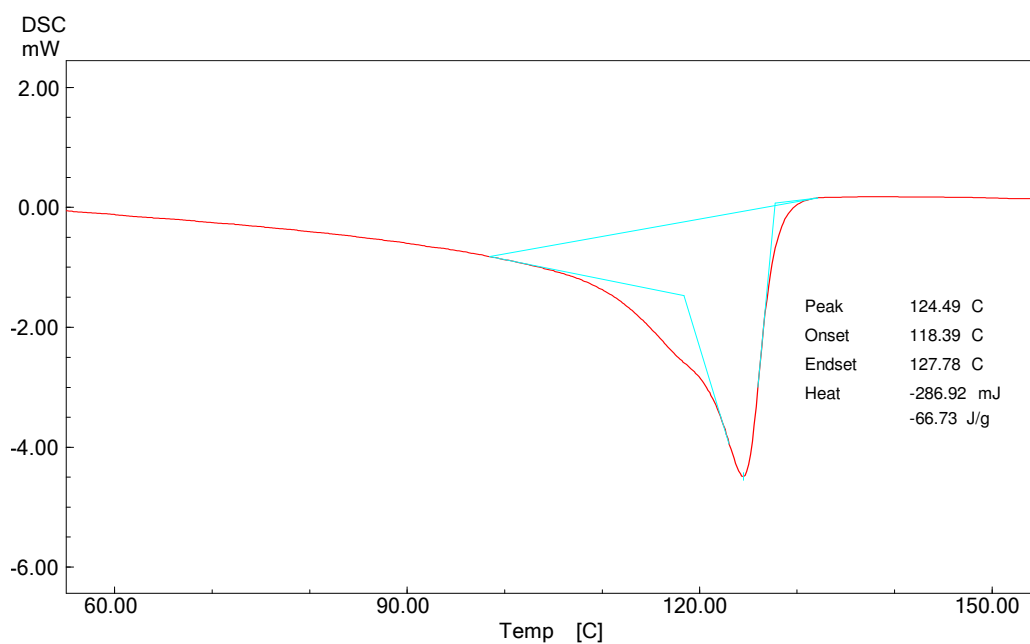


Figure B.21 DSC thermogram of LIN/E-BA-MAH binary blend containing 5 wt % compatibilizer

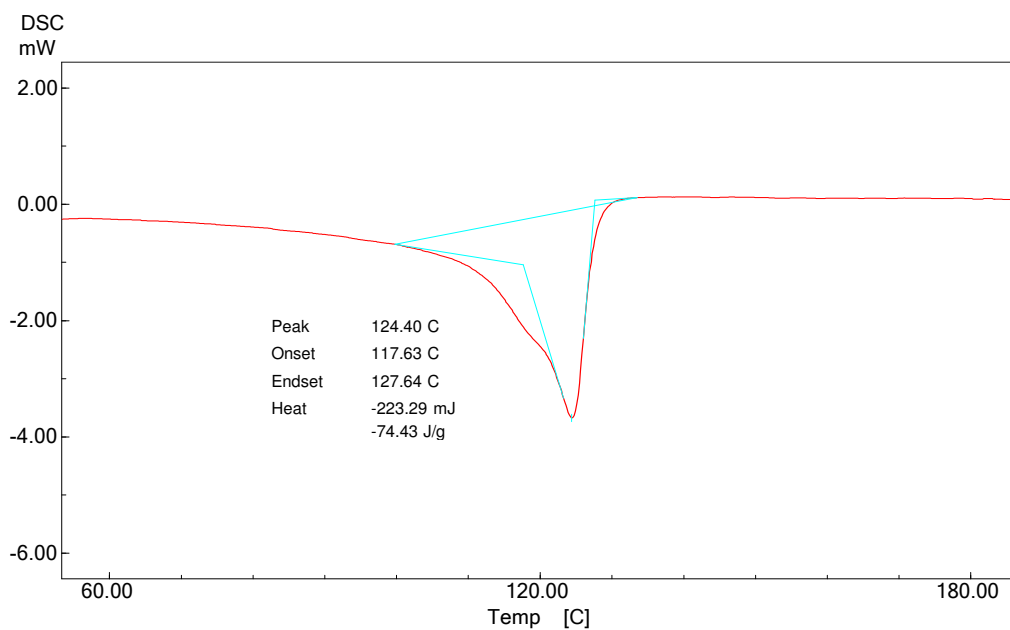


Figure B.22 DSC thermogram of LIN/30B binary nanocomposite containing 2 wt % organoclay

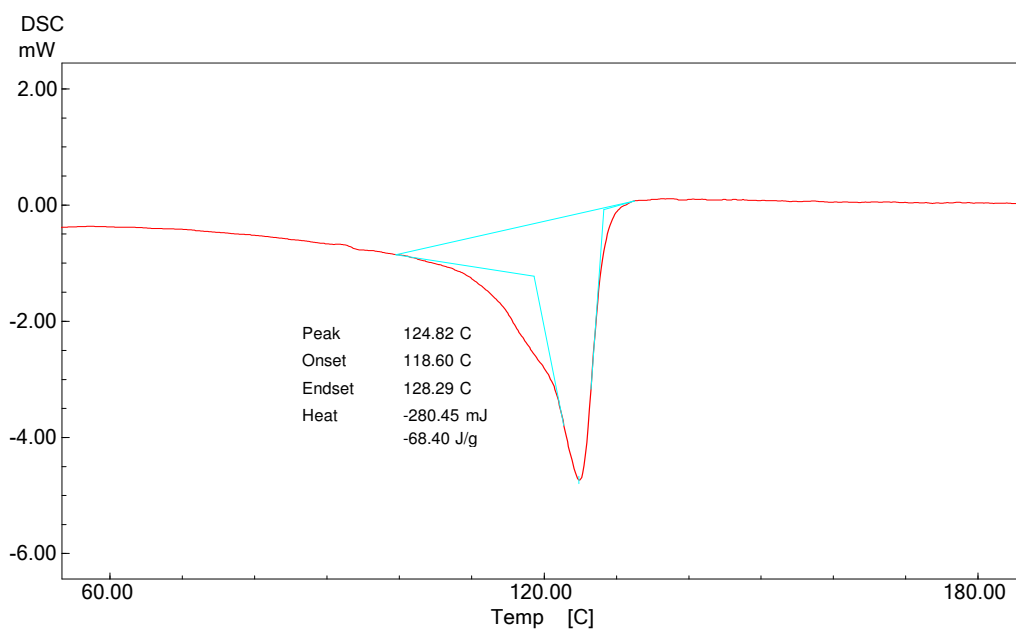


Figure B.23 DSC thermogram of LIN/NF8 binary nanocomposite containing 2 wt % organoclay

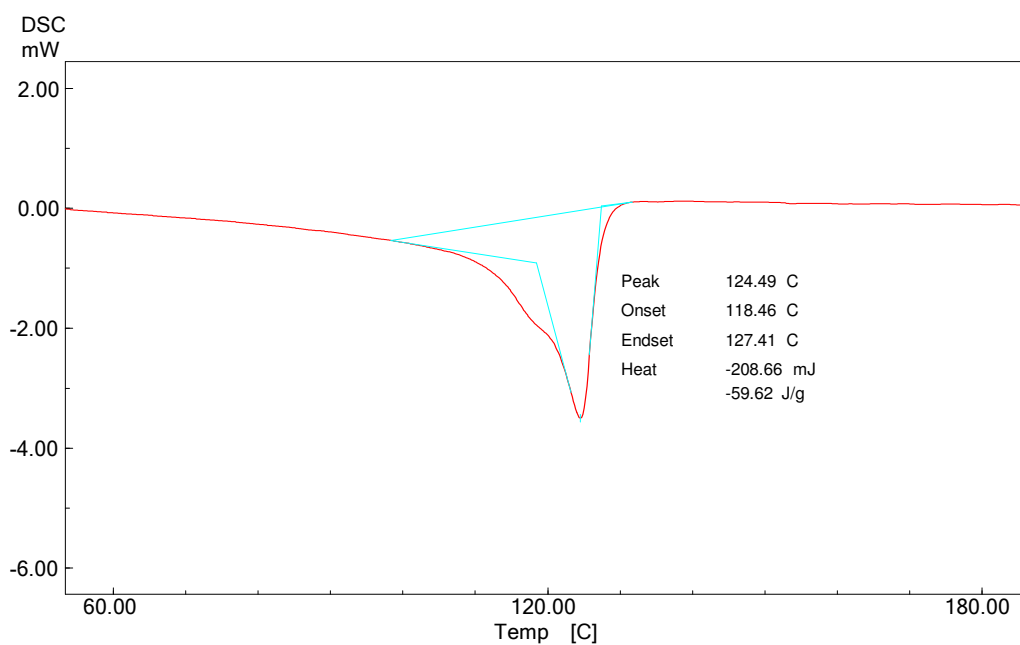


Figure B.24 DSC thermogram of LIN/E-MA-GMA/30B ternary nanocomposite containing 5 wt % compatibilizer and 2 wt % organoclay

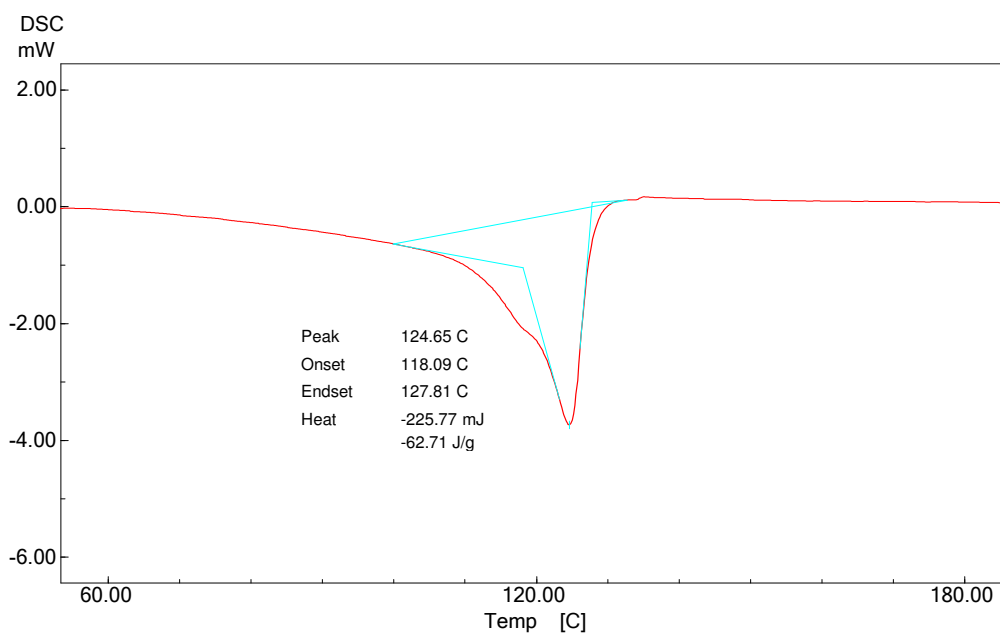


Figure B.25 DSC thermogram of LIN/E-BA-MAH/30B ternary nanocomposite containing 5 wt % compatibilizer and 2 wt % organoclay

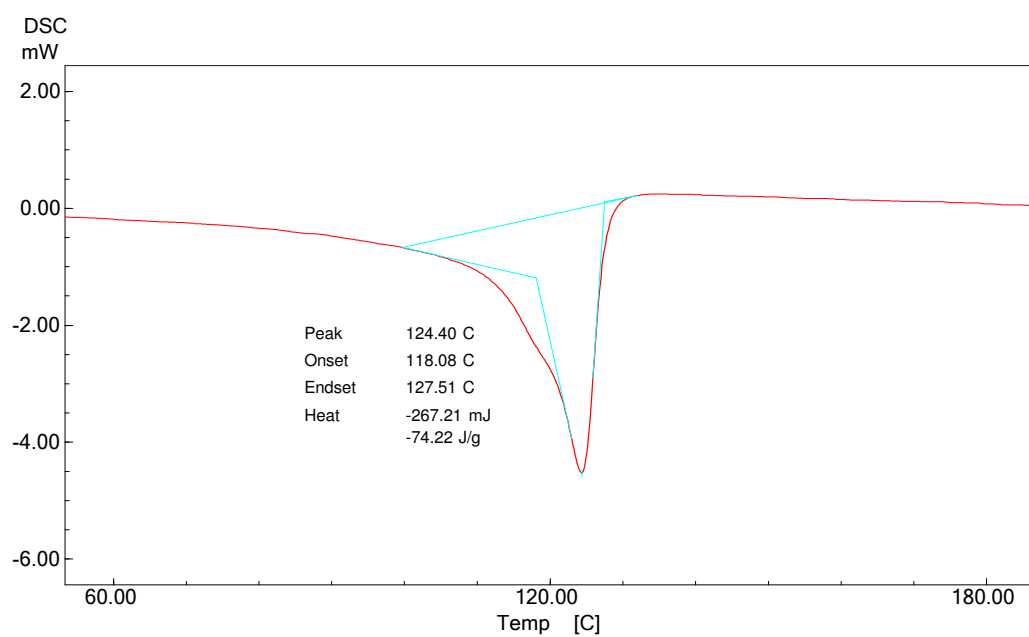


Figure B.26 DSC thermogram of LIN/E-MA-GMA/NF8 ternary nanocomposite containing 5 wt % compatibilizer and 2 wt % organoclay

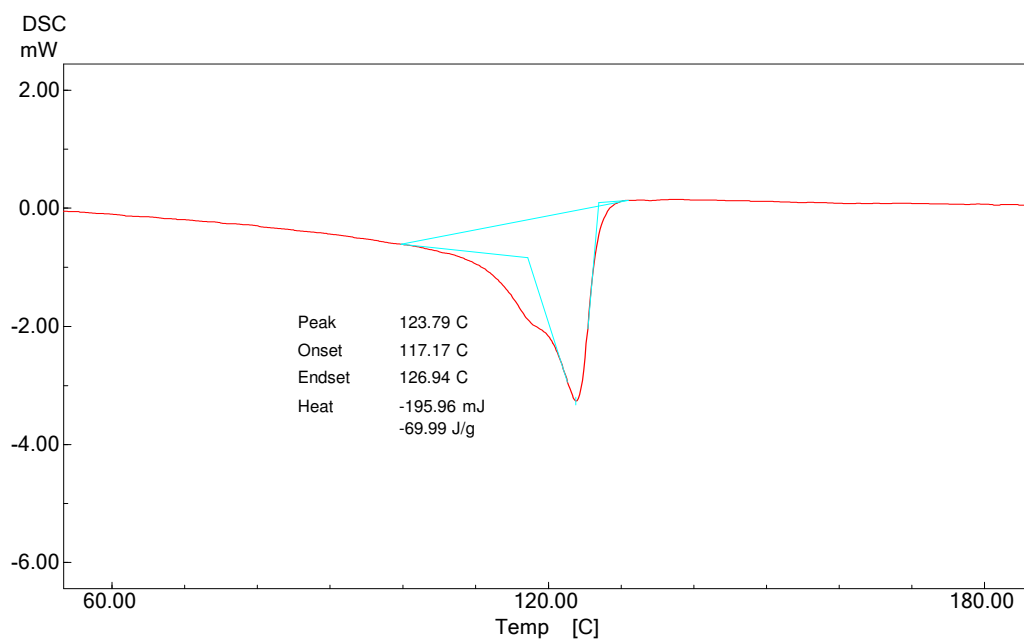


Figure B.27 DSC thermogram of LIN/E-BA-MAH/NF8 ternary nanocomposites containing 5 wt % compatibilizer and 2 wt % organoclay

APPENDIX C

TENSILE TEST RESULTS

Table C.1 Tensile strength data of samples with LDPE matrix

Sample	Tensile Strength (MPa)	Std. Dev.
LDPE	15.1	1.2
LD/E-MA-GMA 5 %	14.9	0.4
LD/E-MA-GMA 10 %	11.7	0.1
LD/E-BA-MAH 5 %	15.4	0.6
LD/E-BA-MAH 10 %	13.2	0.4
LD/30B 2%	15.4	0.1
LD/30B 4%	15.1	0.1
LD/30B 6%	13.9	0.6
LD/NF8 2%	13.0	1.2
LD/NF8 4%	14.7	1.0
LD/NF8 6%	13.7	1.1
LD/E-MA-GMA/30B	15.8	1.3
LD/E-BA-MAH/30B	16.1	1.3
LD/E-MA-GMA/NF8	15.5	1.3
LD/E-BA-MAH/NF8	15.9	0.1

Table C.2 Tensile strength data of samples with HDPE matrix

Sample	Tensile Strength (MPa)	Std. Dev. (\pm)
HDPE	33.8	0.5
HD/E-MA-GMA 5 %	32.5	1.7
HD/E-MA-GMA 10 %	31.8	0.5
HD/E-BA-MAH 5 %	31.9	1.6
HD/E-BA-MAH 10 %	31.4	1.7
HD/30B 2%	33.1	0.6
HD/30B 4%	34.3	1.1
HD/30B 6%	34.5	1.6
HD/NF8 2%	37.9	1.6
HD/NF8 4%	37.5	0.5
HD/NF8 6%	42.6	2.2
HD/E-MA-GMA/30B	36.5	2.9
HD/E-BA-MAH/30B	37.1	2.0
HD/E-MA-GMA/NF8	39.0	0.7
HD/E-BA-MAH/NF8	39.1	0.9

Table C.3 Tensile strength data of samples with LLDPE matrix

Sample	Tensile Strength (MPa)	Std. Dev. (\pm)
LLDPE	15.9	0.2
LIN/E-MA-GMA 5 %	14.6	1.5
LIN/E-MA-GMA 10 %	15.3	2.0
LIN/E-BA-MAH 5 %	16.0	0.2
LIN/E-BA-MAH 10 %	15.1	0.9
LIN/30B 2%	14.7	0.9
LIN/30B 4%	15.6	0.1
LIN/30B 6%	15.2	0.8
LIN/NF8 2%	15.8	0.3
LIN/NF8 4%	14.9	0.3
LIN/NF8 6%	15.8	0.5
LIN/E-MA-GMA/30B	18.0	0.8
LIN/E-BA-MAH/30B	17.7	0.2
LIN/E-MA-GMA/NF8	17.4	1.1
LIN/E-BA-MAH/NF8	16.5	0.8

Table C.4 Young's Modulus data of samples with LDPE matrix

Sample	Young's Modulus (Mpa)	Std. Dev. (\pm)
LDPE	167	10.8
LD/E-MA-GMA 5 %	137	6.1
LD/E-MA-GMA 10 %	123	4.0
LD/E-BA-MAH 5 %	139	5.5
LD/E-BA-MAH 10 %	129	9.26
LD/30B 2%	156	4.2
LD/30B 4%	161	9.3
LD/30B 6%	166	6.6
LD/NF8 2%	164	6.96
LD/NF8 4%	185	6.14
LD/NF8 6%	190	8.17
LD/E-MA-GMA/30B	174	12.8
LD/E-BA-MAH/30B	170	8.5
LD/E-MA-GMA/NF8	180	6.3
LD/E-BA-MAH/NF8	178	4.9

Table C.5 Young's Modulus data of samples with HDPE matrix

Sample	Young's Modulus (MPa)	Std. Dev. (\pm)
HDPE	1132	54.7
HD/E-MA-GMA 5 %	1040	59.9
HD/E-MA-GMA 10 %	625	95.7
HD/E-BA-MAH 5 %	1073	63.1
HD/E-BA-MAH 10 %	733	130
HD/30B 2%	1125	144
HD/30B 4%	1111	203
HD/30B 6%	794	157
HD/NF8 2%	1114	71.9
HD/NF8 4%	1156	58.6
HD/NF8 6%	1188	85.4
HD/E-MA-GMA/30B	1180	41.2
HD/E-BA-MAH/30B	1168	70.8
HD/E-MA-GMA/NF8	1190	80.8
HD/E-BA-MAH/NF8	1240	73.8

Table C.6 Young's Modulus data of samples with LLDPE matrix

Sample	Young's Modulus (Mpa)	Std. Dev. (\pm)
LLDPE	230	12.2
LIN/E-MA-GMA 5 %	233	19.6
LIN/E-MA-GMA 10 %	159	28.2
LIN/E-BA-MAH 5 %	218	16.9
LIN/E-BA-MAH 10 %	203	47.8
LIN/30B 2%	264	36.2
LIN/30B 4%	341	19.2
LIN/30B 6%	290	41.4
LIN/NF8 2%	340	24.2
LIN/NF8 4%	320	18.4
LIN/NF8 6%	294	32.6
LIN/E-MA-GMA/30B	256	11.5
LIN/E-BA-MAH/30B	233	22.2
LIN/E-MA-GMA/NF8	249	28.7
LIN/E-BA-MAH/NF8	226	24.9

Table C.7 Percent elongation at break data of samples with LDPE matrix

Sample	% Elongation at break	Std. Dev. (\pm)
LDPE	121	8.4
LD/E-MA-GMA 5 %	109	9.2
LD/E-MA-GMA 10 %	121	13.5
LD/E-BA-MAH 5 %	131	5.9
LD/E-BA-MAH 10 %	131	9.3
LD/30B 2%	95.5	0.9
LD/30B 4%	92.7	7.4
LD/30B 6%	78.8	6.7
LD/NF8 2%	107	9.4
LD/NF8 4%	104	11.6
LD/NF8 6%	96.1	14.9
LD/E-MA-GMA/30B	81.9	1.4
LD/E-BA-MAH/30B	83.7	1.2
LD/E-MA-GMA/NF8	115	11.4
LD/E-BA-MAH/NF8	109	2.7

Table C.8 Percent elongation at break data of samples with HDPE matrix

Sample	% Elongation at break	Std. Dev. (\pm)
HDPE	456	16.2
HD/E-MA-GMA 5 %	481	7.7
HD/E-MA-GMA 10 %	570	19.3
HD/E-BA-MAH 5 %	507	8.1
HD/E-BA-MAH 10 %	513	11.0
HD/30B 2%	469	25.5
HD/30B 4%	467	17.1
HD/30B 6%	450	21.1
HD/NF8 2%	471	10.4
HD/NF8 4%	447	12.6
HD/NF8 6%	237	51.4
HD/E-MA-GMA/30B	467	8.6
HD/E-BA-MAH/30B	457	4.8
HD/E-MA-GMA/NF8	461	8.3
HD/E-BA-MAH/NF8	420	14.8

Table C.9 Percent elongation at break data of samples with LLDPE matrix

Sample	% Elongation at break	Std. Dev. (\pm)
LLDPE	624	23.4
LIN/E-MA-GMA 5 %	503	64.1
LIN/E-MA-GMA 10 %	489	49.6
LIN/E-BA-MAH 5 %	607	20.6
LIN/E-BA-MAH 10 %	619	48.4
LIN/30B 2%	533	12.7
LIN/30B 4%	521	11.4
LIN/30B 6%	503	8.5
LIN/NF8 2%	572	18.4
LIN/NF8 4%	443	55.9
LIN/NF8 6%	397	71.6
LIN/E-MA-GMA/30B	518	8.10
LIN/E-BA-MAH/30B	495	18.6
LIN/E-MA-GMA/NF8	557	19.9
LIN/E-BA-MAH/NF8	538	0.50

APPENDIX D

STRESS-STRAIN CURVES

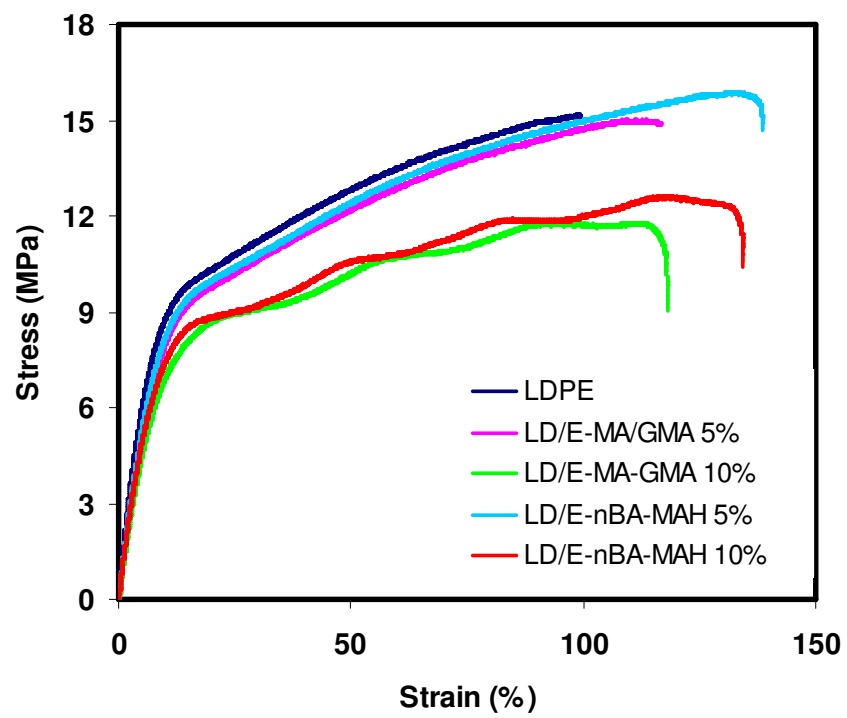


Figure D.1 Tensile stress-strain curve of LD/Compatibilizer blends

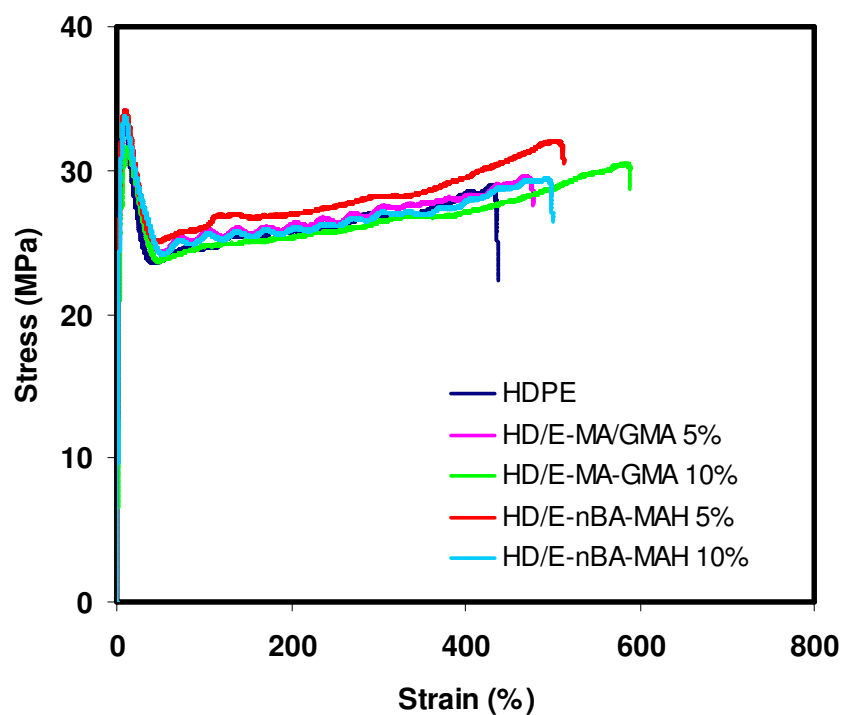


Figure D.2 Tensile stress-strain curve of HD/Compatibilizer blends

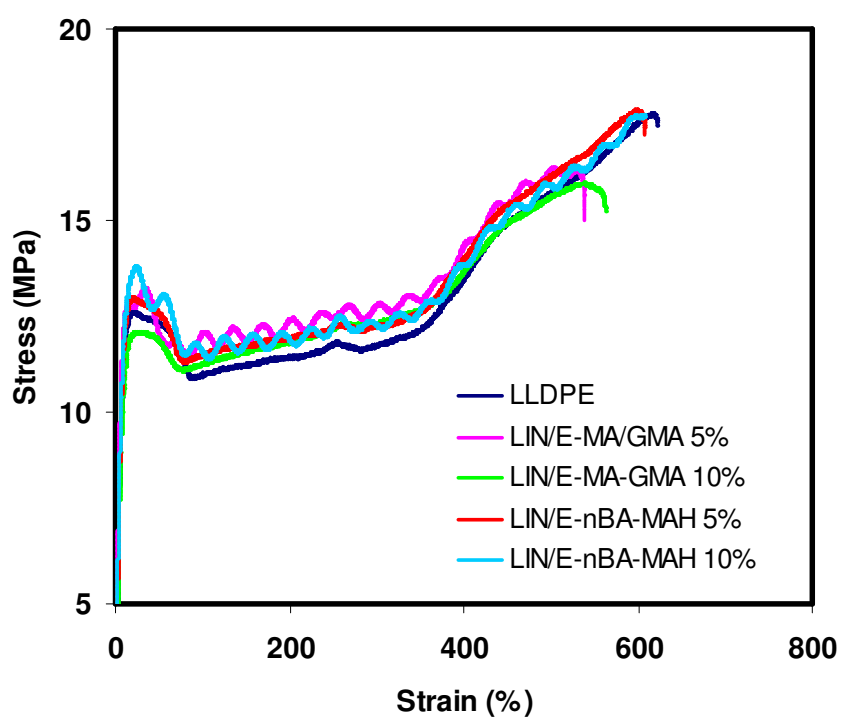


Figure D.3 Tensile stress-strain curve of LIN/Compatibilizer blends

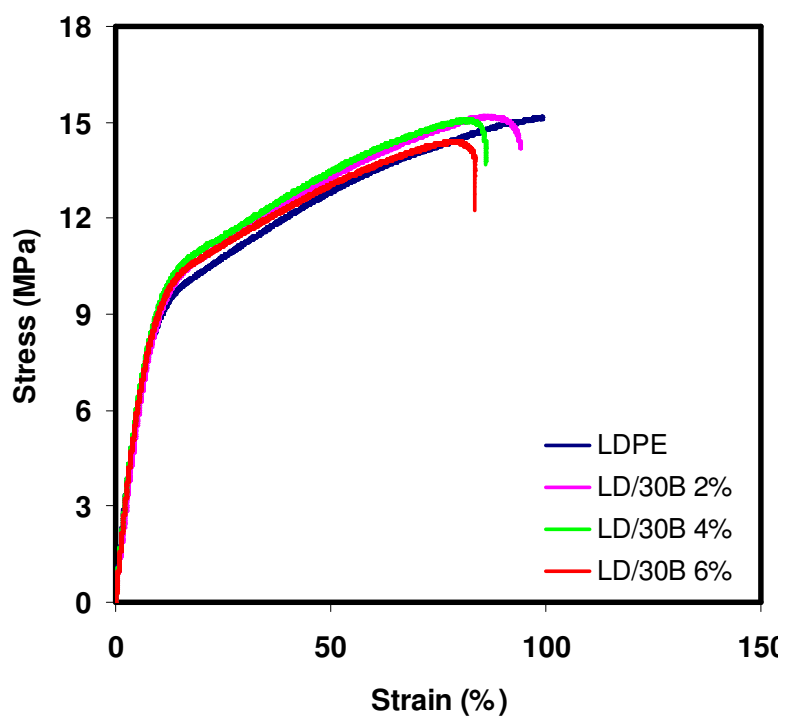


Figure D.4 Tensile stress-strain curves of LD/30B binary nanocomposites

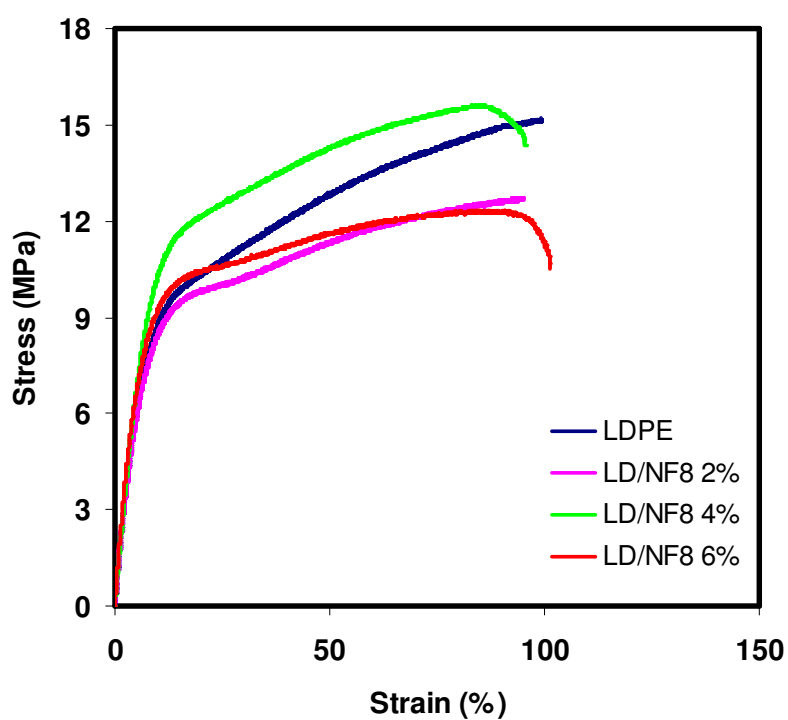


Figure D.5 Tensile stress-strain curves of LD/NF8 binary nanocomposites

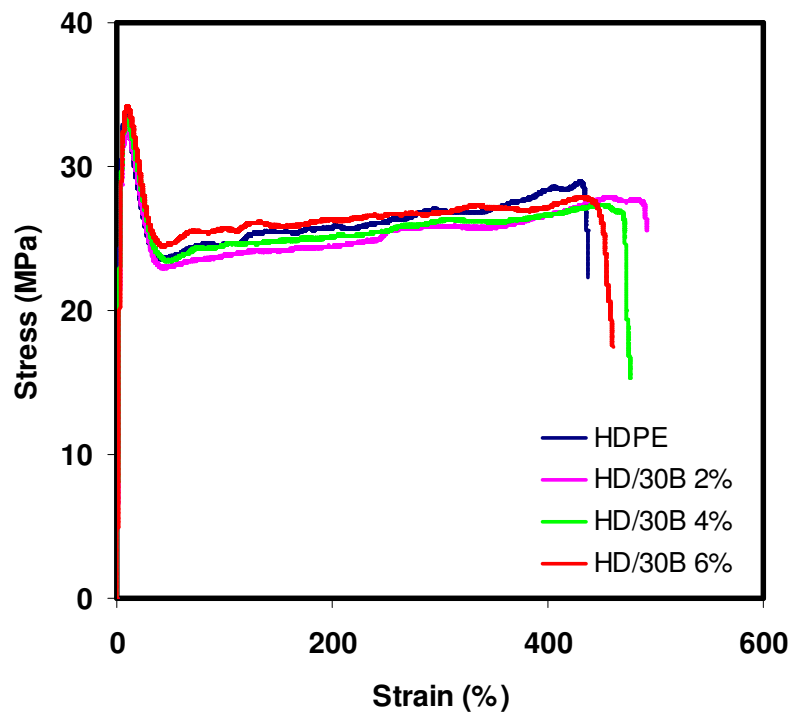


Figure D.6 Tensile stress-strain curves of HD/30B binary nanocomposites

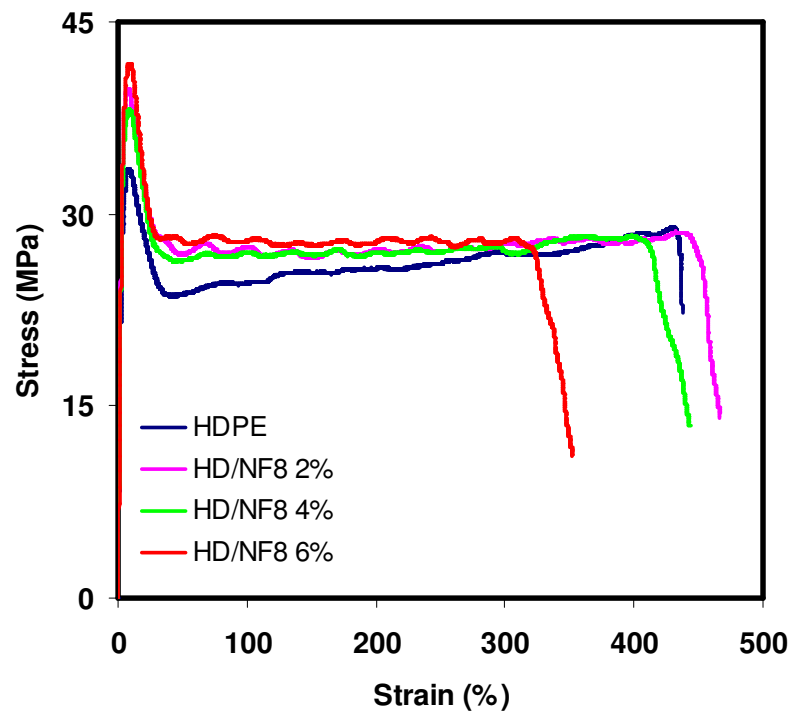


Figure D.7 Tensile stress-strain curves of HD/NF8 binary nanocomposites

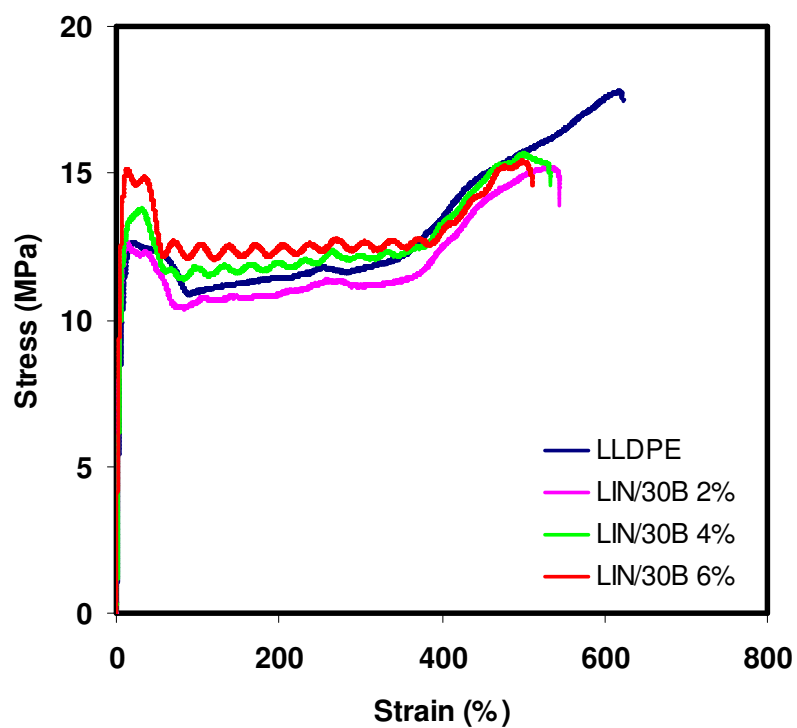


Figure D.8 Tensile stress-strain curves of LIN/30B binary nanocomposites

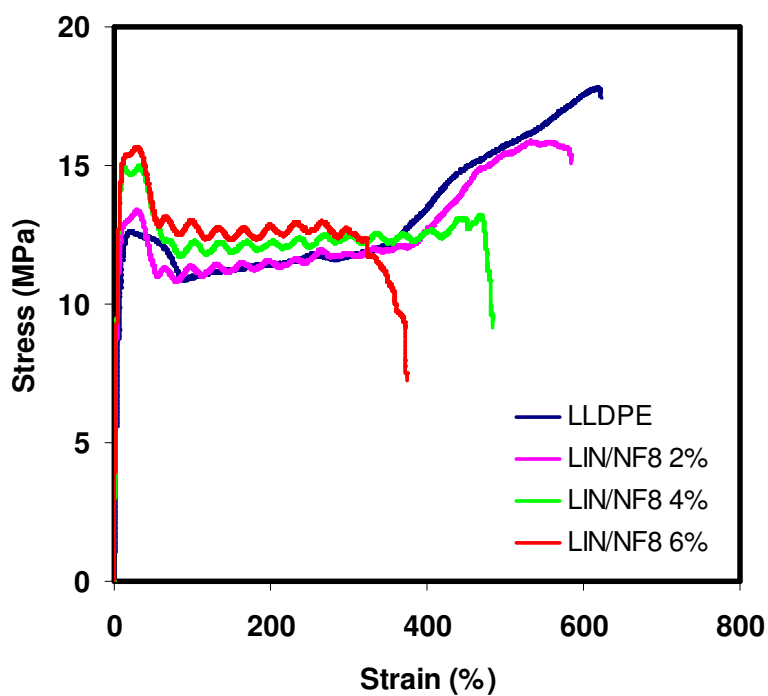


Figure D.9 Tensile stress-strain curves of LIN/NF8 binary nanocomposites

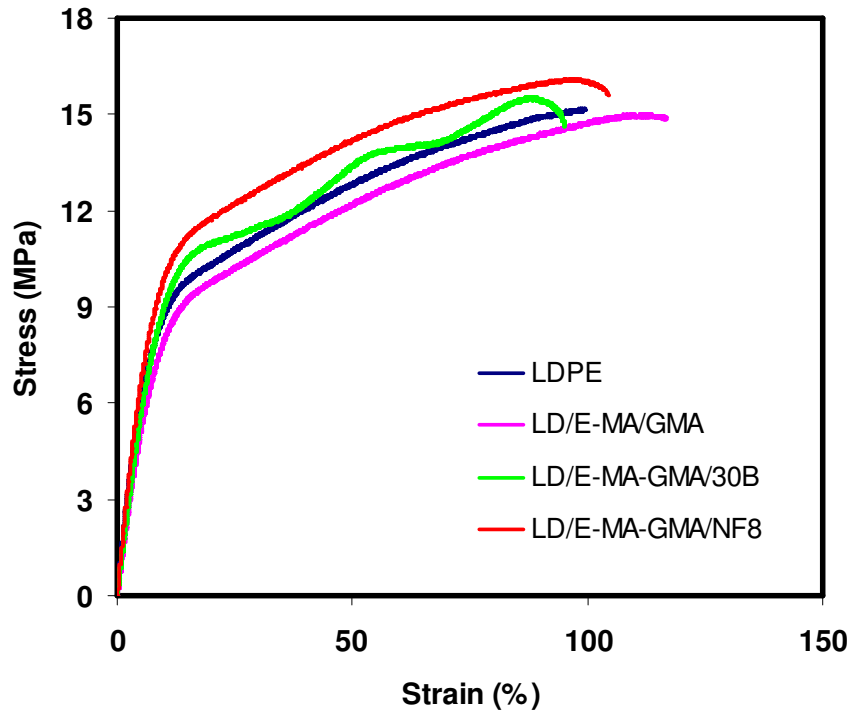


Figure D.10 Tensile stress-strain curves of LD/E-MA-GMA/Organoclay ternary nanocomposites with 5 wt % compatibilizer and 2 wt % organoclay loading

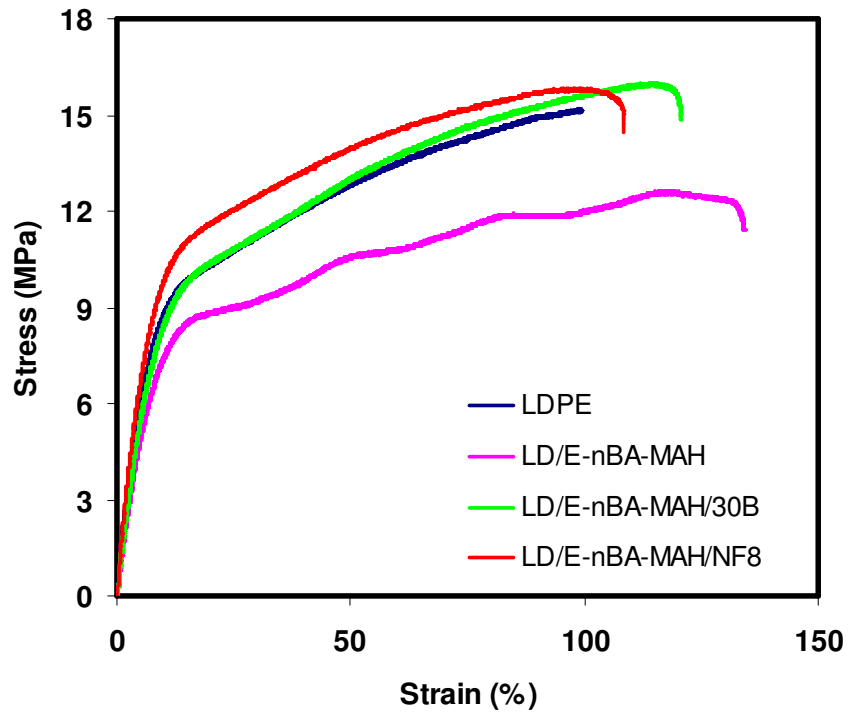


Figure D.11 Tensile stress-strain curves of LD/E-BA-MAH/Organoclay ternary nanocomposites with 5 wt % compatibilizer and 2 wt % organoclay loading

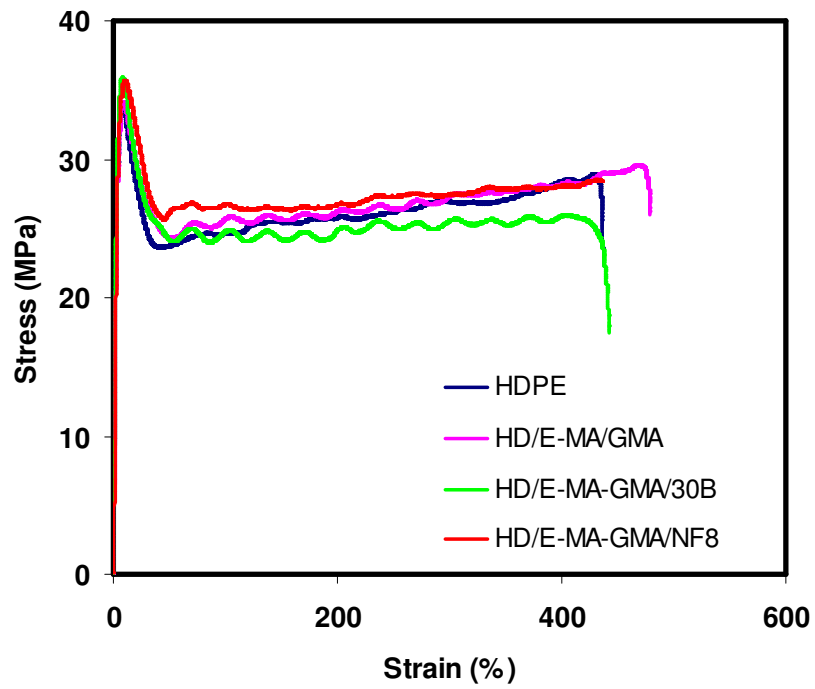


Figure D.12 Tensile stress-strain curves of HD/E-MA-GMA/organoclay ternary nanocomposites with 5 wt % compatibilizer and 2 wt % organoclay loading

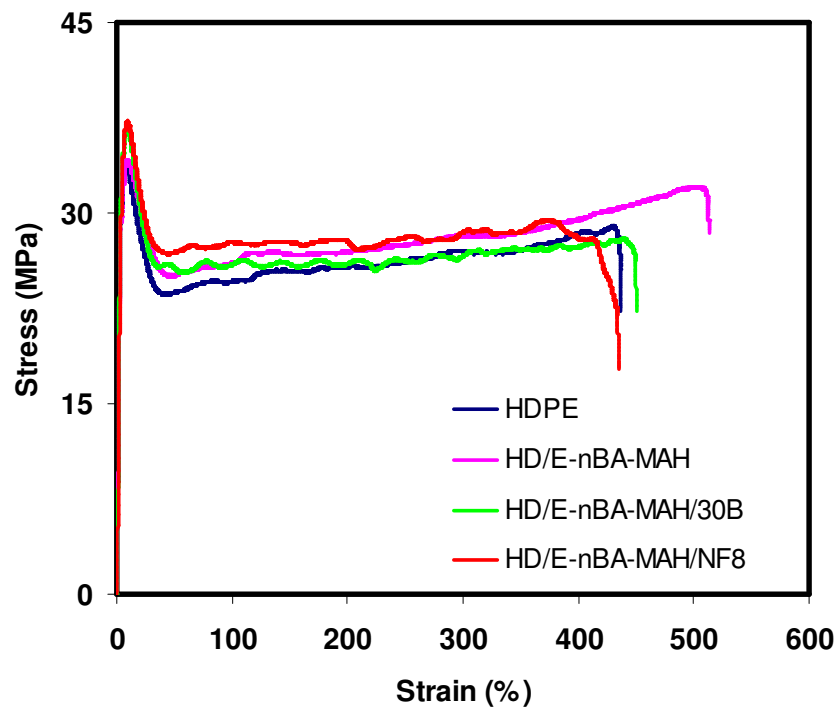


Figure D.13 Tensile stress-strain curves of HD/E-nBA-MAH/organoclay ternary nanocomposites with 5 wt % compatibilizer and 2 wt % organoclay loading

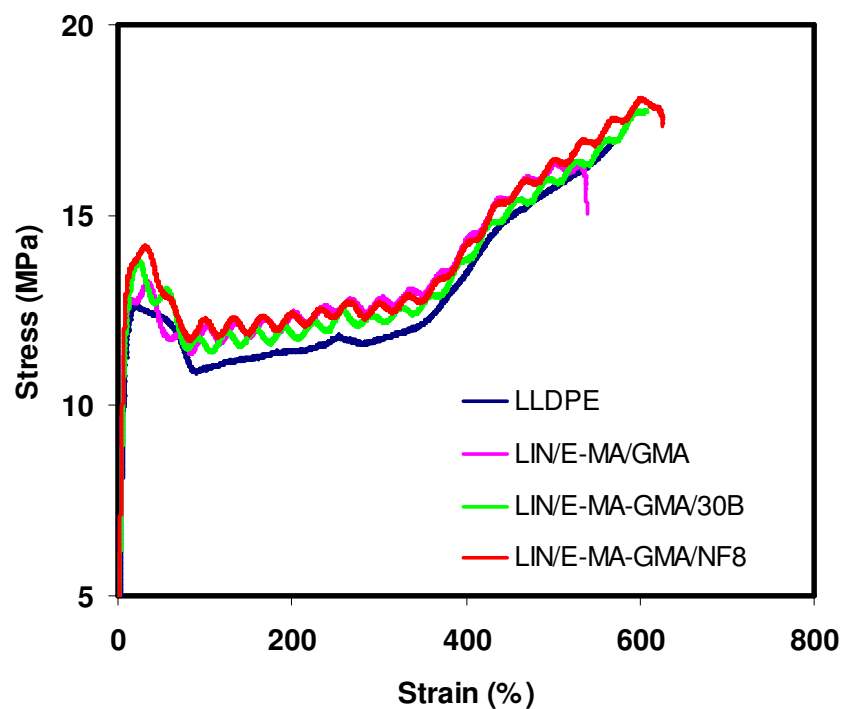


Figure D.14 Tensile stress-strain curves of LIN/E-MA-GMA/Organoclay ternary nanocomposites with 5 wt % compatibilizer and 2 wt % organoclay loading

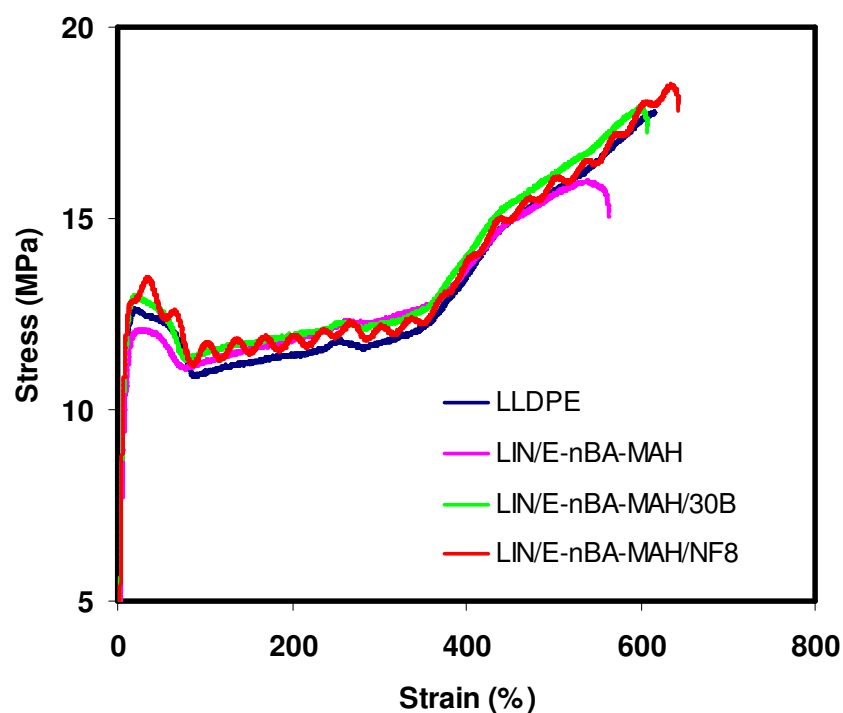


Figure D.15 Tensile stress-strain curves of LIN/E-BA-MAH/Organoclay ternary nanocomposites with 5 wt % compatibilizer and 2 wt % organoclay loading

CURRICULUM VITAE

Personal Information

Surname, Name: Işık Coşkunes, Fatma

Birth: 1980, Gebze,

Address: Karapınar Mh. 1165. Cd. No: 43/B Daire:14 Çamkaya, Ankara

Nationality: Turkish

Marital Status: Married

E-mail: isikfatma@yahoo.com

Mobile: + 90 505 840 88 82

Education

M. Sc. (Chemical Engineering) (C.GPA: 3.64/4.00)

[September 2003 - July 2005]

Middle East Technical University, Department of Chemical Engineering,
Ankara, Turkey

B.Sc. (Chemical Engineering) (C.GPA: 3.48/4.00)

[September 1998 - June 2003]

Middle East Technical University, Department of Chemical Engineering,
Ankara, Turkey

High School

[September 1995 – February 1998]

Kocaeli Körfez Fen Lisesi, Kocaeli, Turkey

Professional Experience

OHS Expert

[July 2005 - To date]

Occupational Health and Safety Center, Ankara

Research Assistant**[January 2005-July 2005]**

Chemical Engineering Department, METU, Ankara

Intern Chemical Engineer (Summer Practice)**[July 2002 – August 2002]**

CAM ELYAF Kocaeli, Turkey

Intern Chemical Engineer (Summer Practice)**[June 2001 – July 2001]****BAYER**, Kocaeli, Turkey**Journal Publications**

- Isik Coskunes F., Yilmazer U., "Preparation and Characterization of Low Density Polyethylene/Ethylene Methyl Acrylate Glycidyl Methacrylate/Organoclay Nanocomposites", Journal of Applied Polymer Science, 120, pg3087-3097, 2011.

Conference Publications

- Yilmazer U., Isik Coskunes F. "Preparation And Characterization Of Low Density Polyethylene / E-Ma-Gma / Organoclay Nanocomposites", "2nd Polymeric Composites Symposium-Exhibition And Brokerage Event", İzmir, TURKEY, 2010.

Computer Related Experience and Skills

- **Programming Languages:** FORTRAN 77
- **Operating Systems:** Windows 98/2000/XP/Vista
- **Commercial and Research Software Packages:** Matlab Microsoft Office XP/2003/2007 (Word, Excel, PowerPoint, Outlook)

Languages**English:** Very good in reading and writing